Frequency-Domain Analysis of "Constant in Gain Lead in Phase (Cglp)" Reset Compensators

Application to precision motion systems

Ahmadi Dastjerdi, A.

DOI
10.4233/uuid:4ada8565-2efe-472b-a182-b94c935048ae

Publication date
2021

Document Version
Final published version

Citation (APA)
Ahmadi Dastjerdi, A. (2021). *Frequency-Domain Analysis of "Constant in Gain Lead in Phase (Cglp)" Reset Compensators: Application to precision motion systems.* [Dissertation (TU Delft), Delft University of Technology]. https://doi.org/10.4233/uuid:4ada8565-2efe-472b-a182-b94c935048ae

Frequency-Domain Analysis of "Constant in gain Lead in phase (CgLp)" Reset Compensators

Application to Precision Motion Systems

FREQUENCY-DOMAIN ANALYSIS OF "CONSTANT IN GAIN LEAD IN PHASE (CGLP)" RESET COMPENSATORS

APPLICATION TO PRECISION MOTION SYSTEMS

Dissertation

for the purpose of obtaining the degree of doctor
at Delft University of Technology,
by the authority of the Rector Magnificus, Prof.dr.ir. T. H. J. J. van der Hagen,
chair of the Board for Doctorates,
to be defended publicly on

by

Ali AHMADI DASTJERDI

Master of Science in Mechanical Engineering-Applied Mechanics,
Sharif University of Technology, Iran,
born in Tehran, Iran.

This dissertation has been approved by

promotor: Prof.dr.ir. J. L. Herder
copromotor: Dr. S.H. Hossein Nia Kani

Composition of the doctoral committee:

Rector Magnificus,	Chairperson
Prof.dr.ir. J. L. Herder,	Delft University of Technology (Propmotor)
Dr. S.H. Hossein Nia Kani,	Delft University of Technology (Copromotor)
Independent members:	
Prof. dr. ir. J. W. van Wingerden,	Delft University of Technology
Prof.dr. L. Zaccarian,	LAAS-CNRS and University of Trento
Prof. dr. A. Banos,	University de Murcia
Prof. dr. M. Heertjes,	Eindhoven University of Technology
Other members:	
Prof. dr. A. Astolfi,	Imperial College of London

Keywords: Constant in gain Lead in phase (CgLp), Frequency-Domain Analysis, Loop-Shaping, Pseudo-Sensitivities, Reset Control Systems, Stability Analysis, Tuning Method

Printed by: Johannes Gutenberg

ISBN 000-00-0000-000-0

An electronic version of this dissertation is available at
http://repository.tudelft.nl/.

To my beloved wife, Azar,
and to my parents, Fezeh and Mohammad Taghi

CONTENTS

Summary xi

Samenvatting xiii

Preface xv

1 Introduction 1
- 1.1 Limitation of linear controllers . . . 2
- 1.2 Reset control systems . . . 4
- 1.3 DF of reset control systems . . . 5
- 1.4 CgLp compensators . . . 5
- 1.5 Research gap . . . 6
- 1.6 Research objectives . . . 7
- 1.7 Outline of the thesis . . . 8
- References . . . 8

2 An overview on linear fractional order controllers 11
- 2.1 Introduction . . . 12
- 2.2 Definitions of FO derivative and integral . . . 13
- 2.3 Common types of linear FO controllers . . . 15
  - 2.3.1 TID controller . . . 15
  - 2.3.2 CRONE controllers . . . 16
  - 2.3.3 lead/lag compensators . . . 16
  - 2.3.4 FO-$PI^{\lambda}D^{\mu}$ controllers . . . 17
- 2.4 Tuning methods of FO-controllers . . . 21
  - 2.4.1 Tuning methods for TID controller . . . 22
  - 2.4.2 Tuning methods for CRONE generations . . . 22
  - 2.4.3 Tuning methods for FO lead/lag compensators . . . 24
  - 2.4.4 Tuning methods for $PI^{\lambda}D^{\mu}$ . . . 25
- 2.5 Realization of FO controllers . . . 29
  - 2.5.1 Continuous approximation methods (S domain) . . . 30
  - 2.5.2 Discrete approximation methods (Z domain) . . . 33
  - 2.5.3 δ domain approximation methods . . . 35
  - 2.5.4 Digital implementation . . . 37
  - 2.5.5 Analogue implementation . . . 37
- 2.6 Several useful codes for FO controllers . . . 40
- 2.7 Discussion . . . 40
- 2.8 Conclusion . . . 42
- References . . . 42

3 Closed-loop frequency analysis of reset control systems 51
3.1 Introduction . . . 52
3.2 Preliminaries . . . 53
3.3 Closed-loop frequency response of reset control systems . . . 54
3.3.1 Stability and convergence . . . 55
3.3.2 HOSIDF of the closed-loop reset control systems . . . 60
3.3.3 Pseudo-sensitivities for reset control systems . . . 63
3.3.4 High frequency analysis . . . 66
3.4 Periodic inputs . . . 68
3.5 Illustrative example . . . 70
3.5.1 The optimal structure for CI . . . 70
3.5.2 Performance of CgLp Compensators . . . 73
3.6 Conclusion . . . 76
3.A lemma 3 . . . 77
3.B Lemma 4 . . . 77
3.C Limit calculation for high frequency analysis . . . 78
References . . . 78

4 Frequency-domain stability methods for reset control systems 83
4.1 Introduction . . . 84
4.2 Preliminaries . . . 85
4.3 Stability analysis of reset control systems with first order reset elements . . . 88
4.4 Stability analysis of reset control systems with second order reset elements 94
4.4.1 Reset control systems with GSORE . . . 94
4.4.2 Reset control systems with SOSRE . . . 102
4.5 Illustrative Examples . . . 103
4.5.1 A Reset control system with GSORE . . . 105
4.5.2 A Reset control system with SOSRE . . . 106
4.6 Conclusion . . . 106
4.A Proof of Lemma 5 . . . 107
4.B Proof of Corollary 9 . . . 109
4.C Proof of Proposition 1 . . . 109
4.D Proof of Corollary 10 . . . 110
References . . . 111

5 A frequency-domain tuning method for CgLp compensators 115
5.1 Introduction . . . 116
5.2 Overview of CgLp compensators . . . 117
5.2.1 Frequency-domain descriptions for reset elements . . . 117
5.2.2 CgLp compensator . . . 118
5.2.3 H_β condition . . . 119
5.2.4 Pseudo-sensitivities for reset control systems . . . 119
5.2.5 Sequence of reset elements . . . 120
5.3 Tuning procedure . . . 120
5.3.1 Solving the optimization problem . . . 122

5.4 Application to a precision motion stage . . . 123
5.4.1 Breaking water-bed effect . . . 126
5.4.2 Time-domain results . . . 127
5.4.3 Investigation of super-position law . . . 132
5.4.4 Changing sequence of reset element . . . 133
5.5 Conclusion . . . 136
References . . . 136

6 Conclusions and recommendations **141**
6.1 Conclusions . . . 142
6.2 Recommendations . . . 145
References . . . 146

Acknowledgements **149**

A A frequency-domain stability method for reset systems **151**
A.1 Introduction . . . 152
A.2 Problem formulation . . . 153
A.3 Frequency-domain stability analysis . . . 154
A.4 Illustrative example . . . 161
A.5 Conclusion . . . 164
References . . . 164

B The optimal sequence for reset controllers **167**
B.1 Introduction . . . 168
B.2 Preliminaries . . . 169
B.2.1 Reset control . . . 169
B.2.2 Pseudo sensitivity functions . . . 170
B.3 Methodology . . . 170
B.4 Closed-loop performance . . . 171
B.4.1 System overview . . . 172
B.4.2 Controller Design . . . 172
B.4.3 Closed-loop performance analysis in simulation . . . 174
B.4.4 Shaping filter . . . 175
B.4.5 Step response . . . 177
B.5 Experimental validation . . . 177
B.6 Conclusion . . . 179
References . . . 180

C Toolbox **183**

Curriculum Vitæ **187**

List of Publications **189**

SUMMARY

Proportional Integral Derivative (PID) controllers dominate the industry and are used in more than 90 percent of machines in this era. One of the reason for the popularity of these controllers is the existence of easy to use frequency-domain analysis tools such as loop-shaping for this type of controller. Due to the advancement of technology in recent decades, industry needs machines with higher speed and precision. Thus, an advanced industry-compatible control capable of a simultaneous increase in precision and speed is needed. Unfortunately, linear controllers, including integer and fractional order controllers, cannot satisfy this requirement of industry because of fundamental limitations such as the “water-bed" effect. In other words, precision and speed are conflicting demands in linear controllers, and designers should consider a proper trade-off between them when they tune these controllers.

The reset control strategy which is one of the well-known non-linear controllers, has shown a great capacity to overcome the limitation of linear controllers. In our group, a new type of reset compensator, which is termed “Constant in gain Lead in phase (CgLp)”, has been proposed as a potential solution for this significant challenge. Considering the first harmonic of the steady-state response of the CgLp compensator, which is called the Describing Function (DF) analysis, this compensator has a constant gain while providing a phase lead. As a result, this novel compensator can improve the precision of the control system, while simultaneously maintaining the high quality level of transient response (throughput of the system). As mentioned before, industry favours designing controllers in the frequency-domain because it provides an easy to use tool for performance analysis of control systems. Therefore, in order to interface this compensator well with the current control design in industry and broaden its applicability, it is important to study this type of reset compensator in the frequency-domain.

So far, CgLp compensators have been studied in the frequency-domain using the DF method. However, there are some major drawbacks which have to be solved in order to make these compensators ready for industry utilization. Essentially, there is a lack of knowledge about the closed-loop steady-state performance of reset control systems. In addition, since the high order harmonics generated by CgLp compensators are neglected in the DF method, this method by itself is not an appropriate method for predicting open-loop and closed-loop steady-state performance, particularly for precision motion applications. Second, it is necessary to develop an intuitive frequency-domain stability method to assess the stability of CgLp compensators, similar to the Nyquist plot for linear controllers. Finally, to achieve a favourable dynamic performance, it is highly needed to propose a systematic frequency-domain tuning method for this type of reset compensators.

The aim of this thesis is to address the three aforementioned major questions and provide a non-linear loop-shaping approach for analyzing CgLp compensators in the frequency-domain. For this purpose, in the first step, sufficient conditions for the exis-

tence of the steady-state response for the closed-loop reset control systems driven by periodic references are given. Furthermore, a framework is developed to obtain the steady-state response and define a notion of closed-loop frequency response, including high order harmonics. From the precision perspective, pseudo-sensitivities for reset control systems are defined which accurately predict the closed-loop performance of reset control systems.

In the next step, an intuitive frequency-domain method for assessing the stability of CgLp compensators is developed. Thanks to this developed approach, similar to linear controllers, it is possible to directly determine the stability of this type of reset control systems using frequency response measurements. To make this non-linear loop-shaping easy to use, most of these calculations, which are provided for frequency-domain analysis of reset control systems, are embedded in a user-friendly toolbox.

Finally, to accomplish the non-linear loop-shaping, the defined pseudo-sensitivities and the frequency-domain stability method are utilized to provide a reliable and systematic frequency-domain tuning method for CgLp compensators. Furthermore, different performance metrics of a CgLp compensator, which is tuned by the proposed method, are compared with those of a PID controller on a precision positioning stage. The results show that this method is effective, and the tuned CgLp can achieve more favourable dynamic performance than the PID controller for the precision motion stage. In this empirical example, it was demonstrated that using CgLp compensator improve the precision performance of the stage by 60% without devastating the transient response. Hence, it was practically shown that CgLp compensators overcome the “water-bed effect".

SAMENVATTING

Proportional Integral Derivative (PID) -regelaars domineren de industrie en worden tegenwoordig in meer dan 90 procent van de machines gebruikt omdat ze eenvoudig te gebruiken zijn vanwege de beschikbaarheid van frequentiedomein analyse tools zoals loop-shaping voor dit type regelaar. De industrie vooruit gemaakt vereist de industrie machines met steeds hogere snelheid en precisie. Bedrijven zijn dus geïnteresseerd in geavanceerde, industrie-compatibele regelaars, voor zowel een toename in precisie als in snelheid. Helaas kunnen lineaire regelaars, zowel de integer als fractional order typen, niet voldoen aan deze eis van de industrie vanwege hun fundamentele beperking: het water-bed effect. Met andere woorden, in lineaire regelaars zijn precisie en snelheid tegenstrijdig waardoor ontwerpers een goede afweging moeten maken tussen beide wanneer ze deze regelaars instellen.

Een van de bekende niet-lineaire regelaars, de Reset regelaar, heeft een groot potentie getoond om de beperking van lineaire regelaars te overwinnen. In onze groep is een nieuw type reset compensator, genaamd de " Constant in gain Lead in phase (CgLp) aangedragen als mogelijke oplossing voor deze belangrijke uitdaging. Lettend op de eerste harmonische van de steady-state respons van de CgLp-compensator, genaamd de Describing Function (DF)-analyse, heeft deze compensator een constante versterking en tegelijkertijd een vasevoorsprong. Hierdoor kan deze nieuwe compensator de precisie van het regelsysteem verbeteren, terwijl het tegelijkertijd in staat is om het van een hoge kwaliteit dynamische respons te voorzien (doorvoer van het systeem). Zoals vermeld geeft de industrie de voorkeur aan het ontwerpen van regelaars in het frequentiedomein omdat het een eenvoudig te gebruiken hulpmiddel is om de prestatie van regelsysteem te analyseren. Daarom, om deze compensator goed te laten aansluiten op het huidige regelontwerp in de industrie en het daardoor breder toepasbaar te maken, is het belangrijk om dit type reset compensator in het frequentiedomein te bestuderen.

Tot nu toe zijn CgLp-compensatoren bestudeerd in het frequentiedomein met behulp van de DF-methode. er zijn echter enkele grote nadelen die moeten worden opgelost om deze compensatoren geschikt te maken voor de industrie. Er is voornamelijk een gebrek aan kennis over de gesloten-keten steady-state-prestaties van reset regelsystemen. Daarnaast worden de harmonischen van hoge orde die worden gegenereerd door CgLp-compensatoren verwaarloosd in de DF-methode. Daarom is deze methode op zichzelf geen geschikte methode voor het voorspellen van steady- state prestaties met open- keten en gesloten- keten; met name voor toepassingen met precisie-beweging. Ten tweede is het essentieel om een intuïtieve frequentiedomein-stabiliteitsmethode te ontwikkelen om de stabiliteit van CgLp-compensatoren te beoordelen welke vergelijkbaar met de Nyquist-plot voor lineaire regelaars. Ten slotte, om een gunstige dynamische prestatie te bereiken, het is hard nodig om een systematische methode voor het afstemmen van het frequentiedomein voor dit type reset compensatoren op te stellen.

Het doel van dit proefschrift is om de hierbovengenoemde drie hoofdvragen te be-

antwoorden en een niet-lineaire loop-shaping-benadering te bieden voor het analyseren van CgLp-compensatoren in het frequentiedomein. Als eerste stap om dit doel te bereiken worden voldoende voorwaarden gegeven voor het verkrijgen van een steady-state respons voor het gesloten-keten reset regelsysteem, aangestuurd door periodieke referenties. Daarna wordt een raamwerk ontwikkeld om de steady- state respons te verkrijgen en om een begrip van closed-loop frequentierespons te definiëren, inclusief harmonischen van hogere orde. Vanuit precisie-perspectief worden pseudo-gevoeligheden voor reset regelsystemen gedefinieerd die nauwkeurig de gesloten-keten prestatie van reset regelsystemen voorspellen.

In de volgende stap worden intuïtieve frequentiedomein methoden ontwikkeld om de stabiliteit van CgLp-compensatoren te beoordelen. Dankzij deze ontwikkelde benadering, welke vergelijkbaar is met lineaire regelaars, is het mogelijk om de stabiliteit van dit type reset regelsystemen rechtstreeks te bepalen met behulp van de frequentierespons metingen. Om deze niet-lineaire loop-shaping gebruiksvriendelijk te maken, zijn de meeste berekeningen die bedoeld zijn voor de frequentiedomeinanalyse van reset regelsystemen ingebed in een gebruiksvriendelijke toolbox.

Ten slotte worden de gedefinieerde pseudo-gevoeligheden en de frequentiedomein-stabiliteits methode gebruikt om een betrouwbare en systematische frequentiedomein afstemmingsmethoden voor CgLp-compensatoren te bieden om niet-lineaire loop-shaping te verkrijgen. Bovendien worden verschillende prestatiematen van de CgLp-compensator, welke is ingesteld met de voorgestelde methode, vergeleken met die van een PID-regelaar op een precisie-positioneerplatform. De resultaten laten zien dat deze methode effectief is en dat de afgestemde CgLp gunstiger dynamische prestaties kan bereiken dan de PID-regelaar voor de bewegingsprecisie het platform. In dit empirische voorbeeld is aangetoond dat het gebruik van de CgLp-compensator de precisie prestaties het platform met 60% verbetert zonder afbreuk te doen aan de dynamische respons. Het voorbeeld leat dat de CgLp methode het water-bed effect overwint zowel in theorie als in de praktijk.

PREFACE

The main outcome of my research during four years on "Frequency-Domain Analyzing of Constant in gain Lead in phase (CgLp) reset compensators" is this thesis, which includes six chapters and three appendices. Although the scientific contribution during my PhD study resulted in seven journal and six conference papers, which can be found the list of publication C, four major of those journal papers are placed in chapters two till five. Also, two of the conference papers are presented in Appendix B and C. Since chapters two till five and Appendix B and C mostly contain papers that are published or submitted for peer review to journals and conferences, there are several repetitions, particularly in the introduction and preliminaries of those chapters. Moreover, since the sequence of those chapters does not follow a chronological pattern, there are some sections in upcoming chapters which are cited in previous chapters. In this regard, the author apologizes for any inconvenience during reading this thesis.

Ali Ahmadi Dastjerdi
Delft, May 2021

1

INTRODUCTION

Ali AHMADI DASTJERDI

In this chapter, the significant challenge that linear controllers are faced with is briefly recalled. Then, the preliminaries about reset controllers, and "Constant in gain Lead in phase (CgLp)" compensators are provided. Next, the research objective is elaborated, and the outline of the thesis is presented.

1

Today, high-tech industry requires machines with ever increasing speed and precision which causes the performance specifications of controllers to become extremely demanding. Consequently, companies are interested in advanced industry-compatible control capable of a significant and simultaneous increase in precision and speed. Linear Proportional-Integral-Derivative (PID) controllers still have been applied in 90% of the high-tech industry are no longer sufficient to meet these new performance specifications [1–3]. Recently, Fractional Order (FO)-PID controllers have tried to solve this significant barrier (see Chapter 2). Although FO-PID controller is offering more design freedom compared to classical PID controller and makes this problem less severe, it is a type of linear controller and its performance is confined [4]. In fact, this limitation comes from the inherent linearity of these FO-PID and classical PID controllers which makes them not suited to handle increasing the precision and speed simultaneously.

1.1. LIMITATION OF LINEAR CONTROLLERS

SINCE there is a relation between Bode's gain and phase of linear control systems, linear controllers are not capable of increasing the precision and speed[1] simultaneously [1–3]. In this section, this limitation is elaborated in both time-domain and frequency-domain. From the frequency-domain viewpoint, in PID controllers, proportional action controls the tracking speed (also known as "bandwidth"), integral action controls tracking precision, and derivative action ensures the stability of the system [1–3].The loop-shaping approach (either manual or automated) is a widespread technique in the frequency-domain for designing PID controllers because it directly gives a deep insight into the stability, precision and bandwidth of the control system by looking at the open-loop of the system.

From the loop-shaping perspective, two requirements have to be fulfilled for control motion applications. First, the control system should have high open-loop gains at low frequencies to ensure an acceptable tracking and disturbance rejection performances, and have low gains at high frequencies to avoid noise amplification. This can be ensured by a constant large negative slope (-2 or lower) as shown with the green and gray line in Figure 1.1. Second, the system should have enough phase margin (the amount of the phase above -180°) at bandwidth to assure the stability. However, this can only be achieved by a gain slope of ($\nu = -1$). Obviously, these two requirements directly conflict with each other. This leads to a trade-off between precision and speed [1].

Recently, FO calculus entails using non-integer orders of derivative and integral action (for more details see Chapter 2). This allows for more flexible control design where the gain slope around the bandwidth is not restricted to -1, but it can be any real number depending on the required phase margin. Also, n_I and n_F (gain slope at low and high frequencies, see Figure 1.1) could be any real number lower than -2. This increased freedom helps in reducing the effect of the precision-speed trade-off. This trade-off can be explained by "water-bed" effect in the noise sensitivity frequency response [1–3].

[1] Note that in this thesis, speed or throughput of a control system means the time it takes that the transient response of the system dies out (settling time).

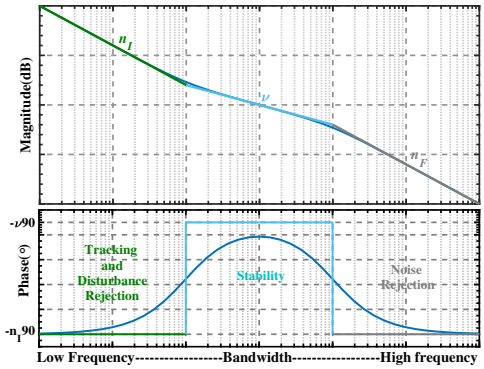

Figure 1.1: Open-loop frequency response of a conventional control system

According to linear control theory,

$$\int_0^\infty \mathrm{Ln}(|S(j\omega)|)d\omega = 0, \tag{1.1}$$

for every stable Linear Time Invariant (LTI) system with no RHP pole and zeros which has at least two more poles than zeros . Thus, if some control action reduces the sensitivity amplitude in a certain frequency range, then the sensitivity will increase in other frequency ranges. For example, if the tracking and disturbance rejection performances of a linear control system are improved using an extra integrator (PI^2D), the phase margin of the system decreases which results in a higher peak of sensitivity (the modules margin).

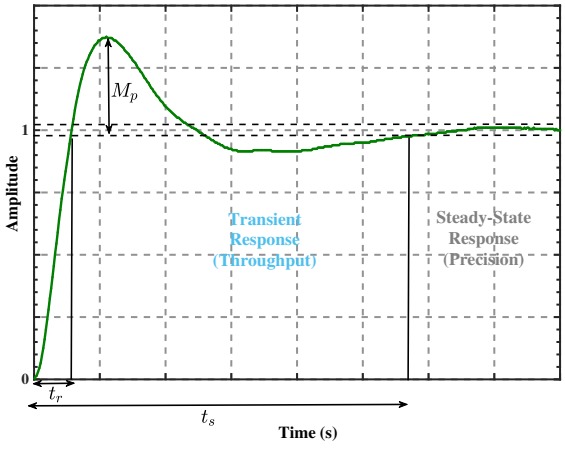

Figure 1.2: Step response of a conventional control system

This limitation can also be explained in the time-domain. To this end, the step response of a precision positioning stage, which is controlled by a PID controller, is shown

in Figure 1.2. The step response of a control system has important specifications which give information about the properties of the system. These specifications are:

- Rise time (t_r): the time at which the output of the system becomes equal to the reference (or in some applications 90% of the reference) for the first time.
- Overshoot (M_p): the difference between the peak of the response of the system and the amplitude of reference step input.
- Settling time (t_s): the time at which the output of the system has entered and remained within a specified error band.
- Steady-state error: the deviation of the output of system from reference during steady-state ($\lim_{t\to\infty} e(t)$).

These specifications have relations with the open-loop frequency response of motion control systems (Figure 1.1). Rise time (t_r) is inversely dependent on the bandwidth of the system. Overshoot (M_p) is inversely related to the phase margin, and settling time (t_s) has approximately inverse relation by the phase margin and bandwidth of the system. The steady-state error of the system is determined by the slope gain of the system at low and high frequencies (n_I and n_F). Thus, if the steady-state error (precision) of the system is improved by decreasing the slope of the system at high and low frequencies, the amplitude of overshoot and settling time will increase (throughput decreases). This also implies the mentioned trade-off between precision and speed in linear controllers [1–3].

1.2. RESET CONTROL SYSTEMS

RECENTLY, it has been shown that concept of "Constant in gain Lead in phase (CgLp)" compensator has prospects to reduce this trade-off [5–8]. It is because (unlike differentiator) CgLp can give a phase lead without changing the gain of the system. Since the CgLp compensator is a type of reset element, it is noteworthy to recall basic principles of reset elements. The state-space representation of a reset elements is,

$$\begin{cases} \dot{x}_r(t) = A_r x_r(t) + B_r e(t), & e(t) \neq 0, \\ x_r(t^+) = A_\rho x(t), & e(t) = 0, \\ u_r(t) = C_r x(t) + D_r r(t), \end{cases} \tag{1.2}$$

where A_r, B_r, C_r, and D_r are the dynamic matrices of the base linear system of the reset element, $e(t)$ and $u(t)$ are the error input and control output, respectively. When the reset condition is not satisfied ($e(t) \neq 0$), the system has a linear dynamic behaviour, and when the reset condition becomes true ($e(t) = 0$), the states reset to new values by A_ρ (reset matrix). Note that the transfer function $BLS(s) = C_r(sI - A_r)^{-1}B_r + D_r$ is called the base linear transfer function of the reset element and $(\overset{A_\rho}{\not{BLS}(s)})$ denotes that the controller with the base linear transfer function $BLS(s)$ resets with the reset matrix A_ρ.

The first reset element, which is a Clegg Integrator (CI), was introduced by Clegg in 1958 [9]. A CI is an integrator which resets its state to zero when its input crosses zero. In comparison with a simple linear integrator, CI provides less overshoot. This

can be justified by the fact that considering only the first harmonic of the output of CI (Describing Function (DF) method), it produces less phase lag at the cross-over frequency than the linear one. To have more design freedom, First Order Reset Element (FORE) [5, 10, 11] and Second Order Reset Element (SORE) have been proposed [5, 12]. In addition, to enhance the performance of reset control systems, several techniques such as reset band [13, 14], fixed reset instants [15], partial Reset (resetting subset of states or resetting to non-zero values), and PI+CI approaches [16] have been studied. Using partial reset technique ($A_\rho \neq 0$) in cases of FORE and SORE, Generalized First Order Reset Element (GFORE) and Generalized Second Order Reset Element (GSORE) have been introduced [5, 17]. Moreover, in order to soften the non-linearity of reset elements, new structures have been developed (for more details, see Chapter 4).

1.3. DF OF RESET CONTROL SYSTEMS

RESET compensators are analyzed using the DF method in the frequency-domain. To study the reset element (1.2) using the DF method, a sinusoidal reference $r(t) = a_0 \sin(\omega t)$, $\omega > 0$ is applied and the output is approximated by the first harmonic of the Fourier series expansion of the steady-state response (provided if exists). In order to have a well-defined steady-state response, it is assumed that A_r has all eigenvalues with negative real part and $A_\rho e^{\frac{A_r \pi}{\omega}}$ has all eigenvalues with magnitude smaller than one [17]. The DF of the reset element (1.2) is obtained in [17] as

$$\mathcal{N}_{DF}(\omega) = \frac{a_1(\omega) e^{j\varphi_1(\omega)}}{a_0} = C_r(j\omega I - A_r)^{-1}(I + j\Theta(\omega))B_r + D_r, \tag{1.3}$$

where

$$\Theta(\omega) = \frac{-2\omega^2}{\pi}(I + e^{\frac{\pi A_r}{\omega}})\left((I + A_\rho e^{\frac{\pi A_r}{\omega}})^{-1} A_\rho (I + e^{\frac{\pi A_r}{\omega}}) - I\right)(\omega^2 I + A_r^2)^{-1}. \tag{1.4}$$

1.4. CGLP COMPENSATORS

IN this section, the concept of CgLp compensators is introduced. A CgLp compensator (1.5) and (1.6) is constructed utilizing a GFORE or a GSORE with the series combination of a corresponding order of lead filter. Considering the DF analysis of GFORE/GSORE, the gain behaviour is the same as a first/second order low-pass filter while the phase lag of these elements are less than the first/second order low-pass filter. Now, if a first/second order lead filter is put in series with GFORE/GSORE, this reset compensator has a constant gain with a lead phase (Figure. 1.3) [5, 6, 18–20]. The first order CgLp compensator is

$$C_{CgLp1}(s) = \left(\frac{1}{\frac{s}{\omega_{r\alpha}} + 1}\right)^{A_\rho} \left(\frac{\frac{s}{\omega_r} + 1}{\frac{s}{\omega_t} + 1}\right), \tag{1.5}$$

where $\omega_{r\alpha} = \omega_r / \alpha$ is the corner frequency of the reset element, $A_\rho = \gamma$ is the reset matrix, and ω_r and ω_t are the corner frequency of the lead filter. To provide a constant gain,

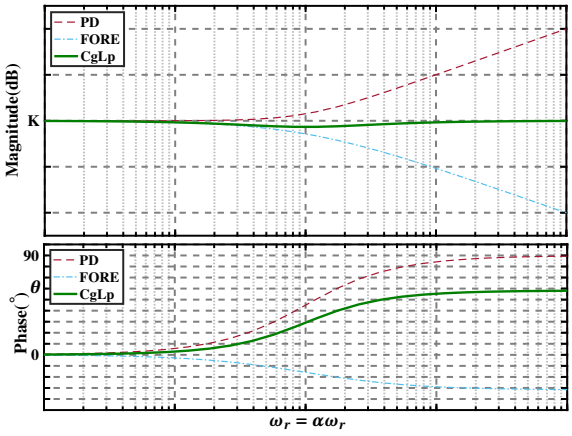

Figure 1.3: The DF of a CgLp compensator

Table 1.1: Correction factors of the first and second order CgLp [5, 19]

γ	-0.9	-0.8	-0.7	-0.6	-0.5	-0.4	-0.3	-0.2	-0.1	0	0.1	0.2	0.3	0.4	0.5	0.6	0.7	0.8	0.9
α	16.71	8.19	5.26	3.85	3.01	2.47	2.09	1.81	1.60	1.44	1.32	1.23	1.16	1.11	1.07	1.04	1.02	1.01	1.0
α_1	30.09	14.11	8.66	5.89	4.23	3.11	2.43	1.92	1.52	1.23	1.03	0.93	0.89	0.90	0.92	0.94	0.96	0.98	0.99
α_2	3.28	3.20	3.01	2.76	2.49	2.21	2.10	1.91	1.63	1.36	1.14	1.02	1.00	1.03	1.06	1.07	1.07	1.05	1.03

parameters $\omega_{r\alpha}$ and ω_r are found using Table 1.1), and $\omega_t \gg \omega_r$. Moreover, the second order CgLp compensator is

$$C_{CgLp2}(s) = \left(\frac{1}{\left(\frac{s}{\omega'_{r\alpha}}\right)^2 + 2\frac{\beta_{r\alpha}}{\omega'_{r\alpha}}s + 1} \right)^{\gamma I} \left(\frac{\left(\frac{s}{\omega'_r}\right)^2 + 2\frac{\beta_r}{\omega'_r}s + 1}{\left(\frac{s}{\omega'_t} + 1\right)^2} \right), \tag{1.6}$$

in which $\omega'_{r\alpha} = \omega_r/\alpha_1$ and $\beta_{r\alpha} = \beta_r/\alpha_2$ are the corner frequency and damping of the reset element, respectively, $A_\rho = \gamma I$ is the reset matrix, β_r is the damping of the lead filter, and ω'_r and ω'_t are the corner frequency of the lead filter. To provide a constant gain, correction factors α_1 and α_2 are provided in Table 1.1 for $\beta_{r\alpha} = 1$, and $\omega'_t \gg \omega'_r$. Since CgLp compensators have a constant gain with a lead phase, they can potentially eliminate the trade-off which is discussed in Section 1.1.

1.5. RESEARCH GAP

As was mentioned, loop-shaping is one of the popular methods for designing controllers in industry. However, the loop-shaping approach is only applicable for analyzing linear controllers in the frequency-domain. In addition, the DF method is only an approximation method and is not reliable enough, particularly in precision motion applications in which we need have to follow a motion trajectory very fast and precisely. Therefore, to interface CgLp compensators well with the current control design in in-

dustry, which favours designing controllers in the frequency-domain, it is important to precisely design this type of reset compensator in the frequency-domain.

1.6. RESEARCH OBJECTIVES

THE main contribution of this thesis is to fulfil the mentioned important research gap by providing a non-linear loop-shaping frame work for analyzing CgLp compensators in the frequency-domain. This is one of the essential scientific gaps which has to be filled towards making these reset compensators ready for industry. For this purpose, this thesis has to achieve the following three key objectives which are how to study steady-state performance, assess the stability, and tune parameters of CgLp compensators in the frequency-domain.

So far, CgLp compensators have been studied in the frequency-domain using the DF method. However, this method has several drawbacks which make this method unreliable. First, the closed-loop steady-state performance of reset control systems has not been yet analyzed in literature. This is challenging because there is no proof of the existence of the steady-state solution for closed-loop reset control systems. Besides, since the high order harmonics generated by reset elements are neglected in the DF method, this method by itself is not an appropriate approach for predicting the open-loop and closed-loop steady-state performance, particularly for precision motion applications. Thus, the first objective of this thesis is: ***to develop theories to analyze the steady-state response of closed-loop reset controllers.***

Stability is one of the important requirements of control systems. However, similar to other non-linear controllers, the stability analysis of these reset control systems is complex and often requires parametric models of systems. Moreover, for the loop-shaping approach is also important to determine the stability of control systems using the frequency-domain response. Although there are some frequency-domain stability tools such as the H_β condition for reset control systems, assessing the conditions of those methods are complex, particularly for high-dimensional plants. In addition, they cannot guarantee uniformly bounded-input bounded-state (UBIBS) property for reset control systems in the case of resetting to non-zero values. Therefore, the second objective of this thesis is: ***to propose a non-parametric frequency-domain stability method to assess the stability of CgLp compensators using Frequency Response Function (FRF) measurement.***

Finally, due to the design flexibility of reset elements, there are different combinations of tuning parameters for CgLp compensators which can provide the same amount of phase lead at the cross-over frequency based on the DF method. However, all of these combinations do not necessarily improve the performance of reset control systems due to the existence of high order harmonics. Hence, it is highly needed to develop a systematic and reliable frequency-domain tuning method for this type of reset compensators to achieve the final important objective: ***to develop a frequency-domain tuning method for CgLp compensators to achieve a favourable dynamic performance for the control system.***

1.7. OUTLINE OF THE THESIS

This thesis includes the main articles either published or submitted to peer review journals[2]. Since most of the papers are about CgLp compensators, the reader might find several repetitions, particularly in the introduction and preliminaries of chapters. The chapters of this thesis are organized as follows.

In Chapter 2, an overview of linear FO-PID controllers in the frequency domain is presented. In this chapter, the pros and cons of linear FO-PID controllers are elaborated. Furthermore, it is shown that although FO-PID controllers provide more design flexibility and improve the performance of control systems, they are faced with the same limitation as classical PID controllers due to their linearity.

In Chapter 3, first, sufficient conditions for the existence of the steady-state response for a closed-loop system with a reset element driven by periodic references are given. Furthermore, a framework to get the steady-state response and define a notion of closed-loop frequency response, including high order harmonics, is presented. From the precision perspective, pseudo-sensitivities for reset control systems are defined which accurately predict the closed-loop performance of reset control systems.

In Chapter 4, an intuitive frequency-domain method for assessing the stability of CgLp compensators is developed utilizing the H_β condition, analytic geometry relations, and optimization methods.

In Chapter 5, the defined pseudo-sensitivities and the frequency-domain stability method are utilized to provide a reliable and systematic frequency-domain tuning method for CgLp compensators. Furthermore, different performance metrics of a CgLp compensator, which is tuned by the proposed method, are compared with those of a PID controller on a precision positioning stage.

In Chapter 6, the main conclusions of this research are given. The advantages and disadvantages of the proposed non-linear loop-shaping framework are discussed. Finally, some recommendations for future study are provided.

REFERENCES

[1] A. A. Dastjerdi, B. M. Vinagre, Y. Chen, and S. H. HosseinNia, *Linear fractional order controllers; a survey in the frequency domain,* Annual Reviews in Control (2019).

[2] R. Middleton, *Trade-offs in linear control system design,* Automatica **27**, 281 (1991).

[3] R. M. Schmidt, G. Schitter, and A. Rankers, *The Design of High Performance Mechatronics High-Tech Functionality by Multidisciplinary System Integration* (IOS Press, 2014).

[4] A. A. Dastjerdi, N. Saikumar, and S. H. HosseinNia, *Tuning guidelines for fractional order PID controllers: Rules of thumb,* Mechatronics **56**, 26 (2018).

[5] N. Saikumar, R. K. Sinha, and S. H. HosseinNia, *'Constant in gain Lead in phase' element-application in precision motion control,* IEEE/ASME Transactions on Mechatronics **24**, 1176 (2019).

[2] There are other published articles which contribute to solve other minor problems of CgLp compensators, which you can find in the list of publication C.

[6] L. Chen, N. Saikumar, and S. H. HosseinNia, *Development of robust fractional-order reset control,* IEEE Transactions on Control Systems Technology **28**, 1404 (2020).

[7] A. Palanikumar, N. Saikumar, and S. H. HosseinNia, *No more differentiator in PID: Development of nonlinear lead for precision mechatronics,* in *European Control Conference (ECC)* (2018) pp. 991–996.

[8] N. Karbasizadeh, A. Ahmadi Dastjerdi, N. Saikumar, D. Valerio, and S. HosseinNia, *Benefiting from linear behaviour of a nonlinear reset-based element at certain frequencies,* in *Australian and New Zealand Control Conference (ANZCC)* (2020).

[9] J. C. Clegg, *A nonlinear integrator for servomechanisms,* Transactions of the American Institute of Electrical Engineers, Part II: Applications and Industry **77**, 41 (1958).

[10] L. Zaccarian, D. Nesic, and A. R. Teel, *First order reset elements and the Clegg integrator revisited,* in *American Control Conference* (2005) pp. 563–568 vol. 1.

[11] I. Horowitz and P. Rosenbaum, *Non-linear design for cost of feedback reduction in systems with large parameter uncertainty,* International Journal of Control **21**, 977 (1975).

[12] L. Hazeleger, M. Heertjes, and H. Nijmeijer, *Second-order reset elements for stage control design,* in *American Control Conference (ACC)* (2016) pp. 2643–2648.

[13] A. Barreiro, A. Baños, S. Dormido, and J. A. González-Prieto, *Reset control systems with reset band: Well-posedness, limit cycles and stability analysis,* Systems & Control Letters **63**, 1 (2014).

[14] A. Baños and M. A. Davó, *Tuning of reset proportional integral compensators with a variable reset ratio and reset band,* IET Control Theory & Applications **8**, 1949 (2014).

[15] J. Zheng, Y. Guo, M. Fu, Y. Wang, and L. Xie, *Improved reset control design for a pzt positioning stage,* in *2007 IEEE International Conference on Control Applications* (IEEE, 2007) pp. 1272–1277.

[16] A. Baños and A. Barreiro, *Reset control systems* (Springer Science & Business Media, 2011).

[17] Y. Guo, Y. Wang, and L. Xie, *Frequency-domain properties of reset systems with application in hard-disk-drive systems,* IEEE Transactions on Control Systems Technology **17**, 1446 (2009).

[18] N. Karbasizadeh, N. Saikumar, and S. H. Hoseinnia, *Fractional-order single state reset element,* Nonliner Dynamics (2021).

[19] X. Hou, *Tuning of the "Constant in gain Lead in phase" Element for Mass-like Systems*, Master's thesis, Delft University of Technology (2019).

[20] C. Cai, *The Optimal Sequence for Reset Controllers*, Master's thesis, Delft University of Technology (2019).

2

AN OVERVIEW ON LINEAR FRACTIONAL ORDER CONTROLLERS

Ali AHMADI DASTJERDI

The scope of this chapter is to describe state-of-the-art related to linear fractional order control system in the frequency-domain. In this chapter, the concept of fractional calculus and their applications in the control problems are introduced. In addition, basic definitions of the fractional order differentiation and integration are presented. Then, four common types of fractional order controllers are briefly presented and after that their representative tuning methods are introduced. Furthermore, some useful continuous and discrete approximation methods of fractional order controllers and their digital and analogue implementation methods are elaborated. Then, some Matlab toolboxes which facilitate utilizing fractional order calculus in the control field are presented. Finally, advantages and disadvantages of using fractional order calculus in the control area are discussed. It is concluded that although fractional order controllers improve the performance of linear controllers, they could not fill our research gap due to their inherent linearity.

This chapter has been published in Annual Reviews in Control **51**, 47 (2019 [1]).

2.1. INTRODUCTION

FRACTIONAL Order (FO) calculus has attracted attention from academic and industrial associations because its applications have been increased in many aspects of science and engineering [2–5]. The control field is no exception and utilizing of FO-calculus has been raised in the modelling and controlling of dynamic systems. Basically, in control applications, there are four combinations for closed-loop systems: Integer Order (IO) plants with IO controllers, IO plants with FO controllers, FO plants with FO controllers and FO plants with IO controllers [6, 7].

Using FO-calculus in the modelling of system dynamics is increased since many phenomena such as the voltage-current relation of a semi-infinite lossy transmission line, the diffusion of heat through a semi-infinite solid, viscoelasticity, damping and chaos, fractals etc. inherently show FO behaviour [6, 8–10]. Particularly, when the dynamic of a system has a distributed parameter nature, the best solution for modeling is using FO-calculus [6, 7]. Moreover, it has been reported that FO-calculus models the behaviour of biomimetic systems the best [7]. Furthermore, in the electrical engineering field, there are some electrical devices which show intermediate properties between resistances and capacitances. These devices are known as "fractance" and are modelled by means of FO-calculus [11]. Hence, FO-models can help engineers to simulate the dynamic behaviour of many systems more precisely than IO-ones.

FO-calculus has high potential to improve performances of controllers since designers have more flexibility in selecting power of FO-controllers in comparison with IO-controllers [12–16]. Moreover, since FO-calculus can provide a proper trade-off between the first and second order integrator or differentiator part of controllers, linear FO-controllers particularly the FO-PID types become very popular among control engineers. In this manner, researchers have tried to develop FO-linear controllers in both time [2, 17–23] and frequency domain [3, 9, 11, 24–27]. In the time domain, most of research is based on optimization methods and in the frequency domain, the most widely-used methods are H_∞ norm, loop-shaping, iso-damping, etc.

Despite all the comments, IO-controllers are predominately used in the control field [28]. Apart from the “water-bed" effect from which all linear controllers suffer [29], there are other significant barriers which confine development of FO-controllers. First, direct analytical methods for solving FO differential and integral equations are very complicated [6]. Secondly, the implementation of FO-controllers is more difficult than IO ones owing to certain reasons which are elaborated in the next sections. Finally, the existing tuning methods are sophisticated and proper for specialists and most of them are applicable for process control problems (first order plant with low bandwidth requirement).

During these years, several investigations have been done about reviewing FO-controllers [6, 7, 30]. Chen *et al.* introduced and compared four common types of FO-controllers [6]. Also, investigation [6] presents several realization methods for FO-controllers. Moreover, they talked about potential advantages of FO-controllers and their application in [7]. In [30], aspects of linear and non-linear Fractional Order Proportional Integral and Derivative (FO-PID) controllers such as tuning, history, and toolboxes are discussed in both time and frequency domains. These review papers give general insight about the FO-controllers; however, some of them are very specific which do not cover all aspects about these controllers, or some of them are very broad that can-

not give enough information about each concept. Thus, this article focuses on the linear FO-controllers in the frequency domain. This paper gives enough information efficiently and comprehensively about linear FO-controllers in the frequency domain by which beginners can understand FO-calculus, select a proper type for their application, tune and implement these controllers.

This review paper is organized so that, the basic definitions of the FO derivative and integral are presented in Section 2.2. Then, common types of FO-controllers which are introduced in the literature are commented in Section 2.3 and their representative tuning methods are delineated in Section 2.4. Section 2.5 is devoted to the realization of FO-controllers in which approximation methods in the S, Z and δ domain, and analogue and digital implementation methods are presented. Then, some useful toolboxes are introduced which facilitate design, approximation and realization of FO-controllers in the frequency domain in Section 2.6. Finally, the advantages and disadvantages of FO-controllers are discussed in Section 2.7 and some conclusions and remarks are given in Section 2.8.

2.2. DEFINITIONS OF FO DERIVATIVE AND INTEGRAL

ALTHOUGH FO calculus which means the generalization of the integration and differentiation operator to a FO operator is a 300-years-old topic [31], it has only gained attention in the last two decades to facilitate modelling and control problems. There are various definitions like Riemann, Letnikov, Liouville, Caputo for FO derivative and integral [6, 29, 32–34]. Based on Cauchy's formula, Riemann defined the general FO integral as below for a general complex order v [29, 33, 35, 36] as

$$I_{t_o}^{v} f(t) \triangleq \frac{1}{\Gamma(v)} \int_{t_o}^{t} \frac{f(\tau)}{(t-\tau)^{1-v}} d\tau, \quad \begin{cases} t > t_o, \\ t_o \in R, \\ v \in C, \end{cases} \tag{2.1}$$

in which $\Gamma(v)$ is the Gamma function

$$\Gamma(v) = \int_0^{\infty} e^{-x} x^{v-1} dx. \tag{2.2}$$

When v is a real FO number, (2.1) can be re-written as [29, 33, 35, 36]

$$I_{t_o}^{v} f(t) \triangleq \int_{t_o}^{t} \frac{f(\tau)(t-\tau)^{v-1}}{\Gamma(v)} d\tau = \int_{t_o}^{t} g_v(t-\tau) f(\tau) d\tau = g * f, \tag{2.3}$$

where

$$g_v(t-\tau) = \frac{(t-\tau)^{v-1}}{\Gamma(v)}. \tag{2.4}$$

Now, the Laplace transform of the FO integral can be interpolated from the convolution (2.3) [29]:

$$\mathscr{L}\{I_{t_o}^{v} f(t)\} = \mathscr{L}\left\{\frac{(t)^{v-1} u(t)}{\Gamma(v)}\right\} \mathscr{L}\{f(t)\} = \frac{1}{s^v} F(s). \tag{2.5}$$

Lioviolle simply calculated FO derivative. In his method, the exponential presentation function $f(t) = \sum_{n=0}^{\infty} c_n e^{a_n t}$ is used for this purpose. In this respect, the FO derivative is obtained as [33, 35]

$$D^{\nu} f(t) = \sum_{n=0}^{\infty} c_n a_n^{\nu} e^{a_n t}. \tag{2.6}$$

The Riemann-Liouville's definition of the general FO derivative is [6, 29, 33, 35, 36]

$$D_{t_o}^{\nu} f(t) \triangleq \frac{1}{\Gamma(n-\nu)} \frac{d^n}{dt^n} \left(\int_{t_o}^{t} \frac{f(\tau)}{(t-\tau)^{1+\nu-n}} d\tau \right), \quad n = [\text{integer real part of } \nu] + 1. \tag{2.7}$$

The second popular definition of FO derivative is given by Caputo [33, 35, 36] as

$$D_{t_o}^{\nu} f(t) = \frac{1}{\Gamma(\nu-n)} \int_{t_o}^{t} \frac{f^{(n)}(\tau) d\tau}{(t-\tau)^{\nu+1-n}}, \quad (n-1 \le \nu < n). \tag{2.8}$$

This definition is improved in [37] as

$$\mathcal{D}_{t_o}^{\nu} = \frac{M(\nu)}{1-\nu} \int_{t_o}^{t} \dot{f}(\tau) e^{-\frac{\nu(1-\tau)}{1-\nu}} d\tau, \tag{2.9}$$

where $M(\nu)$ is a normalized function so that $M(0) = M(1) = 1$. Another general definition of the FO derivative is given by Grünwald-Letnikov [6, 29, 30, 33, 35, 36]:

$$D^{\nu} f(t) = \lim_{h \to 0} \frac{\sum_{k=1}^{\infty} (-1)^k \binom{\nu}{k} f(t-kh)}{h^{\nu}}, \quad \binom{\nu}{k} = \frac{\Gamma(\nu+1)}{k!\Gamma(\nu-k+1)}. \tag{2.10}$$

Eventually, the Laplace transform of a real FO derivative can be achieved by using the Riemann-Liouville's and Caputo's definition ((2.7) and (2.8)) [6, 29] as

$$\mathscr{L}\{D_{t_0}^{\nu} f(t)\} = sF(s) - \sum_{k=0}^{n-1} s^{\nu-k-1} D_{t_0}^{k} f(t)\Big|_{t=0}, \quad (n-1 < \nu \le n). \tag{2.11}$$

By considering definitions of the FO derivative and integral which are described above, the continuous integro-diffrential operator for a general complex value of ν is introduced in [6] by

$$D_{t_o}^{\nu} = \begin{cases} \dfrac{d^{\nu}}{dt^{\nu}}, & \mathcal{R}e(\nu) > 0, \\ 1, & \mathcal{R}e(\nu) = 0, \\ \displaystyle\int_{t_o}^{t} (d\tau)^{-\nu}, & \mathcal{R}e(\nu) < 0. \end{cases} \tag{2.12}$$

The two main properties of the continuous integro-diffrential operator are listed [6, 29]:

1. This is a linear operator:

$$D_{t_o}^{\nu}(af(t) + bg(t)) = aD_{t_o}^{\nu} f(t) + bD_{t_o}^{\nu} g(t)$$

2. It follows the additive index law:

$$D_{t_o}^{\nu} D_{t_o}^{\alpha} f(t) = D_{t_o}^{\alpha} D_{t_o}^{\nu} f(t) = D_{t_o}^{\alpha+\nu} f(t)$$

2.3. COMMON TYPES OF LINEAR FO CONTROLLERS

IN this section, four common types of linear FO-controllers which are represented in the literature are described shortly. In what follows, Tilted Integral Derivative (TID) controllers, CRONE controllers, FO lead/lag compensators and (FO-PID) controllers shall be introduced.

2.3.1. TID CONTROLLER

By substituting the proportional component in the PID controller with the FO integrator ($s^{-\frac{1}{n}}, n \in N$), the TID controller was introduced [38]. The configuration of TID controllers is shown in Figure. 2.1. Figure. 2.2 compares the frequency response of TID and PID controllers such that both controllers provide the same phase margin and gain values at high frequencies. As was shown, the TID controller has better performance in rejecting disturbances than the PID controller since it has higher gain before the crossover frequency (i.e $\omega_{i-TID} \leq \omega \leq \omega_d$). A method for tuning of TID controller parameters will be elaborated in Section 2.4.1. From practical viewpoint, this controller must be used with a low-pass filter to make it a proper transfer function, so the lag phase of the low-pass filter have to be considered in tuning process.

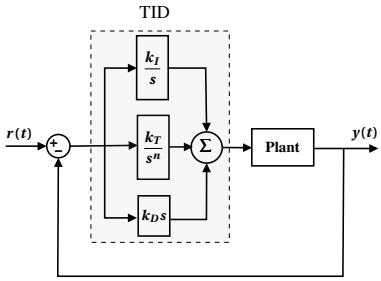

Figure 2.1: Block diagram of TID controller

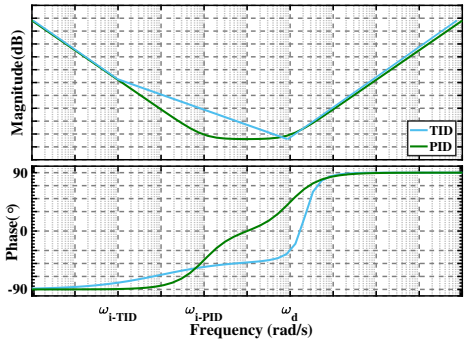

Figure 2.2: Bode diagram of TID controller

2.3.2. CRONE CONTROLLERS

CRONE (French abbreviation for Commande Robuste d'Ordre Non Entier, which means non-integer robust control) controllers have been established by Oustaloup since the 1980s in tracking fractal robustness [29]. Three CRONE generations were proposed in the frequency domain in which the open-loop transfer function has FO integrators and differentiators. These three generations are used for controlling robustly against plant uncertainties. The first generation of CRONE has the simplest configuration among CRONE generations and can be considered as a simple FO-PID controller. As it is shown in Figure. 2.3, the open-loop transfer function of the second generation is shaped following the Bode's ideal cut-off frequency characteristic.

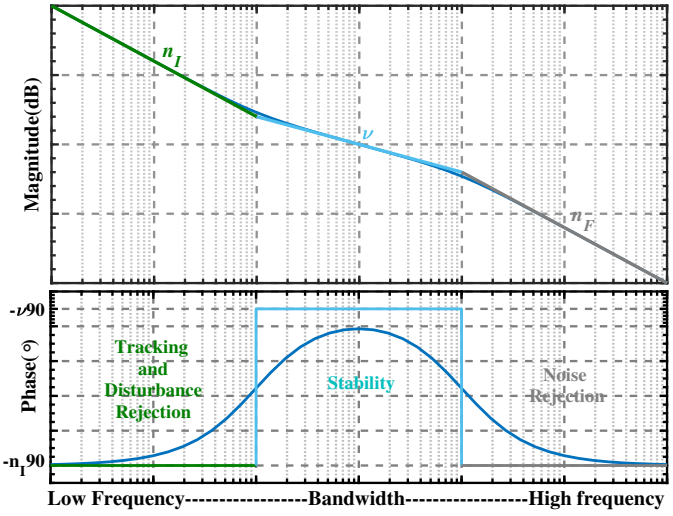

Figure 2.3: Open-loop transfer function in the second generation of CRONE while $n_F = n_I$

The third generation of CRONE widens the application of the second generation of CRONE so that it is applicable to plants which have general uncertainties than just gain-like perturbations. The configurations and tuning methods of CRONE generations will be delineated in Section 2.4.2.

2.3.3. LEAD/LAG COMPENSATORS

The generalization of classical lead/lag compensators to FO lead/lag compensators has been studied in some investigations [6, 7, 29]. FO lead/lag compensators are obtained by

$$C(s) = k_p\left(\frac{1+\frac{s}{\omega_L}}{1+\frac{s}{\omega_h}}\right)^{\mu}, \quad \omega_L < \omega_h, \quad \begin{cases} \text{Lead}, & \mu \in (0,+\infty), \\ \text{Lag}, & \mu \in (-\infty,0). \end{cases} \tag{2.13}$$

Sometimes, FO lead/lag compensators are also defined in [3, 39] as

$$C(s) = k_p x^{\mu}\left(\frac{1+\Delta s}{1+\Delta x s}\right)^{\mu}, \quad 0 < x < 1, \quad \begin{cases} \text{Lead}, & \mu > 0, \\ \text{Lag}, & \mu < 0. \end{cases} \tag{2.14}$$

Another configuration of these compensators is [40]

$$C(s) = k_p\left(\frac{1+x\Delta s^{\mu}}{1+\Delta s^{\mu}}\right), \quad 0<\mu<2, \quad \begin{cases}\text{Lead}, & 1<x,\\ \text{Lag}, & 0<x<1,\end{cases} \tag{2.15}$$

where Δ is a tuning knob which determines corner frequencies of these compensators. It must be recalled that it is not possible to consider $\mu \geq 2$ because the transfer function of the controller is not bounded-input bounded-output (BIBO) stable [41]. The bode plot of a lead compensator is shown in Figure. 2.4.

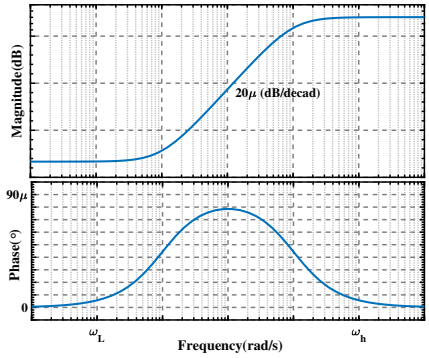

Figure 2.4: Bode diagram of FO-lead compensator

In the lead compensators, the more distance between ω_L and ω_h, the more robustness and stability (phase margin) for the controller. Also, the phase margin can be increased by increasing μ and the maximum achievable phase by FO lead compensators is $\mu 90°$. However, increasing μ or the distance between the corner frequencies (ω_L and ω_h) leads to have high magnitudes in high frequencies. Consequently, the controller has less noise rejection characteristic which may cause practical complications. So, similar to integer lead/lag compensators, the stability and robustness have conflict with the precision in this type of FO-controllers. In Section 2.4.3, tuning methods of these controllers will be discussed.

2.3.4. FO-$PI^{\lambda}D^{\mu}$ CONTROLLERS

Podlubny introduced the first FO-PID controller in 1994 [42]. FO-PID controllers are the general form of the conventional integer order PID controllers. The parallel or ideal form of this controller is

$$C(s) = k_p + \frac{k_i}{s^{\lambda}} + k_d s^{\mu}, \quad \lambda, \mu \in R. \tag{2.16}$$

Figure. 2.5 shows the various types of controller (2.16) versus λ and μ. It can be stated that all families of (PID) controller can be derived from (2.16) as follows:

1. P controllers can be obtained when $\lambda = \mu = 0$:

$$C(s) = k_p. \tag{2.17}$$

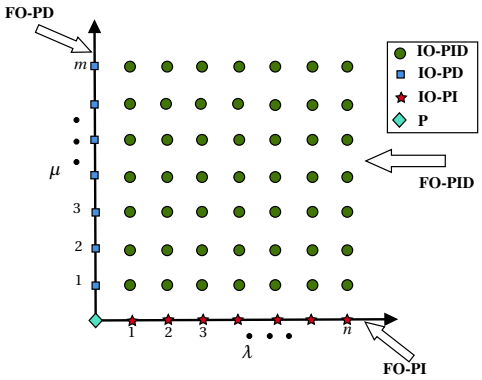

Figure 2.5: Various types of PID controllers

2. IO-PI controllers can be obtained when $\mu = 0, \lambda = n \in N$;

$$C(s) = k_p\left(1 + \frac{k_i}{s^n}\right). \tag{2.18}$$

3. FO-PI controllers can be obtained when $\mu = 0, \lambda \notin N$:

$$C(s) = k_p\left(1 + \frac{k_i}{s^\lambda}\right). \tag{2.19}$$

4. IO-PD controllers can be obtained when $\lambda = 0, \mu = m \in N$:

$$C(s) = k_p\left(1 + k_d s^m\right). \tag{2.20}$$

5. FO-PD controllers can be obtained when $\lambda = 0, \mu \notin N$:

$$C(s) = k_p\left(1 + k_d s^\mu\right). \tag{2.21}$$

6. IO-PID controllers can be obtained when $(\lambda = n, \mu = m) \in N$:

$$C(s) = k_p + \frac{k_i}{s^n} + k_d s^m. \tag{2.22}$$

There are some drawbacks of parallel FO-PID controllers. First, if $\lambda \in (0,1)$ in the integration part of this controller, the settling time is very high. So, sometimes $\frac{1}{s^\lambda}$ is replaced with $\frac{1}{s}s^{1-\lambda}$ to decrease the settling time value [3, 29, 43]. Also, it is necessary to tame the derivative part of the parallel FO-PID controller for avoiding saturation phenomenon and having the better noise rejection feature. Hence, (2.16) becomes

$$C(s) = k_p + \frac{k_i}{s^\lambda} + \frac{k_d s^\mu}{1 + \tau_f s^\gamma}, \quad \gamma \geq \mu. \tag{2.23}$$

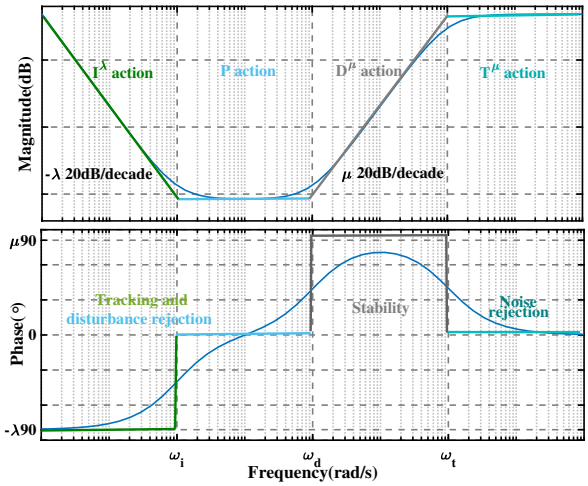

Figure 2.6: Bode plot of FO-PID controllers

If $\mu \neq \gamma$ a memory with a high capacity is required for implementing the discrete time or continuous-time approximation of this controller. So, it is better to consider ($\gamma - \mu = n, \quad n \geq 0$) [29]. By increasing n, the phase margin decreases and the system has the better noise rejection feature and vice versa. In most cases, n is equal to zero. The most widely-used parallel FO-PID controller is

$$C(s) = k_p + \frac{k_i}{s^\lambda} + \frac{k_d s^\mu}{1 + \tau_f s^\mu}. \tag{2.24}$$

Moreover, for the ease of practical implementation, FO-PID controllers can be represented in the series form as

$$C(s) = k_p \left(1 + \frac{k_i}{s^\lambda}\right) \left(\frac{1 + \dfrac{s}{\omega_l}}{1 + \dfrac{s}{\omega_h}}\right)^\mu. \tag{2.25}$$

Bode plot of FO-PID controllers is shown in Figure. 2.6. As was shown, the maximum phase which is achievable by these controllers is about 90μ degree. In [44, 45], the FO-[PD] and and FO-[PI] controller is defined as

$$C(s) = k_p(1 + k_d s)^\mu, \tag{2.26}$$

$$C(s) = k_p \left(1 + \frac{k_i}{s}\right)^\lambda, \tag{2.27}$$

respectively. The comparison between FO-PD (2.21) and FO-[PD] controller is performed in Figure. 2.7. It is concluded that the FO-[PD] controller outperforms the FO-PD controller for FO-systems [44] while the FO-PI and FO-[PI] do not have significant differences in the performance for the FO process plants [45].

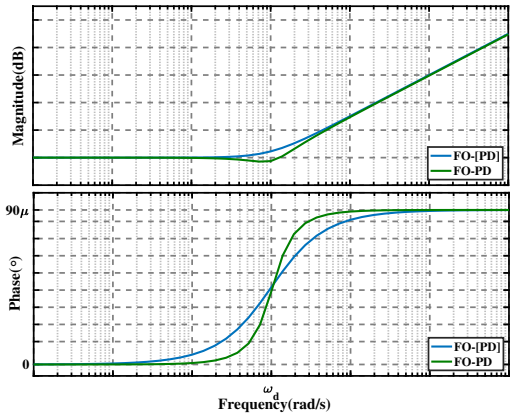

Figure 2.7: Bode plot of FO-PD and FO-[PD] controllers

Another type of FO-controllers which is presented in the literature is $D^{1-\lambda}I^{\lambda}$ [43, 46, 47]:

$$C(s) = \frac{k_i + k_d s}{s^{\lambda}}. \tag{2.28}$$

The bode plots of controller (2.28) for several values of λ are drawn in Figure. 2.8. It is obvious that when $\lambda = 0$, this is an IO-PD controller and when $\lambda = 1$ this is an IO-PI controller. So, the $D^{1-\lambda}I^{\lambda}$ controller is a trade-off between IO-PD and IO-PI controllers. When λ increases, the gain at low frequencies increases while the phase at cross-over frequency decreases. Having higher gains at low frequencies (increasing integral action of the controller) leads to improving the tracking performance of this controller. Consequently, stability decreases and precision improves for this controller by increasing λ and vice versa. Therefore, it can be said that this controller is a trade-off between stability and precision.

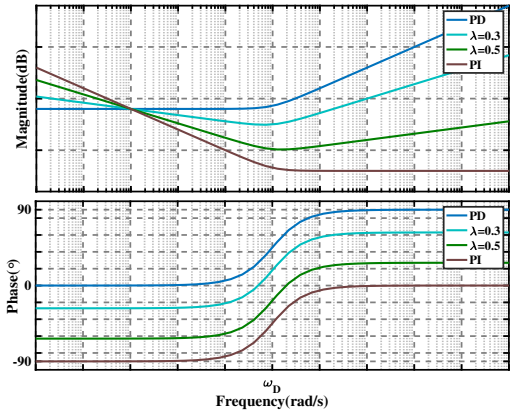

Figure 2.8: Bode plot of $D^{1-\lambda}I^{\lambda}$ controller for various values of λ

2.4. TUNING METHODS OF FO-CONTROLLERS

IN this section, representative tuning methods for FO-controllers which are developed in the frequency domain are discussed. Similar to Section 2.3, tuning methods are fallen down into four categories including tuning methods for TID controllers, tuning methods for CRONE generations, tuning methods for FO lead/lag compensators, and tuning methods for $PI^{\lambda}D^{\mu}$ controllers. Let's describe some general equations and constraints which are used in a lot of literature in order to tune FO-controllers [9, 18, 29, 39, 48–51]. These constraints are:

1. The phase margin definition:

$$\text{Arg}[G(j\omega_c)C(j\omega_c)] = -\pi + \varphi_m, \tag{2.29}$$

where $G(j\omega)$ and $C(j\omega)$ are the plant and control transfer functions, respectively.

2. The cross-over frequency definition:

$$|G(j\omega_c)C(j\omega_c)| = 1. \tag{2.30}$$

3. The flatness of the phase curve of the open-loop transfer function near the cross-over frequency which leads to the robustness of the system against gain variations in a specific range (iso-damping):

$$\frac{d(\text{Arg}[G(j\omega)C(j\omega)])}{d\omega}\Big|_{\omega=\omega_c} = 0. \tag{2.31}$$

4. The gain margin definition:

$$\text{Arg}(G(\omega_{cp})C(\omega_{cp})) = -\pi \Rightarrow |G(\omega_{cp})C(\omega_{cp})| = \frac{-1}{M_g}. \tag{2.32}$$

5. The complementary sensitivity constraints [29]:

$$\inf\left|T(j\omega) = \frac{CG}{1+CG}\right| \geq T_l(\omega), \tag{2.33}$$

$$M_r = \sup|T(j\omega)| \leq T_u(\omega). \tag{2.34}$$

Low frequency characteristics of bound T_l and T_u are used to avoid slow response of the system to a step variation of reference signals or disturbances. Middle frequency behaviours of T_l and T_u confine the highest value of the settling time (enhance the speed of the system) and high values of the resonant peak. Sometimes, high frequency properties of T_u increase the noise rejection feature of the system.

6. The modulus margin constraint (the sensitivity function constraint):

$$M_s = \sup\left|S(j\omega) = \frac{1}{1+CG}\right| \leq S_u(\omega), \tag{2.35}$$

where $S(j\omega)$ is the sensitivity transfer function and S_u is a desire bound. This constraint can be used for improving the disturbance rejection characteristic of the system. The lower values of the modules margin, the more robustness of the system against disturbances.

7. The control sensitivity constraint:

$$\sup|CS(j\omega)| \leq CS_u(\omega), \tag{2.36}$$

where CS_u is a desire bound.This constraint limits the control effort in respect of noises and disturbances, so this increases the energy efficiency of the controller.

8. The process sensitivity constraint:

$$\sup|GS(j\omega)| \leq GS_u(\omega), \tag{2.37}$$

where GS_u is a desire bound. This constraint improves disturbance rejection of the plant, so it leads to enhancing the precision of the system.

2.4.1. TUNING METHODS FOR TID CONTROLLER

As discussed in section 2.3.1, TID controller has the simplest configuration among FO-controllers. It is noteworthy to recall that auto-tuning methods for PID controllers are applicable for TID controllers since they are very similar to PID controllers. Apart from this fact, there is one explicit tuning method in the frequency domain for this type of FO-controllers [38]. As it was shown in Figure. 2.1, three parameters k_I, k_T and k_D must be tuned for these controllers. In this respect, these three simple steps must be followed:

1. Assume $k_I = k_D = 0$ and set k_T in order to satisfy constraint (2.30)
2. $k_I = \frac{k_T}{4}\left(\frac{\omega_c}{2\pi}\right)^{\left(1-\frac{1}{n}\right)}$
3. At the end, considering the phase margin 5° above the desired phase margin, k_D is obtained using (2.29)

2.4.2. TUNING METHODS FOR CRONE GENERATIONS

As was described in section 2.3.2, three generations of CRONE controllers exist and each generation has its tuning method and can be used in a special condition. The first generation of CRONE is used to robustly control a plant with an uncertain gain but constant phase around the cross-over frequency. In other words, if the cross-over frequency (ω_c) of a controlled system changes due to gain variation of the plant in a frequency range $[\omega_A, \omega_B]$, its phase stays unchanged within this frequency range. The configuration of the first generation of CRONE controllers is provided in [29, 48] as

$$C_{R_1}(s) = k\left(1+\frac{\omega_I}{s}\right)^{n_I}\left(\frac{1+\frac{s}{\omega_L}}{1+\frac{s}{\omega_h}}\right)^{n}\left(\frac{1}{1+\frac{s}{\omega_f}}\right)^{n_F}, \tag{2.38}$$
$$n_I, n_f \in N,\ n \in R,\ \omega_I < \omega_L < \omega_A < \omega_B < \omega_h < \omega_f.$$

It is suggested that ω_L and ω_h must be set so that they ensure a constant phase for the open loop response within the range of $[\omega_A, \omega_B]$ (for more details, see [29]). Parameters

n and k are obtained by using constraints (2.29) and (2.30) [29] as

$$n = \frac{-\pi + \varphi_m - \arg(G(j\omega_c)) + n_F \arctan\left(\frac{\omega_c}{\omega_f}\right) + n_I\left(\frac{\pi}{2} - \arctan\left(\frac{\omega_c}{\omega_I}\right)\right)}{\arctan\left(\frac{\omega_c}{\omega_L}\right) - \arctan\left(\frac{\omega_c}{\omega_h}\right)}, \tag{2.39}$$

$$k = \frac{\left(1 + \frac{\omega_c^2}{\omega_F^2}\right)^{0.5n_F}}{|G(j\omega_c)|\left(\frac{\omega_h}{\omega_L}\right)^{0.5n}\left(1 + \frac{\omega_I^2}{\omega_c^2}\right)^{0.5n_I}}. \tag{2.40}$$

When the gain and phase of a plant change in a frequency range $[\omega_A, \omega_B]$, the second generation of CRONE must be used to make the system robust against uncertainties. The configuration of the second generation of CRONE controller [29, 48, 52, 53] is

$$C_{R_2}(s) = kG^{-1}(s)\left(1 + \frac{\omega_I}{s}\right)^{n_I}\left(\frac{1 + \frac{s}{\omega_h}}{1 + \frac{s}{\omega_L}}\right)^{\nu}\left(\frac{1}{1 + \frac{s}{\omega_f}}\right)^{n_F}, \tag{2.41}$$
$$n_I, n_f \in N,\ \nu \in R,\ \omega_I < \omega_L < \omega_A < \omega_B < \omega_h < \omega_f.$$

Similar to the first generation of CRONE, ν and k are obtained using (2.29) and (2.30) as

$$\nu = \frac{-\pi + \varphi_m + n_F \arctan\left(\frac{\omega_c}{\omega_f}\right) + n_I\left(\frac{\pi}{2} - \arctan\left(\frac{\omega_c}{\omega_I}\right)\right)}{\arctan\left(\frac{\omega_c}{\omega_h}\right) - \arctan\left(\frac{\omega_c}{\omega_L}\right)}, \tag{2.42}$$

$$k = \frac{\left(1 + \frac{\omega_c^2}{\omega_f^2}\right)^{0.5n_F}}{\left(\frac{\omega_L}{\omega_h}\right)^{0.5\nu}\left(1 + \frac{\omega_I^2}{\omega_c^2}\right)^{0.5n_I}}. \tag{2.43}$$

Parameters n_I and n_F must be set so that $n_I \geq n_{pl}$ and $n_F \geq n_{ph}$ if the order of plant at low frequencies ($\omega < \omega_I$) and high frequencies ($\omega > \omega_f$) is n_{pl} and n_{ph}, respectively (for more details see [29]).

Although the second generation of CRONE controller extends the frequency range for choosing the cross-over frequency, in some cases such as existing delay on the system, this configuration is not able to ensure robustness of a system. Hence, the third generation of CRONE is utilized when uncertainties of a plant are more general than just gain-like perturbations. In the basic idea of the third generation of CRONE, the open-loop transfer function (2.44) has a complex integration order ($\nu = a + ib$) which leads to have a general template in the Nichols chart [29, 48] as

$$\beta = k\left(\cosh(b\frac{\pi}{2})\right)\left(\frac{\omega_c}{s}\right)^a\left(\mathscr{R}e_{li}\left(\left(\frac{\omega_c}{s}\right)^{ib}\right)\right)^{-\text{sign}(b)}. \tag{2.44}$$

Tuning of the third generation of CRONE controller is very complicated (for more information see [29]). A designer can set the number of tuning parameters by considering more general templates based on how a plant is sophisticated as

$$\beta_T = \sum_{j=1}^{N} \beta_j \Rightarrow CR_3(s) = G^{-1}\beta_T. \tag{2.45}$$

When the number of tuning parameters are determined, a designer must select a proper cost function and solve an optimization problem under some constraints which definitely include constraints (2.29) and (2.30). Four optimization problems are recommended for tuning the third generation of CRONE controller [29, 54].

1. Considering $J = \sup|T(j\omega)| - M_r$ as the cost function in which M_r is the desired resonant peak. Minimization must be done under constraint (2.33) to (2.37).
2. Considering $J = \frac{20}{2\pi} log(\int_{\omega_{min}}^{\omega_{max}} \max|e(j\omega)|^2 d\omega)$ as the cost function in which $e(t) = y_{ref}(t) - y(t)$. Minimization must be done under the constraints (2.36).
3. Considering $J = \max\sup\left|\frac{G(j\omega)S(j\omega)}{j\omega}\right|_{dB}$. Minimization must be done under the constraints (2.33) to (2.37).
4. Considering $J = \max\sup\left|\frac{S(j\omega)}{j\omega}\right|_{dB}$. Minimization must be done under the constraints (2.33) to (2.37).

CRONE generations have been successfully applied to some practical systems [55]. The second generation was implemented mechanically to a suspension system of a vehicle [26]. The third generation was applied to a resonant plant (flexible transmission) [25], a four mass-spring system with low damping [56], and a nonlinear hydraulic actuator [24]. To sum up, it appears that the CRONE generations are very useful for designing a robust controller against plant uncertainties.

2.4.3. TUNING METHODS FOR FO LEAD/LAG COMPENSATORS

In this part, tuning methods which are applicable for tuning FO-lead lag compensators are presented. Monje *et al.* obtained a method for auto-tuning of these compensators (2.14) [39]. The magnitude of $|G(j\omega_c)|$ and $\arg(G(j\omega_c))$ are found by using the relay test (see [39] for more information). For this purpose, the constraints (2.29), (2.30), and the definition of the static error constant

$$k_{ss} = \lim_{s\to 0} s^n C(s)G(s), \tag{2.46}$$

where n is type of the plant are used for tuning of an FO-lead/lag compensator. There are four unknown parameters (x, μ, Δ, k_p) with three equations, so an optimization problem has to be solved. The objective function has been chosen to minimize μ since the less value of μ, the less value of x which results in more robust compensator. Following a trial and error approach is taken to solve this optimization problem:

1. Consider a minimum value for μ (for instance, $\mu = 0.05$).
2. Calculate x, Δ, and k_p.
3. If x is positive, the compensator is tuned. Otherwise, μ is increased with a fixed value and repeat steps (2)-(3).

In a similar way, Tavazoei and Tavakoli-Kakhki obtained a general method for tuning controller (2.15). In this way, the constraints (2.29), (2.30) and the definition of the static error constant (2.46), and the maximum value of the controller output (to avoid saturation) are considered for tuning of its four parameters [40].

2.4.4. TUNING METHODS FOR $PI^{\lambda}D^{\mu}$

As discussed before, the most popular type of FO-controller is the FO-PID controller. In this section, tuning methods for these controllers in the frequency domain are reviewed.

Several researchers proposed tuning methods using optimization techniques. Zhao *et al.* tuned FO-PID controller (2.16) for one type of FO-plant ($G(s) = \frac{1}{a_1 s^{\alpha} + a_2 s^{\beta} + a_3}$) [9]. For a given phase and gain margin, (2.29), (2.30), and (2.32) are accounted for tuning. This leads to four equations with seven unknown parameters $(\omega_c, \omega_{cp}, k_p, k_i, k_d, \mu, \lambda)$ as

(i) $f(\omega_c, \omega_{cp}, \mu, \lambda, \varphi_m, M_g) = 0$,

(ii) $k_p = g(\omega_c, \omega_{cp}, \mu, \lambda, \varphi_m, M_g)$,

(iii) $k_i = y(\omega_c, \omega_{cp}, \mu, \lambda, \varphi_m, M_g)$,

(iv) $k_d = z(\omega_c, \omega_{cp}, \mu, \lambda, \varphi_m, M_g)$.

This problem is solved through an optimization method in which four parameters (ω_c, ω_{cp}, μ, λ) form a desired cost function $J = \mathcal{L}(\omega_c, \omega_{cp}, \mu, \lambda)$ based on the required performance (robustness, stability, etc). The optimization problem is solved under constraint (i). After finding these four parameters through a suitable optimization algorithm, parameters (k_p, k_i, k_d) are obtained using equations (ii)-(iv). This method is flexible and users are able to add their requirements as an objective function in the optimization part. They also concluded that FO-PID controller has better performance than IO-one for FO-plants.

In addition, Zhong and Li proposed a tuning method for FO-PID controllers for a specific type of FO-plants ($G(s) = \frac{1}{a_1 s^{\alpha_1} + a_2 s^{\alpha_2} + a_3 s^{\alpha_3} + a_4}$, $a_i > 0$) [57]. In this method, constraints (2.29), (2.30), and (2.31) are used for tuning, so there are seven unknown parameters $(\omega_c, \varphi_m, k_p, k_d, k_i, \mu, \lambda)$ and three equations. Then, the feasible region for unknown parameters based on the stability analyses is found. Next, one of the suggested cost functions including (IAE=$J = \int_0^{\infty} |e(t)| dt$) , (2.33), and (2.35) is used for optimization under constraints (2.29), (2.30), and (2.31). A fixed-step search method is utilized for solving. If the obtained controller satisfies the desired performances, the tuning is finished; otherwise, two narrow intervals for μ and λ are taken so that previous obtained

optimal λ and μ are placed in the middle of intervals. After that, the step-size is reset to a smaller value the procedure is repeated, and the controller is finally tuned.
Valério and da Costa obtained a tuning method similar the Ziegler-Nichols method for FO-PID controllers (2.16) [49]. It is assumed that each plant frequency response can be approximated by an S-shaped response ($G(s) = \frac{e^{-Ls}}{1+Ts}$). Then, to solve the problem, (2.29) is supposed as the minimization cost function and (2.30), (2.31), (2.34), and (2.35) are counted for constraints. For many different L and T, the Nelder-Mead's simple optimization method is applied to solve this optimization problem for a specific requirement and then the least-squares method is used to find a relation between L, T and tuning parameters for the given specifications. For any requirement, this procedure can be done to find a relation between dynamic parameters of the system and tuning knobs. They reported that the FO-PID which is tuned by this method is more robust against gain variations than IO-PID (2.22) which is tuned by the Ziegler-Nichols method.
Similarly, Saidi *et al.* proposed a tuning method for FO-PID controllers for any general plant [58]. In the proposed approach, (2.29), (2.30), (2.31), (2.34), and (2.35) are considered for tuning. Also, they assumed flatness of the phase in a desired band $[\omega_l, \omega_h]$ and then considered N frequencies belonging to this band. They changed constraints (2.29) and (2.31) to (2.47) and (2.48), respectively.

$$\sum_{i=1}^{N} (\arg[C(j\omega_i)G(\omega_i)] + \pi - \varphi_m)^2 = 0, \quad \forall \omega_i \in [\omega_l, \omega_h], \tag{2.47}$$

$$\sum_{i=1}^{N} \left(\frac{d \arg[C(j\omega)G(j\omega)]}{d\omega}\Big|_{\omega=\omega_i} \right)^2 = 0, \quad \forall \omega_i \in [\omega_l, \omega_h]. \tag{2.48}$$

Then, they supposed (2.30) as the minimization cost function under constraints (2.29), (2.31), (2.34), and (2.35) to tune the controller.
Chen *et al.* generalized Modulus margin constrained Integral Gain Optimization (MIGO) based controller tuning method for FO-PI controllers (2.19) and called it the F-MIGO method [59]. In this respect, they faced with an optimization problem which is:

- $R = \frac{M_s + M_r - 1}{2M_s(M_r^2 - 1)}$. M_r and M_s are respectively the resonant peak (2.34) and the modules margin (2.35).
- $f(k_p, k_i, \omega, \lambda) = |1 + C(j\omega)G(j\omega)|^2$.
- Objective function: $\max\{k_i\}$
- Constraints: $f(k_p, k_i, \omega, \lambda) \geq R^2$

This optimization problem is solved for a fixed value of λ through

$$f(k_p, k_i, \omega, \lambda) = R^2, \ \frac{\partial f}{\partial \omega} = 0, \ \frac{\partial f}{\partial k_p} = 0, \ \frac{d^2 f}{d\omega^2} > 0. \tag{2.49}$$

Then, this procedure is performed for a range of λ and best λ is selected to minimize (ISE $= \int_0^\infty e^2(t)dt$) for a step response. This method is applied to a first order system

plus time delay ($G(s) = \frac{ke^{-Ls}}{1+Ts}$) and relations between controller parameters and process parameters (L and T) are obtained. This method is compared with IO-PI controllers (2.18) tuned by the Ziegler-Nichols, modified Ziegler-Nichols and AMIGO [60] for six different plants. It is concluded that if the relative dead time ($\frac{L}{L+T}$) is very small, the FO-PI controllers are better than IO-PI controllers, for systems with a balanced lag and delay value ($L \approx T$), there is no difference between IO-PI and FO-PI controllers and for systems with high relative dead time, FO-PI controller responses are faster with higher values of the overshoot than IO-PI controller responses.

Vu and Lee developed this tuning method and introduced a new tuning guideline [61]. In this approach, the open-loop transfer function is considered as $(\frac{s}{\omega_c})^{\gamma}$, and then, λ is selected based on the previous method. Next, k_p, γ, and ω_c are tuned based on one of the suggested optimization criteria under constraint (2.33). In the end, k_i is found through $CG(j\omega) = (\frac{j\omega}{\omega_c})^{\gamma}$.

Padula and Visioli found tuning methods for integral ($G(s) = \frac{ke^{-Ls}}{s}$), stable ($G(s) = \frac{ke^{-Ls}}{Ts+1}$), and unstable ($G(s) = \frac{ke^{-Ls}}{Ts-1}$) process plants [18, 50]. Three types of controllers including the tamed series FO-PID (similar to the controller (2.25)), the tamed series IO-PID controller ((2.25) with $\lambda = \mu = 1$ and $\omega_h = 10\omega_l$) and the ideal or parallel tamed FO-PID ((2.24) with a low-pass filter) are tuned for this purpose. For tuning integral and stable plant, IAE and (2.35) are respectively selected as the cost function and constraint for an optimization problem. For tuning the unstable plant, the cost function remains the same but the constraint is substituted with checking stability. In this respect, the stability condition of the closed-loop transfer function is checked at the first step for each trial. If the trial makes the system unstable, the objective function will get a high value, so it is discarded automatically. This tuning method is performed for a step disturbance and reference signal response separately and relations between controller parameters, L and T are found for each controller in each scenario (disturbance rejection or reference tracking). They recognized that FO calculus has significant effects on differentiator part of FO-PID and does not provide any advantages for integral part since the integral order became one in all optimization solutions. In addition, FO-PID controllers outperform IO-PID controllers in three considered systems.

Monje *et al.* proposed a method for tuning FO-PI controllers (2.19) robustly against plant uncertainties and changing the time delay for the second order plus time delay process systems ($G(s) = \frac{ke^{-Ls}}{(T_1 s+1)(T_2 s+1)}$) [43]. In the robust design against the time delay variation (L), (2.30) is assumed as the cost function and (2.29) and (2.31) are considered as constraints. In the robust design against the variation of time constants (T_1 or T_2), the cost function remains the same as time delay variation and constraints are replaced with (2.29) and (2.32). The nonlinear optimization method (FMINCON in MATLAB) is used for solving these optimization problems. As it was discussed before, $\frac{1}{s^{\lambda}}$ was replaced with $\frac{1}{s}s^{1-\lambda}$ in their controller to improve the settling time. In a similar way, they

tuned FO-PID controller (2.16) for the first order systems plus time delay ($G(s)=\frac{ke^{-Ls}}{1+Ts}$). In this respect, they use the same cost function under constraints (2.29), (2.31), (2.34), and (2.35) [3].

Moreover, similar to their method for FO-lead/lag compensator [39], they proposed an auto-tuning method for series FO-PID controller (2.25) [3]. The magnitudes of $|G(j\omega_c)|$ and $\text{Arg}(G(j\omega_c))$ are found by using the relay test and FO-PID is reshaped as an FO-PI controller (2.19) multiplied to an FO-lead compensator (2.14). First, the FO-PI part is designed so that it makes the slope of the phase of the open loop-transfer function to zero while $k_i=\frac{1}{\omega_c}$ (in order to minimize the value of λ). Next, the FO-lead compensator is tuned for the plant multiplied FO-PI part using method described in [39] (elaborated in Section 2.4.3).

In addition, De Keyser *et al.* developed an auto-tuning for FO-PD (2.21) and FO-PI (2.19) controllers [62]. In this method, $\frac{d(\text{Arg}[G(j\omega)])}{d\omega}\Big|_{\omega=\omega_c}$, $\text{Arg}[G(j\omega_c)]$, and $|G(j\omega_c)|$ are found through a novel experiment for an unknown plant, and then, the controller is tuned using constraints (2.29), (2.30), and (2.31) (for more details see [62]).

Some people try to tune FO controllers utilizing loop-shaping tools. Krijnen *et al.* combined the loop-shaping with optimization methods for tuning a series FO-PID controllers (2.50) for a precision positioning system (a mass-spring damper system) to maximize crossover frequency (bandwidth frequency) [27]. Controller (2.50) is a FO-PID controller which is multiplied by a FO-low pass filter as

$$C(s)=k_p(1+\frac{\omega_i}{s})\Big(\frac{1+\frac{s}{\omega_z}}{1+\frac{s}{\omega_p}}\Big)^{\mu}LP_{(n,r)}(s), \tag{2.50}$$

in which

$$LP_{(n,r)}(s)=\begin{cases} n=1, & \dfrac{1}{1+\frac{s}{\omega_{lp}}}, \\ n=2, & \left(\dfrac{1}{1+\left(\frac{s}{\omega_{lp}}\right)^r}\right)\left(\dfrac{1}{1+\frac{s}{\omega_{lp}}}\right), \\ n=3, & \left(\dfrac{1}{1+\left(\frac{s}{\omega_{lp}}\right)^r+\left(\frac{s}{\omega_{lp}}\right)^{2r}}\right)\left(\dfrac{1}{1+\frac{s}{\omega_{lp}}}\right). \end{cases} \tag{2.51}$$

In their method, tuning parameters $x=[k_p,\omega_i,\omega_z,\omega_p,\omega_{lp},n,r,\mu]$ are found through an optimization procedure in which $\min\{\frac{\omega_{c,bm}}{\omega_c(x)}\}$ ($\omega_{c,bm}$ is the target bandwidth) is considered as a cost function under constraints (2.29), (2.30), and (2.32). The tuned FO-PID controller is compared with an IO-PID controller ((2.25) with $\lambda=\mu=1$) which is tuned by an empirical method [63] and it is revealed that the FO-PID controller increases the

achievable bandwidth frequency in comparison with IO-PID controller.
Dastjerdi *et al.* proposed an industrially applicable tuning method using the loop-shaping method for controller (2.50) without FO-low pass filter ($LP_{(n,r)}$) [64]. In that method, knowing the value of the phase and gain margin, the controller is tuned using some curves which are obtained based on the loop-shaping approach (for more details see [64]). The advantage of this method is that it does not need to solve complicated equations, so it is very convenient for industrial applications.
Moreover, another tuning method based on the combination of Internal Model Control (IMC), loop-shaping, and second generation of CRONE is proposed in [65]. This method is very simple and straightforward and FO-PID controllers are tuned for all process plants based on the phase margin, cross-over frequency, and type of the plant. In addition, Cervera *et al.* considered combination of FO lead compensator (2.14), FO-PI (2.19), and an IO low-pass filter and tuned it upon constraints (2.29), (2.30), (2.34), and (2.35) using loop-shaping tools [66].

Some researchers introduced tuning methods based on solving these nonlinear equations ((2.29) to (2.37)) by utilizing mathematical methods such as the graphical method, the Newton-Raphson numerical iterative algorithm and so on. Feliu-Batlle *et al.* carried out research to tune controller $D^{1-\lambda}I^{\lambda}$ (2.28) for the second order plus time delay process systems ($G(s)=\frac{ke^{-Ls}}{(T_1s+1)(T_2s+1)}$) [46]. It is noteworthy to say that the controller is multiplied by $(1+\frac{\alpha}{s})$ where α is very small and set by the trial and error method in order to decrease the settling time value. The constraints (2.29), (2.30) and (2.32) were solved using the Newton-Raphson numerical iterative algorithm. They assert that $D^{1-\lambda}I^{\lambda}$ controllers are more robust and stable than IO-PID controllers (2.22) against changes in T_1. Moreover, in [67], an accurate approximation method is used to directly solve constraints (2.29), (2.30), and (2.31) to tune FO-PI controllers (2.19) for any general plant.
Luo and Chen tuned three controllers including IO-PID (2.22), FO-PD ((2.21), $\mu\in(0,2)$), and FO-[PD] (2.26, $\mu\in(0,2)$) controllers for FO plants ($G(s)=\frac{1}{s(Ts^{\alpha}+1)}$) [44]. The constraints (2.29), (2.30) and (2.31) are solved using the graphical method for designing a robust controller against gain variations. It is concluded that IO-PID controllers are not proper for some cases because they cause systems to become unstable and also FO-[PD] controllers are more robust and have better performances than FO-PD ones. Moreover, they used this approach for tuning FO-PI and FO-[PI] for the similar type of FO plants [45]. They concluded that there are no differences between FO-PI (2.19) and FO-[PI] (2.27) controllers for this type of plant [45]. Similarly, Luo *et al.* followed this method to tune the FO-PD controller for a servo hard disk drive [68]. This method is also used to tune FO-PI controllers (2.19) for the first order plants [69].

2.5. REALIZATION OF FO CONTROLLERS

CONTROL engineers are faced with a big difficulty which is the realization of FO-controllers when they want to utilize this type of controllers. Implementation of FO-controllers will be done in two steps. First, the irrational function s^{ν} must be approximated with a rational function. There are some methods for obtaining the rational

approximation functions of s^ν in the S, Z and δ domain. In other words, there are continuous approximation functions (S domain) and discrete approximation functions (Z and δ domain). Second, the rational transfer functions can be implemented by analogue circuits (for continuous transfer functions) or by special digital devices such as PLC, PIC, FPGA and so forth (for discrete approximation functions).

2.5.1. CONTINUOUS APPROXIMATION METHODS (S DOMAIN)

One of the important problems in implementing of FO controllers can be addressed as finding a way for the rational approximation of the irrational transfer function s^ν. There are several mathematical methods for the rational approximation of s^ν. In control theory, the Continuous Fractional Expansion (CFE) method, which is a well-known method for function evaluation, is a proper way among many other mathematical methods. In this way, any irrational function $G(s)$ can be expressed as [70, 71]

$$G(s) \approx a_0(s) + \cfrac{b_1(s)}{a_1(s) + \cfrac{b_2(s)}{a_2(s) + \cfrac{b_3(s)}{a_3(s) + \ldots}}}. \tag{2.52}$$

This technique yields to approximate the irrational function $G(s)$ by a rational function which is achieved by dividing two polynomial functions of the variable s as

$$G(s) \approx \frac{P_n(s)}{Q_m(s)} = \frac{p_0 + p_1 s + \ldots + p_n s^n}{q_0 + q_1 s + \ldots + q_m s^m}, \tag{2.53}$$

which is passed through these points $(s_1, G(s_1)), \ldots, (s_{1+a}, G(s_{1+a}))$ where $a = m + n + 1$. A method upon the CFE technique is suggested by Matsuda in selected logarithmically spaced points $(s_k, k = 0, 1, 2, \ldots)$. His approximation method is [70, 71]

$$H(s) \approx a_0 + \cfrac{s - s_0}{a_1 + \cfrac{s - s_1}{a_2 + \cfrac{s - s_2}{a_3 + \ldots}}}, \tag{2.54}$$

where $V_0(s) = H(s)$, $V_{i+1}(s) = \dfrac{s - s_i}{V_i(s) - a_i}$, $a_i = V_i(s_i)$.

The most widely applicable method for the approximation of s^ν in a limited frequency range is Oustaloup's method [29, 70–73] which is

$$s^\nu \approx C_o \prod_{k=-N}^{k=N} \frac{\left(1 + \dfrac{s}{\omega'_k}\right)}{\left(1 + \dfrac{s}{\omega_k}\right)}, \tag{2.55}$$

with $C_o = \left(\dfrac{\omega_h}{\omega_b}\right)^{0.5\nu}$, $\omega'_k = \omega_b \left(\dfrac{\omega_h}{\omega_b}\right)^{\frac{k+N+\frac{1-\nu}{2}}{2N+1}}$, $\omega_k = \omega_b \left(\dfrac{\omega_h}{\omega_b}\right)^{\frac{k+N+\frac{1+\nu}{2}}{2N+1}}$, and $\omega_h > \omega_b$ are frequency bands on which s^ν acts. Quality of Oustaloup's method near frequency bands

may not be satisfactory when ω_h is very high and ω_b is very low. So, an extension of this method is proposed to overcome this problem by combining the Taylor's series and Oustaloup's method [72] as

$$s^{\nu} \approx C_o \left(\frac{d s^2 + b\omega_h s}{d(1-\nu)s^2 + b\omega_h s + d\nu} \right) \prod_{k=-N}^{k=N} \frac{s + \omega\prime_k}{s + \omega_k}, \tag{2.56}$$

in which $C_o = \left(\frac{d\omega_b}{b}\right)^{\nu} \prod_{k=-N}^{k=N} \frac{\omega_k}{\omega\prime_k}$. The suggested values for b and d are, respectively, 10 and 9 [72].

Similar to the Oustaloup's method, Chareff proposed an approximation for functions in the form of $G(s) = \frac{1}{\left(1 + \frac{s}{P_T}\right)^{\nu}}$ as [71]

$$\frac{1}{\left(1 + \frac{s}{P_T}\right)^{\nu}} \approx \frac{\prod_{i=1}^{N-1} \left(1 + \frac{s}{z_i}\right)}{\prod_{i=1}^{N} \left(1 + \frac{s}{p_i}\right)}, \tag{2.57}$$

where $a = 10^{\frac{\nu}{10(1-\nu)}}$, $b = 10^{\frac{\nu}{10\nu}}$, $p_0 = P_T\sqrt{b}$, $p_i = p_0(ab)^i$, $z_i = a p_0 (ab)^i$, $N = \text{Integer}\left[\frac{log\left(\frac{\omega_{max}}{p_0}\right)}{log(ab)}\right] + 1$, and ω_{max} is the desired bandwidth. These coefficients are computed such that deviation from the original magnitude response in the frequency domain becomes less than $y(dB)$. Yüce *et al.* introduced an approximation method based on Laplace transform of FO integrator (2.4) by utilizing the least square fitting tool of Matlab. In this way [74],

$$\mathscr{L}^{-1}\left\{\frac{1}{s^{\nu+1}}\right\} = \frac{t^{\nu}}{\nu\Gamma(\nu)} = \mathscr{F}(t). \tag{2.58}$$

It is assumed that function $\mathscr{Y}$ (2.59) is fitted properly to the function $\mathscr{F}$ and then m_i and n_i parameters are achieved by using the least square fitting tool in Matlab as

$$\mathscr{F}(t) \approx \mathscr{Y}(t) = m_1 e^{-n_1 t} + m_2 e^{-n_2 t} + m_3 e^{-n_3 t} + m_4 e^{-n_4 t} + m_5 e^{-n_5 t} + c. \tag{2.59}$$

Then, the inverse Laplace transform is applied to (2.59) and the approximation function is obtained as

$$\mathscr{L}\{\mathscr{Y}\} = \frac{m_1}{s+n_1} + \frac{m_2}{s+n_2} + \frac{m_3}{s+n_3} + \frac{m_4}{s+n_4} + \frac{m_5}{s+n_5} + \frac{c}{s}. \approx \frac{1}{s^{\nu+1}} \tag{2.60}$$

Upon Newton's iterative method for solving nonlinear equations, Carlson introduced an approximation method for FO transfer functions. In this respect [73, 75, 76]

$$G(s)^{\nu} \approx H_n(s) = H_{n-1}(s) \frac{(a-1)(H_{n-1}(s))^a + (a+1)G(s)}{(a+1)(H_{n-1}(s))^a + (a-1)G(s)}, \tag{2.61}$$

where $a = \frac{1}{\nu}$, $H_0(s) = 1$. It is obvious that this method is restricted to that a must be an integer number. So, some researchers tried to overcome this limitation. Shrivastava and Varshney considered that Carlson's method is applicable for $\nu = 0.1,\ 0.2$, and 0.5. Then, they built other ν values in the range of $[0.1, 0.9]$ by combination of these three values (for example, $0.3 = 0.1 + 0.2$ or $0.8 = 0.3 + 0.5$) and obtained a table for approximation of $(s^\nu,\ \nu \in [0.1, 0.9])$ [75]. Moreover, Tepljakov *et al.* modified the Carlson's method in order to approximate s^ν in a frequency range. They declared that the behaviour of s^ν in a frequency band is similar to an FO lead/lag compensator (2.14). If ν^{-1} is not an integer number, it will be decomposed by a special algorithm (for more information see [76]) as

$$\nu = \sum_{i=1}^{i=k} \frac{1}{m_i}. \tag{2.62}$$

Then, the approximation function in the frequency band is calculated as

$$G(s)^\nu \approx \prod_{i=1}^{i=k} \left(\frac{1+\Delta s}{1+x\Delta s}\right)^{\frac{1}{m_i}} \approx \prod_{i=1}^{i=k} H_n^{\frac{1}{m_i}}, \tag{2.63}$$

where $H_n^{\frac{1}{m_i}}$ is calculated through (2.61) while $a = m_i$.
In addition, Aware *et al.* introduced a new method for approximation of s^ν in the frequency band of (ω_L, ω_H) [77]. They obtained this method by optimizing the number of poles and zeros to maintain the phase value of s^ν within the ϵ° tolerance of its actual value as follows.

$$s^\nu \approx \frac{(s-z_1)(s-z_2)...(s-z_n)}{(s-p_1)(s-p_2)...(s-p_n)}, \tag{2.64}$$

in which $p_1 = 10^{2\nu+\log(\omega_L)+1}$, $p_n = 10^{\log(p_{n-1})+2-\mu}$, $z_1 = 10\omega_L$, $z_n = 10^{\log(z_{n-1})+2-\mu}$, $\mu = 0.64\epsilon$, $n = \min_{p_n > \omega_H}(n)$.
Lino and Maione obtained an approximation method for FO lead/lag compensator (2.14) which is [78]

$$C(s) = k_p x^\mu \left(\frac{1+\Delta s}{1+\Delta x s}\right)^\nu \approx \frac{\sum_{k=0}^{N} B_{N-k} s^k}{\sum_{k=0}^{N} A_{N-k} s^k},\ \nu > 0,\ \begin{cases} \text{Lead}, & 0 < x < 1, \\ \text{Lag}, & 1 < x, \end{cases} \tag{2.65}$$

where

- $A_{N-k} = \sum_{i=1}^{N} a_{N-i} L_{ki}^C,\ B_{N-k} = \sum_{i=1}^{N} b_{N-i} L_{ki}^C,\ L_{ki}^C = T^k \sum_{j=j_1}^{j_2} \binom{i}{j}\binom{N-i}{k-j} x^{k-j},$
- $j_1 = \max\{0, k+i-N\},\quad j_2 = \min\{i, k\},$
- $a_i = \binom{N}{i}(N-i+1+\nu)_{(i)}(N-\nu)_{(N-i)^*},\quad b_i = \binom{N}{i}(i+1+\nu)_{(N-i)}(N-\nu)_{(i)^*},$
- $(\nu+i+1)_{(N-i)} = (\nu+i+1)(\nu+i+2)...(\nu+N),$
- $(N-\nu)_{(i)^*} = (N-\nu)(N-\nu-1)...(N-\nu-i+1),$

Table 2.1: Discrete Time Conversion Rules

Methods	$s \rightarrow z$ Conversion	Taylor series [8]
Backward-Difference (Euler) [6, 8, 71, 80]	$s^{\nu} \approx \left[\frac{1-z^{-1}}{T}\right]^{\nu}$	$(\frac{1}{T})^{\nu}\left[1-\nu z^{-1}+\frac{\nu(\nu-1)}{2!}z^{-2}+...\right]$
Trapezoidal (Tustin) [6, 8, 71, 80]	$s^{\nu} \approx \left[\frac{2(1-z^{-1})}{T(1+z^{-1})}\right]^{\nu}$	$(\frac{2}{T})^{\nu}\left[1-2\nu z^{-1}+2\nu^2 z^{-2}+...\right]$
Al-Alaoui [6, 80]	$s^{\nu} \approx \left[\frac{56(1-z^{-1})}{49T(7+z^{-1})}\right]^{\nu}$	-
Simpson [8]	$s^{\nu} \approx \left[\frac{3(1-z^{-1})(1+z^{-1})}{T(1+4z^{-1}+z^{-2})}\right]^{\nu}$	$(\frac{3}{T})^{\nu}\left[1-4\nu z^{-1}+2\nu(4\nu+3)z^{-2}+...\right]$

Table 2.2: β and γ tuning parameters

Methods	Forward Euler	Tustin	Al-Alaoui	Backward Euler	Implicit Adams
γ	0	0.5	$\frac{7}{8}$	1	1.5
β	1				

- $(\nu+N+1)_{(0)} = (\nu-N)_{(0)} = (N-\nu)_{(0)^*} = 1$.

As it asserts that s^{ν} in a frequency band can be considered as an FO lead/lag compensator [76], this method can be applied to approximate s^{ν} in a frequency range.

2.5.2. DISCRETE APPROXIMATION METHODS (Z DOMAIN)

In this age, using digital logic in some applications such as controller implementation has been increased because of development of digital computers. FO-controllers are not exceptional and there are many investigations for digital implementation of these controllers. Tenreiro Machado was one of the pioneer researchers who proposed an algorithm for the digital implementation of FO-controllers [79]. The first step in digital implementation is the discretization of the FO-transfer function. For this purpose, there are several methods which are categorized into two main groups: direct discretization and indirect discretization methods [80].

DIRECT DISCRETIZATION METHODS

In these methods, two steps must be taken for obtaining a discrete function of FO differentiators. At first, it is important to select a proper generating function. Generating functions express the discretization of FO differentiators ($s = \omega(z^{-1})$) and usually have the general configuration [81]

$$\omega(z^{-1}) = \frac{1-z^{-1}}{\beta T\left(\gamma+(1-\gamma)z^{-1}\right)}, \tag{2.66}$$

in which β, γ, and T are respectively the gain tuning parameter, phase tuning parameter, and sample period. The most commonly used generating functions are most usable for the discretization are listed in Table 2.1. Most of these generating functions can be obtained using (2.66) by considering gain and phase tuning parameters listed in Table 2.2. Obviously, the generating functions which are listed in Table 2.1 are irrational. So, in the

second step, it is necessary to approximate these irrational formulas with finite order rational formulas. To obtain this goal, two most applicable mathematics methods (Power Series Expansion (PSE) and CFE) are utilized in direct discretization methods in many studies. In other words, it can be said that

$$D^{\pm\nu}(z) \approx CFE\{\omega(z^{-1})^{\nu}\} \quad \text{or} \quad D^{\pm\nu}(z) \approx PSE\{\omega(z^{-1})^{\nu}\}. \tag{2.67}$$

As it was shown in Table2.1, Machado *et al.* proposed some discrete approximation functions by applying the Taylor series, which is one of the mostly used PSE methods, to several generating functions [8].
One of the well-known approximation functions is obtained based on the PSE method by utilizing the Euler generating function and the Grünwald-Letnikov definition (2.10). In this respect, the discrete approximation of the FO integro-differential operator is gotten by using the short memory principle [6, 71, 80] as

$$(s)^{\pm\nu} = T^{\mp\nu} z^{-[\frac{L}{T}]} \sum_{j=0}^{[\frac{L}{T}]} c_j^{\nu} z^{[\frac{L}{T}]-j}, \tag{2.68}$$

in which L is the memory length, $c_j^{\nu} = \left(1 - \frac{(1+\nu)}{j}\right) c_{j-1}^{\nu}$, and $c_0^{\nu} = 1$. In order to improve the accuracy of the discrete approximation functions in high frequencies, Chen *et al.* introduced a new generating function by combining the Tustin and Simpson generating functions. Their new generating function is [80],

$$s^{\nu} \approx k_0 \left(\frac{1 - z^{-2}}{1 + r_2 z^{-1}}\right)^{\nu}, \tag{2.69}$$

where $k_0 = \frac{6r_2}{T(3-a)}$, $r_2 = \frac{3 + a - 2\sqrt{3a}}{3-a}$, $a \in [0,1]$ is a weighting factor or a tuning knob. Then, this generating function is expanded rationally by the implementation of the CFE method using MATLAB Symbolic Toolbox [80].
Chen *et al.* proposed a discrete approximation method upon the Muir-recursion formula, which is applicable in the geophysical data processing, in order to express the Tustin generating function rationally [6] and claimed that their method is as accurate as the Taylor series expansion method. In this method,

$$s^{\nu} \approx \left(\frac{2}{T}\right)^{\nu} \left(\frac{1 - z^{-1}}{1 + z^{-1}}\right)^{\nu} = \left(\frac{2}{T}\right)^{\nu} \lim_{n\to\infty} \frac{A_n(z^{-1}, \nu)}{A_n(z^{-1}, -\nu)}, \tag{2.70}$$

In which: $A_0(z^{-1}, \nu) = 1$, $A_n(z^{-1}, \nu) = (1 - c_n z^n) A_{n-1}(z^{-1}, \nu)$, $c_n = \begin{cases} \frac{\nu}{n}, & n \text{ is odd}, \\ 0, & n \text{ is even}. \end{cases}$
Similar to (2.65), a closed-form formula is obtained for discrete approximation of FO lead/lag compensators [78] as

$$C(s) = k_p x^{\mu} \left(\frac{1 + \Delta s}{1 + \Delta x s}\right)^{\nu} \approx \frac{\sum_{h=0}^{N} D_{N-h} z^h}{\sum_{h=0}^{N} C_{N-h} z^h}, \ \nu > 0, \begin{cases} \text{Lead}, & 0 < x < 1, \\ \text{Lag}, & 1 < x, \end{cases} \tag{2.71}$$

with,

- $C_{N-h} = \sum_{k=0}^{N} A_{N-k} L_{hk}^{D}$, $D_{N-h} = \sum_{k=0}^{N} B_{N-k} L_{hk}^{D}$, $j_2 = \min\{h,k\}$,
- $L_{hk}^{D} = (\frac{2}{T})^k \sum_{j=j_1}^{j_2} (-1)^{k-j} \binom{k}{j} \binom{N-k}{h-j} x^{k-j}$, $j_1 = \max\{0, k+h-N\}$,
- A_{N-k} and B_{N-k} are described in (2.65),

INDIRECT DISCRETIZATION METHODS

There are two stages in indirect discretization methods. At the first stage, the irrational transfer function s^{ν} is approximated by a rational transfer function by using methods which are described in Section 2.5.1. Then, by replacing s in the approximation function with generating functions which are represented in Table(2.1) ($s \rightarrow \omega(z^{-1})$), the discrete approximation function is obtained. In other words,

$$s^{\nu} \approx \frac{P_n(s)}{Q_m(s)} \xrightarrow{s=\omega(z^{-1})} s^{\nu} \approx G(z). \tag{2.72}$$

For instance, Folea *et al.* approximated s^{ν} with Oustaloup's method (2.55) firstly. Then, to obtain the discrete approximate transfer function, they replaced s with

$$s = \frac{(1+\alpha)(z-1)}{T(z+\alpha)}, \tag{2.73}$$

where T is sampling period and $\alpha \in [0,1]$) is a weighting factor [82, 83]. This method is generalized for any non-rational continuous-time transfer function by passing following steps or a general [84]. After replacing s with (2.73), the frequency response is obtained replacing $z = e^{j\omega t}$ where ω is a vector of equally-spaced frequencies. Then, the impulse response of the discrete-time FO system is obtained using the inverse Fast Fourier Transform (FFT) to the previous calculated frequency response. The approximated transfer function is achieved from the impulse response using some techniques such as Steiglitz-McBride in the form of

$$G(z^{-1}) = \frac{a_0 + a_1 z^{-1} + \ldots + a_n z^{-N}}{b_0 + b_1 z^{-1} + \ldots + b_n z^{-n}}, \; n \text{ is the order of approximation.} \tag{2.74}$$

2.5.3. δ DOMAIN APPROXIMATION METHODS

Although the digital implementation is widely used in this era because of the development of digital computers, there is a big concern in discrete approximation methods. As it is known, stable poles and minimum-phase zeros in the s-plane are lain inside the unit circle in the z-plane when the bilinear transformation is utilized. So, the high resolution presentation of compensators with long words are essential for ensuring stability. But, it is impossible to get infinite accuracy in designing values of coefficients in a software and hardware implementation because a finite number of bits are available [78]. Furthermore, when the sampling rate is increased, zeros and poles of discrete approximation

functions get close to each other and concentrate at the point (1,0). Hence, discrete approximation functions are very sensitive to small variations of coefficients in high sampling rates and even may lose their stability in some cases [78, 85]. To overcome these dilemmas, the δ operator can be a proper solution because it allows a gradual transformation from the discrete to continuous time domain. For this purpose, the continuous transfer function is converted to the δ domain through [78, 85]:

$$s = \frac{1}{T}\ln(\delta T + 1) \approx \frac{\delta}{0.5\delta T + 1}, \tag{2.75}$$

where T is the sampling period. Similar to indirect discretization methods, it is possible to approximate irrational transfer functions with presented methods in Section 2.5.1 and then use the preceding equation to obtain δ domain approximation functions.
Moreover, some researchers introduced some direct methods to obtain rational δ domain transfer functions. Similar to (2.71) and (2.65), a closed-form formula is obtained for the approximation of FO lead/lag compensators δ domain as [78]:

$$C(s) = k_p x^{\mu}\left(\frac{1+\Delta s}{1+\Delta x s}\right)^{\nu} \approx \frac{\sum_{h=0}^{N} F_{N-h}\delta^h}{\sum_{h=0}^{N} E_{N-h}\delta^h},\ \nu > 0,\ \begin{cases}\text{Lead}, & 0 < x < 1,\\ \text{Lag}, & 1 < x,\end{cases} \tag{2.76}$$

with $E_{N-j} = \sum_{k=0}^{j}\binom{N-k}{j-k}(0.5T)^{j-k}A_{N-k}$, $F_{N-j} = \sum_{k=0}^{j}\binom{N-k}{j-k}(0.5T)^{j-k}B_{N-k}$, A_{N-k} and B_{N-k} are described in (2.65). As it has been explained, all methods (2.65), (2.71), and (2.76) can be used for s^{ν} which acts on a frequency band. In addition, Maione introduced a formula to approximate s^{ν} in δ domain as [85]

$$s^{\nu} \approx G_{\delta}^{(N)} = \frac{\sum_{k=0}^{N} c_k \delta^{N-k}}{\sum_{k=0}^{N} d_k \delta^{N-k}}, \tag{2.77}$$

In which

- $c_{(N-j)}(\nu) = \sum_{r=0}^{j} p_{(N-r)}(\nu)(0.5T)^{j-r}\binom{N-r}{j-r}$, $d_{(N-j)}(\nu) = \sum_{r=0}^{j} q_{(N-r)}(\nu)(0.5T)^{j-r}\binom{N-r}{j-r}$,
- $p_j(\nu) = q_{(N-j)}(\nu) = (-1)^j\binom{N}{j}(\nu+j+1)_{(N-j)}(\nu-N)_{(j)}$,
- $(\nu-N)_{(j)} = (\nu-N)(\nu-N-1)...(\nu-N+j-1)$, $(\nu-N)_{(0)} = 1$,
- $(\nu+j+1)_{(N-j)} = (\nu+j+1)(\nu+j+2)...(\nu+N)$, and N is the order of approximation.

It must be noted that for the implementation of the δ transfer functions [85], relation

$$\delta^{-1} = \frac{Tz^{-1}}{1-z^{-1}} \tag{2.78}$$

can be used.

2.5.4. DIGITAL IMPLEMENTATION

The first step in the digital implementation is getting the finite difference equation which is achieved by the discrete approximation methods elaborated in Sections 2.5.2 and 2.5.3. Then, all discrete approximation of FO transfer functions can be implemented directly to any microprocessor based devices like as PLC, PIC, PCL I/O card, FPGA, FPAA, switched capacitors, etc [86, 87]. Figure. 2.9 shows the implementation of the canonical form (2.74) of discrete approximation of FO transfer functions. To implement this form, two codes are needed: initialization and loop code (see the pseudo-code in [6, 88]).

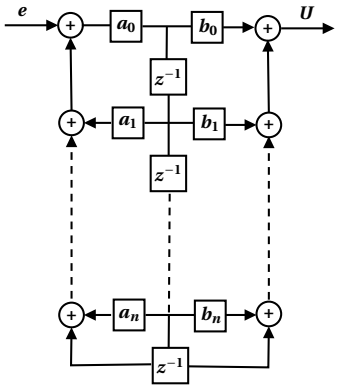

Figure 2.9: Block diagram of the canonical representation

2.5.5. ANALOGUE IMPLEMENTATION

Although digital controllers are used widely nowadays because of the revolution of cost-effective digital computers, they have some limitations in some aspects. The first problem comes from the nature of the discretization. This is related to the sampling period which must be significantly more than the time of computation length. Also, a memory with high capacity is needed for high order discrete approximations. Digital controllers are not as fast as analogue controllers. As a result, although several digital controllers have been recently used to control relatively high modes of systems, they are not proper for very fast processes such as vibration control [70]. As some limitations are mentioned, analogue realization is the only solution in some cases.

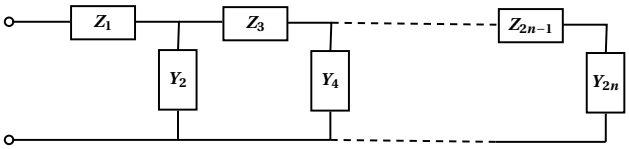

Figure 2.10: Finite ladder circuit

A circuit which represents FO behaviour is termed a "fractance". Basically, there are three fractance devices: domino ladder network, tree structure of electrical elements and transmission line circuit [6]. It asserts that ladder lattice networks can approximate

FO transfer functions more accurate than the lumped networks [89]. Consider the finite ladder circuit which is depicted in Figure. 2.10, in which $Z_{2k-1}(s)$, $Y_{2k}(s)$, $k = 1, ..., n$ are the impedance of circuit elements. The equivalent impedance of the whole circuit $Z(s)$ is obtained by [70]

$$Z(s) = Z_1(s) + \cfrac{1}{Y_2(s) + \cfrac{1}{Z_3(s) + \cfrac{1}{Y_4(s) + \cfrac{1}{\ddots \cfrac{1}{Y_{2n-2}(s) + \cfrac{1}{Z_{2n-1}(s) + \cfrac{1}{Y_{2n}(s)}}}}}}}, \tag{2.79}$$

so, first, continuous approximation function of FO-controllers must be expressed in the form of (2.79). Then, $Z_{2k-1}(s)$ and $Y_{2k}(s)$, $k = 1, ..., n$ will give the type of necessary electrical elements using the first Cauer's canonic LC circuit [90] (for more information, see examples in [70]). If $b_i < 0$, then the circuit is depicted in Figure. 2.11 is considered [70]. The entire circuit has equivalent impedance of $-Z$ in which Z can be a resistor, capacitor or coil.

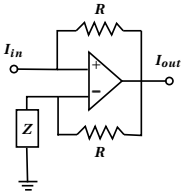

Figure 2.11: Negative-impedance converter

There are also some methods for the direct implementation of FO derivatives s^v which lead to increase the accuracy of the realization of FO controllers. In these methods, there is no need for approximation of FO transfer functions. Bohannan found some electrical elements, named as "fractor", exhibit fractance attributes [91]. It is revealed that Lithium Hydrazinium Sulfate ($LiN_2H_5SO_4$) behaves in a wide range of temperatures and frequencies like an electrical element with the impedance of [91]

$$Z_F = \frac{k}{s^{0.5}}. \tag{2.80}$$

Figure. 2.12 shows a circuit which implements the half order integrator by using a fractor made from ($LiN_2H_5SO_4$) material [91]. It is hoped that many investigations will be done in the future in materials to build fractors with a wide range of exponents. Then, it facilitates introducing FO control elements to engineering applications without using approximation methods.

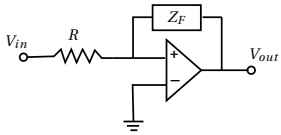

Figure 2.12: Schematic of a simple circuit of half order integrator

Another way for direct realization of FO controllers is using a new electrical element whose name is "Memristor" [92]. Memristor is an electrical element which exhibits a FO behaviour with the impedance of [92]

$$Z_{MS} = Ks^{\nu},\ (\nu, K) \in R. \tag{2.81}$$

Two configurations which are shown in Figure. 2.13a and 2.13b are considered for the analogue implementation of FO controllers. The equivalent impedance of the entire circuit Figures 2.13a and 2.13b are respectively $Z(s) = -\frac{M}{K}s^{-\nu}$ and $Z(s) = -\frac{K}{M}s^{\nu}$, $(\nu \in R)$ in which M called memristance with the physical unit of Ohm [92]. Although this method is promising, further research has to be conducted to prove this method can implement the FO transfer functions.

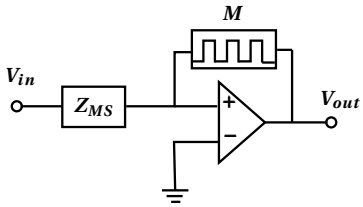

(a) Type I

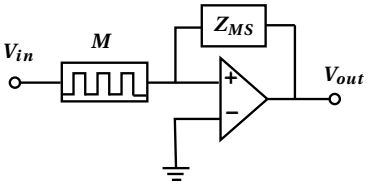

(b) Type II

Figure 2.13: Analogue fractional-order operators

In addition, Aware *et al.* developed an analogue implementation technique based on their approximation method (2.64) [77]. In this technique, first, s^{ν} is approximated using (2.64), and then, each set of zero and pole (z_i, p_i) is implemented as shown in Figure. 2.14. In Figure. 2.14, firstly, any available capacitor (C_i) is selected. Then,

$$\begin{cases} R_i = \dfrac{1}{p_i C_i},\ R_i' = \dfrac{1}{z_i - p_i}, & \nu < 0, \\ R_i = \dfrac{1}{z_i C_i},\ R_i' = \dfrac{1}{p_i - z_i}, & \nu > 0. \end{cases} \tag{2.82}$$

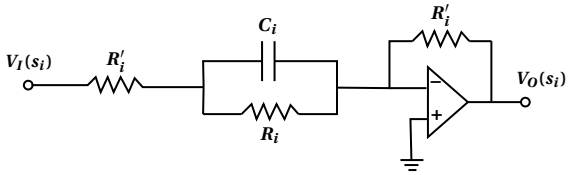

Figure 2.14: Schematic of implementing each set of zero-pole pair of s^v

2.6. SEVERAL USEFUL CODES FOR FO CONTROLLERS

NOW, it is noteworthy to introduce some Matlab codes which simplify using FO calculus in the control field. One of these toolboxes is the CRONE CSD toolbox which is designed for tuning all generations of CRONE controllers [29]. The online version of this toolbox is available through this link.
Valério and Sa da Costa introduced a general and user friendly toolbox which is termed Ninteger [73]. It has three identification methods. Also, it has many approximation methods which have been described in this article. Moreover, it is proper for tuning all generations of CRONE and FO-PID controllers (2.16) in both time and frequency domain.
One of the useful software for tuning FO-PID controllers (2.16), FO-lead lag compensators and all IO-filters in both time and frequency domain is designed at the mechatronic system design group of TU Delft University by S.H. HosseinNia et al. Also, it has several approximation methods like Ninteger software and is free and available through the following link.
Furthermore, there are some simple codes for the frequency domain analysis of FO functions in [6]. Lachhab *et al.* designed a FO toolbox which automatically tune an FO-PID controller based on given specifications and dynamics of the plant. Moreover, this software includes some approximation methods [93]. Tepljakov *et al.* developed a very general toolbox whose name is FOMCON [94] which has several options including both time and frequency analysis, FO controllers in the state-space, CRONE controllers, approximation methods, optimization criteria for tuning FO-controllers, and identification with FO-models. In addition, it has some FO-blocks which can be added in Simulink library of Matlab. It can be downloaded through this link.
Dingy wrote a book about FO controllers and also designed a toolbox which contains every method which is described in his book [95]. This toolbox which is termed FOTF includes several approximation methods, functions for analyzing FO controllers in both time and frequency domain, Simulink blocks for FO functions, and tuning methods for FO controllers. This toolbox is available through this link.

2.7. DISCUSSION

IN this section, the advantages and disadvantages of using FO calculus in the control area are commented based on the literature reviewed in this article. Many researchers believe that FO controllers outperform IO ones [11, 43, 49, 96–101]. In the case of linear controllers, on the one hand, it can be asserted that FO-PID controllers give more flexibility to designers to select the tuning parameters due to two important factors. First,

the orders of integration and differentiator of the controller are not restricted to integer numbers. Second, the stability region of tuning knobs (k_p, k_i, and k_d in controller (2.16)) which guarantees the stability of the whole system for a specific phase margin value is bigger than one for IO-PID controllers as proposed by Hamamci in [102]. On the other hand, the tuning knobs of FO-PID controllers are more than classical IO ones, so, designers can consider more efficient constraints for tuning FO-PID compared to classical IO ones. In comparison with high order IO-PID controllers, since FO-PID controllers are approximated with several zeros-and poles, their performances are similar with high order IO-PID. But the tuning of FO-PID is easier because two extra orders must be tuned in FO-PID instead of determining places of several zeros-poles in high order IO-PID controllers.

Among several constraints, iso-damping behaviour (constraint (2.31)) has attracted a lot of attention from researchers in tuning FO controllers. It is reported that FO-PID controllers are more robust against plant uncertainties than IO-PID ones [11, 43, 49, 103]. It is asserted that the third generation of CRONE is one of the most appropriate solutions when uncertainties of a plant are more general than just gain-like perturbations [24, 25, 56]. Hence, from robustness viewpoint, FO controllers are more effective in comparison with IO ones.

Furthermore, some researchers believe that it is possible to consider the energy efficiency constraint for tuning FO-PID controllers [104–106]. As a result, from the energy perspective, FO-PID can outperform classical IO-PID controllers; for instance, using FO-PID decreases averagely 20% power consumption of a DC motor [104]. Another example, it is shown that using FO-PID controllers for a magnetic levitation system leads to a better fuel efficiency in comparison with classical IO-PID controllers [105].

In addition, FO controllers can properly compensate disturbances due to undesired nonlinearities such as dead zone, backlash, hysteresis, and static distortion in the systems which results in increasing the precision of the system [107–109]. Moreover, some research manifests that using FO transfer functions for describing the dynamic characteristics of some special plant is more precise than IO ones [6–9, 110]. Also, it is concluded that FO controllers are more proper than IO controllers for FO plants [11, 102]. Therefore, for some special plants, it is necessary to use FO calculus in both modelling and control.

It can be concluded that FO controllers have better performance than IO ones and improve significantly the performance of systems. However, there are two big barriers which confine the adoption of FO controllers in the industry. Firstly, tuning of the FO controllers is more complex than IO ones. This problem is solved to some extent by present tuning methods and toolboxes which are elaborated in Sections 2.4 and 2.6, respectively. Even though, based on the knowledge of the author, there are few reports about tuning of FO controllers for motion systems (high cross-over frequency is required). Secondly, realization of FO controllers need devices with high memory capacity because FO controllers are approximated with high order transfer functions. Since there is no direct method for realization of FO controllers, approximation methods must be used for this purpose. In order to increase accuracy of the approximation methods, the order of estimated functions must be increased which leads to a high order controller. Although some researchers are trying to solve this problem, their methods need further efforts to

be complete [91, 92]. It is hoped that researchers can propose a direct method for realization of FO controllers using some special materials such as Memristor and ($Li N_2 H_5 SO_4$).

To wrap up, FO calculus advances the control area in many aspects. It can be claimed that FO calculus facilitates modelling of complicated dynamic systems such as distributed parameter systems, biomimetics materials, smart materials, etc. [7, 97, 98, 111]. Moreover, it improves performance of both linear and nonlinear controllers particularly from the robustness viewpoint. In addition, it is claimed that FO calculus has potential to shape the phase and gain of the frequency response independently and achieve the Bode ideal transfer function [7]. However, nobody attempted to solve this significant problem. All in all, it is predicted that overcoming mentioned barriers leads to substitution of IO-PID controllers with FO ones in the near future.

2.8. CONCLUSION

FO controllers have attracted much attention from academia and industrial associations. In this article, linear FO controllers are reviewed with the focus on the frequency domain. In this respect, FO calculus including basic definitions of FO derivative and integrator were introduced. Next, four well-known linear FO controllers which are TID controller, CRONE generations, FO lead/lag compensators, and FO-PID controllers were commented and after that, their representative tuning methods were elaborated. Although many simple tuning methods for FO controllers were reported, most of them are useful for process control problems (low bandwidth and high time delay systems) and motion control problems (high bandwidth systems) have not been considered much in the literature yet. Then, continuous and discrete approximation methods of FO controllers and their analogue and digital implementation were explained. Approximation methods lead to high order functions which makes the implementation of FO controllers to be more difficult than IO ones. Although much of recent research resolved this problem to some extent, further investigations are required. Then, some useful codes which facilitate using FO calculus in the control field were presented. Finally, it is anticipated that IO-PID controllers are replaced with FO ones in the near future by finding a direct method for implementation of FO controllers. All in all, this review paper helps beginners to get started rapidly and learn how to select, tune, approximate, and implement FO-controllers.

REFERENCES

[1] A. A. Dastjerdi, B. M. Vinagre, Y. Chen, and S. H. HosseinNia, *Linear fractional order controllers; a survey in the frequency domain,* Annual Reviews in Control (2019).

[2] F. Padula, A. Visioli, and M. Pagnoni, *On the anti-windup schemes for fractional-order pid controllers,* in *Emerging Technologies & Factory Automation (ETFA), 2012 IEEE 17th Conference on* (IEEE, 2012) pp. 1–4.

[3] C. A. Monje, B. M. Vinagre, V. Feliu, and Y. Chen, *Tuning and auto-tuning of fractional order controllers for industry applications,* Control engineering practice **16**, 798 (2008).

[4] K. Rajagopal, A. Karthikeyan, and P. Duraisamy, *Hyperchaotic chameleon: fractional order fpga implementation,* Complexity **2017** (2017).

[5] L. Liu, H. Xing, X. Cao, Z. Fu, and S. Song, *Guaranteed cost finite-time control of discrete-time positive impulsive switched systems,* Complexity **2018** (2018).

[6] Y. Chen, I. Petras, and D. Xue, *Fractional order control-a tutorial,* in *American Control Conference, 2009. ACC'09.* (IEEE, 2009) pp. 1397–1411.

[7] Y. Chen, *Ubiquitous fractional order controls?* IFAC Proceedings Volumes **39**, 481 (2006).

[8] J. T. Machado *et al.*, *Discrete-time fractional-order controllers,* Fractional Calculus and Applied Analysis **4**, 47 (2001).

[9] C. Zhao, D. Xue, and Y. Chen, *A fractional order PID tuning algorithm for a class of fractional order plants,* in *Mechatronics and automation, 2005 IEEE international conference*, Vol. 1 (IEEE, 2005) pp. 216–221.

[10] Y. Zhao, Y. Li, F. Zhou, Z. Zhou, and Y. Chen, *An iterative learning approach to identify fractional order kibam model,* IEEE/CAA Journal of Automatica Sinica **4**, 322 (2017).

[11] Y. Luo, Y. Chen, and Y. Pi, *Experimental study of fractional order proportional derivative controller synthesis for fractional order systems,* Mechatronics **21**, 204 (2011).

[12] S. H. HosseinNia, I. Tejado, D. Torres, B. M. Vinagre, and V. Feliu, *A general form for reset control including fractional order dynamics,* IFAC Proceedings Volumes **47**, 2028 (2014).

[13] I. Tejado, S. Hosseinnia, and B. Vinagre, *Adaptive gain-order fractional control for network-based applications,* Fractional Calculus and Applied Analysis **17**, 462 (2014).

[14] S. H. HosseinNia, I. Tejado, B. M. Vinagre, and Y. Chen, *Iterative learning and fractional reset control,* in *ASME 2015 International Design Engineering Technical Conferences and Computers and Information in Engineering Conference* (American Society of Mechanical Engineers, 2015) pp. V009T07A041–V009T07A041.

[15] S. H. HosseinNia, I. Tejado, and B. M. Vinagre, *A method for the design of robust controllers ensuring the quadratic stability for switching systems,* Journal of Vibration and Control **20**, 1085 (2014).

[16] S. M. RakhtAla, M. Yasoubi, and H. HosseinNia, *Design of second order sliding mode and sliding mode algorithms: a practical insight to dc-dc buck converter,* IEEE/CAA Journal of Automatica Sinica **4**, 483 (2017).

[17] S. Khubalkar, A. Chopade, A. Junghare, M. Aware, and S. Das, *Design and realization of stand-alone digital fractional order pid controller for buck converter fed dc motor,* Circuits, Systems, and Signal Processing **35**, 2189 (2016).

[18] F. Padula and A. Visioli, *Tuning rules for optimal pid and fractional-order pid controllers,* Journal of process control **21**, 69 (2011).

[19] S. Das, I. Pan, and S. Das, *Multi-objective lqr with optimum weight selection to design fopid controllers for delayed fractional order processes,* ISA transactions **58**, 35 (2015).

[20] C. Wang, H. Li, and Y. Chen, *H_∞ output feedback control of linear time-invariant fractional-order systems over finite frequency range,* IEEE/CAA Journal of Automatica Sinica **3**, 304 (2016).

[21] H. Chen and Y. Chen, *Fractional-order generalized principle of self-support (fogpss) in control system design,* IEEE/CAA Journal of Automatica Sinica **3**, 430 (2016).

[22] M. Zarghami, S. H. Hosseinnia, and M. Babazadeh, *Optimal control of egr system in gasoline engine based on gaussian process,* IFAC-PapersOnLine **50**, 3750 (2017).

[23] S. H. HosseinNia, *Robust model predictive control using iterative learning,* in *Control Conference (ECC), 2015 European* (IEEE, 2015) pp. 3514–3519.

[24] V. Pommier, J. Sabatier, P. Lanusse, and A. Oustaloup, *Crone control of a nonlinear hydraulic actuator,* Control Engineering Practice **10**, 391 (2002).

[25] A. Oustaloup, B. Mathieu, and P. Lanusse, *The crone control of resonant plants: application to a flexible transmission,* European Journal of control **1**, 113 (1995).

[26] A. Oustaloup, X. Moreau, and M. Nouillant, *The crone suspension,* Control Engineering Practice **4**, 1101 (1996).

[27] M. E. Krijnen, R. A. van Ostayen, and H. HosseinNia, *The application of fractional order control for an air-based contactless actuation system,* ISA transactions (2017).

[28] A. O'Dwyer, *Handbook of PI and PID controller tuning rules* (World Scientific, 2009).

[29] J. Sabatier, P. Lanusse, P. Melchior, and A. Oustaloup, *Fractional order differentiation and robust control design*, Vol. 77 (Springer, 2015).

[30] P. Shah and S. Agashe, *Review of fractional pid controller,* Mechatronics **38**, 29 (2016).

[31] B. Vinagre, I. Petráš, I. Podlubny, and Y. Chen, *Using fractional order adjustment rules and fractional order reference models in model-reference adaptive control,* Nonlinear Dynamics **29**, 269 (2002).

[32] J. Sabatier, O. P. Agrawal, and J. T. Machado, *Advances in fractional calculus*, Vol. 4 (Springer, 2007).

[33] M. Dalir and M. Bashour, *Applications of fractional calculus,* Applied Mathematical Sciences **4**, 1021 (2010).

[34] R. E. Gutiérrez, J. M. Rosário, and J. Tenreiro Machado, *Fractional order calculus: basic concepts and engineering applications,* Mathematical Problems in Engineering **2010** (2010).

[35] C. Li and W. Deng, *Remarks on fractional derivatives,* Applied Mathematics and Computation **187**, 777 (2007).

[36] B. Ross, *The development of fractional calculus 1695–1900,* Historia Mathematica **4**, 75 (1977).

[37] M. Caputo and M. Fabrizio, *A new definition of fractional derivative without singular kernel,* Progr. Fract. Differ. Appl **1**, 1 (2015).

[38] B. J. Lurie, *Three-parameter tunable tilt-integral-derivative (tid) controller,* (1994).

[39] C. A. Monje, B. M. Vinagre, A. J. Calderon, V. Feliu, and Y. Chen, *Auto-tuning of fractional lead-lag compensators,* IFAC Proceedings Volumes **38**, 319 (2005).

[40] M. S. Tavazoei and M. Tavakoli-Kakhki, *Compensation by fractional-order phase-lead/lag compensators,* IET Control Theory & Applications **8**, 319 (2014).

[41] M. Aoun, R. Malti, F. Levron, and A. Oustaloup, *Synthesis of fractional laguerre basis for system approximation,* Automatica **43**, 1640 (2007).

[42] I. Podlubny, *Fractional-order systems and fractional-order controllers,* Institute of Experimental Physics, Slovak Academy of Sciences, Kosice **12**, 1 (1994).

[43] C. A. Monje, A. J. Calderon, B. M. Vinagre, Y. Chen, and V. Feliu, *On fractional PI^{λ} controllers: some tuning rules for robustness to plant uncertainties,* Nonlinear Dynamics **38**, 369 (2004).

[44] Y. Luo and Y. Chen, *Fractional order [proportional derivative] controller for a class of fractional order systems,* Automatica **45**, 2446 (2009).

[45] H. Malek, Y. Luo, and Y. Chen, *Identification and tuning fractional order proportional integral controllers for time delayed systems with a fractional pole,* Mechatronics **23**, 746 (2013).

[46] V. Feliu-Batlle, R. R. Perez, and L. S. Rodriguez, *Fractional robust control of main irrigation canals with variable dynamic parameters,* Control Engineering Practice **15**, 673 (2007).

[47] S. Folea, C. I. Muresan, R. De Keyser, and C. M. Ionescu, *Theoretical analysis and experimental validation of a simplified fractional order controller for a magnetic levitation system,* IEEE transactions on control systems technology **24**, 756 (2016).

[48] A. Oustaloup and P. Melchior, *The great principles of the crone control,* in *Systems, Man and Cybernetics, 1993.'Systems Engineering in the Service of Humans', Conference Proceedings., International Conference on*, Vol. 2 (IEEE, 1993) pp. 118–129.

[49] D. Valério and J. S. da Costa, *Tuning of fractional PID controllers with ziegler–nichols-type rules,* Signal Processing **86**, 2771 (2006).

[50] F. Padula and A. Visioli, *Optimal tuning rules for proportional-integral-derivative and fractional-order proportional-integral-derivative controllers for integral and unstable processes,* IET Control Theory & Applications **6**, 776 (2012).

[51] F. Merrikh-Bayat, N. Mirebrahimi, and M. R. Khalili, *Discrete-time fractional-order pid controller: Definition, tuning, digital realization and some applications,* International Journal of Control, Automation and Systems **13**, 81 (2015).

[52] J. Cervera and A. Baños, *Automatic loop shaping in qft by using crone structures,* IFAC Proceedings Volumes **39**, 207 (2006).

[53] J. Sabatier, A. Oustaloup, A. G. Iturricha, and P. Lanusse, *Crone control: principles and extension to time-variant plants with asymptotically constant coefficients,* Nonlinear Dynamics **29**, 363 (2002).

[54] P. Lanusse, M. Lopes, J. Sabatier, and B. Feytout, *New optimization criteria for the simplification of the design of third generation crone controllers,* IFAC Proceedings Volumes **46**, 355 (2013).

[55] A. Oustaloup, J. Sabatier, P. Lanusse, R. Malti, P. Melchior, X. Moreau, and M. Moze, *An overview of the crone approach in system analysis, modeling and identification, observation and control,* IFAC Proceedings Volumes **41**, 14254 (2008).

[56] J. Sabatier, S. Poullain, P. Latteux, J. L. Thomas, and A. Oustaloup, *Robust speed control of a low damped electromechanical system based on crone control: application to a four mass experimental test bench,* Nonlinear Dynamics **38**, 383 (2004).

[57] J. Zhong and L. Li, *Tuning fractional-order $PI^{\lambda}D^{\mu}$ controllers for a solid-core magnetic bearing system,* IEEE transactions on control systems technology **23**, 1648 (2015).

[58] B. Saidi, M. Amairi, S. Najar, and M. Aoun, *Bode shaping-based design methods of a fractional order pid controller for uncertain systems,* Nonlinear Dynamics **80**, 1817 (2015).

[59] Y. Chen, T. Bhaskaran, and D. Xue, *Practical tuning rule development for fractional order proportional and integral controllers,* Journal of Computational and Nonlinear Dynamics **3**, 021403 (2008).

[60] T. Hägglund and K. J. Åström, *Revisiting the ziegler-nichols tuning rules for pi control,* Asian Journal of Control **4**, 364 (2002).

[61] T. N. L. Vu and M. Lee, *Analytical design of fractional-order proportional-integral controllers for time-delay processes,* ISA transactions **52**, 583 (2013).

[62] R. De Keyser, C. I. Muresan, and C. M. Ionescu, *A novel auto-tuning method for fractional order pi/pd controllers,* ISA transactions **62**, 268 (2016).

[63] R. M. Schmidt, G. Schitter, and A. Rankers, *The Design of High Performance Mechatronics-: High-Tech Functionality by Multidisciplinary System Integration* (IOS Press, 2014).

[64] A. A. Dastjerdi, N. Saikumar, and S. H. HosseinNia, *Tuning guidelines for fractional order pid controllers: Rules of thumb,* Mechatronics **56**, 26 (2018).

[65] B. Maâmar and M. Rachid, *Imc-pid-fractional-order-filter controllers design for integer order systems,* ISA transactions **53**, 1620 (2014).

[66] J. Cervera, A. Banios, C. A. Monje, and B. M. Vinagre, *Tuning of fractional PID controllers by using qft,* in *IEEE Industrial Electronics, IECON 2006-32nd Annual Conference on* (IEEE, 2006) pp. 5402–5407.

[67] Y. Chen, H. Dou, B. M. Vinagre, and C. A. Monje, *A robust tuning method for fractional order pi controllers,* IFAC Proceedings Volumes **39**, 22 (2006).

[68] Y. Luo, T. Zhang, B. Lee, C. Kang, and Y. Chen, *Fractional-order proportional derivative controller synthesis and implementation for hard-disk-drive servo system,* IEEE Transactions on Control Systems Technology **22**, 281 (2014).

[69] C. I. Muresan, S. Folea, G. Mois, and E. H. Dulf, *Development and implementation of an fpga based fractional order controller for a dc motor,* Mechatronics **23**, 798 (2013).

[70] I. Podlubny, I. Petraš, B. M. Vinagre, P. O'leary, and L. Dorčák, *Analogue realizations of fractional-order controllers,* Nonlinear dynamics **29**, 281 (2002).

[71] B. Vinagre, I. Podlubny, A. Hernandez, and V. Feliu, *Some approximations of fractional order operators used in control theory and applications,* Fractional calculus and applied analysis **3**, 231 (2000).

[72] D. Xue, C. Zhao, and Y. Chen, *A modified approximation method of fractional order system,* in *Mechatronics and Automation, Proceedings of the 2006 IEEE International Conference on* (IEEE, 2006) pp. 1043–1048.

[73] D. Valério and J. Sa da Costa, *Ninteger: A non-integer control toolbox for matlab,* Proceedings of the Fractional Differentiation and its Applications, Bordeaux (2004).

[74] A. Yüce, F. N. Deniz, and N. Tan, *A new integer order approximation table for fractional order derivative operators,* IFAC-PapersOnLine **50**, 9736 (2017).

[75] N. Shrivastava and P. Varshney, *Rational approximation of fractional order systems using carlson method,* in *Soft Computing Techniques and Implementations (ICSCTI), 2015 International Conference on* (IEEE, 2015) pp. 76–80.

[76] A. Tepljakov, E. Petlenkov, and J. Belikov, *Application of newton's method to analog and digital realization of fractional-order controllers,* International Journal of Microelectronics and Computer Science **2**, 45 (2012).

[77] M. V. Aware, A. S. Junghare, S. W. Khubalkar, A. Dhabale, S. Das, and R. Dive, *Design of new practical phase shaping circuit using optimal pole–zero interlacing algorithm for fractional order pid controller,* Analog Integrated Circuits and Signal Processing **91**, 131 (2017).

[78] P. Lino and G. Maione, *Realization of new robust digital fractional-order compensators,* IFAC-PapersOnLine **50**, 8580 (2017).

[79] J. Tenreiro Machado, *Theory of fractional integrals and derivatives, application to motion control,* International Confrerence on Recent Advances in Mechatronics, 1995 (1995).

[80] Y. Chen, B. M. Vinagre, and I. Podlubny, *Continued fraction expansion approaches to discretizing fractional order derivatives—an expository review,* Nonlinear Dynamics **38**, 155 (2004).

[81] R. S. Barbosa, J. T. Machado, and M. F. Silva, *Time domain design of fractional differintegrators using least-squares,* Signal Processing **86**, 2567 (2006).

[82] S. Folea, R. De Keyser, I. R. Birs, C. I. Muresan, and C.-M. Ionescu, *Discrete-time implementation and experimental validation of a fractional order pd controller for vibration suppression in airplane wings,* Acta Polytechnica Hungarica **14**, 191 (2017).

[83] R. De Keyser and C. I. Muresan, *Analysis of a new continuous-to-discrete-time operator for the approximation of fractional order systems,* in *Systems, Man, and Cybernetics (SMC), 2016 IEEE International Conference on* (IEEE, 2016) pp. 003211–003216.

[84] R. De Keyser, C. I. Muresan, and C. M. Ionescu, *An efficient algorithm for low-order direct discrete-time implementation of fractional order transfer functions,* ISA transactions **74**, 229 (2018).

[85] G. Maione, *High-speed digital realizations of fractional operators in the delta domain,* IEEE Transactions on Automatic Control **56**, 697 (2011).

[86] I. Petráš, L. Dorcák, I. Podlubny, J. Terpák, and P. O'Leary, *Implementation of fractional-order controllers on plc b&r 2005,* in *Proceedings of the ICCC* (2005) pp. 24–27.

[87] I. Petráš, *Tuning and implementation methods for fractional-order controllers,* Fractional Calculus and Applied Analysis **15**, 282 (2012).

[88] R. Caponetto, *Fractional order systems: modeling and control applications*, Vol. 72 (World Scientific, 2010).

[89] S. Roy, *On the realization of a constant-argument immittance or fractional operator,* IEEE Transactions on Circuit Theory **14**, 264 (1967).

[90] J. Kvasil and J. Čajka, *An introduction to synthesis of linear circuits,* SNTL/ALFA, Prague (1981).

[91] G. W. Bohannan, *Analog realization of a fractional control element-revisited,* in *Proc. of the 41st IEEE int. conf. on decision and control, tutorial workshop*, Vol. 2 (2002) pp. 203–208.

[92] C. Coopmans, I. Petráš, and Y. Chen, *Analogue fractional-order generalized memristive devices,* in *Proc. of the ASME 2009 International Design Engineering Technical Conferences & Computers and Information in Engineering Conference* (2009).

[93] N. Lachhab, F. Svaricek, F. Wobbe, and H. Rabba, *Fractional order PID controller (FOPID)-toolbox,* in *Control Conference (ECC), 2013 European* (IEEE, 2013) pp. 3694–3699.

[94] A. Tepljakov, E. Petlenkov, and J. Belikov, *Fomcon: Fractional-order modeling and control toolbox for matlab,* in *Mixed Design of Integrated Circuits and Systems (MIXDES), 2011 Proceedings of the 18th International Conference* (IEEE, 2011) pp. 684–689.

[95] X. Dingy, *Fractional-order Control Systems - Fundamentals and Numerical Implementations* (de Gruyter Press, Berlin, 2017).

[96] J. Liu, T. Zhao, and Y. Chen, *Maximum power point tracking with fractional order high pass filter for proton exchange membrane fuel cell,* IEEE/CAA Journal of Automatica Sinica **4**, 70 (2017).

[97] F. Ge, Y. Chen, and C. Kou, *Cyber-physical systems as general distributed parameter systems: three types of fractional order models and emerging research opportunities,* IEEE/CAA Journal of Automatica Sinica **2**, 353 (2015).

[98] K. Cao, Y. Chen, and D. Stuart, *A fractional micro-macro model for crowds of pedestrians based on fractional mean field games,* IEEE/CAA Journal of Automatica sinica **3**, 261 (2016).

[99] S. H. Hosseinnia, I. Tejado, V. Milanés, J. Villagrá, and B. M. Vinagre, *Experimental application of hybrid fractional-order adaptive cruise control at low speed,* IEEE transactions on control systems technology **22**, 2329 (2014).

[100] L. Marinangeli, F. Alijani, and S. H. HosseinNia, *Fractional-order positive position feedback compensator for active vibration control of a smart composite plate,* Journal of Sound and Vibration **412**, 1 (2018).

[101] M. Zarghami, M. Babazadeh, and S. H. Hosseinnia, *Performance enhancement of spark ignition engines by using fractional order controller,* in *Control Conference (ECC), 2016 European* (IEEE, 2016) pp. 1248–1252.

[102] S. E. Hamamci, *An algorithm for stabilization of fractional-order time delay systems using fractional-order PID controllers,* IEEE Transactions on Automatic Control **52**, 1964 (2007).

[103] M. E. Meral and D. Çelík, *A comprehensive survey on control strategies of distributed generation power systems under normal and abnormal conditions,* Annual Reviews in Control (2018).

[104] S. Das, M. Aware, A. Junghare, and S. Khubalkar, *Energy/fuel efficient and enhanced robust systems demonstrated with developed fractional order pid controller,* Innov Ener Res **7**, 2576 (2018).

[105] A. S. Chopade, S. W. Khubalkar, A. Junghare, M. Aware, and S. Das, *Design and implementation of digital fractional order pid controller using optimal pole-zero approximation method for magnetic levitation system,* IEEE/CAA Journal of Automatica Sinica **5**, 977 (2018).

[106] S. Khubalkar, A. Junghare, M. Aware, and S. Das, *Modeling and control of a permanent-magnet brushless dc motor drive using a fractional order proportional-integral-derivative controller,* Turkish Journal of Electrical Engineering & Computer Sciences **25**, 4223 (2017).

[107] C. Ma and Y. Hori, *The application backlash of fractional order control to vibration suppression,* in *American Control Conference, 2004. Proceedings of the 2004*, Vol. 3 (IEEE, 2004) pp. 2901–2906.

[108] S. H. HosseinNia, R. L. Magin, and B. M. Vinagre, *Chaos in fractional and integer order nsg systems,* Signal Processing **107**, 302 (2015).

[109] P. P. Singh and B. K. Roy, *Comparative performances of synchronisation between different classes of chaotic systems using three control techniques,* Annual Reviews in Control **45**, 152 (2018).

[110] I. Tejado, S. H. HosseinNia, D. Torres, B. M. Vinagre, Á. López-Bernal, F. J. Villalobos, L. Testi, and I. Podlubny, *Fractional models for measuring sap velocities in trees,* in *Fractional Differentiation and Its Applications (ICFDA), 2014 International Conference on* (IEEE, 2014) pp. 1–6.

[111] J. Huang, Y. Chen, H. Li, and X. Shi, *Fractional order modeling of human operator behavior with second order controlled plant and experiment research,* IEEE/CAA Journal of Automatica Sinica **3**, 271 (2016).

3

CLOSED-LOOP FREQUENCY ANALYSIS OF RESET CONTROL SYSTEMS

Ali AHMADI DASTJERDI

As was mentioned, to increase the applicability of CgLp compensators in industry, it is necessary to provide a solid frequency-domain frame work for analyzing reset control systems. This chapter introduces a closed-loop frequency analysis tool for reset control systems. To begin with, sufficient conditions for the existence of the steady-state response for a closed-loop system with a reset element driven by periodic references are provided. It is then shown that, under specific conditions, such a steady-state response for periodic inputs is periodic with the same period as the input. Furthermore, a framework to obtain the steady-state response and define a notion of closed-loop frequency response, including high order harmonics, is presented. Finally, pseudo-sensitivities for reset control systems are defined. All of these calculations are embedded in a user-friendly toolbox to make this approach easy of use. To show the effectiveness of the proposed analysis method, the position control problem for a precision positioning stage is studied. In particular, comparison with the results achieved using methods based on the Describing Function shows that the proposed method predicts the closed-loop performance more precisely.

This chapter has been submitted to IEEE-Transaction on Automatic Control.

3.1. INTRODUCTION

PROPORTIONAL Integral Derivative (PID) controllers are used in more than 90% of industrial control applications [1–3]. However, cutting-edge industrial applications have control requirements that cannot be fulfilled by PID controllers. To overcome this problem linear controllers may be substituted by non-linear ones. Reset controllers are one such non-linear controllers which have attracted attention due to their simple structure and their ability to improve closed-loop performance [4–20].

A traditional reset controller consists of a linear element the state of which is reset to zero when the input equals zero. The simplest reset element is the Clegg Integrator (CI), which is a linear integrator with a reset mechanism [4]. To provide design freedom and applicability, reset controllers such as First Order Reset Elements (FORE) [21, 22] and Second Order Reset Elements (SORE) have also been introduced [14]. These reset elements are utilized to construct new compensators to achieve significant performance enhancement [17, 23–27]. In order to further improve the performance of reset control systems several techniques, such as the considerations of non-zero reset values [9, 22], reset bands [28, 29], fixed reset instants, and $PI+CI$ configurations [30–32] have been introduced.

Frequency-domain analysis is preferred in industry since this allows ascertaining closed-loop performance measures in an intuitive way. However, the lack of such methods for non-linear controllers is one of the reasons why non-linear controllers are not widely popular in industry. The Describing Function (DF) method is one of the few methods for approximately studying non-linear controllers in the frequency-domain and this has been widely used also in the literature of reset controllers [9, 17, 27, 33, 34]. The DF method relies on a quasi-linear approximation of the steady-state output of a non-linear system considering only the first harmonic of the Fourier series expansion of the input and output signals (assumed periodic). The general formulation of the DF method for reset controllers is presented in [33], which however does not provide any information on the closed-loop steady-state response.

In this chapter, first, sufficient conditions for the existence of the steady-state response for a closed-loop system with a reset element and driven by a periodic input are given. Then, a notion of closed-loop frequency response for reset control systems, including high order harmonics, is introduced. Pseudo-sensitivities to combine harmonics and facilitate analyzing reset control systems in the closed-loop configuration are then defined. All of these ideas can be utilized to develop a toolbox which is briefly discussed. Furthermore, the method is used to analyze the performance of a precision positioning stage. Note finally that, contrary to the DF method, which provides only approximations for the periodic steady-state response of reset control systems, the proposed tools allow computing exact steady-state responses to periodic excitations.

The chapter is organized as follows. Preliminaries on the frequency analysis for reset controllers are presented in Section 3.2. In Section 3.3 sufficient conditions to define a notion of frequency response are presented. Then, a method to obtain closed-loop frequency responses for reset control systems, including high order harmonics, is developed, and pseudo-sensitivities are defined. In Section 3.4 the steady-state response of reset controllers to periodic inputs is studied. In Section 3.5 the performance of our proposed methods is assessed on an illustrative example. Finally, some concluding remarks

and suggestions for future studies are given in Section 3.6.

3.2. PRELIMINARIES

IN this section frequency-domain descriptions for reset controllers are briefly recalled. The state-space representation of a reset element is given by equations of the form

$$\begin{cases} \dot{x}_r(t) = A_r x_r(t) + B_r r(t), & r(t) \neq 0, \\ x_r(t^+) = A_\rho x(t), & r(t) = 0, \\ u_r(t) = C_r x(t) + D_r r(t), \end{cases} \tag{3.1}$$

in which $x_r(t) \in \mathbb{R}^{n_r}$ are the reset states, $r(t) \in \mathbb{R}$ is an external signal, $u_r(t)$ is the control input, A_r, B_r, C_r and D_r are the dynamic matrices of the reset element, and matrix A_ρ determines the value of the reset states after the reset action. The transfer function $C_r(sI - A_r)^{-1}B_r + D_r$ is called the base transfer function of the reset controller. To study the reset controller (3.1) in the frequency-domain one could use various approaches. For example, in order to find the DF, a sinusoidal reference $r(t) = a_0 \sin(\omega t)$, $\omega > 0$ is applied and the output is approximated by means of the first harmonic of the Fourier series expansion of the steady-state response (provided if exists). In order to have a well-defined steady-state response we assume that A_r has all eigenvalues with negative real part and $A_\rho e^{\frac{A_r \pi}{\omega}}$ has all eigenvalues with magnitude smaller than one [33]. In this case, the state-space representation of the reset element (3.1) can be re-written as

$$\begin{cases} \dot{x}_r(t) = A_r x_r(t) + a_0 B_r \sin(\omega t), & t \neq t_k, \\ x_r(t^+) = A_\rho x(t), & t = t_k, \\ u_r(t) = C_r x(t) + a_0 D_r \sin(\omega t), \end{cases} \tag{3.2}$$

with $\omega > 0$, in which $t_k = \frac{k\pi}{\omega}$, with $k \in \mathbb{N}$, are the reset instants. According to [33], the DF associated to system (3.2) is given by

$$\mathcal{N}_{DF}(\omega) = \frac{a_1(\omega)e^{j\varphi_1(\omega)}}{a_0} = C_r(j\omega I - A_r)^{-1}(I + j\theta(\omega))B_r + D_r, \tag{3.3}$$

where

$$\theta(\omega) = \frac{-2\omega^2}{\pi}(I + e^{\frac{\pi A_r}{\omega}})\left((I + A_\rho e^{\frac{\pi A_r}{\omega}})^{-1}A_\rho(I + e^{\frac{\pi A_r}{\omega}}) - I\right)(\omega^2 I + A_r^2)^{-1}. \tag{3.4}$$

Recently, a new tool, called Higher-Order Sinusoidal Input Describing Functions (HOSIDF), for studying non-linearities in the frequency-domain has been introduced in [35]. In this method a non-linear system is considered as a virtual harmonic generator and the HOSIDF is defined as [35]:

$$H_n(j\omega) = \frac{a_n(\omega)e^{j\varphi_n(a_0,\omega)}}{a_0}, \tag{3.5}$$

in which $a_n(\omega)$ and $\varphi_n(a_0,\omega)$ are the n^{th} components of the Fourier series expansion of the steady-state output of the system to a sinusoidal input. This framework has been

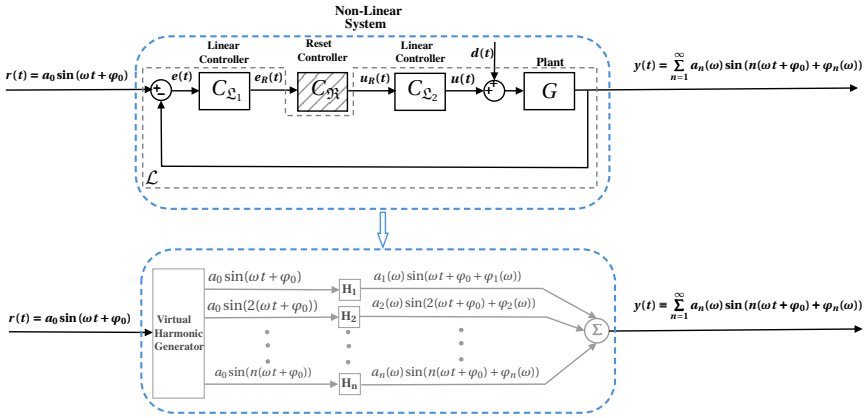

Figure 3.1: Closed-loop architecture with reset controller (top). HOSIDF representation of the closed-loop configuration (bottom).

extended to the reset controller (3.1) in [36] as

$$H_n(j\omega) = \begin{cases} C_r(j\omega I - A_r)^{-1}(I + j\theta(\omega))B_r + D_r, & n = 1, \\ C_r(jn\omega I - A_r)^{-1} j\theta(\omega) B_r, & n > 1 \text{ odd}, \\ 0, & n \text{ even}. \end{cases} \tag{3.6}$$

Note that the above frequency analysis is made simple by the fact that the reset instants are known, that is the reset controller is studied in the open-loop. Frequency properties of reset controllers as part of a closed-loop system in the presence of a periodic reference or disturbance input are much more difficult to study, and are the subject of the next section.

3.3. CLOSED-LOOP FREQUENCY RESPONSE OF RESET CONTROL SYSTEMS

CONSIDER the single-input single-output (SISO) control architecture in the top diagram of Figure. 3.1. This includes as particular cases all schemes discussed in Section 3.1. The closed-loop system consists of a linear plant with transfer function $G(s)$, two linear controllers with proper transfer function $C_{\mathfrak{L}_1}(s)$ and $C_{\mathfrak{L}_2}(s)$, and a reset controller with base transfer function $C_{\mathcal{R}}(s)$. Let $\mathcal{L}$ be the LTI part of the system and assume that $G(s)$ is strictly proper. The state-space realization of $\mathcal{L}$ is described by the equations

$$\mathcal{L}: \begin{cases} \dot{\zeta}(t) = A\zeta(t) + Bw(t) + B_u u_R(t), \\ u(t) = C_u\zeta(t) + D_u r(t), \\ e_R(t) = C_{e_R}\zeta(t) + D_{e_R} r(t), \\ y(t) = C\zeta(t), \end{cases} \tag{3.7}$$

where $\zeta(t) \in \mathbb{R}^{n_p}$ describes the states of the plant and of the linear controllers (n_p is the number of states of the linear part), A, B, C, B_u, C_{e_R}, C_u, D_u and D_{e_R} are the correspond-

ing dynamic matrices, $y(t) \in \mathbb{R}$ is the output of the plant and $w(t) = [r(t)\ d(t)]^T \in \mathbb{R}^2$ is an external input. The state-space representation of the reset controller is given by the equations

$$\begin{cases} \dot{x}_r(t) = A_r x_r(t) + B_r e_R(t), & e_R(t) \neq 0, \\ x_r(t^+) = A_\rho x_r(t), & e_R(t) = 0, \\ u_R(t) = C_r x_r(t) + D_r e_R(t). \end{cases} \tag{3.8}$$

The closed-loop state-space representation of the overall system can, therefore, be written as

$$\begin{cases} \dot{x}(t) = \bar{A}x(t) + \bar{B}w(t), & e_R(t) \neq 0, \\ x(t^+) = \bar{A}_\rho x(t), & e_R(t) = 0, \\ u(t) = \bar{C}_u x(t) + \bar{D}_u r(t), \\ e_R(t) = \bar{C}_{e_R} x(t) + D_{e_R} r(t), \\ y(t) = \bar{C}x(t), \end{cases} \tag{3.9}$$

where $x(t) = [x_r(t)^T \quad \zeta(t)^T]^T \in \mathbb{R}^{n_p+n_r}$, and $\bar{A} = \begin{bmatrix} A_r & B_r C_{eR} \\ B_u C_r & A + B_u D_r C_{eR} \end{bmatrix}$, $\bar{C} = \begin{bmatrix} 0_{1\times n_r} & C \end{bmatrix}$, $\bar{B} = \begin{bmatrix} 0_{n_r\times 2} \\ B \end{bmatrix} + \begin{bmatrix} B_r D_{eR} & 0_{n_r\times 1} \\ B_u D_r D_{eR} & 0_{n_p\times 1} \end{bmatrix}$, $\bar{A}_\rho = \begin{bmatrix} A_\rho & 0_{n_r\times n_p} \\ 0_{n_p\times n_r} & I_{n_p\times n_p} \end{bmatrix}$, $\bar{C}_{e_R} = \begin{bmatrix} 0_{1\times n_r} & C_{e_R} \end{bmatrix}$, $\bar{C}_u = \begin{bmatrix} C_r D_{\mathfrak{L}_2} & C_{e_R} D_r D_{\mathfrak{L}_2} + C_u \end{bmatrix}$, and $\bar{D}_u = D_u D_{e_R} D_r$ with $D_{\mathfrak{L}_2}$ the feedthrough matrix of $C_{\mathfrak{L}_2}(s)$.

3.3.1. STABILITY AND CONVERGENCE

In this section sufficient conditions for the existence of a steady-state solution for the closed-loop reset control system (3.9) driven by periodic inputs is provided. This is based on the H_β condition [5, 37–39], which we recall in what follows. Let

$$C_0 = \begin{bmatrix} \rho & \beta C_{eR} \end{bmatrix}, \quad B_0 = \begin{bmatrix} I_{n_r\times n_r} \\ 0_{n_p\times n_r} \end{bmatrix}, \quad \rho = \rho^T > 0, \quad \rho \in \mathbb{R}^{n_r\times n_r}, \quad \beta \in \mathbb{R}^{n_r\times 1}. \tag{3.10}$$

The H_β condition states that the reset control system (3.9) with $w = 0$ is quadratically stable if and only if there exist $\rho = \rho^T > 0$ and β such that the transfer function

$$H(s) = C_0(sI - \bar{A})^{-1}B_0 \tag{3.11}$$

is Strictly Positive Real (SPR), $(\bar{A}, B_0)$ and $(\bar{A}, C_0)$ are controllable and observable, respectively, and

$$A_\rho^T \rho A_\rho - \rho < 0. \tag{3.12}$$

Definition 1. *A time $\bar{T} > 0$ is called a reset instant for the reset control system (3.9) if $e_R(\bar{T}) = 0$. For any given initial condition and input w the resulting set of all reset instants defines the reset sequence $\{t_k\}$, with $t_k \leq t_{k+1}$, for all $k \in \mathbb{N}$. The reset instants t_k of the reset control system (3.9) have the well-posedness property if for any initial condition x_0 and any input w, all reset instants are distinct, and there exists a $\lambda > 0$ such that for all $k \in \mathbb{N}$, $\lambda \leq t_{k+1} - t_k$ [9, 40].*

Remark 1. If the H_β condition holds, then the reset control system (3.9) has the uniform bounded-input bounded-state (UBIBS) property and the reset instants have the well-posedness property (see Lemma 5 in Chapter 4). Therefore, the reset control system (3.9) has a unique well-defined solution for $t \geq t_0$ for any initial condition x_0 and input $w(t)$ which is a Bohl function [9, 40].

To develop a frequency analysis for the reset control system (3.9), the following assumption is required.

Assumption 1. *The initial condition of the reset controller is zero. In addition, there are infinitely many reset instants and* $\lim_{k\to\infty} t_k = \infty$.

The second term in Assumption 1 is introduced to rule out a trivial situation. In fact, if $\lim_{k\to\infty} t_k = T_K$, then for all $t \geq T_K$ the reset control system (3.9) is a stable linear system. Two important technical lemmas, which are used in the proof of the following theorem, are now formulated and proved.

Lemma 1. *Let* $\{t_k\}$ *and* $\{\tilde{t}_k\}$ *be the reset sequences of the reset control system (3.9) for two different initial conditions* ζ_0 *and* $\tilde{\zeta}_0$ *of the linear part and for the same input. Suppose Assumption 1 and the* H_β *condition hold and* w *is a Bohl function. Then* $\lim_{k\to\infty}(t_k - \tilde{t}_k) = 0$.

Proof. To begin with note that, for any initial condition $x_0 = \begin{bmatrix} 0^T & \zeta_0^T \end{bmatrix}^T$, the signal $e_R(t)$ in (3.9) can be obtained through the equation (see Lemma 3 in the Appendix 3.A)

$$\begin{cases} \dot{x}_I(t) = \bar{A}x_I(t) + \bar{B}w(t) + \begin{bmatrix} B_r \\ 0_{n_p\times 2} \end{bmatrix} w_I(t), & e_R(t) \neq 0, \\ x_I(t^+) = \bar{A}_\rho x_I(t), & e_R(t) = 0, \\ e_R(t) = \bar{C}_{e_R} x_I(t) + D_{e_R} r(t) + [1\ 0]\, w_I(t), \end{cases} \tag{3.13}$$

with $x_I(0) = 0$ and

$$\begin{cases} \dot{Z}(t) = AZ(t), \\ w_I(t) = \begin{bmatrix} C_{eR} \\ 0 \end{bmatrix} Z(t), \end{cases} \quad Z(0) = \zeta_0. \tag{3.14}$$

Since the linear part of the system contains the internal model (3.14) of w_I, and $w(t)$ is a Bohl function, based on [5, 38] $e_R(t)$ is asymptotically independent of $w_I(t)$. This implies that $\lim_{k\to\infty}(t_k - \tilde{t}_k) = 0$. □

Lemma 2. *Consider the reset control system (3.9). Suppose Assumption 1 holds,* w *is a Bohl function, and the* H_β *condition is satisfied. Then the reset control system (3.9) is uniformly exponentially convergent.*

Proof. To begin with note that the property of uniformly exponentially convergence is as given in [41]. Since the H_β condition is satisfied, according to Remark 1, the reset control system (3.9) has a unique well-defined solution for any initial condition x_0 and any w which is a Bohl function. Let x and $\tilde{x}$ be two solutions of the reset control system (3.9) corresponding to the some input w and to two different initial conditions. Since the H_β

condition is satisfied $x(t)$ and $\tilde{x}(t)$ are bounded for all t. Let $\Delta x := x(t) - \tilde{x}(t)$, and let $\{t_k\}$ and $\{\tilde{t}_k\}$ be the reset sequences of $x(t)$ and $\tilde{x}(t)$. Define $\mathcal{M} = \{t \in \mathbb{R}^+ |\ t \neq t_k \wedge t \neq \tilde{t}_k\}$. By Lemma 1

$$\forall\ \delta > 0,\ \exists\ \Pi > 0 \text{ such that } k > \Pi \Rightarrow |t_k - \tilde{t}_k| < \delta. \tag{3.15}$$

Moreover, by the well-posedness property, there exists a $\lambda > 0$ such that $\lambda \leq t_{k+1} - t_k$ and $\lambda \leq \tilde{t}_{k+1} - \tilde{t}_k$. Thus, selecting δ sufficiently small yields

$$x(t_k + \delta) = e^{\bar{A}\delta}\bar{A}_\rho x(t_k) + \int_{t_k}^{t_k+\delta} e^{\bar{A}(t_k+\delta-\tau)}\bar{B}w(\tau)d\tau, \tag{3.16}$$

for all t_k sufficiently large. By (3.15), $\tilde{t}_k = t_k + \delta'$, with $0 \leq \delta' \leq \delta$. Thus

$$\tilde{x}(t_k+\delta) = e^{\bar{A}(\delta-\delta')}\bar{A}_\rho\left(e^{\bar{A}\delta'}\tilde{x}(t_k) + \int_{t_k}^{t_k+\delta'} e^{\bar{A}(t_k+\delta'-\tau)}\bar{B}w(\tau)d\tau\right) + \int_{t_k+\delta'}^{t_k+\delta} e^{\bar{A}(t_k+\delta-\tau)}\bar{B}w(\tau)d\tau. \tag{3.17}$$

Now, by (3.16) and (3.17)

$$\begin{aligned}\Delta x(t_k+\delta) =& \bar{A}_\rho\Delta x(t_k) + (e^{\bar{A}\delta}\bar{A}_\rho - e^{\bar{A}(\delta-\delta')}\bar{A}_\rho e^{\bar{A}\delta'})\tilde{x}(t_k)\int_{t_k}^{t_k+\delta'} e^{\bar{A}(t_k+\delta-\tau)}\bar{B}w(\tau)d\tau \\ &- e^{\bar{A}(\delta-\delta')}\bar{A}_\rho\int_{t_k}^{t_k+\delta'} e^{\bar{A}(t_k+\delta'-\tau)}\bar{B}w(\tau)d\tau - (e^{\bar{A}\delta} - I)\bar{A}_\rho\Delta x(t_k) \\ =& \bar{A}_\rho\Delta x(t_k) + O(\delta, \tilde{x}(t_k), x(t_k)),\end{aligned} \tag{3.18}$$

and, using (3.15), $\lim_{k\to\infty} O(\delta, \tilde{x}(t_k), x(t_k)) = 0$. The same discussion applies for $\tilde{t}_k$. Hence, for t sufficiently large we have

$$\begin{cases}\Delta\dot{x}(t) = \bar{A}\Delta x(t), & t \in \mathcal{M},\\ \Delta x(t^+) = \bar{A}_\rho\Delta x(t), & t \notin \mathcal{M}.\end{cases} \tag{3.19}$$

Due to the satisfaction of the H_β condition [5, 37, 38], there exist a matrix $P = P^T > 0$, $P \in \mathbb{R}^{(n_p+n_r)\times(n_p+n_r)}$, and a scalar $\alpha > 0$ such that

$$P\bar{A} + \bar{A}^T P \leq -2\alpha P, \tag{3.20}$$

$$\bar{A}_\rho^T P\bar{A}_\rho - P \leq 0. \tag{3.21}$$

Using the candidate Lyapunov function $V(\Delta x) = \frac{1}{2}(\Delta x)^T P(\Delta x)$ yields

$$\begin{cases}\dot{V} \leq -\alpha V, & t \in \mathcal{M},\\ V(\Delta x(t^+)) = V(\Delta x(t)) + \Xi(t,\delta), & t \notin \mathcal{M}.\end{cases} \tag{3.22}$$

Thus, using (3.19) and (3.21) for t sufficiently large yields $\Xi(t,\delta) \leq 0$. Hence, since Δx is bounded, there exist $\alpha_m > 0$ and $\mathcal{K} > 0$ such that

$$||x_2(t) - x_1(t)||_P^2 \leq \mathcal{K}e^{-\alpha_m t}, \tag{3.23}$$

for all $t \geq 0$ (see Lemma 4 in the Appendix 3.B). This implies that the reset control system (3.9) is uniformly exponentially convergent. □

Theorem 1. *Consider the reset control system (3.9). Suppose Assumption 1 holds, $w(t) = w_0 \sin(\omega t)$[1], and the H_β condition is satisfied. Then the reset control system (3.9) has a periodic steady-state solution which can be expressed as $\bar{x}(t) = \mathcal{S}(\sin(\omega t), \cos(\omega t), \omega)$ for some function $\mathcal{S} : \mathbb{R}^3 \to \mathbb{R}^{n_r+n_p}$.*

Proof. Since the H_β condition holds and $w(t) = w_0 \sin(\omega t)$ is a Bohl function, by Remark 1 the reset control system (3.9) has a unique solution for any initial condition x_0. In addition, the reset control system (3.9) has the UBIBS property and, according to Lemma 2, it is uniformly exponentially convergent. Hence, the proof of the existence of the function $\mathcal{S}$ relies on the results in [41]. We only need to show that $\mathcal{S}$ is unique. To this end, similarly to [42], assume that the reset control system (3.9) has two steady-state solutions $\bar{x}_2(t) = \mathcal{S}_2(\sin(\omega t), \cos(\omega t), \omega)(t)$ and $\bar{x}_1(t) = \mathcal{S}_1(\sin(\omega t), \cos(\omega t), \omega)(t)$, for $w(t) = w_0 \sin(\omega t)$. Since the H_β condition holds, by Lemma 2 there exist $\alpha_m > 0$ and $\mathcal{K} > 0$ such that

$$||\bar{x}_2(t) - \bar{x}_1(t)||_P^2 \leq \mathcal{K} e^{-\alpha_m t}, \tag{3.24}$$

hence, the claim. □

Corollary 1. *Consider the reset control system (3.9) with $r(t) = r_0 \sin(\omega t)$ and $d = 0$, for all $t \geq 0$. Then the even harmonics and the subharmonics of the steady-state response have zero amplitude, and the sequence of reset instants is periodic with period $\frac{\pi}{\omega}$.*

Proof. The response of (3.9) for $r = r_0 \sin(\omega t)$ and $d = 0$, for all $t \geq 0$, is given by

$$x(t) = r_0 \left(e^{\bar{A}(t-t_k)} \left(\xi_k + \psi(t_k) \right) - \psi(t) \right), \quad t \in (t_k, t_{k+1}], \tag{3.25}$$

where

$$\begin{aligned} \psi(t) &= (\omega I \cos(\omega t) + \bar{A} \sin(\omega t))\mathcal{F}, \ \mathcal{F} = (\omega^2 I + \bar{A}^2)^{-1} \bar{B} \begin{bmatrix} 1 \\ 0 \end{bmatrix}, \\ t_k &= \{ t_k \in \mathbb{R}^+, \ k \in \mathbb{Z}^+ \mid e_R(t_k) = 0 \}, \ \xi_k = \frac{1}{r_0} x(t_k^+) = \frac{1}{r_0} \bar{A}_\rho x(t_k). \end{aligned} \tag{3.26}$$

Thus

$$\bar{x}(t) = r_0 \left(e^{\bar{A}(t-t_s)} \left(\xi_s + \psi(t_s) \right) - \psi(t) \right), \quad t \in (t_s, t_{s+1}], \tag{3.27}$$

with

$$\begin{aligned} \xi_s = \bar{A}_\rho e^{\bar{A}(t_s - t_{s-1})} \Big(& \bar{A}_\rho e^{\bar{A}(t_{s-1} - t_{s-2})} \dots \bar{A}_\rho e^{\bar{A}(t_1 - t_0)} (\xi_0 + \psi(t_0)) + \bar{A}_\rho e^{\bar{A}(t_{s-1} - t_{s-2})} \dots \bar{A}_\rho e^{\bar{A}(t_2 - t_1)} \\ & (I - \bar{A}_\rho)\psi(t_1) + \bar{A}_\rho e^{\bar{A}(t_{s-1} - t_{s-2})} \dots \bar{A}_\rho e^{\bar{A}(t_2 - t_1)} (I - \bar{A}_\rho)\psi(t_2) + \dots + (I - \bar{A}_\rho)\psi(t_{s-1}) \Big) \\ & - \bar{A}_\rho \psi(t_s). \end{aligned} \tag{3.28}$$

According to [43], uniformly convergent systems forget their initial conditions. By Lemma 1 and Lemma 2, ξ_s and the reset instants are unique for any t_0 and ζ_0. Hence, the transient

[1] For ease of the notation we consider $w(t) = w_0 \sin(\omega t)$. However, Theorem 1 is also applicable in the case in which $w(t) = [r_0 \sin(\omega_t + \phi_1) \ d_0 \sin(\omega_t + \phi_2)]^T$.

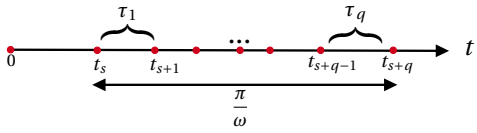

Figure 3.2: Steady-state reset instants of the reset control system (3.9)

response of ξ_s converges to zero which implies that

$$\begin{aligned}\xi_s = \bar{A}_\rho e^{\bar{A}(t_s-t_{s-1})}\Big((I-\bar{A}_\rho)\psi(t_{s-1}) + \bar{A}_\rho e^{\bar{A}(t_{s-1}-t_{s-2})}(I-\bar{A}_\rho)\psi(t_{s-2}) \\ + \bar{A}_\rho e^{\bar{A}(t_{s-1}-t_{s-2})}\bar{A}_\rho e^{\bar{A}(t_{s-2}-t_{s-3})}(I-\bar{A}_\rho)\psi(t_{s-3}) + \dots \\ + \bar{A}_\rho e^{\bar{A}(t_{s-1}-t_{s-2})}\dots\ \bar{A}_\rho e^{\bar{A}(t_{s-m+1}-t_{s-m})}(I-\bar{A}_\rho)\psi(t_{s-m})\Big) - \bar{A}_\rho\psi(t_s). \end{aligned} \tag{3.29}$$

Therefore, since reset occurs when

$$\bar{C}_{e_R}\bar{x}(t) + D_{e_R} r_0 \sin(\omega t) = 0, \tag{3.30}$$

if $\{t_s, t_{s-1}, ..., t_{s-m}\}$ are reset instants and satisfy (3.30), then $\{t_s, t_{s-1}, ..., t_{s-m}\} + \frac{\pi}{\omega}$ also satisfy (3.30), which implies that the sequence of reset instants is periodic with period $\frac{\pi}{\omega}$. Using this property in (3.27) shows that $\bar{x}(t) = -\bar{x}(t+\frac{\pi}{\omega})$ and $t_{s+q} - t_s = \frac{\pi}{\omega}$, hence $\xi_s = -\xi_{s+q}$. This means that the even harmonics of the steady-state response of the reset control system (3.9) have zero amplitude. In addition, $\bar{x}(t) = \bar{x}(t+\frac{2\pi}{\omega})$, which implies that the steady-state response of the reset control system (3.9) does not contain any sub-harmonic. □

Remark 2. The reset sequence $\{t_k\}$ and the reset values ζ_k are independent of the input amplitude for $r(t) = r_0\sin(\omega_t)$.

We now show that the function $\mathcal{S}$ can be derived explicitly for $r(t) = r_0\sin(\omega_t)$ and $d = 0$. Suppose there are $q-1$ reset instants between t_s and $t_s + \frac{\pi}{\omega}$ (Figure. 3.2). Assume $\sin(\omega t_s) = \kappa$, then $\cos(\omega t_s) = \pm\sqrt{1-\kappa^2}$ (without loss of generality we consider the positive value). Using trigonometry relations, one has that

$$\begin{aligned}\psi(t_s) &= f_0(\kappa), \\ \psi(t_s+\tau_1) &= f_1(\kappa,\tau_1), \\ &\vdots \\ \psi(t_s+\tau_1+\dots+\tau_q) &= f_q(\kappa,\tau_1,\tau_2,...,\tau_q).\end{aligned} \tag{3.31}$$

Moreover,

$$\xi_{s+i} = \underbrace{\bar{A}_\rho\Big(e^{\bar{A}\tau_i}(g_{i-1}(\kappa,\xi_s,\tau_1,..,\tau_{i-1}) + f_{i-1}(\kappa,\tau_1,..,\tau_{i-1})) - f_i(\kappa,\tau_1,\tau_2,...,\tau_i)\Big)}_{g_i(\kappa,\xi_s,\tau_1,\tau_2,...,\tau_i)}, \tag{3.32}$$

with $i = 1,2,...,q$ and $g_0(\kappa,\xi_s) = \xi_s$. Now, since $e_R(t)$ is zero at reset instants, one has that

$$E_i(\kappa,\xi_s,\tau_1,...,\tau_i) = \bar{C}_{e_R}\left(e^{\bar{A}\tau_i}(g_{i-1}(\kappa,\xi_s,\tau_1,..,\tau_{i-1}) + f_{i-1}(\kappa,\tau_1,..,\tau_{i-1})) - f_i(\kappa,\tau_1,\tau_2,...,\tau_i)\right) + D_{eR}\sin(\omega(t_s+\tau_1+...+\tau_i)) = 0 \tag{3.33}$$

with $i = 1,2,...,q$. In addition,

$$\begin{aligned} \tau_1+\tau_2+...+\tau_q &= \frac{\pi}{\omega}, \\ \xi_s = -\xi_{s+q} \Rightarrow g_q(\kappa,\xi_s,\tau_1,\tau_2,...,\tau_q) + \xi_s &= 0. \end{aligned} \tag{3.34}$$

Moreover, by the well-posedness property of reset instants (see Definition 1), reset instants are distinct. Hence, there are $q+2$ independent equations and $q+2$ parameters $(\kappa,\xi_s,q,\tau_1,\tau_2,...,\tau_q)$, $q \in \mathbb{N}$. In addition, the well-posedness property implies that the reset intervals are lower bounded [9]. Hence,

$$\exists\, \lambda \le \tau_i \Rightarrow q \le \frac{\pi}{\lambda\omega} - 1. \tag{3.35}$$

Furthermore, for $q = 1$, the equations have always a unique solution. Thus, there exists a bounded non-empty set $Q = \{Q_i \in \mathbb{N} | Q_i \le q_{\max}\}$ such that for $q \in Q$, the equations have a solution. Hence, $\bar{x}(t)$, the steady-state response of the reset control system (3.9) to $r(t) = r_0\sin(\omega t)$, is the solution of (3.33)-(3.34) for $q = q_{\max}$. Since $\bar{x}(t)$ is periodic with period $\frac{2\pi}{\omega}$, one has

$$\bar{x}(t) = \sum_{n=1}^{\infty} a_n\cos((2n+1)\omega t) + b_n\sin((2n+1)\omega t). \tag{3.36}$$

According to Theorem 1, $\bar{x}$ is unique and equal to the function $\mathcal{S}$. Thus,

$$\bar{x}(t) = \sum_{n=1}^{\infty} a_n\cos((2n+1)\omega t) + b_n\sin((2n+1)\omega t) = \mathcal{S}(\sin(\omega t),\cos(\omega t),\omega). \tag{3.37}$$

Finally, one could also use De Moivre's formula to find a formal polynomial expansion for $\mathcal{S}$ in terms of $\sin(\omega t)$ and $\cos(\omega t)$.

3.3.2. HOSIDF OF THE CLOSED-LOOP RESET CONTROL SYSTEMS

In Section 3.3.1 sufficient conditions for the existence of the steady-state solution for the reset control system (3.9) driven by periodic inputs have been presented. Moreover, the steady-state solution has been explicitly calculated. In this section the HOSIDF technique [35] is applied to the steady-state response of the system to derive a notion of frequency response for the reset control system (3.9), which allows analyzing tracking and disturbance rejection performance (see the bottom diagram of Figure. 3.1).

TRACKING PERFORMANCE

Consider the reset control system (3.9) with $r(t) = r_0\sin(\omega t)$ and $d(t) = 0$, for all $t \ge 0$. We now derive relations between the input $r(t)$ and the steady-state response of the

output y, of the error e, and of the control input u. To this end, consider the steady-state reset instants $t_s, t_{s+1}, ..., t_{s+q}$ and their associated reset values $\xi_s, \xi_{s+1}, ..., \xi_{s+q}$ which are calculated through (3.33) and (3.34).

Theorem 2. *Consider the reset control system (3.9) with $r(t) = r_0 \sin(\omega t)$ and $d(t) = 0$, for all $t \geq 0$. Let $T_n(j\omega)$ be the ratio of the n^{th} harmonic component of the output signal y to the first harmonic component of r. Then*

$$T_n(j\omega) = \begin{cases} \frac{2j\omega\bar{C}}{\pi}(\bar{A} - j\omega I)^{-1}(\sum_{i=1}^{q}\mathcal{R}(i,1,\omega)) - \bar{C}(j\omega I + \bar{A})\mathcal{F}, & n = 1, \\ \frac{2j\omega\bar{C}}{\pi}(\bar{A} - jn\omega I)^{-1}(\sum_{i=1}^{q}\mathcal{R}(i,n,\omega)), & n > 1 \text{ odd}, \\ 0, & n \text{ even}, \end{cases} \tag{3.38}$$

in which

$$\mathcal{R}(i,n,\omega) = \left(\frac{e^{\bar{A}(t_{s+i} - t_{s+i-1})}}{e^{jn\omega t_{s+i}}} - \frac{I}{e^{jn\omega t_{s+i-1}}}\right)\left(\xi_{s+i-1} + \psi(t_{s+i-1})\right). \tag{3.39}$$

Proof. By [33, 35]

$$T_n(j\omega) = \frac{\int_{t_s}^{t_s + \frac{2\pi}{\omega}} y(t)e^{-jn\omega t}dt}{\int_{t_s}^{t_s + \frac{2\pi}{\omega}} r_0 \sin(\omega t)e^{-j\omega t}dt}. \tag{3.40}$$

Using (3.27), (3.40) is rewritten as

$$T_n(j\omega) = \frac{j\omega\bar{C}}{\pi}\left(\sum_{i=1}^{2q}\left(\int_{t_{s+i-1}}^{t_{s+i}} \mathcal{X}_i(t)e^{-jn\omega t}dt\right) - \int_{t_s}^{t_s + \frac{2\pi}{\omega}} \psi(t)e^{-jn\omega t}dt\right), \tag{3.41}$$

where

$$\mathcal{X}_i(t) = e^{\bar{A}(t - t_{s+i-1})}\left(\xi_{s+i-1} + \psi(t_{s+i-1})\right). \tag{3.42}$$

For n even the first part of (3.41) is zero by Corollary 1, while for n odd one has

$$\begin{aligned} \int_{t_{s+i-1}}^{t_{s+i}} \mathcal{X}_i(t)e^{-jn\omega t}dt &= \int_{t_{s+i-1}}^{t_{s+i}} e^{\bar{A}(t - t_{s+i-1})}\left(\xi_{s+i-1} + \psi(t_{s+i-1})\right)e^{-jn\omega t}dt \\ &= \int_{t_{s+i-1} + \frac{\pi}{\omega}}^{t_{s+i} + \frac{\pi}{\omega}} e^{\bar{A}(t - t_{s+i-1})}\left(-\xi_{s+i-1} - \psi(t_{s+i-1})\right)\frac{e^{-jn\omega t}}{e^{-jn\pi}}dt \\ &= \int_{t_{s+i-1} + \frac{\pi}{\omega}}^{t_{s+i} + \frac{\pi}{\omega}} \mathcal{X}_i(t)e^{-jn\omega t}dt = (A - jn\omega I)^{-1}\mathcal{R}_{(i,n)}, \end{aligned} \tag{3.43}$$

while the second term in (3.41) is given by

$$\int_{t_{ss_0}}^{t_{ss_m}} \psi(t)e^{-jn\omega dt} = \begin{cases} \pi(I - \frac{j\bar{A}}{\omega})\mathcal{F}, & n = 1, \\ 0, & n > 2. \end{cases} \tag{3.44}$$

Thus, substituting (3.43) and (3.44) to (3.41) yields the claim. □

Definition 2. *The family of complex valued functions $T_n(j\omega)$, $n = 1,2,...$ is the complementary sensitivity of the reset control system (3.9).*

Corollary 2. *Consider the reset control system (3.9) with $r(t) = r_0 \sin(\omega t)$ and $d(t) = 0$, for all $t \geq 0$. Let $S_n(j\omega)$ be the ratio of the n^{th} harmonic component of the error signal e to the first harmonic component of r. Then*

$$S_n(j\omega) + T_n(j\omega) = \begin{cases} 1, & n = 1, \\ 0, & n > 1. \end{cases} \tag{3.45}$$

Corollary 3. *Consider the reset control system (3.9) with $r(t) = r_0 \sin(\omega t)$ and $d(t) = 0$, for all $t \geq 0$. Let $CS_n(j\omega)$ be the ratio of the n^{th} harmonic component of the control input signal u to the first harmonic component of r. If the plant is stable, then*

$$CS_n(j\omega) = \frac{T_n(j\omega)}{G(nj\omega)}. \tag{3.46}$$

Definition 3. *The families of complex valued functions $S_n(j\omega)$ and $CS_n(j\omega)$, $n = 1,2,...$, are the sensitivity and the control sensitivity of the reset control system (3.9), respectively.*

DISTURBANCE REJECTION

In this section relations between $d(t) = \sin(\omega t)$ and the error $e(t)$ and the control input $u(t)$ are found in the case in which $r(t) = 0$ for the reset control system (3.9) using the same procedure provided in Section 3.3.2. The matrix $\psi(t)$ has to be replaced by

$$\begin{aligned} \psi_{\mathcal{D}}(t) &= (\omega I \cos(\omega t) + \bar{A} \sin(\omega t)) \mathcal{F}_{\mathcal{D}}, \\ \mathcal{F}_{\mathcal{D}} &= (\omega^2 I + \bar{A}^2)^{-1} \bar{B} \begin{bmatrix} 0 \\ 1 \end{bmatrix}. \end{aligned} \tag{3.47}$$

Let $t'_s, t'_{s+1}, ..., t'_{s+q'}$ and $\xi'_s, \xi'_{s+1}, ..., \xi'_{s+q'}$ be the steady-state reset instants and their associated reset values for the reset control system (3.9) with $d(t) = d_0 \sin(\omega t)$ and $r(t) = 0$, respectively. In addition, since $r(t) = 0$, (3.33) is changed to

$$\underbrace{\bar{C}_{e_R}\left(e^{\bar{A}\tau'_i}(g_{i-1}(\kappa', \xi'_s, \tau'_1, .., \tau'_{i-1}) + f_{i-1}(\kappa', \tau'_1, .., \tau'_{i-1})) - f_i(\kappa', \tau'_1, \tau'_2, ..., \tau'_i)\right)}_{E_i(\kappa', \xi'_s, \tau'_1, ..., \tau'_i)} = 0, \tag{3.48}$$

with $i = 1,2,...,q'$. Now, substituting $\psi(t)$ with $\psi_{\mathcal{D}}(t)$ in relations (3.31) and (3.32), and considering (3.48) instead of (3.33), the steady-state response of the reset control system (3.9) for $d(t) = d_0 \sin(\omega t)$ and $r(t) = 0$ can be found using the same procedure provided in Section 3.3.1.

Corollary 4. *Consider the reset control system (3.9) with $d(t) = d_0 \sin(\omega t)$ and $r(t) = 0$, for all $t \geq 0$. Let $PS_n(j\omega)$ be the ratio of the n^{th} harmonic component of the error signal e*

to the first harmonic component of d. Then

$$PS_n(j\omega) = \begin{cases} \frac{2j\omega\bar{C}}{\pi}(j\omega I - \bar{A})^{-1}(\sum_{i=1}^{q'}\mathcal{R}_{\mathcal{D}}(i,1,\omega)) + \bar{C}(j\omega I + \bar{A})\mathcal{F}_{\mathcal{D}}, & n = 1, \\ \frac{2j\omega\bar{C}}{\pi}(jn\omega I - \bar{A})^{-1}(\sum_{i=1}^{q'}\mathcal{R}_{\mathcal{D}}(i,n,\omega)), & n > 1 \text{ odd}, \\ 0, & n \text{ even}, \end{cases} \tag{3.49}$$

in which

$$\mathcal{R}_{\mathcal{D}}(i,n,\omega) = \left(\frac{e^{\bar{A}(t'_{s+i} - t'_{s+i-1})}}{e^{jn\omega t'_{s+i}}} - \frac{I}{e^{jn\omega t'_{s+i-1}}}\right)\left(\xi'_{s+i-1}\psi_{\mathcal{D}}(t'_{s+i-1})\right). \tag{3.50}$$

Corollary 5. *Consider the reset control system (3.9) with $d(t) = d_0\sin(\omega t)$ and $r(t) = 0$, for all $t \geq 0$. Let $CS_{d_n}(j\omega)$ be the ratio of the n^{th} harmonic component of the control input signal u to the first harmonic component of d. If the plant is stable, then*

$$CS_{d_n}(j\omega) = \begin{cases} \frac{-PS_1(j\omega)}{G(j\omega)} - 1, & n = 1, \\ \frac{-PS_n(j\omega)}{G(nj\omega)}, & n > 1. \end{cases} \tag{3.51}$$

Definition 4. *The families of complex valued functions $PS_n(j\omega)$ and $CS_{d_n}(j\omega)$, $n = 1, 2, \ldots$, are the process-sensitivity and the control sensitivity due to the presence of the disturbance of the reset control system (3.9), respectively.*

3.3.3. PSEUDO-SENSITIVITIES FOR RESET CONTROL SYSTEMS

The analysis of the error signal e and of the control input u is one of the main factors while designing a controller. In linear systems this analysis is performed using the closed-loop transfer functions [44]. As discussed in Section 3.1, although reset control systems may be analyzed using the DF of the reset controller in the closed-loop sensitivity equations, this yields an approximation which is not precise due to the existence of high order harmonics. On the other hand, it is not trivial to analyze reset controllers considering all harmonics. In order to perform the analysis of reset control systems straightforwardly we combine all harmonics into one frequency function for each closed-loop frequency response. In the literature, there are several studies about definition of Bode plot for non-linear systems [45, 46]. However, all of these focus only on the gain of the system. In the following, pseudo-sensitivities, which have both gain and phase components, are defined.

It has been proven that the error and the control input signals of the reset control system (3.9) are periodic with period $\frac{2\pi}{\omega}$ (Figure. 3.3) under provided conditions Theorem 1. We define the pseudo-sensitivity as the ratio of the maximum error of the reset control system (3.9), for $r(t) = r_0\sin(\omega t)$ and $d(t) = 0$, for all $t \geq 0$, to the amplitude of the reference at each frequency.

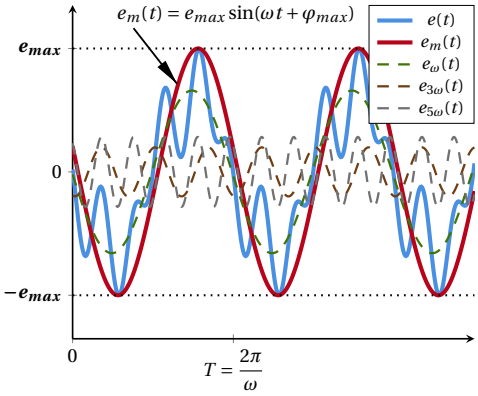

Figure 3.3: The error signal $e(t)$ with its 1st, 3rd, and 5th harmonics. $e_m(t)$ is fitted to $e(t)$ and it is an indicator of the maximum error of the system.

Definition 5. *The Pseudo-sensitivity S_∞ is, for all $\omega \in \mathbb{R}^+$,*

$$S_\infty(j\omega) = e_{\max}(\omega)e^{j\varphi_{\max}(\omega)},$$

where $\varphi_{\max} = \frac{\pi}{2} - \omega t_{\max}$,

$$e_{\max}(\omega) = \frac{\max\limits_{t_s \le t \le t_{s+2q}} (r(t) - y(t))}{r_0} = \sin(\omega t_{\max}) - \frac{1}{r_0}\bar{C}\bar{x}(t_{\max}),$$
$$t_{\max} \in \{t_{ext} \mid \dot{e}(t_{ext}) = 0,\ t_s \le t_{ext} \le t_{s+2q}\} \cup \{t_{s+i} \mid i \in \mathbb{Z},\ 0 \le i \le 2q\}.$$

Using (3.9) and (3.27) t_{ext} can be obtained from

$$\dot{e}(t_{ext}) = 0 \Rightarrow \omega\cos(\omega t_{ext}) - \bar{C}\bar{B}\begin{bmatrix}1\\0\end{bmatrix}\sin(\omega t_{ext}) = \bar{C}\bar{A}\Big(e^{\bar{A}(t_{ext}-t_{s+i})}\big(\xi_{s+i} + \psi(t_{s+i})\big) - \psi(t_{ext})\Big),$$
$$t_{ext} \in (t_{s+i}, t_{s+i+1}],\ i = \{i \in \mathbb{Z}^+ \mid i < 2q\}.$$

Similarly, the pseudo-process sensitivity is defined as the ratio of the maximum error signal of the reset control system (3.9) for $d(t) = d_0\sin(\omega t)$ and $r(t) = 0$, for all $t \ge 0$, to the amplitude of the disturbance at each frequency.

Definition 6. *The Pseudo-process sensitivity PS_∞ is, for all $\omega \in \mathbb{R}^+$,*

$$PS_\infty(j\omega) = e_{\max_d}(\omega)e^{j\varphi_{\max_d}(\omega)},$$

where $\varphi_{\max_d} = \frac{\pi}{2} - \omega t_{\max_d}$,

$$e_{\max_d}(\omega) = \frac{\max\limits_{t'_s \le t \le t'_{s+2q}} -y(t)}{d_0} = -\frac{1}{d_0}\bar{C}\bar{x}(t_{\max_d}),\ t_{\max_d} \in \{t_{ext_d}\} \cup \{t'_{s+i}, i \in \mathbb{Z}, 0 \le i \le 2q'\}.$$

In a similar way t_{ext_d} is obtained from

$$\dot{e}(t_{ext_d}) = \frac{1}{d_0}\bar{C}\dot{\bar{x}}(t_{ext_d}) = 0 \Rightarrow \bar{C}\bar{B}\begin{bmatrix}0\\1\end{bmatrix}\sin(\omega t_{ext_d}) = \bar{C}\bar{A}\Big(\psi_{\mathcal{D}}(t_{ext_d}) - e^{\bar{A}(t_{ext_d}-t'_{s+i})}\big(\xi'_{s+i}+\psi_{\mathcal{D}}(t'_{s+i})\big)\Big),$$
$$t_{ext_d} \in (t'_{s+i}, t'_{s+i+1}],\ i = \{i \in \mathbb{Z}^+ \mid i < 2q'\}. \tag{3.52}$$

In order to analyze the noise rejection capability of the system the pseudo-complementary sensitivity is defined as the ratio of the maximum output of the reset control system (3.9) for $r(t) = r_0\sin(\omega t)$ and $d = 0$, for all $t \geq 0$, to the amplitude of the reference at each frequency.

Definition 7. *The Pseudo-complementary sensitivity T_∞ is, for all $\omega \in \mathbb{R}^+$,*

$$T_\infty(j\omega) = y_{\max}(\omega)e^{j\varphi_{\max_y}(\omega)},$$

where $\varphi_{\max_y} = \frac{\pi}{2} - \omega t_{\max_y}$,

$$y_{\max}(\omega) = \frac{\max\limits_{t_s\leq t\leq t_{s+2q}} y(t)}{r_0} = \frac{1}{r_0}\bar{C}\bar{x}(t_{\max_y}),\ t_{\max_y} \in \{t_{ext_y}\}\cup\{t_{s+i}, i \in \mathbb{Z}, 0 \leq i \leq 2q\}.$$

Similarly,

$$\dot{y}(t_{ext_y}) = \frac{1}{r_0}\bar{C}\dot{\bar{x}}(t_{ext_y}) = 0 \Rightarrow \bar{C}\bar{B}\begin{bmatrix}1\\0\end{bmatrix}\sin(\omega t_{ext_y}) = \bar{C}\bar{A}\Big(\psi(t_{ext_y}) - e^{\bar{A}(t_{ext_y}-t_{s+i})}\big(\xi_{s+i}+\psi(t_{s+i})\big)\Big),$$
$$t_{ext_y} \in (t_{s+i}, t_{s+i+1}],\ i = \{i \in \mathbb{Z}^+ \mid i < 2q\}. \tag{3.53}$$

The pseudo-control sensitivity is defined as the ratio of the maximum control input signal of the reset control system (3.9) for $r(t) = r_0\sin(\omega t)$ and $d = 0$, for all $t \geq 0$, to the amplitude of the reference at each frequency.

Definition 8. *The Pseudo-control sensitivity CS_∞ is, for all $\omega \in \mathbb{R}^+$,*

$$CS_\infty(j\omega) = u_{\max}(\omega)e^{j\varphi_{\max_u}(\omega)},$$

where $\varphi_{\max_u} = \frac{\pi}{2} - \omega t_{\max_u}$,

$$u_{\max}(\omega) = \frac{\max\limits_{t_s\leq t\leq t_{s+2q}} u(t)}{r_0} = \frac{1}{r_0}\bar{C}_u\bar{x}(t_{\max_u}) + \bar{D}_u\sin(\omega t_{\max_u}),$$
$$t_{\max_u} \in \{t_{ext_u}\}\cup\{t'_{s+i}, i \in \mathbb{Z}, 0 \leq i \leq 2q'\}.$$

In addition, t_{ext_u} can be found utilizing the relation $\dot{u}(t_{ext_u}) = 0$ as

$$\bar{D}_u\omega\cos(\omega t_{ext_u}) + \bar{C}_u\bar{B}\begin{bmatrix}1\\0\end{bmatrix}\sin(\omega t_{ext_u}) = \bar{C}_u\bar{A}\Big(\psi(t_{ext_u}) - e^{\bar{A}(t_{ext_u}-t_{s+i})}\big(\xi_{s+i}+\psi(t_{s+i})\big)\Big),$$
$$t_{ext_u} \in (t_{s+i}, t_{s+i+1}],\ i = \{i \in \mathbb{Z}^+ \mid i < 2q\}. \tag{3.54}$$

In linear control theory, the transfer function of the closed-loop system from the disturbance input d to the control input u is equal to minus the transfer function from the

reference signal r to the output signal y. However, this relation does not hold for the pseudo-sensitivities due to the non-linear nature of the controller. Hence, the pseudo-control sensitivity of the disturbance is defined as the ratio of the maximum amplitude of the control input, for $d(t) = d_0 \sin(\omega t)$ and $r = 0$ for all $t \geq 0$, to the amplitude of the disturbance, at each frequency.

Definition 9. *The Pseudo-control sensitivity of the disturbance CS_{d_∞} is, for all $\omega \in \mathbb{R}^+$,*

$$CS_{d_\infty}(j\omega) = u_{\max_d}(\omega) e^{j\varphi_{\max_{u_d}}(\omega)},$$

where $\varphi_{\max_{u_d}} = \frac{\pi}{2} - \omega t_{\max_{u_d}}$,

$$u_{\max_d}(\omega) = \frac{\max\limits_{t'_s \leq t \leq t'_{s+2q}} u(t)}{d_0} = \frac{1}{d_0} \bar{C}_u \bar{x}(t_{\max_{u_d}}),\ t_{\max_{u_d}} \in \{t_{ext_{u_d}}\} \cup \{t'_{s+i}, i \in \mathbb{Z}, 0 \leq i \leq 2q'\}.$$

Finally, $t_{ext_{u_d}}$ is calculated through the relation

$$\dot{u}(t_{ext_{u_d}}) = 0 \Rightarrow \bar{C}_u \bar{B} \begin{bmatrix} 0 \\ 1 \end{bmatrix} \sin(\omega t_{ext_{u_d}}) = \bar{C}_u \bar{A} \Big(\psi_{\mathcal{D}}(t_{ext_{u_d}}) - e^{\bar{A}(t_{ext_u} - t'_{s+i})} \big(\xi'_{s+i} + \psi_{\mathcal{D}}(t'_{s+i}) \big) \Big),$$
$$t_{ext_{u_d}} \in (t'_{s+i}, t'_{s+i+1}],\ i = \{i \in \mathbb{Z}^+ \mid i < 2q'\}. \tag{3.55}$$

We conclude this series of definitions with the following result.

Corollary 6. *Consider the reset control system (3.9). The pseudo-sensitivities and the closed-loop HOSIDFs are independent of the amplitude of the harmonic excitation input.*

3.3.4. HIGH FREQUENCY ANALYSIS

The evaluation of the sensitivities and the pseudo-sensitivities may be computationally expensive, particularly at high frequencies. In order to simplify these relations the reset instants at high frequencies can be approximated. For sufficiently large frequencies, since the open-loop transfer function is strictly proper and (3.38) and (3.25) hold, one has

$$\lim_{\omega \to \infty} \frac{\max\limits_{t_s \leq t \leq t_{s+q}} |e_R(t) - e_{R_1}(t)|}{\max\limits_{t_s \leq t \leq t_{s+q}} |e_{R_1}(t)|} = 0, \tag{3.56}$$

where $e_{R_1}(t) = R_1 \sin(\omega t + \varphi_{e_{R_1}})$ is the first harmonic of $e_R(t)$ (see Appendix 3.C). Thus,

$$\forall \epsilon \in (0,1)\ \exists\, \omega_h \in \mathbb{R}^+ \mid \forall\, \omega \geq \omega_h : \frac{\max\limits_{t_s \leq t \leq t_{s+q}} |e_R(t) - e_{R_1}(t)|}{\max\limits_{t_s \leq t \leq t_{s+q}} |e_{R_1}(t)|} \leq \epsilon. \tag{3.57}$$

Therefore, if ϵ is chosen sufficiently small, the steady-state reset instants for $\omega \geq \omega_h$ can be approximated as

$$t_k \approx \frac{k\pi - \varphi_{e_{R_1}}}{\omega}, \tag{3.58}$$

in which

$$\varphi_{e_{R_1}} \approx \angle \frac{C_{\mathfrak{L}_1}(j\omega)}{1+C_{\mathfrak{L}_1}C_{\mathcal{R}_{DF}}C_{\mathfrak{L}_2}G(j\omega)}, \tag{3.59}$$

where $C_{\mathcal{R}_{DF}}$ is the DF of $C_{\mathcal{R}}$ obtained using (3.3).

Remark 3. The accuracy of the approximation depends on the magnitude of ϵ. The smaller the value of ϵ, the more accurate the approximation is.

Let $\omega \geq \omega_h$ and $r(t) = \sin(\omega t - \varphi_{e_{R_1}})$. Then (3.9) can be re-written as

$$\begin{cases} \dot{\bar{x}}(t) = \bar{A}\bar{x}(t) + \bar{B}\sin(\omega t - \varphi_{e_{R_1}}), & t \neq \dfrac{k\pi}{\omega}, \\ \bar{x}(t^+) = \bar{A}_\rho \bar{x}(t), & t = \dfrac{k\pi}{\omega}, \\ y(t) = \bar{C}\bar{x}(t). \end{cases} \tag{3.60}$$

Thus, $\psi(t)$ in (3.25) is given by

$$\psi_\varphi(t) = (\omega I\cos(\omega t - \varphi_{e_{R_1}}) + \bar{A}\sin(\omega t - \varphi_{e_{R_1}}))\mathcal{F}. \tag{3.61}$$

The steady-state reset instants are $\{\frac{(2k)\pi}{\omega}, \frac{(2k+1)\pi}{\omega}\}$, $k \in \mathbb{N}$. Therefore,

$$\xi_s = -\xi_{s+1} = \frac{-\bar{A}_\rho(I + e^{\frac{\bar{A}\pi}{\omega}})\psi_\varphi(0)}{I + \bar{A}_\rho e^{\frac{\bar{A}\pi}{\omega}}} \Rightarrow \mathcal{R}(1,n,\omega) = -(e^{\frac{\bar{A}\pi}{\omega}} + I)(\xi_s + \psi_\varphi(0)). \tag{3.62}$$

Hence, for $\omega \geq \omega_h$, $T_n(j\omega)$ for the reset control system (3.9) are approximated by

$$\begin{cases} \bar{C}(\bar{A} - j\omega I)^{-1}\theta_\varphi(\omega) - \bar{C}(j\omega I + \bar{A})\mathcal{F}, & n = 1, \\ \bar{C}(\bar{A} - jn\omega I)^{-1}\theta_\varphi(\omega), & n > 1 \text{ odd}, \\ 0, & n \text{ even}, \end{cases} \tag{3.63}$$

in which

$$\theta_\varphi(\omega) = \frac{-2j\omega e^{j\varphi_{e_{R_1}}}}{\pi}(I + e^{\frac{\bar{A}\pi}{\omega}})\left(I - (I + \bar{A}_\rho e^{\frac{\bar{A}\pi}{\omega}})^{-1}(\bar{A}_\rho(I + e^{\frac{\bar{A}\pi}{\omega}}))\right)\psi_\varphi(0). \tag{3.64}$$

A similar analysis holds for the steady-state response of the reset control system (3.9) to a disturbance input. Similarly, let $d = \sin(\omega t - \varphi_{e_{d_1}})$. Then

$$\varphi_{e_{d_1}} \approx \angle \frac{-C_{\mathfrak{L}_1}(j\omega)G(j\omega)}{1+C_{\mathfrak{L}_1}C_{\mathcal{R}_{DF}}C_{\mathfrak{L}_2}G(j\omega)}, \tag{3.65}$$

and $\psi_{\mathcal{D}}$ in (3.47) is given by

$$\psi_{\mathcal{D}_\varphi}(t) = (\omega I\cos(\omega t - \varphi_{e_{d_1}}) + A\sin(\omega t - \varphi_{e_{d_1}}))\mathcal{F}_{\mathcal{D}}. \tag{3.66}$$

Similarly,

$$\xi'_s=-\xi'_{s+1}=\frac{-\bar{A}_\rho(I+e^{\frac{\bar{A}\pi}{\omega}})\psi_{\mathcal{D}_\varphi}(0)}{I+\bar{A}_\rho e^{\frac{\bar{A}\pi}{\omega}}}\Rightarrow\mathcal{R}_\mathcal{D}(1,n,\omega)=-(e^{\frac{\bar{A}\pi}{\omega}}+I)(\xi'_s+\psi_{\mathcal{D}_\varphi}(0)). \quad (3.67)$$

Therefore, for ω sufficiently large $PS_n(j\omega)$ for the reset control system (3.9) are approximated as

$$\begin{cases}\bar{C}(j\omega I-\bar{A})^{-1}\theta_{\mathcal{D}_\varphi}(\omega)+\bar{C}(j\omega I+\bar{A})\mathcal{F}_\mathcal{D}, & n=1,\\ \bar{C}(jn\omega I-\bar{A})^{-1}\theta_{\mathcal{D}_\varphi}(\omega), & n>1 \text{ odd},\\ 0, & n \text{ even},\end{cases} \quad (3.68)$$

in which

$$\theta_{\mathcal{D}_\varphi}(\omega)=\frac{-2j\omega e^{j\varphi_{e_{d_1}}}}{\pi}(I+e^{\frac{\bar{A}\pi}{\omega}})\left(I-(I+\bar{A}_\rho e^{\frac{\bar{A}\pi}{\omega}})^{-1}(\bar{A}_\rho(I+e^{\frac{\bar{A}\pi}{\omega}}))\right)\psi_{\mathcal{D}_\varphi}(0). \quad (3.69)$$

Remark 4. The presented results have been integrated into an open source toolbox, which has been developed using Matlab, see [47]. This toolbox facilitates the analysis and design for reset control systems.

3.4. PERIODIC INPUTS

IN Section 3.3 a notion of frequency response and pseudo-sensitivities for reset control systems have been defined. These serve as graphical tools for performance analysis of reset controllers. The pseudo-sensitivities determine how a system amplifies harmonic inputs at various frequencies, information which is essential for control designers. However, this information is obtained for a single harmonic excitation and since the superposition principle does not hold, it provides only an approximation in the case of multi-harmonics excitation. In this section the steady-state performance in the presence of multi-harmonics excitation and periodic inputs is investigated. This is reasonable since most references and disturbances are periodic [12, 48].

For ease of notation let $\text{lcm}\left(\frac{a_1}{b_1},\frac{a_2}{b_2},...,\frac{a_i}{b_i}\right)$ denote the least common multiple of $\frac{a_1}{b_1},\frac{a_2}{b_2}$, ..., and $\frac{a_i}{b_i}$ and $\text{gcd}\left(\frac{a_1}{b_1},\frac{a_2}{b_2},...,\frac{a_i}{b_i}\right)$ denote the greatest common divisor of $\frac{a_1}{b_1},\frac{a_2}{b_2},...,$ and $\frac{a_i}{b_i}$ in which $a_i\in\mathbb{N}$ and $b_i\in\mathbb{N}$.

Theorem 3. *Consider the reset control system (3.9). Suppose the H_β condition and Assumption 1 hold. Then for any periodic excitation of the form*

$$w(t)=w_0\sin(\frac{2\pi}{T_0}t)+w_1\sin(\frac{2\pi}{T_1}t)+...+w_N\sin(\frac{2\pi}{T_N}t), \quad (3.70)$$

with $w_i=[r_i,\ d_i]^T$, the reset control system (3.9) has a periodic steady-state solution of the form

$$\bar{x}(t)=a_0+\sum_{n=1}^{\infty}a_n\cos(n\omega_M t)+b_n\sin(n\omega_M t),\ \omega_M=2\pi\times gcd(\frac{1}{T_0},\frac{1}{T_1},...,\frac{1}{T_N}).$$

Proof. Let $t_{s_{M+i}}$ be the steady-state reset instants of the reset control system (3.9) for w is given in (3.70). By (3.9) the steady-state solution for w as in (3.70) is given by

$$\bar{x}(t) = e^{\bar{A}(t-t_{s_M})}\Big(\xi_{s_M} + \psi_M(t_{s_M})\Big) - \psi_M(t),\ t \in (t_{s_M}, t_{s_M+1}], \tag{3.71}$$

where

$$\psi_M(t) = \sum_{i=0}^{N} \psi_i(t),\ \psi_i(t) = (\omega_i I \cos(\omega_i t) + \bar{A}\sin(\omega_i t))\mathcal{F}_i,\ \mathcal{F}_i = (\omega_i^2 I + \bar{A}^2)^{-1}\bar{B}w_i.$$

By Lemma 2 the reset control system (3.9) forgets the initial condition; thus, using as similar procedure as the one in Section 3.3.1, yields

$$\begin{aligned}\bar{x}(t) = & e^{\bar{A}(t-t_{s_M})}\Big((I-\bar{A}_\rho)\psi_M(t_{s_M}) + e^{\bar{A}(t_{s_M}-t_{s_M-1})}\Big((I-\bar{A}_\rho)\psi_M(t_{s_M-1}) + \dots \\ & + \bar{A}_\rho e^{\bar{A}(t_{s_M-1}-t_{s_M-2})}\dots\bar{A}_\rho e^{\bar{A}(t_{s_M-m+1}-t_{s_M-m})}(I-\bar{A}_\rho)\psi_M(t_{s_M-m})\Big)\Big) \\ & - \psi_M(t),\ t \in (t_{s_M}, t_{s_M+1}].\end{aligned}$$

Since the reseting condition is

$$\bar{C}_{e_R}\bar{x}(t) + D_{e_R}[1\ 0]w_M(t) = 0, \tag{3.72}$$

if $\{t_{s_M}, t_{s_M-1}, \dots, t_{s_M-m}\}$ are reset instants and satisfy (3.72), then $t \in \{t_{s_M}, t_{s_M-1}, \dots, t_{s_M-m}\} + \frac{2\pi}{\omega_M}$ are such that (3.72) holds, which implies that the sequence of reset instants is periodic with period $\frac{2\pi}{\omega_M}$; hence, $\bar{x}(t) = \bar{x}(t + \frac{2\pi}{\omega_M})$, and using the Fourier series representation yields

$$\bar{x}(t) = a_0 + \sum_{n=1}^{\infty} a_n \cos(n\omega_M t) + b_n \sin(n\omega_M t). \tag{3.73}$$

□

Corollary 7. *Consider the reset control system (3.9). Suppose the H_β condition and Assumption 1 hold. Then for any periodic input $w_P(t) = w_P(t + T_P)$ the reset control system (3.9) has a steady-state periodic solution with the same period time T_P.*

Proof. A periodic function can be written as

$$w_P(t) = a_0' + \sum_{n=1}^{\infty} a_n' \cos(n\frac{2\pi}{T_P}t) + b_n' \sin(n\frac{2\pi}{T_P}t). \tag{3.74}$$

Using Theorem 3 the steady-state solution of (3.9) for the input (3.74) is

$$\bar{x}(t) = a_0 + \sum_{n=1}^{\infty} a_n \cos(n\omega_M t) + b_n \sin(n\omega_M t),\ \omega_M = 2\pi \times gcd(\frac{1}{T_P}, \frac{2}{T_P}, \dots, \frac{n}{T_P}) = \frac{2\pi}{T_P},$$

hence the claim. □

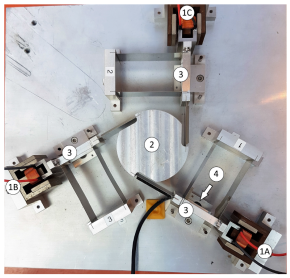

Figure 3.4: A 3 DOF planar precision positioning Spyder stage. The voice coil actuators 1A, 1B and 1C control three masses (labelled as 3) which are constrained by leaf flexures. The three masses are connected to a central mass (labelled as 2) through leaf flexures. A Linear encoder (labelled as 4) is placed under mass 3 to provide the position feedback

3.5. ILLUSTRATIVE EXAMPLE

IN this section an illustrative example showing the effectiveness of the developed results is presented. A 3DOF precision positioning system, see Figure. 3.4, [1] and [49], is selected for this purpose. In this system we only consider mass 3 and actuator 1A (see Figure. 3.4) which can be modelled via the transfer function, see [50],

$$G(s) = \frac{8695}{s^2 + 4.36s + 7627}. \tag{3.75}$$

Note that all of the controllers in the following subsections are designed such that the H_β condition holds.

3.5.1. THE OPTIMAL STRUCTURE FOR CI

The closed-loop frequency responses of the system with two reset controllers are compared against the closed-loop frequency responses achievable with a “tamed" PID controller [1] with base linear transfer function

$$C_{PID}(s) = k_p\left(1 + \frac{\omega_i}{s}\right)\left(\frac{\frac{s}{\omega_d}+1}{\frac{s}{\omega_t}+1}\right). \tag{3.76}$$

The first reset controller is obtained by replacing the integrator in (3.76) with a CI yielding

$$C_{SP(CI)D}(s) = k_p\left(1 + \frac{\omega_i}{s}\right)\left(\frac{\frac{s}{\omega_d}+1}{\frac{s}{\omega_t}+1}\right), \tag{3.77}$$

and the second reset controller is the parallel form of (3.77), that is

$$C_{PP(CI)D}(s) = k_p\left(1 + \frac{\omega_i}{s} + \frac{\frac{s}{\omega_d}}{\frac{s}{\omega_t}+1}\right). \tag{3.78}$$

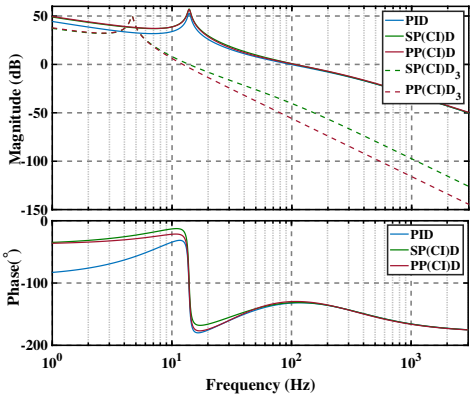

Figure 3.5: The DFs and the amplitudes of the third harmonics of the open-loop system with the controllers $C_{SPI(CI)D}$ and $C_{PPI(CI)D}$, and open-loop frequency response of the system with the controller C_{PID}

Note that, unlike the case of linear controllers, the parallel and series configuration of reset controllers can result in totally different responses. In this example we show that in contrast with the DF method, our method is capable of exposing this difference. Setting 100 Hz as the crossover frequency ω_c, the control parameters have been tuned based on the method proposed in [1, 44, 51] as $K_p = \dfrac{1}{3|G(j\omega_c)|} = 14.35$, $\omega_t = 3\omega_c = 600\pi$, $\omega_i = \dfrac{\omega_c}{10} = 20\pi$, and $\omega_d = \dfrac{\omega_c}{3} = 66.6\pi$. All frequency responses are obtained utilizing the toolbox in [47].

The open-loop frequency response of the system with the controller C_{PID}, and the DFs and the amplitudes of third harmonics of the system with the controllers $C_{SP(CI)D}$, $C_{PP(CI)D}$ are shown in Figure. 3.5. Based on the DF analysis it is expected that the tracking performances and the disturbance rejection capabilities of the system with controllers $C_{PP(CI)D}$ and $C_{SP(CI)D}$ are the same, and these performance capabilities are superior to those of the system with the controller C_{PID}. In addition, the control inputs and the noise attenuation capabilities of the system with these controllers are expected to be almost the same. However, the magnitude of high order harmonics of the reset controllers is different.

The time-domain results (Figure. 3.6) disprove the predictions which rely on the DF method. In this figure the tracking errors and the amplitude of the control inputs of the system with these controllers are displayed for $r(t) = 100\sin(2\pi t)$. It is seen that the control input of the system with the controller $C_{SP(CI)D}$ is much larger than the amplitude of the control inputs of the system with the controllers C_{PID} and $C_{PP(CI)D}$, whereas the tracking performance of the system with the controller $C_{SP(CI)D}$ is worse than the tracking performances of the system with the controllers C_{PID} and $C_{PP(CI)D}$. Note that similar to results presented in [17, 25, 52, 53], the amplitudes of even harmonics of the response are zero.

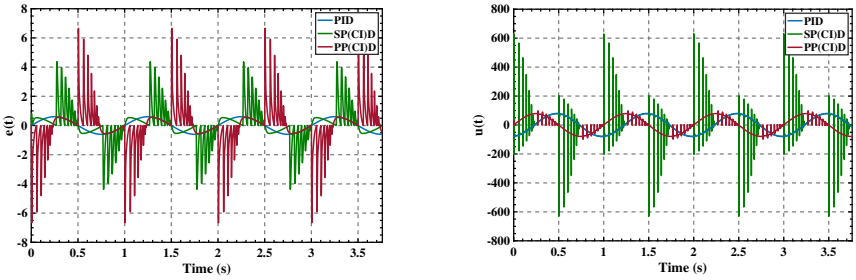

(a) Tracking error

(b) Control input

Figure 3.6: Time histories of the tracking errors and of the control inputs of the system with the controllers $C_{PP(CI)D}$, $C_{SP(CI)D}$ and C_{PID} for $r(t) = 100\sin(2\pi t)$

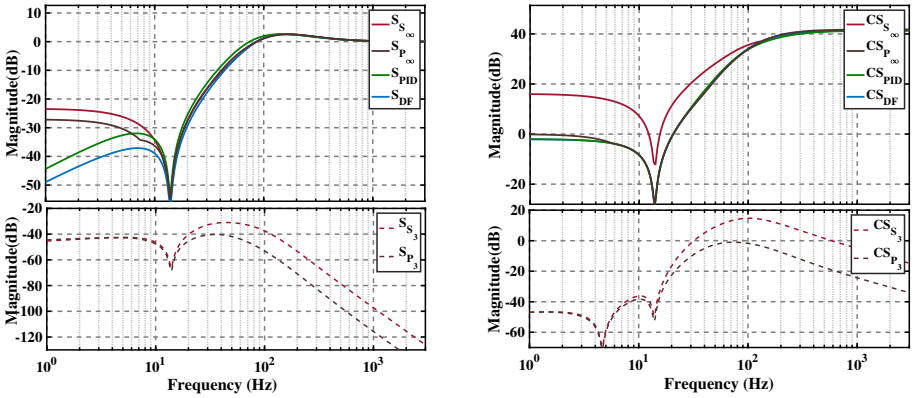

(a) Sensitivity

(b) Control sensitivity

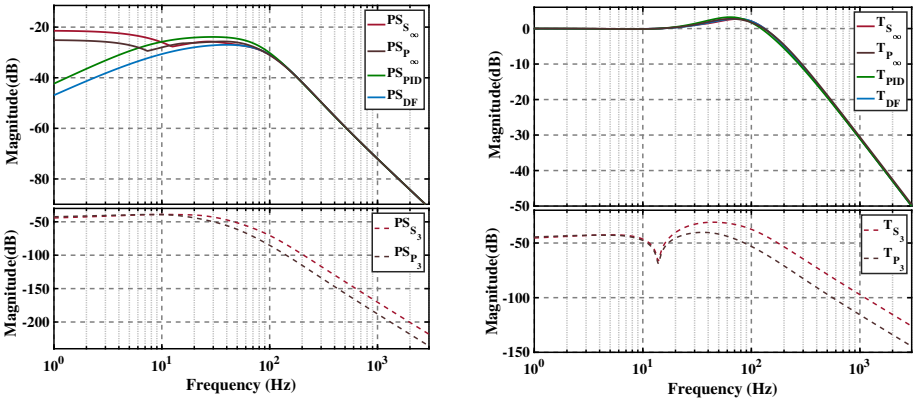

(c) Process sensitivity

(d) Complementary sensitivity

Figure 3.7: The DFs (._ DF), amplitudes of the third harmonics of the sensitivities (._3), and amplitudes of pseudo-sensitivities (._ ∞) of the closed-loop system with the controllers $C_{SP(CI)D}$, $C_{PP(CI)D}$, and closed-loop sensitivities of the system with the controller C_{PID}

Unlike the DF method, the pseudo-sensitivities (Figure. 3.7) allows justifying why the performance of the system with the controller C_{PID} is superior to the performances of the system with the controllers $C_{PP(CI)D}$ and $C_{SP(CI)D}$ in terms of precision and control effort. As illustrated in Figure. 3.7a, at low frequency the tracking performance of the system with the controller C_{PID} is better than that of the system with the controllers $C_{PP(CI)D}$ and $C_{SP(CI)D}$. Moreover, the tracking performance of the system with the controller $C_{PP(CI)D}$ is better than the tracking performance of the system with the controller $C_{SP(CI)D}$ at frequencies around the cross-over frequency. As it can be seen in Figure. 3.7b, the amplitude of the function CS_∞ of the system with the controller $C_{SP(CI)D}$ is much higher than that of the system with the controller $C_{PP(CI)D}$ and of the control sensitivity of the system with the controller C_{PID}. Thus, to avoid saturation problems designers should use the function CS_∞ instead of using the result obtained from the DF method when reset controllers are used.

In addition, as shown in Figure. 3.7c, the low frequency disturbance rejection capability of the system with the controller C_{PID} is better than that of the system with the controllers $C_{PP(CI)D}$ and $C_{SP(CI)D}$. Furthermore, as illustrated in Figure. 3.7d, the noise attenuating capabilities of the system with these three controllers are the same. The differences between the performances of the system with the controllers $C_{PP(CI)D}$ and $C_{SP(CI)D}$ are due to the differences in the amplitude and phase of the high order harmonics produced by these controllers.

To sum up, although it has been shown that using CIs, instead of linear integrators, improves the transient response of the system, the proposed results show that this deteriorates the tracking performance of the system, and the system needs a “stronger" actuator. Moreover, the actual implementation of the CI has significant effects on the performance of the system which cannot be exposed by using the results obtained with the DF method. This analysis reveals that the CI should be used in the parallel architecture (3.78), yielding a system with better precision and lower control input once compared with the system with the CI in the series architecture (3.77).

3.5.2. PERFORMANCE OF CGLP COMPENSATORS

Reset elements are utilized to introduce new compensators to enhance performance of control systems [17, 23–27]. In this section a new reset compensator called Constant in gain Lead in phase (CgLp) is analyzed. It consists of a reset filter FORE and a Proportional Derivative (PD) filter in series [17, 25]. The DF of a CgLp compensator is given in Figure. 3.8. Note that the combination of a PD and a FORE produces a compensator with a constant gain, while providing a phase lead. To study the effects of the “position" of the control elements on the performance of systems with reset controllers, two controllers (see Figure. 3.9) with CgLp compensators are considered. Both controllers are described by

$$C_{g_i}(s) = k_p \overbrace{\overbrace{\left(\frac{1}{\frac{s}{\omega_r}+1}\right)}^{\text{FORE}}\overbrace{\left(\frac{\frac{s}{\omega_d}+1}{\frac{s}{\omega_t}+1}\right)}^{\text{Lead}}}^{\text{CgLp}}\overbrace{\left(1+\frac{\omega_i}{s}\right)}^{\text{PI}}\overbrace{\left(\frac{\frac{s}{\omega_l}+1}{\frac{s}{\omega_f}+1}\right)}^{\text{Lead}}. \tag{3.79}$$

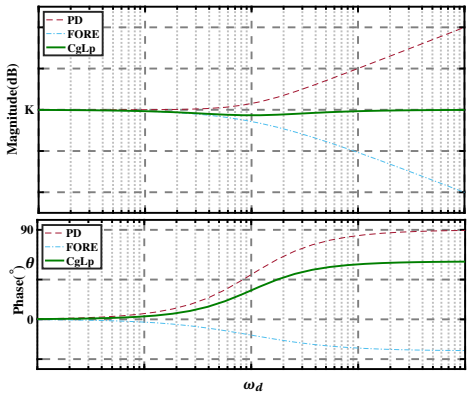

Figure 3.8: The DF of a CgLp compensator

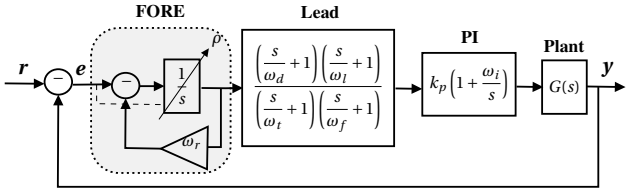

(a) The system with control C_{g_1}

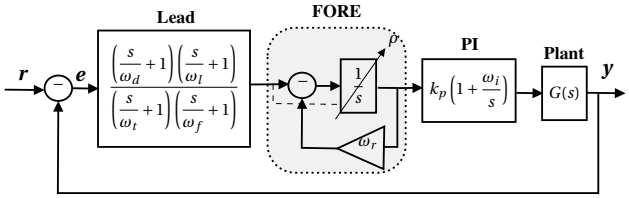

(b) The system with control C_{g_2}

Figure 3.9: Block diagrams of the Spyder plant with controllers C_{g_1} (top), and C_{g_2} (bottom)

The parameters of these two controllers are the same and tuned optimally based on the method described in [52], yielding $k_p = 25.5$, $\omega_r = 111\pi$, $\omega_d = 105.2\pi$, $\omega_t = 1640\pi$, $\omega_i = 20\pi$, $\omega_l = 105.2\pi$, $\omega_f = 260\pi$, and $\gamma = 0.3$. The only difference between these two controllers is in the "position" of the filters. For C_{g_1} is FORE-lead-proportional-integrator, while for C_{g_2} one has lead-FORE-proportional-integrator. The DFs and the amplitudes of the third harmonic of the open-loop system with both controllers are given in Figure. 3.10. The DFs of the open-loop system with both controllers are the same, but the amplitudes of their third harmonic are different which yields different performances. In Figure. 3.11 the closed-loop frequency responses of the system with both controllers, including the amplitudes of the third harmonics, the DFs and amplitudes of pseudo-sensitivities, are presented. Note that there are significant differences between the results obtained using the DF method and the proposed tools.

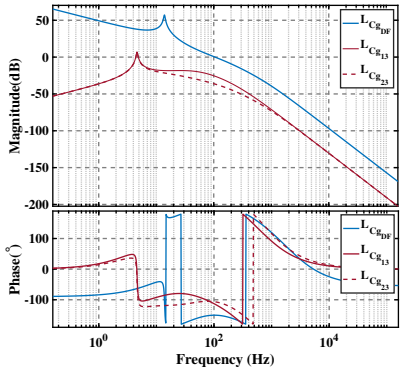

Figure 3.10: The DFs and the amplitudes of the third harmonics of the open-loop system with the controllers C_{g_1} and C_{g_2}

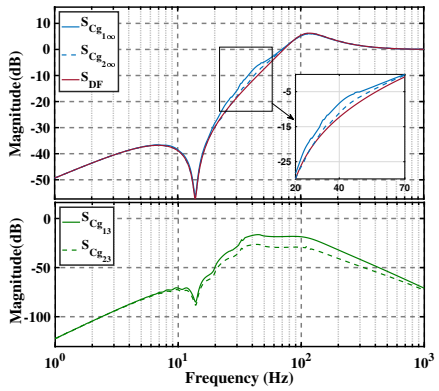

(a) Sensitivity

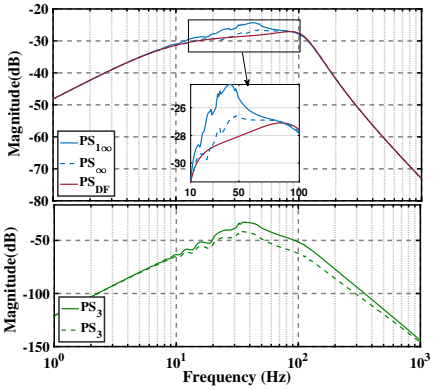

(b) Process sensitivity

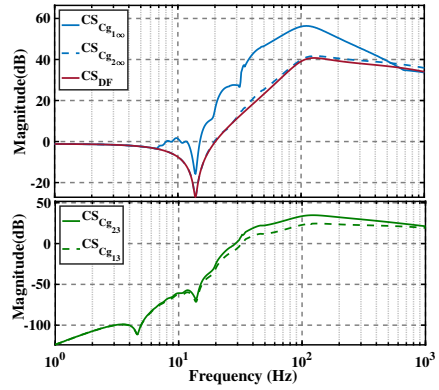

(c) Control sensitivity

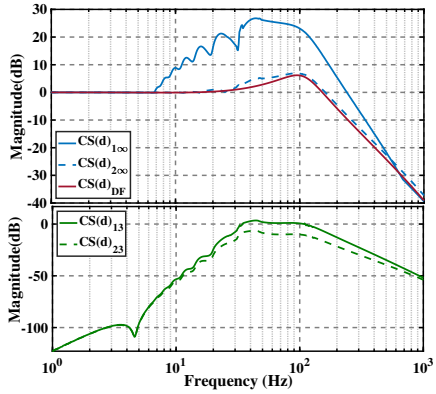

(d) Control sensitivity to disturbance

Figure 3.11: The DFs (._ DF), amplitudes of the third harmonics of the sensitivities (._3), and amplitudes of pseudo-sensitivities (._ ∞) of the closed-loop system with the controllers C_{g_1} and C_{g_2}

Unlike the DF method, the proposed tools reveal the effects of the “position" of the control filters on the performance of the reset control systems. The differences in magnitude and phase of the high order harmonics of the open-loop system with these controllers (Figure. 3.10) leads to discrepancies between the closed-loop frequency responses. As shown in Figure. 3.11a, the system with the controller C_{g_2} has better tracking performance than that of the system with the controller C_{g_1}. In addition, the amplitude of the third harmonic of the sensitivity of the system with C_{g_2} is smaller than that resulting from the use of the controller C_{g_1} around the cross-over frequency. Moreover, as illustrated in Figure. 3.11b, the system with the controller C_{g_2} has better disturbance rejection capability than the system with the controller C_{g_1}. As shown in Figure. 3.11c and Figure. 3.11d, the system with the controller C_{g_1} has larger control input in comparison with the system with the controller C_{g_2}. As discussed, unlike the case of linear controller and the results obtained using the DF method, the control sensitivity due to the disturbance CS_{d_∞} is different from the complementary sensitivity, particularly at middle frequencies.
In addition, the tracking error and the error due to the presence of disturbance of the system with the controller C_{g_1} at 5 Hz are obtained experimentally (Table 3.1). As was shown, there are negligible differences between experimental and our proposed results. These small differences between the theoretical and the experimental results are due to quantization, digitalization of the controller, numerical approximations, and the presence of noise.

In summary the proposed methods allow predicting the closed-loop performance of reset control systems more accurately than the DF method. In addition, it reveals important features of reset controllers which are not exposed by the DF method.

Table 3.1: Comparison between the theoretical and experimental results in terms of tracking performance and disturbance rejection

Performance	C_{g_1}	
	Theory	Experiment
Tracking $\frac{e_r}{\lvert r\rvert}$(dB)	-37.57	-35.8
Disturbance rejection $\frac{e_w}{\lvert w\rvert}$(dB)	-33.1	-34

3.6. CONCLUSION

THIS chapter has proposed an analytical approach to obtain closed-loop frequency responses for reset control systems, including high order harmonics. To this end, sufficient conditions for the existence of the steady-state solution of the closed-loop reset control systems driven by periodic inputs have been presented. Moreover, pseudo-sensitivities, which serve as a graphical tool for performance analysis of reset controllers, have been defined: these relate the error and control input of the system to the reference and the disturbance. All calculations can be performed in a user-friendly toolbox to make this approach easy of use. To show the effectiveness of the proposed method, the performances of a high-precision positioning stage with reset controllers have been assessed using the DF method and our proposed method. The results confirm that the

proposed method predicts the closed-loop performance of reset control systems more accurately than the DF method.

3.A. LEMMA 3

Lemma 3. *Consider the linear systems* $\dot{x}_{p_1}(t) = A_p x_{p_1}(t) + B_p u(t)$, $y_{p_1}(t) = C_p x_{p_1}(t)$, *with* $x_{p_1}(0) = x_0$, $\dot{x}_{p_2}(t) = A_p x_{p_2}(t) + B_p u(t)$, $y_{p_2}(t) = C_p x_{p_2}(t) + W_I(t)$, *with* $x_{p_2}(0) = 0$, *and* $\dot{z}(t) = A_p z(t)$, $W_I(t) = C_p z(t)$, *with* $z(0) = x_0$, *in which* A_p, B_p, *and* C_p *describe a realization of transfer function* $P(s)$ *(see Figure. 3.12). Then* $y_{p_1}(t) = y_{p_2}(t)$, *for all* $t \geq 0$.

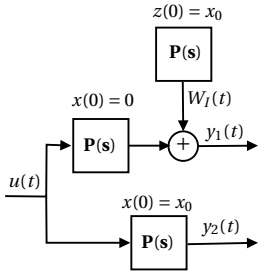

Figure 3.12: Diagram of the result in Lemma 3

Proof. Note that $W_I(t) = C_p e^{A_p t} x_0$. Thus,

$$y_{p_2}(t) = y_{p_1}(t) = C_p e^{A_p(t)} x_0 + \int_0^t e^{A_p(t-\tau)} B_p u(\tau) d\tau.$$

□

3.B. LEMMA 4

Lemma 4. *Consider a positive and bounded function* $V(t)$. *Suppose that there exists a* $\alpha > 0$ *such that*

$$\begin{cases} \dot{V} \leq -\alpha V & t \in \mathcal{M}, \\ V(\Delta x(t^+)) = V(\Delta x(t)) + \Xi(t,\delta), & t \notin \mathcal{M}. \end{cases} \tag{3.80}$$

If for t *sufficiently large*

$$\Xi(t,\delta) \leq 0, \tag{3.81}$$

then there exist $\alpha_m > 0$ *and* $\mathcal{K} > 0$ *such that*

$$V(t) \leq \mathcal{K} e^{-\alpha_m t}, \text{ for all } t \geq 0. \tag{3.82}$$

Proof. Since V is bounded, by (3.80) and (3.81), V achieves its maximum value at some time $t_{v_m} < \infty$. In other words, there exists a time $0 \leq t_{v_m} < \infty$ such that

$$\begin{cases} V(t_{v_m}) \geq V(t), & t \leq t_{v_m}, \\ V(t_{v_m}) > V(t). & t > t_{v_m}, \end{cases} \tag{3.83}$$

Therefore, by (3.81) and well-posedness property, there exists a bounded set $\mathcal{T} = \{t_i > t_{v_m} |\ t_i \notin \mathcal{M} \wedge \Xi(t_i, \delta) > 0,\ i \in \mathbb{N}\}$. Thus, using (3.83) there exists a bounded set $\mathcal{A} = \{\alpha_i > 0 |\ V(t_i) = e^{-\alpha_i (t_i - t_{v_m})} V(t_{v_m}),\ t_i \in \mathcal{T}\}$. Since the set $\mathcal{A}$ is bounded, there exists a $\alpha' > 0$ such that for all $\alpha_i \in \mathcal{A}$ one has that $\alpha' \leq \alpha_i$. Now considering $\alpha_m = \min(\alpha, \alpha')$, based on (3.80) and (3.81), yields

$$V(t) \leq e^{-\alpha_m (t - t_{v_m})} V(t_{v_m}) = \mathcal{K} e^{-\alpha_m t}, \text{ for all } t \geq 0. \tag{3.84}$$

Finally, if $\mathcal{T}$ and $\mathcal{A}$ are empty sets, then selecting $\alpha_m = \alpha$ the claim yields. □

3

3.C. LIMIT CALCULATION FOR HIGH FREQUENCY ANALYSIS

Note that by (3.25) and (3.38), $\lim_{\omega \to \infty} \bar{y}(t) = 0$ and $\lim_{\omega \to \infty} T_n(j\omega) = 0$. In addition, since $y(t) = r_0 \sum_{n=1}^{\infty} T_n(j\omega)$, $\lim_{\omega \to \infty} \sum_{n=1}^{\infty} T_n(j\omega) = 0$. On the other hand, if the transfer function of the controller $C_{\mathfrak{L}_1}$ is proper, then $\lim_{\omega \to \infty} C_{\mathfrak{L}_1}(nj\omega) = K_{c1}$; otherwise, $\lim_{\omega \to \infty} (nj\omega)^{n_c} C_{\mathfrak{L}_1}(nj\omega) = 1$, with $n_c \geq 1$. In the case in which $C_{\mathfrak{L}_1}$ is proper.

$$\lim_{\omega \to \infty} \frac{\max\limits_{t_s \leq t \leq t_{s+q}} |e_R(t) - e_{R_1}(t)|}{\max\limits_{t_s \leq t \leq t_{s+q}} |e_{R_1}(t)|} \leq \lim_{\omega \to \infty} \frac{K_{c1} r_0 |\sum_{n=3}^{\infty} T_n(j\omega)|}{K_{c1} r_0} \Rightarrow \lim_{\omega \to \infty} \frac{\max\limits_{t_s \leq t \leq t_{s+q}} |e_R(t) - e_{R_1}(t)|}{\max\limits_{t_s \leq t \leq t_{s+q}} |e_{R_1}(t)|} = 0. \tag{3.85}$$

In the case in which $C_{\mathfrak{L}_1}$ is strictly proper.

$$\lim_{\omega \to \infty} \frac{\max\limits_{t_s \leq t \leq t_{s+q}} |e_R(t) - e_{R_1}(t)|}{\max\limits_{t_s \leq t \leq t_{s+q}} |e_{R_1}(t)|} < \lim_{\omega \to \infty} \frac{\frac{r_0}{\omega^{n_c}} |\sum_{n=3}^{\infty} \frac{T_n(j\omega)}{n^{n_c}}|}{\frac{r_0}{\omega^{n_c}}} \Rightarrow \lim_{\omega \to \infty} \frac{\max\limits_{t_s \leq t \leq t_{s+q}} |e_R(t) - e_{R_1}(t)|}{\max\limits_{t_s \leq t \leq t_{s+q}} |e_{R_1}(t)|} = 0. \tag{3.86}$$

REFERENCES

[1] A. A. Dastjerdi, N. Saikumar, and S. H. HosseinNia, *Tuning guidelines for fractional order PID controllers: Rules of thumb,* Mechatronics **56**, 26 (2018).

[2] A. O'Dwyer, *Handbook of PI and PID controller tuning rules* (World Scientific, 2009).

[3] Y. Chen, *Ubiquitous fractional order controls?* IFAC Proceedings Volumes **39**, 481 (2006), 2nd IFAC Workshop on Fractional Differentiation and its Applications.

[4] J. C. Clegg, *A nonlinear integrator for servomechanisms,* Transactions of the American Institute of Electrical Engineers, Part II: Applications and Industry **77**, 41 (1958).

[5] O. Beker, C. Hollot, Y. Chait, and H. Han, *Fundamental properties of reset control systems,* Automatica **40**, 905 (2004).

[6] O. Beker, C. V. Hollot, and Y. Chait, *Plant with integrator: an example of reset control overcoming limitations of linear feedback,* IEEE Transactions on Automatic Control **46**, 1797 (2001).

[7] D. Nesic, A. R. Teel, and L. Zaccarian, *Stability and performance of siso control systems with first-order reset elements,* IEEE Transactions on Automatic Control **56**, 2567 (2011).

[8] A. F. Villaverde, A. B. Blas, J. Carrasco, and A. B. Torrico, *Reset control for passive bilateral teleoperation,* IEEE Transactions on Industrial Electronics **58**, 3037 (2011).

[9] A. Baños and A. Barreiro, *Reset control systems* (Springer Science & Business Media, 2011).

[10] S. van Loon, K. Gruntjens, M. Heertjes, N. van de Wouw, and W. Heemels, *Frequency-domain tools for stability analysis of reset control systems,* Automatica **82**, 101 (2017).

[11] D. Wu, G. Guo, and Y. Wang, *Reset integral-derivative control for HDD servo systems,* IEEE Transactions on Control Systems Technology **15**, 161 (2007).

[12] A. Pavlov, B. Hunnekens, N. Wouw, and H. Nijmeijer, *Steady-state performance optimization for nonlinear control systems of Lur'e type,* Automatica **49**, 2087 (2013).

[13] F. S. Panni, H. Waschl, D. Alberer, and L. Zaccarian, *Position regulation of an EGR valve using reset control with adaptive feedforward,* IEEE Transactions on Control Systems Technology **22**, 2424 (2014).

[14] L. Hazeleger, M. Heertjes, and H. Nijmeijer, *Second-order reset elements for stage control design,* in *American Control Conference (ACC)* (2016) pp. 2643–2648.

[15] R. Beerens, A. Bisoffi, L. Zaccarian, W. Heemels, H. Nijmeijer, and N. van de Wouw, *Reset integral control for improved settling of PID-based motion systems with friction,* Automatica **107**, 483 (2019).

[16] N. Saikumar, R. K. Sinha, and S. Hassan HosseinNia, *Resetting disturbance observers with application in compensation of bounded nonlinearities like hysteresis in piezo-actuators,* Control Engineering Practice **82**, 36 (2019).

[17] N. Saikumar, R. K. Sinha, and S. H. HosseinNia, *'Constant in gain Lead in phase' element-application in precision motion control,* IEEE/ASME Transactions on Mechatronics **24**, 1176 (2019).

[18] W. P. M. H. Heemels, G. E. Dullerud, and A. R. Teel, *$\mathcal{L}_2$-gain analysis for a class of hybrid systems with applications to reset and event-triggered control: A lifting approach,* IEEE Transactions on Automatic Control **61**, 2766 (2016).

[19] F. Fichera, C. Prieur, S. Tarbouriech, and L. Zaccarian, *Lmi-based reset $\mathcal{H}_\infty$ design for linear continuous-time plants,* IEEE Transactions on Automatic Control **61**, 4157 (2016).

[20] A. Banos and A. Barreiro, *Delay-independent stability of reset systems,* IEEE Transactions on Automatic Control **54**, 341 (2009).

[21] L. Zaccarian, D. Nesic, and A. R. Teel, *First order reset elements and the Clegg integrator revisited,* in *American Control Conference* (2005) pp. 563–568 vol. 1.

[22] I. Horowitz and P. Rosenbaum, *Non-linear design for cost of feedback reduction in systems with large parameter uncertainty,* International Journal of Control **21**, 977 (1975).

[23] B. Hunnekens, N. van de Wouw, M. Heertjes, and H. Nijmeijer, *Synthesis of variable gain integral controllers for linear motion systems,* IEEE Transactions on Control Systems Technology **23**, 139 (2014).

[24] S. J. A. M. Van den Eijnden, Y. Knops, and M. F. Heertjes, *A hybrid integrator-gain based low-pass filter for nonlinear motion control,* in *IEEE Conference on Control Technology and Applications (CCTA)* (2018) pp. 1108–1113.

[25] A. Palanikumar, N. Saikumar, and S. H. HosseinNia, *No more differentiator in PID: Development of nonlinear lead for precision mechatronics,* in *European Control Conference (ECC)* (2018) pp. 991–996.

[26] L. Chen, N. Saikumar, and S. H. HosseinNia, *Development of robust fractional-order reset control,* IEEE Transactions on Control Systems Technology **28**, 1404 (2020).

[27] D. Valério, N. Saikumar, A. A. Dastjerdi, N. Karbasizadeh, and S. H. HosseinNia, *Reset control approximates complex order transfer functions,* Nonlinear Dynamics , 1 (2019).

[28] A. Barreiro, A. Baños, S. Dormido, and J. A. González-Prieto, *Reset control systems with reset band: Well-posedness, limit cycles and stability analysis,* Systems & Control Letters **63**, 1 (2014).

[29] A. Baños and M. A. Davó, *Tuning of reset proportional integral compensators with a variable reset ratio and reset band,* IET Control Theory & Applications **8**, 1949 (2014).

[30] A. Vidal and A. Banos, *QFT-based design of PI+CI reset compensators: Application in process control,* in *16th Mediterranean Conference on Control and Automation* (2008) pp. 806–811.

[31] U. R. Nair, R. Costa-Castelló, and A. Baños, *Grid voltage regulation using a reset PI+CI controller for energy storage systems,* **51**, 226 (2018), 3rd IFAC Conference on Advances in Proportional-Integral-Derivative Control PID.

[32] S. H. HosseinNia, I. Tejado, D. Torres, B. M. Vinagre, and V. Feliu, *A general form for reset control including fractional order dynamics,* IFAC Proceedings Volumes **47**, 2028 (2014).

[33] Y. Guo, Y. Wang, and L. Xie, *Frequency-domain properties of reset systems with application in hard-disk-drive systems,* IEEE Transactions on Control Systems Technology **17**, 1446 (2009).

[34] W. E. Vander Velde *et al.*, *Multiple-input describing functions and nonlinear system design,* McGraw lill (1968).

[35] P. Nuij, O. Bosgra, and M. Steinbuch, *Higher-order sinusoidal input describing functions for the analysis of non-linear systems with harmonic responses,* Mechanical Systems and Signal Processing **20**, 1883 (2006).

[36] K. Heinen, *Frequency analysis of reset systems containing a Clegg integrator,* Master's thesis, Delft University of Technology (2018).

[37] Y. Guo, L. Xie, and Y. Wang, *Analysis and Design of Reset Control Systems* (Institution of Engineering and Technology, 2015).

[38] C. Hollot, O. Beker, Y. Chait, and Q. Chen, *On establishing classic performance measures for reset control systems,* in *Perspectives in robust control* (Springer, 2001) pp. 123–147.

[39] A. A. Dastjerdi, A. Astolfi, and S. H. HosseinNia, *A frequency-domain stability method for reset systems,* in *IEEE 59th Conference on Decision and Control* (2020).

[40] A. Banos, J. I. Mulero, A. Barreiro, and M. A. Davo, *An impulsive dynamical systems framework for reset control systems,* International Journal of Control **89**, 1985 (2016).

[41] A. Pavlov, N. van de Wouw, and H. Nijmeijer, *Frequency response functions for nonlinear convergent systems,* IEEE Transactions on Automatic Control **52**, 1159 (2007).

[42] A. Pavlov, A. Pogromsky, N. van de Wouw, and H. Nijmeijer, *Convergent dynamics, a tribute to Boris Pavlovich Demidovich,* Systems & Control Letters **52**, 257 (2004).

[43] A. Pavlov, N. van de Wouw, and H. Nijmeijer, *Convergent piecewise affine systems: analysis and design part i: continuous case,* in *Proceedings of the 44th IEEE Conference on Decision and Control* (2005) pp. 5391–5396.

[44] R. M. Schmidt, G. Schitter, and A. Rankers, *The Design of High Performance Mechatronics High-Tech Functionality by Multidisciplinary System Integration* (IOS Press, 2014).

[45] O. Beker, *Analysis of reset control systems.*, Ph.D. thesis, University of Massachusetts Amherst (2002).

[46] A. Pavlov, N. van de Wouw, and H. Nijmeijer, *Frequency response functions and bode plots for nonlinear convergent systems,* in *Proceedings of the 45th IEEE Conference on Decision and Control* (2006) pp. 3765–3770.

[47] A. A. Dastjerdi, *Toolbox for frequency analysis of reset control systems,* .

[48] W.-Y. Huang, C.-P. Chao, J.-R. Kang, and C.-K. Sung, *The application of ball-type balancers for radial vibration reduction of high-speed optic disk drives,* Journal of Sound and Vibration **250**, 415 (2002).

[49] N. Saikumar, D. Valerio, and S. H. HosseinNia, *Complex order control for improved loop-shaping in precision positioning,* in *IEEE 58th Conference on Decision and Control* (2019) pp. 7956–7962.

[50] H. Xiaojun, A. Ahmadi Dastjerdi, N. Saikumar, and S. HosseinNia, *Tuning of 'Constant in gain Lead in phase (CgLp)' reset controller using Higher-Order Sinusoidal Input Describing Function (HOSIDF),* in *Australian and New Zealand Control Conference (ANZCC)* (2020).

[51] M. E. Krijnen, R. A. van Ostayen, and H. HosseinNia, *The application of fractional order control for an air-based contactless actuation system,* ISA Transactions **82**, 172 (2018), fractional Order Signals, Systems, and Controls: Theory and Application.

[52] A. A. Dastjerdi, N. Saikumar, and S. H. HosseinNia, *Tuning of a class of reset elements using pseudo-sensitivities,* arXiv preprint arXiv:2005.02887 (2020).

[53] N. Karbasizadeh, A. Ahmadi Dastjerdi, N. Saikumar, D. Valerio, and S. HosseinNia, *Benefiting from linear behaviour of a nonlinear reset-based element at certain frequencies,* in *Australian and New Zealand Control Conference (ANZCC)* (2020).

4

FREQUENCY-DOMAIN STABILITY METHODS FOR RESET CONTROL SYSTEMS

Ali AHMADI DASTJERDI

As was discussed in the previous chapter, satisfaction of the H_β condition is necessary for the existence of a steady-state solution. Moreover, a frequency-domain stability method is highly needed for providing non linear loop-shaping for reset control systems. In this chapter, an intuitive frequency-domain method for assessing the stability of reset elements based on the H_β condition is proposed. To this end, the H_β method, analytic geometry, and optimization methods are utilized to develop a frequency-domain method for stability analysis for different configurations of the first and second order reset elements. The method can also guarantee an uniformly bounded-input bounded-state (UBIBS) property for reset control systems in the case of resetting to non-zero values. Finally, an illustrative example is presented to demonstrate the effectiveness of the proposed approach to use frequency response measurements directly to assess the stability of the closed-loop reset control systems.

The preliminary results of this chapter are presented in CDC 2020 (see appendix A), and the extended version (this chapter) has been submitted to Automatica.

4.1. INTRODUCTION

High-tech precision industrial applications have control requirements which are hard to fulfil by means of linear controllers. One way to increase the performance of these systems is to replace linear controllers with non linear ones, for instance reset controllers. Owing to their simple structure, these controllers have attracted significant attention from academia and industry [1–10]. In particular, reset controllers have been utilized to improve the performance of several mechatronic systems (see, e.g. [11–20]).

The first reset element was introduced by Clegg [1] in 1958. The Clegg Integrator (CI) is an integrator which resets its state to zero whenever its input signal is zero. To provide additional design freedom and flexibility, extensions of the CI including First Order Reset Elements (FORE) [11, 21], Generalized First Order Reset Elements (GFORE) [17], Second Order Reset Elements (SORE) [12], Generalized Second Order Reset Elements (GSORE) [17], and Second Order Single State Reset Elements (SOSRE) [22] have been developed. Moreover, to improve the performances of these controllers several methods such as reset bands [23, 24], fixed reset instants, partial reset techniques (resetting to a non-zero value or resetting a selection of the controller states) [25], use of shaping filters in the reset instants line [26], and the PI+CI approach [25] have also been investigated.

Similar to every control system, stability is one of the most essential requirements of reset control systems [2, 6, 7, 9, 27–30]. Stability properties for reset control systems have been studied using quadratic Lyapunov functions [6, 9, 31, 32], reset instants dependent methods [29, 33, 34], passivity, small gain, and IQC approaches [27, 35–37]. However, most of these methods are complex, require parametric models of the system and the solution of LMI's, and are only applicable to specific types of systems. Thus, since industry often favors the use of frequency-domain methods, these methods are not well matched with the current control design requirements in industry. To overcome this challenge, some frequency-domain approaches for assessing stability properties of reset control systems have been proposed [2, 7, 38]. A method for determining stability properties of a FORE in closed-loop with a mass-spring-damper system has been developed in [38]. However, this sector-bounded method is only applicable to a specific type of systems. Under the specific reset condition $e(t)u(t) < \dfrac{u^2(t)}{\varepsilon}$, for some $\varepsilon > 0$, in which e and u are the input and the output of the reset element, respectively, the approach in [7] is applicable to reset control systems. However, this method is not applicable to architecture illustrated in Figure. 4.1. In addition, in the case of traditional reset control systems in which the reset condition occurs at $e(t) = 0$, the base linear system of the closed-loop must be positive which implies that it is not appropriate for plants with the relative order more that one.

The H_β condition is one of the widely-used methods for assessing stability properties of reset control systems [2, 9, 29]. In particular, when the base linear system of the reset element has a first order transfer function, it gives sufficient frequency-domain conditions for uniform bounded-input bounded-state (UBIBS) stability. However, assessing the H_β condition in the frequency-domain is not intuitive, especially for plants with high order transfer functions. In addition, the effect of a shaping filter in the reset line on the H_β condition has not been studied yet. Furthermore, there is a lack of methods to assess the H_β condition for GSORE using Frequency Response Function (FRF) mea-

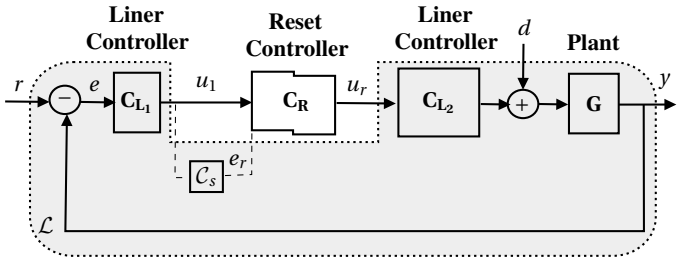

Figure 4.1: The closed-loop architecture of a reset control system

surements. Finally, the H_β condition is not applicable to assess UBIBS stability of reset control systems in the case of partial reset techniques. Hence, obtaining a general easy-to-use frequency-domain method for assessing UBIBS stability of reset control systems is an important open question.

In this paper, on the basis of the H_β condition, novel frequency-domain stability conditions for control systems with first and second order reset elements with a shaping filter in the reset line are proposed. This approach allows for assessing UBIBS stability of reset control systems in the frequency-domain. In this approach, the H_β condition does not have to be explicitly tested and stability properties are directly determined on the basis of the FRF measurements of the base linear open-loop system. In addition, the approach can be used in the case of partial reset techniques.

The remainder of the paper is organized as follows. In Section 4.2 preliminaries about reset elements are presented and the problem is formulated. The frequency-domain approaches for assessing stability properties of control systems with first and second order reset elements are presented in Section 4.3 and Section 4.4, respectively. In Section 4.5 the effectiveness of these approaches is demonstrated via a practical example. Finally, conclusions and suggestions for future studies are given in Section 4.6.

4.2. PRELIMINARIES

In this section the description of reset elements and the H_β condition are breifly recalled and some preliminaries are given. The focus of the paper is on the single-input single-output (SISO) control architecture illustrated in Figure. 4.1. The closed-loop system consists of a linear plant with transfer function $G(s)$ (which we assume strictly proper), linear controllers with proper transfer functions $C_{L_1}(s)$ and $C_{L_2}(s)$, a reset element with base transfer function $C_R(s)$, and a shaping filter with a proper stable transfer function $\mathcal{C}_s(s)$.

The state-space representation of the reset element is

$$\begin{cases} \dot{x}_r(t) = A_r x_r(t) + B_r u_1(t), & e_r(t) \neq 0, \\ x_r(t^+) = A_\rho x_r(t), & e_r(t) = 0 \wedge (I - A_\rho) x_r(t) \neq 0, \\ u_r(t) = C_r x_r(t) + D_r u_1(t), \end{cases} \tag{4.1}$$

in which $x_r(t) \in \mathbb{R}^{n_r}$ is the vector containing the reset state, A_r, B_r, C_r, and D_r are the dynamic matrices of the reset element, A_ρ is the reset matrix, which determines the values of the reset state after the reset action, and $u_1(t) \in \mathbb{R}$ and $u_r(t) \in \mathbb{R}$ are the input and

output of the reset element, respectively. The transfer function $C_r(sI-A_r)^{-1}B_r+D_r$ is called the base transfer function of the reset element. The base transfer function in case of GFORE is (in all cases $\omega_r>0$)

$$C_R(s)=\frac{1}{\frac{s}{\omega_r}+1}, \tag{4.2}$$

for CI and Proportional Clegg Integrator (PCI) one has

$$C_R(s)=\frac{1}{s}, \tag{4.3}$$

$$C_R(s)=1+\frac{\omega_r}{s}, \tag{4.4}$$

and for GSORE one has

$$C_R(s)=\frac{1}{s^2+2\xi\omega_r s+\omega_r^2},\ \xi>0. \tag{4.5}$$

Thus, for GFORE, $A_r=-C_r=-\omega_r$ (ω_r is the so-called corner frequency), $D_r=0$, and $B_r=1$, whereas for the PCI, $A_r=0$, $C_r=\omega_r$, and $B_r=D_r=1$. In the case of CI, $A_r=D_r=0$, $B_r=C_r=1$, and if we consider the controllable canonical form realization for GSORE, we obtain

$$A_r=\begin{bmatrix}-2\xi\omega_r & -\omega_r^2\\ 1 & 0\end{bmatrix},\ B_r=\begin{bmatrix}1\\0\end{bmatrix},\ C_r=\begin{bmatrix}0 & 1\end{bmatrix},\text{ and } D_r=0. \tag{4.6}$$

Let $\mathcal{L}$ be the linear time-invariant (LTI) part of the system, see Figure. 4.1, with input $u_r(t)\in\mathbb{R}$, external disturbance $w(t)=\begin{bmatrix}r(t) & d(t)\end{bmatrix}^T\in\mathbb{R}^2$, and outputs $y(t)\in\mathbb{R}$, $e_r(t)\in\mathbb{R}$, and $u_1(t)\in\mathbb{R}$. The state-space realization of $\mathcal{L}$ is given by equations

$$\mathcal{L}:\begin{cases}\dot{\zeta}(t)=A\zeta(t)+B_u u_r(t)+Bw(t),\\ y(t)=C\zeta(t),\\ e_r(t)=C_e\zeta(t)+D_e r(t),\\ u_1(t)=C_u\zeta(t)+D_1 r(t),\end{cases} \tag{4.7}$$

where $\zeta(t)\in\mathbb{R}^{n_p}$ describes the states of the plant and of the linear controllers (n_p is the number of states of the whole linear part), and A, B, B_u, and C are the corresponding dynamic matrices. The closed-loop state-space representation of the overall system can, therefore, be written as

$$\begin{cases}\dot{x}(t)=\bar{A}x(t)+\bar{B}w(t), & e_r(t)\neq 0,\\ x(t^+)=\bar{A}_\rho x(t), & e_r(t)=0\wedge(I-\bar{A}_\rho)x(t)\neq 0,\\ y(t)=\bar{C}x(t),\\ e_r(t)=\bar{C}_e x(t)+D_e r(t),\end{cases} \tag{4.8}$$

where $x(t)=\begin{bmatrix}x_r(t)^T & \zeta(t)^T\end{bmatrix}^T\in\mathbb{R}^{n_r+n_p}$, $\bar{A}=\begin{bmatrix}A_r & B_rC_u\\ B_uC_r & A+B_uD_rC_u\end{bmatrix}$, $\bar{C}=\begin{bmatrix}0_{1\times n_r} & C\end{bmatrix}$, $\bar{B}=\begin{bmatrix}0_{n_r\times 2}\\ B\end{bmatrix}+\begin{bmatrix}B_rD_1 & 0_{n_r\times 1}\\ B_uD_rD_1 & 0_{n_p\times 1}\end{bmatrix}$, $\bar{C}_e=\begin{bmatrix}0_{1\times n_r} & C_e\end{bmatrix}$, and $\bar{A}_\rho=\begin{bmatrix}A_\rho & 0_{n_r\times n_p}\\ 0_{n_p\times n_r} & I_{n_p\times n_p}\end{bmatrix}$.

Definition 10. *A time $\bar{T} > 0$ is called a reset instant for the reset control system (4.8) if $e_R(\bar{T}) = 0 \wedge (I - \bar{A}_\rho)x(T) \neq 0$. For any given initial condition and input w the resulting set of all reset instants defines the reset sequence $\{t_k\}$, with $t_k \leq t_{k+1}$, for all $k \in \mathbb{N}$. The reset instants t_k have the well-posedness property if for any initial condition x_0 and any input w, all the reset instants are distinct, and there exists $\lambda > 0$ such that, for all $k \in \mathbb{N}$, $\lambda \leq t_{k+1} - t_k$ [6, 39].*

One of the methods for determining stability properties of reset control systems is the H_β condition [2, 6, 9, 29, 40], which is briefly recalled. Let

$$C_0 = [\varrho \quad \beta C], \quad B_0 = \begin{bmatrix} I_{n_r \times n_r} \\ 0_{n_p \times n_r} \end{bmatrix}, \quad \varrho = \varrho^T > 0, \quad \varrho \in \mathbb{R}^{n_r \times n_r}, \ \beta \in \mathbb{R}^{n_r \times 1}. \tag{4.9}$$

The H_β condition [2, 6, 9, 29, 40] states that the zero equilibrium of the reset control system (4.8) with $C_{L_1} = C_s = 1$ and $w = 0$ is globally uniformly asymptotically stable if and only if there exist $\varrho = \varrho^T > 0$ and β such that the transfer function

$$H(s) = C_0(sI - \bar{A})^{-1}B_0 \tag{4.10}$$

is Strictly Positive Real (SPR), $(\bar{A}, B_0)$ and $(\bar{A}, C_0)$ are controllable and observable, respectively, and

$$A_\rho^T \varrho A_\rho - \varrho \ \leq 0. \tag{4.11}$$

Evaluating the H_β condition requires finding the parameters ϱ and β, which may be very difficult when the system has a high order transfer function. Furthermore, in the case of GSORE there is no direct frequency-domain method to assess this condition. Besides, the UBIBS property of GSORE and GFORE have not yet been studied, and the effects of the shaping filter on the H_β condition have not been considered yet. In the current paper, frequency-domain methods to determine stability properties without finding ϱ and β for GFORE and GSORE with considering the shaping filter are proposed.

Assumption 2. *There are infinitely many reset instants and* $\lim_{k\to\infty} t_k = \infty$.

Assumption 2 is introduced to rule out a trivial situation. In fact, if there is a finite T_K as the last rest instant, then for all $t \geq T_K$ the reset control system (4.8) is a linear stable system if the H_β condition is satisfied. In addition to Assumption 2, we need the following assumption, which is instrumental to study the UBIBS property of reset control systems.

Assumption 3. *In the case of partial reset technique, if A_ρ has the structure*

$$A_\rho = \begin{bmatrix} I_{\bar{n}_r} & 0 \\ 0 & A'_{n'_r} \end{bmatrix},$$

then A_r has the structure

$$A_r = \begin{bmatrix} A_{r_1} & A_{r_2} \\ 0_{\bar{n}_r \times n'_r} & A_{r_3} \end{bmatrix}.$$

Remark 5. In the case of GFORE, GSORE, PCI, and CI in which all states of the reset element reset, Assumption 3 holds.

Before stating the main theorem, an important technical lemma, which is instrumental for all proofs, is formulated and proved.

Lemma 5. *Consider the reset control system (4.8). Suppose that*

- *Assumption 2 holds;*
- $A_\rho^T \varrho A_\rho - \varrho < 0$*;*
- *the H_β condition holds;*
- *at least one of the following conditions holds:*
  1. $\mathcal{C}_s = 1$ *and Assumption 3 holds;*
  2. *the reset instants have the well-posedness property.*

Then the reset control system (4.8) has a well-defined unique left-continuous solution for any initial condition x_0 and any input w which is a Bohl function[1]*. In addition, this solution is UBIBS and the reset instants have the well-posedness property.*

Proof. See Appendix 4.A. □

4.3. STABILITY ANALYSIS OF RESET CONTROL SYSTEMS WITH FIRST ORDER RESET ELEMENTS

In this section frequency-domain methods for assessing stability properties of the reset control system (4.8) with GFORE (4.2), CI (4.3), and PCI (4.4) are proposed on the basis of the H_β condition. To this end, the Nyquist Stability Vector (NSV=$\vec{\mathcal{N}}(\omega) \in \mathbb{R}^2$) in a plane with axis $\chi - \Upsilon$ (see Figure. 4.2) is defined as follows.

Definition 11. *The Nyquist Stability Vector is, for all $\omega \in \mathbb{R}^+$, the vector*

$$\begin{aligned}\vec{\mathcal{N}}(\omega) &= [\mathcal{N}_\chi \quad \mathcal{N}_\Upsilon]^T \\ &= [\Re(L(j\omega)\mathcal{C}_s(j\omega)\kappa(j\omega)) \quad \Re(\kappa(j\omega)C_R(j\omega))]^T,\end{aligned}$$

in which $L(s) = C_{L_1}(s)C_R(s)C_{L_2}(s)G(s)$, $L(j\omega) = a(\omega) + b(\omega)j$, and $\kappa(j\omega) = 1 + L^*(j\omega)$ ($L^*(j\omega)$ is the conjugate of $L(j\omega)$).

For simplicity, and without loss of generality, let $\angle\vec{\mathcal{N}}(\omega) = \theta_\mathcal{N} \in [-\frac{\pi}{2}, \frac{3\pi}{2})$ and define the open sets

$$\mathcal{I}_1 = \left\{\omega \in \mathbb{R}^+ \mid 0 < \angle\vec{\mathcal{N}}(\omega) < \frac{\pi}{2}\right\},$$

$$\mathcal{I}_2 = \left\{\omega \in \mathbb{R}^+ \mid \frac{\pi}{2} < \angle\vec{\mathcal{N}}(\omega) < \pi\right\},$$

[1] See definition Bohl function in [39]

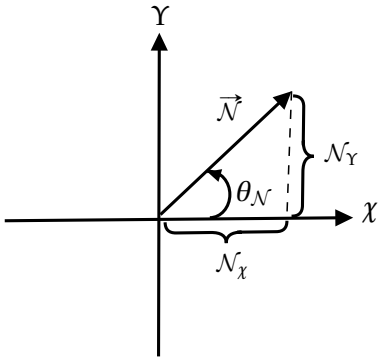

Figure 4.2: Representation of the NSV in the $\chi - \Upsilon$ plane

$$\mathcal{I}_3 = \left\{\omega \in \mathbb{R}^+ \,|\, \pi < \angle\vec{\mathcal{N}}(\omega) < \frac{3\pi}{2}\right\},$$

$$\mathcal{I}_4 = \left\{\omega \in \mathbb{R}^+ \,|\, -\frac{\pi}{2} < \angle\vec{\mathcal{N}}(\omega) < 0\right\}.$$

Let $L(s)\mathcal{C}_s(s) = \dfrac{K_m s^m + K_{m-1}s^{m-1} + \ldots + K_0}{s^n + K'_{n-1}s^{n-1} + \ldots + K'_0}$ and $\mathcal{C}_s(s) = \dfrac{K_{s_m}s^{n_m} + K_{s_{m-1}}s^{m_s-1} + \ldots + K_{s_0}}{K'_{s_n}s^{n_s} + K'_{s_{n-1}}s^{n_s-1} + \ldots + 1}$.
On the basis of the definition of the NSV, systems of Type I and of Type II, which are used to assess stability properties of the reset control system (4.8), are defined.

Definition 12. *The reset control system (4.8) is of Type I if the following conditions hold.*

(1) If $C_{L_1}(s)C_{L_2}(s)G(s)$ has at least one pole at the origin, then $K_{s_0} > 0$.

(2) In the case of CI (4.3), $K_{s_0} < 0$.

(3) For all $\omega \in \mathcal{M} = \{\omega \in \mathbb{R}^+ \,|\, \mathcal{N}_\chi(\omega) = 0\}$ one has $\mathcal{N}_\Upsilon(\omega) > 0$.

(4) For all $\omega \in \mathcal{Q} = \{\omega \in \mathbb{R}^+ \,|\, \mathcal{N}_\Upsilon(\omega) = 0\}$ one has $\mathcal{N}_\chi(\omega) > 0$.

(5) At least one of the following statements is true:

(a) $\forall\, \omega \in \mathbb{R}^+ : \mathcal{N}_\Upsilon(\omega) \geq 0$.

(b) $\forall\, \omega \in \mathbb{R}^+ : \mathcal{N}_\chi(\omega) \geq 0$.

(c) Let $\delta_1 = \max\limits_{\omega\in\mathcal{I}_4}\left|\dfrac{\mathcal{N}_\Upsilon(\omega)}{\mathcal{N}_\chi(\omega)}\right|$ and $\Psi_1 = \min\limits_{\omega\in\mathcal{I}_2}\left|\dfrac{\mathcal{N}_\Upsilon(\omega)}{\mathcal{N}_\chi(\omega)}\right|$. Then $\delta_1 < \Psi_1$ and $\mathcal{I}_3 = \varnothing$.

Remark 6. Let

$$\theta_1 = \min_{\omega\in\mathbb{R}^+}\angle\vec{\mathcal{N}}(\omega) \text{ and } \theta_2 = \max_{\omega\in\mathbb{R}^+}\angle\vec{\mathcal{N}}(\omega). \tag{4.12}$$

Then the conditions identifying Type I systems are equivalent to the following conditions.

(1) If $C_{L_1}(s)C_{L_2}(s)G(s)$ has at least one at the origin, then $K_{s_0} > 0$.

(2) In the case of CI (4.3), $K_{s_0} < 0$.

(3) The condition

$$\left(-\frac{\pi}{2} < \theta_1 < \pi\right) \wedge \left(-\frac{\pi}{2} < \theta_2 < \pi\right) \wedge (\theta_2 - \theta_1 < \pi) \tag{4.13}$$

holds.

Definition 13. *The reset control system (4.8) is of Type II if the following conditions hold.*

(1) If $C_{L_1}(s)C_{L_2}(s)G(s)$ has at least one at the origin, then $K_{s_0} < 0$.

(2) In the case of CI (4.3), $K_{s_0} > 0$.

(3) For all $\omega \in \mathcal{M}$ one has $\mathcal{N}_\Upsilon(\omega) > 0$.

(4) For all $\omega \in \mathcal{Q}$ one has $\mathcal{N}_\chi(\omega) < 0$.

(5) At least, one of the following statements is true:

(a) $\forall\, \omega \in \mathbb{R}^+ : \mathcal{N}_\Upsilon(\omega) \geq 0$;

(b) $\forall\, \omega \in \mathbb{R}^+ : \mathcal{N}_\chi(\omega) \leq 0$;

(c) Let $\delta_2 = \max\limits_{\omega \in \mathcal{I}_3} \left| \dfrac{\mathcal{N}_\Upsilon(\omega)}{\mathcal{N}_\chi(\omega)} \right|$ and $\Psi_2 = \min\limits_{\omega \in \mathcal{I}_1} \left| \dfrac{\mathcal{N}_\Upsilon(\omega)}{\mathcal{N}_\chi(\omega)} \right|$. Then, $\delta_2 < \Psi_2$ and $\mathcal{I}_4 = \varnothing$.

Remark 7. The conditions identifying Type II systems are equivalent to the following conditions.

(1) If $C_{L_1}(s)C_{L_2}(s)G(s)$ has at least one at the origin, then $K_{s_0} < 0$.

(2) In the case of CI (4.3), $K_{s_0} > 0$.

(3) The condition

$$\left(0 < \theta_1 < \frac{3\pi}{2}\right) \wedge \left(0 < \theta_2 < \frac{3\pi}{2}\right) \wedge (\theta_2 - \theta_1 < \pi) \tag{4.14}$$

holds.

Theorem 4. *The zero equilibrium of the reset control system (4.8) with GFORE (4.2), or CI (4.3), or PCI (4.4) is globally uniformly asymptotically stable when $w = 0$, and the system has the UBIBS property for any input w which is a Bohl function if all of the following conditions are satisfied.*

- *The base linear system is stable and the open-loop transfer function does not have any pole-zero cancellation.*
- *In the case of CI (4.3), $C_{L_1}(s)C_{L_2}(s)G(s)$ does not have any pole at the origin and $n - m = 2$ (i.e. the slope gain at high frequency is equal to -2).*
- *The reset control system (4.8) is either of Type I and/or of Type II.*

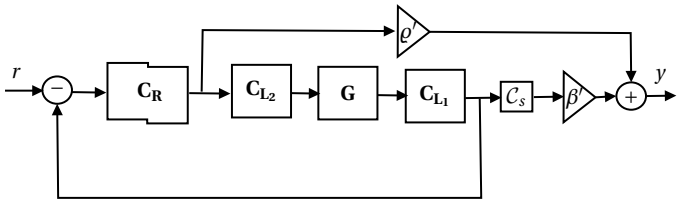

Figure 4.3: The block diagram of the H_β condition for the closed-loop architecture Figure. 4.1 with GFORE or PCI

- $A_\rho = \gamma,\ -1 < \gamma < 1$.
- $\mathcal{C}_s(s) = 1$ *and/or the reset instants have the well-posedness property.*

Proof. For $w(t) = 0$, for all $t \geq 0$, reset happens when $x(t) \in \ker(\bar{C}_e)$. Looking at the proof of the H_β condition, which is given in [2, 6, 9], when there is a shaping filter in the reset line, C_0 in the H_β condition is changed to

$$C_0 = [\varrho \quad \beta\bar{C}_e]. \tag{4.15}$$

Theorem 4 is now proved in several steps.

- Step 1: It is shown that there is a β and $\varrho > 0$ such that $\Re(H(j\omega)) > 0$, for all $\omega \in \mathbb{R}^+$.
- Step 2: For systems with poles at the origin it is shown that $\lim_{\omega\to 0} \Re(H(j\omega)) > 0$.
- Step 3: It is shown that either $\lim_{s\to\infty} H(s) > 0$ or $\lim_{\omega\to\infty} \omega^2\Re(H(j\omega)) > 0$.
- Step 4: It is shown that (A, C_0) and (A, B_0) are observable and controllable, respectively.

Step 1: For simplicity take $\beta' = -\beta$ and $\varrho' = \dfrac{\varrho}{C_r}$. The transfer function (4.10) with the modified C_0 as in (4.15) can be rewritten as (see also Figure. 4.3)

$$H(s) = \frac{y}{r} = \frac{\beta' L(s)\mathcal{C}_s(s) + \varrho' C_R(s)}{1 + L(s)}. \tag{4.16}$$

Thus[2]

$$\Re(H(j\omega)) = \frac{\beta'\mathcal{N}_\chi + \varrho'\mathcal{N}_\upsilon}{(a+1)^2 + b^2}. \tag{4.17}$$

Define now the vector $\vec{\xi}$ in the χ–υ plane as $\vec{\xi} = [\beta' \quad \varrho']^T$. Using Definition 11, equation (4.17) can be re-written as

$$\Re(H(j\omega)) = \frac{\vec{\xi}\cdot\vec{\mathcal{N}}}{(a+1)^2 + b^2}. \tag{4.18}$$

[2] Omitting arguments for simplicity

Therefore

$$\begin{aligned}\forall\omega\in\mathbb{R}^+:\ \Re(H(j\omega))>0 \iff \vec{\xi}\cdot\vec{\mathcal{N}}>0 \iff\\ -\tfrac{\pi}{2}<\angle(\vec{\xi},\vec{\mathcal{N}})<\tfrac{\pi}{2}\ \wedge\ \left|\vec{\mathcal{N}}\right|\neq 0\ \wedge\ \left|\vec{\xi}\right|\neq 0.\end{aligned} \tag{4.19}$$

The rest of the proof of this step are the same as the proof of Step 1 provided in [41] (see Appendix A).

Step 2: When the open-loop system has poles at the origin and C_R is a GFORE, equation (4.16) becomes

$$\lim_{\omega\to 0}\Re(H(j\omega))=K_{s_0}\beta'>0, \tag{4.20}$$

whereas in the case of PCI and CI when $C_{L_1}(s)C_{L_2}(s)G(s)$ does not have any pole at the origin, (4.16) becomes

$$\lim_{\omega\to 0}\Re(H(j\omega))=K_{s_0}\beta'+\varrho'\frac{\omega_r}{C_{L_1}(0)C_{L_2}(0)G(0)}>0. \tag{4.21}$$

Setting $\vec{\mathcal{N}'}=[K_{s_0}\quad \frac{\omega_r}{C_{L_1}(0)C_{L_2}(0)G(0)}]^T$, yields

$$\lim_{\omega\to 0}\Re(H(j\omega))=\vec{\xi}\cdot\vec{\mathcal{N}'}. \tag{4.22}$$

In addition

$$\angle\vec{\mathcal{N}'}=\lim_{\omega\to 0}\angle\vec{\mathcal{N}}\overset{(4.12)}{\Longrightarrow}\theta_1\leq\angle\vec{\mathcal{N}'}\leq\theta_2. \tag{4.23}$$

As a result, by Step 1, $\lim_{\omega\to 0}\Re(H(j\omega))=\vec{\xi}\cdot\vec{\mathcal{N}'}>0$. For PCI, when $C_{L_1}(s)C_{L_2}(s)G(s)$ has poles at the origin,

$$\lim_{\omega\to 0}\Re(H(j\omega))=K_{s_0}\beta'>0. \tag{4.24}$$

Note that for CI in equations (4.21)-(4.23), $\omega_r=1$. It is therefore concluded that if $C_{L_1}(s)C_{L_2}(s)G(s)$ has poles at the origin, then $K_{s_0}\beta'>0$. If $C_{L_1}(s)C_{L_2}(s)G(s)$ does not have any pole at the origin, β can be either positive or negative.

Step 3: In the case of GFORE with $n-m=2$, setting $\vec{\mathcal{N}''}=[-K_n\quad \omega_r^2]^T$ yields

$$\lim_{\omega\to\infty}\omega^2\Re(H(j\omega))=-\beta'K_n+\varrho'\omega_r^2=\vec{\xi}\cdot\vec{\mathcal{N}''}. \tag{4.25}$$

In addition,

$$\angle\vec{\mathcal{N}''}=\lim_{\omega\to\infty}\angle\vec{\mathcal{N}}\overset{(4.12)}{\Longrightarrow}\theta_1\leq\angle\vec{\mathcal{N}''}\leq\theta_2. \tag{4.26}$$

Thus, by Step 1 $\lim_{\omega\to\infty}\omega^2\Re(H(j\omega))=\vec{\xi}\cdot\vec{\mathcal{N}''}>0$. For GFORE with $n-m>2$, $\lim_{\omega\to\infty}\omega^2\Re(H(j\omega))=\varrho'\omega_r^2>0$. For PCI $\lim_{s\to\infty}H(s)=\varrho'>0$. Moreover, in the case of CI when $n-m>2$,

$$\lim_{\omega\to\infty}\omega^2\Re(H(j\omega))=0, \tag{4.27}$$

which implies that $H(s)$ is not SPR in the case of $n-m>2$. Whereas in the case of CI with $n-m=2$,

$$\lim_{\omega\to\infty}\omega^2\Re(H(j\omega))=-K_{s_0}\beta'>0, \tag{4.28}$$

which means that in the case of CI, $C_{L_1}(s)C_{L_2}(s)G(s)$ must not have any pole at the origin. Step 4: In order to show that the pairs (A, C_0) and (A, B_0) are observable and controllable, respectively, it is sufficient to show that the denominator and the numerator of $H(s)$ do not have any common root. Let $a_0 + jb_0$ be a root of the denominator. Then

$$1 + R_L(a_0, b_0) + jI_L(a_0, b_0) = 0 \Rightarrow \begin{cases} R_L(a_0, b_0) = -1, \\ I_L(a_0, b_0) = 0. \end{cases} \tag{4.29}$$

Now, the numerator must not have a root at $a_0 + jb_0$, that is

$$\begin{aligned} &\beta'\left(R_{\mathcal{C}_s}(a_0, b_0) + jI_{\mathcal{C}_s}(a_0, b_0)\right) \neq \varrho'\left(R_{C_R}(a_0, b_0) + jI_{C_R}(a_0, b_0)\right) \\ &\Rightarrow \beta' R_{\mathcal{C}_s}(a_0, b_0) \neq \varrho' R_{C_R}(a_0, b_0) \ \vee \ \beta' I_{\mathcal{C}_s}(a_0, b_0) \neq \varrho' I_{C_R}(a_0, b_0). \end{aligned} \tag{4.30}$$

Therefore, using Step 1 and (4.30) it is possible to find a pair (β', ϱ') such that $H(s)$ does not have any pole-zero cancellation. According to Step 1-4, $H(s)$ is SPR [27], $(\bar{A}, C_0)$ is observable and $(\bar{A}, B_0)$ is controllable, and the base linear system is stable. Moreover, since $-1 < \gamma < 1$, one has that $A_\rho^T \varrho A_\rho - \varrho < 0$. As a result, the H_β condition is satisfied for the reset control system (4.8) with GFORE (4.2), or CI (4.3), or PCI (4.4). Hence, the zero equilibrium of the reset control system (4.8) is globally uniformly asymptotically stable when $w = 0$, and according to Lemma 5, it has the UBIBS property for any initial condition x_0 and any input w which is a Bohl function. □

Corollary 8. *Let $\mathcal{C}_s(s) = 1$, $\theta_L = \angle L(j\omega)$, and $\theta_{C_R} = \angle C_R(j\omega)$. Suppose that the base linear system of the reset control system (4.8) is stable, $A_\rho = \gamma$, $-1 < \gamma < 1$, $L(s)$ and the open-loop system does not have any pole-zero cancellation. Then the zero equilibrium of the reset control system (4.8) with GFORE (4.2), or CI (4.3), or PCI (4.4) is globally uniformly asymptotically stable when $w = 0$, and the system has the UBIBS property for any input w which is a Bohl function if at least one of the following conditions hold.*

1. *For all $\omega \in \mathbb{R}^+$, $\sin(\theta_L) \geq 0$.*
2. *For all $\omega \in \mathbb{R}^+$, $\cos(\theta_L - \theta_{C_R}) \geq 0$ and the reset element is not CI (4.3).*

Proof. When $\mathcal{C}_s(s) = 1$, $\mathcal{N}_\chi(\omega) = a(\omega)^2 + b(\omega)^2 + b(\omega)$. By Hypothesis 1, $b(\omega) \geq 0$, for all $\omega \in \mathbb{R}^+$, which implies that $\mathcal{N}_\chi(\omega) > 0$. Thus, the reset control system (4.8) is of Type I. In addition, defining $C_R(j\omega) = a_R(\omega) + jb_R(\omega)$, yields $\mathcal{N}_\Upsilon(\omega) = a(\omega)a_R(\omega) + b(\omega)b_R(\omega) + a_R(\omega)$. By Hypothesis 2,

$$\forall\, \omega \in \mathbb{R}^+ : \cos(\theta_L - \theta_{C_R}) \geq 0 \Rightarrow \frac{a(\omega)a_R(\omega) + b(\omega)b_R(\omega)}{|L(j\omega)C_R(j\omega)|} \geq 0, \tag{4.31}$$

and since $a_R(\omega) > 0$ in the cases of PCI and GFORE, $\mathcal{N}_\Upsilon(\omega) > 0$, for all $\omega \in \mathbb{R}^+$. Therefore, the reset control system (4.8) is of Type I and/or Type II, hence the claim. □

In [42] the GFORE, CI and PCI architectures have been modified to improve the performance of reset control systems. Using the same procedure as Theorem 4 a frequency-domain method to assess stability properties of these reset control systems illustrated in Figure. 4.4 is proposed.

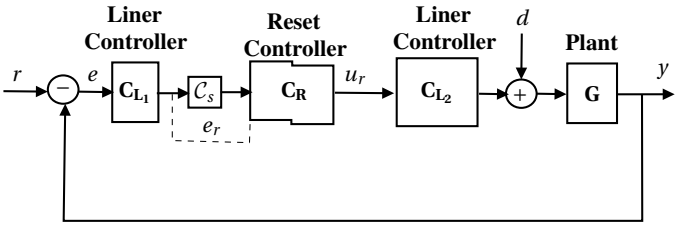

Figure 4.4: The closed-loop architecture of a modified reset element

Corollary 9. *Let the NSV vector for the reset control system shown in Figure. 4.4 be*

$$\begin{aligned}\overrightarrow{\mathcal{N}}_{MF}(\omega) &= [\mathcal{N}_{MF_\chi} \quad \mathcal{N}_{MF_\Upsilon}]^T \\ &= \left[\Re\left(\frac{L'(j\omega)\kappa(j\omega)}{\mathcal{C}_s(j\omega)}\right) \quad \Re(\kappa(j\omega)C_R(j\omega))\right]^T, \end{aligned} \tag{4.32}$$

in which $L'(s) = C_{L_1}(s)C_R(s)C_{L_2}(s)\mathcal{C}_s(s)G(s)$. Then, the zero equilibrium of the reset control system (4.8) in the configuration of Figure. 4.4 with GFORE (4.2), or CI (4.3), or PCI (4.4) is globally uniformly asymptotically stable when $w = 0$, and the system has the UBIBS property for any input w which is a Bohl function if all of the following conditions are satisfied.

- *The base linear system is stable and the open-loop transfer function does not have any pole-zero cancellation.*
- *In the case of CI (4.3), $C_{L_1}(s)C_{L_2}(s)G(s)$ does not have any pole at the origin and $n - m = 2$ (i.e. slope gain at high frequency is equal to -2).*
- *The reset control system (4.8) is either of Type I and/or of Type II.*
- $A_\rho = \gamma$, $-1 < \gamma < 1$.
- $\mathcal{C}_s(s) = 1$ *and/or the reset instants have the well-posedness property.*

Proof. See Appendix 4.B. □

4.4. STABILITY ANALYSIS OF RESET CONTROL SYSTEMS WITH SECOND ORDER RESET ELEMENTS

4.4.1. RESET CONTROL SYSTEMS WITH GSORE

In this section a frequency-domain method for assessing stability properties of the reset control system (4.8) with GSORE (4.5), which has the canonical controllable form state-space realization (4.6), is proposed. In this method the H_β condition is combined with optimization tools to provide sufficient conditions to guarantee stability properties of the reset control system (4.8). Before presenting the main result, one preliminary fact, which is useful for assessing stability properties of the reset control system (4.8) with GSORE (4.5), is presented.

Proposition 1. *Let* $\vec{\mathcal{Q}} \in \mathbb{R}^2$ *and* $\vec{\mathcal{F}} \in \mathbb{R}^2$ *be defined as* $\vec{\mathcal{Q}} = \begin{bmatrix} Q_1 & Q_2 \end{bmatrix}^T$ *and* $\vec{\mathcal{F}}(\omega) = \begin{bmatrix} \mathcal{F}_1(\omega) & \mathcal{F}_2(\omega) \end{bmatrix}^T$. *Let* $\underline{/\vec{\mathcal{Q}}, \vec{\mathcal{F}}(\omega)} = \vartheta(\omega, \frac{Q_2}{Q_1})$, $\omega_p = \{\omega \in \mathbb{R}^+ | \ \mathcal{F}_3(\omega) \geq 0\}$, $\omega_N = \mathbb{R}^+ - \omega_p$, $g_p = \left\{ \frac{Q_2}{Q_1} \in \mathbb{R} | \ \forall \omega \in \omega_p : \ Q_1\mathcal{F}_1(\omega) + Q_2\mathcal{F}_2(\omega) > 0 \right\}$, *and*

$$g_N = \left\{ \frac{Q_2}{Q_1} \in \mathbb{R} | \ \forall \omega \in \omega_N : \ Q_1\mathcal{F}_1(\omega) + Q_2\mathcal{F}_2(\omega) > 0 \right\}.$$

Then the condition

$$Q_1\mathcal{F}_1(\omega) + Q_2\mathcal{F}_2(\omega) > \mathcal{F}_3(\omega), \tag{4.33}$$

holds for all $\omega \in \mathbb{R}$ *if and only if*

- $\eta_1(\frac{Q_2}{Q_1}) < \sqrt{Q_1^2 + Q_2^2} < \eta_2(\frac{Q_2}{Q_1})$,
- $\frac{Q_2}{Q_1} \in \left\{ \frac{Q_2}{Q_1} \in g_p | \ \eta_1(\frac{Q_2}{Q_1}) < \eta_2(\frac{Q_2}{Q_1}) \right\}$,

where

$$\eta_1(\frac{Q_2}{Q_1}) = \begin{cases} -\infty & \omega_p = \varnothing, \\ \max\limits_{\omega \in \omega_p} \dfrac{\mathcal{F}_3(\omega)}{\cos(\vartheta)\sqrt{\mathcal{F}_1^2(\omega) + \mathcal{F}_2^2(\omega)}}, & \omega_p \neq \varnothing, \end{cases}$$

$$\eta_2(\frac{Q_2}{Q_1}) = \begin{cases} +\infty & \dfrac{Q_2}{Q_1} \in g_N \vee \omega_N = \varnothing, \\ \min\limits_{\omega \in \omega_N} \dfrac{\mathcal{F}_3(\omega)}{\cos(\vartheta)\sqrt{\mathcal{F}_1^2(\omega) + \mathcal{F}_2^2(\omega)}}, & \dfrac{Q_2}{Q_1} \notin g_N. \end{cases} \tag{4.34}$$

Proof. See Appendix 4.C. □

Remark 8. The sets g_p and g_N can be easily obtained using the method described in [41].

Define now

$$
\begin{aligned}
f_1(\mathcal{X}_1,\mathcal{X}_2,\mathcal{X}_3,\omega)&=\mathcal{X}_1\Re(C_R(j\omega)\kappa(\omega)j\omega)+\mathcal{X}_2\Re(C_R(j\omega)\kappa(\omega))+\mathcal{X}_3\Re(\mathcal{C}_s(j\omega)(a^2+b^2+a)),\\
f_2(\mathcal{X}_1,\mathcal{X}_2,\mathcal{X}_3,\omega)&=\mathcal{X}_1\Re(C_R(j\omega)\kappa(\omega)(j\omega+2\xi\omega_r))+\mathcal{X}_3\Re(L(j\omega)\kappa(\omega)\mathcal{C}_s(j\omega)(j\omega+2\xi\omega_r))\\
&\quad+\mathcal{X}_2\Re(C_R(j\omega)\kappa(\omega)(2j\xi\omega_r\omega-\omega^2)-(a+1)^2-b^2),\\
G_1(Q_1,Q_2,Q_3,Q_4)&=\sup_{\omega\in(0,\infty)}\left[\frac{f_1(Q_1,Q_2,1,\omega)}{f_1(Q_2,\frac{Q_2Q_3}{Q_4},\frac{Q_2}{Q_4},\omega)+f_2(Q_2,Q_1,1,\omega)}\right.\\
&\quad\left.\times\frac{f_2(Q_3,Q_4,1,\omega)}{f_1(Q_4,Q_3,1,\omega)+f_2(Q_4,\frac{Q_1Q_4}{Q_2},\frac{Q_4}{Q_2},\omega)}\right],\\
G_2(Q_1,Q_2,Q_3,Q_4)&=\sup_{\omega\in[0,\infty)}\left[\frac{f_1(1,Q_2,Q_1,\omega)}{f_1(Q_2,\frac{Q_2}{Q_4},\frac{Q_2Q_3}{Q_4},\omega)+f_2(Q_2,1,Q_1,\omega)}\right.\\
&\quad\left.\times\frac{f_2(1,Q_4,Q_3,\omega)}{f_1(Q_4,1,Q_3,\omega)+f_2(Q_4,\frac{Q_4}{Q_2},\frac{Q_1Q_4}{Q_2},\omega)}\right],\\
\Gamma(\gamma_1,\gamma_2)&=\frac{(\gamma_1\gamma_2-1)^2}{(\gamma_1^2-1)(\gamma_2^2-1)}.
\end{aligned}
$$

We define systems of Type III, of Type IV, and of Type V to assess stability properties of the reset control system (4.8) with GSORE (4.6).

Definition 14. *The reset control system (4.8) with GSORE (4.6) is of Type III if the following conditions hold.*

(1) $M<4$, where $M=\min_{Q_1,Q_2,Q_3,Q_4} G_1(Q_1,Q_2,Q_3,Q_4)$, in which Q_1, Q_2, Q_3, and Q_4 are such that the following constraints hold:

$$
\begin{aligned}
&\mathcal{S}_1: \quad \forall\omega\in(0,\infty):\ K_{s_0}f_1(Q_1,Q_2,1,\omega)>0,\\
&\mathcal{S}_2: \quad \forall\omega\in(0,\infty):\ K_{s_0}f_2(Q_3,Q_4,1,\omega)>0,\\
&\mathcal{S}_3: \quad K_{s_0}\left(\frac{2\xi\omega_r}{Q_1}+\frac{Q_2}{Q_1Q_4}+\frac{2}{Q_1}\sqrt{\frac{2Q_2\xi\omega_r}{Q_4}-\frac{Q_2}{K_{s_0}}}\right)>1,\\
&\mathcal{S}_4: \quad K_{s_0}\left(\frac{2\xi\omega_r}{Q_1}+\frac{Q_2}{Q_1Q_4}-\frac{2}{Q_1}\sqrt{\frac{2Q_2\xi\omega_r}{Q_4}-\frac{Q_2}{K_{s_0}}}\right)<1,\\
&\mathcal{S}_5: \quad \frac{\omega_r^2Q_1}{Q_2}+2\omega_r\left(\xi+2\sqrt{\frac{2Q_1\xi\omega_r}{Q_2}-1}\right)>\frac{Q_3}{Q_4},\\
&\mathcal{S}_6: \quad \frac{\omega_r^2Q_1}{Q_2}+2\omega_r\left(\xi-2\sqrt{\frac{2Q_1\xi\omega_r}{Q_2}-1}\right)<\frac{Q_3}{Q_4},\\
&\mathcal{S}_7: \quad K_{s_0}Q_i>0,\ 2\xi\omega_r>\frac{Q_4}{K_{s_0}},\ 2\xi\omega_r>\frac{Q_2}{Q_1},\ \frac{Q_1Q_3}{Q_2Q_4}>\Gamma(\gamma_1,\gamma_2).
\end{aligned}
\tag{4.35}
$$

(2) The pairs $(\bar{A}, C_0)$ *and* $(\bar{A}, B_0)$ *where* $C_0 = \begin{bmatrix} \begin{bmatrix} 1 \\ \frac{Q_2}{Q_4} \end{bmatrix} \bar{C}_e & \begin{bmatrix} Q_1 & Q_2 \\ Q_2 & \frac{Q_2 Q_3}{Q_4} \end{bmatrix} \end{bmatrix}$ *and* $B_0 = \begin{bmatrix} 0_{n_p \times 2} \\ I_2 \end{bmatrix}$ *are observable and controllable, respectively.*

(3) The open-loop system has at least one pole at the origin and $K_{s_0} \neq 0$.

Definition 15. *The reset control system (4.8) with GSORE (4.6) is of Type IV if the following conditions hold.*

(1) $M < 4$, *where* $M = \min_{Q_1,Q_2,Q_3,Q_4} G_2(Q_1, Q_2, Q_3, Q_4)$, *in which* Q_1, Q_2, Q_3, *and* Q_4 *are such that the following constraints hold:*

$$\begin{aligned}
&\mathcal{S}_1: \quad \forall \omega \in [0,\infty): \ f_1(1, Q_2, Q_1, \omega) > 0, \\
&\mathcal{S}_2: \quad \forall \omega \in [0,\infty): \ f_2(1, Q_4, Q_3, \omega) > 0, \\
&\mathcal{S}_3: \quad \omega_r^2 + 2\omega_r \left(\xi Q_2 + 2\sqrt{2Q_2 \xi \omega_r - Q_2^2} \right) > \frac{Q_2}{Q_4}, \\
&\mathcal{S}_4: \quad \omega_r^2 + 2\omega_r \left(\xi Q_2 - 2\sqrt{2Q_2 \xi \omega_r - Q_2^2} \right) < \frac{Q_2}{Q_4}, \\
&\mathcal{S}_5: \quad Q_4 > 0, \ 0 < Q_2 < 2\xi\omega_r, \ Q_2 Q_4 < \frac{1}{\Gamma(\gamma_1, \gamma_2)}, \ Q_1 \in \mathbb{R}, \ Q_3 \in \mathbb{R}.
\end{aligned} \tag{4.36}$$

(2) The pairs $(\bar{A}, C_0)$ *and* $(\bar{A}, B_0)$ *where* $C_0 = \begin{bmatrix} \begin{bmatrix} Q_1 \\ \frac{Q_2 Q_3}{Q_4} \end{bmatrix} \bar{C}_e & \begin{bmatrix} 1 & Q_2 \\ Q_2 & \frac{Q_2}{Q_4} \end{bmatrix} \end{bmatrix}$ *and* $B_0 = \begin{bmatrix} 0_{n_p \times 2} \\ I_2 \end{bmatrix}$ *are observable and controllable, respectively.*

(3) The open-loop system does not have any pole at the origin.

(4) $n - m > 3$ *(the slope gain at high frequencies is less than -3).*

Definition 16. *The reset control system (4.8) with GSORE (4.6) is of Type V if the following conditions hold.*

(1) $M < 4$, *where* $M = \min_{Q_1,Q_2,Q_3,Q_4} G_2(Q_1, Q_2, Q_3, Q_4)$, *in which* Q_1, Q_2, Q_3, *and* Q_4 *are*

such that the following constraints hold:

$$
\begin{aligned}
&\mathcal{S}_1: \quad \forall \omega \in [0,\infty): \ f_1(1,Q_2,Q_1,\omega) > 0,\\
&\mathcal{S}_2: \quad \forall \omega \in [0,\infty): \ f_2(1,Q_4,Q_3,\omega) > 0,\\
&\mathcal{S}_3: \quad \omega_r^2 - K_n Q_1 + 2\xi\omega_r Q_2 + 2\sqrt{2\xi\omega_r^3 Q_2 + \frac{Q_2^2 Q_3 K_n}{Q_4} - \omega_r^2 Q_2^2} > \frac{Q_2}{Q_4},\\
&\mathcal{S}_4: \quad \omega_r^2 - K_n Q_1 + 2\xi\omega_r Q_2 - 2\sqrt{2\xi\omega_r^3 Q_2 + \frac{Q_2^2 Q_3 K_n}{Q_4} - \omega_r^2 Q_2^2} < \frac{Q_2}{Q_4},\\
&\mathcal{S}_5: \quad 2\xi\omega_r^3 Q_2 + \frac{Q_2^2 Q_3 K_n}{Q_4} > \omega_r^2 Q_2^2,\\
&\mathcal{S}_6: \quad Q_i \in \mathbb{R},\ Q_2 < 2\xi\omega_r,\ K_n Q_3 < \omega_r^2 Q_4,\ 0 < Q_2 Q_4 < \frac{1}{\Gamma(\gamma_1,\gamma_2)}.
\end{aligned}
\tag{4.37}
$$

(2) The pairs $(\bar{A}, C_0)$ *and* $(\bar{A}, B_0)$ *where* $C_0 = \begin{bmatrix} \begin{bmatrix} Q_1 \\ \frac{Q_2 Q_3}{Q_4} \end{bmatrix} \bar{C}_e & \begin{bmatrix} 1 & Q_2 \\ Q_2 & \frac{Q_2}{Q_4} \end{bmatrix} \end{bmatrix}$ *and* $B_0 = \begin{bmatrix} 0_{n_p \times 2} \\ I_2 \end{bmatrix}$ *are observable and controllable, respectively.*

(3) The open-loop system does not have any pole at the origin.

(4) $n - m = 3$ *(the slope gain at high frequency is equal to -3).*

Theorem 5. *The zero equilibrium of the reset control system (4.8) with GSORE (4.6) is globally uniformly asymptotically stable when* $w = 0$*, and the system has the UBIBS property for any input* w *which is a Bohl function if all of the following conditions are satisfied.*

- *The base linear system is stable.*
- $A_\rho = \begin{bmatrix} \gamma_1 & 0 \\ 0 & \gamma_2 \end{bmatrix}$ *and* $-1 < \gamma_i < 1$*, for* $i = 1, 2$.
- *The reset control system is either of Type III, or of Type IV, or of Type V.*
- $\mathcal{C}_s(s) = 1$ *and/or the reset instants have the well-posedness property.*

Proof. Theorem 5 is proved in the following steps.

- Step 1: The transfer function $H(s)$ in (4.10) for the reset control system (4.8) with GSORE (4.6) is calculated. Then, it is shown that $A_\rho^T \varrho A_\rho - \varrho < 0$.
- Step 2: It is shown that $\lim_{\omega\to\infty} \omega^2 (H(j\omega) + H(-j\omega)^T) > 0$.
- Step 3: For systems with poles at the origin it is shown that $\lim_{\omega\to 0} H(j\omega) + H(-j\omega)^T > 0$.
- Step 4: It is shown that $H(j\omega) + H(-j\omega)^T > 0$, for all $\omega \in \mathbb{R}^+$.

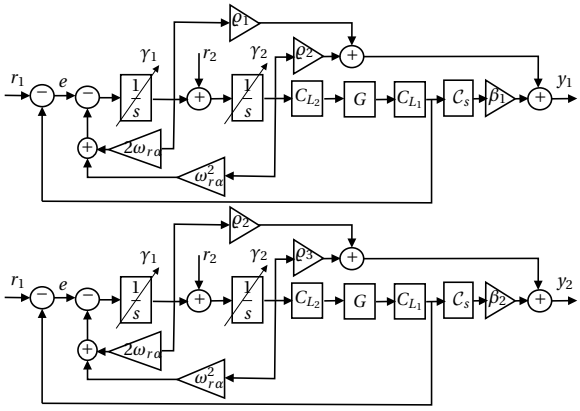

Figure 4.5: The block diagram of the H_β condition for the closed-loop architecture Figure. 4.1 with GSORE

Step 1: In the case of GSORE let $\beta = -\begin{bmatrix}\beta_1 & \beta_2\end{bmatrix}$ and $\varrho = \begin{bmatrix}\varrho_1 & \varrho_2 \\ \varrho_2 & \varrho_3\end{bmatrix} > 0$ be such that

$$\beta_i \in \mathbb{R},\ \varrho_3 > 0,\ \varrho_1 > 0,\ \varrho_1\varrho_3 > \varrho_2^2. \tag{4.38}$$

In addition, since $A_\rho = \begin{bmatrix}\gamma_1 & 0 \\ 0 & \gamma_2\end{bmatrix}$, we have the condition

$$A_\rho^T \varrho A_\rho - \varrho = \begin{bmatrix}(\gamma_1^2-1)\varrho_1 & (\gamma_1\gamma_2-1)\varrho_2 \\ (\gamma_1\gamma_2-1)\varrho_2 & (\gamma_2^2-1)\varrho_3\end{bmatrix} < 0. \tag{4.39}$$

Since $-1 < \gamma_i < 1$, using (4.38) and (4.39), yields

$$\frac{\varrho_1\varrho_3}{\varrho_2^2} > \Gamma(\gamma_1,\gamma_2) = \frac{(\gamma_1\gamma_2-1)^2}{(\gamma_1^2-1)(\gamma_2^2-1)} \geq 1. \tag{4.40}$$

With the considered matrix ϱ and vector β, $H(s)$ in (4.10) with C_0 as in (4.15) is equal to (see also Figure. 4.5)

$$H(s) = \begin{bmatrix}\text{transfer function from } r_1 \text{ to } y_1 & \text{transfer function from } r_2 \text{ to } y_1 \\ \text{transfer function from } r_1 \text{ to } y_2 & \text{transfer function from } r_2 \text{ to } y_2\end{bmatrix}. \tag{4.41}$$

Thus,

$$H(j\omega) + H(-j\omega)^T = \begin{bmatrix}2\Re(\frac{y_1}{r_1}) & \Re(\frac{y_1}{r_2}+\frac{y_2}{r_1}) \\ \Re(\frac{y_1}{r_2}+\frac{y_2}{r_1}) & 2\Re(\frac{y_2}{r_2})\end{bmatrix} > 0 \Rightarrow$$
$$\frac{1}{|\kappa(\omega)|^2}\begin{bmatrix}2f_1(\varrho_1,\varrho_2,\beta_1,\omega) & f_1(\varrho_2,\varrho_1,\beta_2,\omega)+f_2(\varrho_2,\varrho_1,\beta_2,\omega) \\ f_1(\varrho_2,\varrho_1,\beta_2,\omega)+f_2(\varrho_2,\varrho_1,\beta_2,\omega) & 2f_2(\varrho_3,\varrho_2,\beta_2,\omega)\end{bmatrix} > 0. \tag{4.42}$$

Step 2: Since the transfer functions $\frac{y_i}{r_j}$, with $i,j=1,2$, are strictly proper, $\lim_{s\to\infty} H(s)=0$. Therefore, it is necessary to have $\lim_{\omega\to\infty}\omega^2(H(j\omega)+H(-j\omega)^T)>0$. Note that in the case of SORE, $n-m\geq 3$. By (4.42), if $n-m>3$,

$$\lim_{\omega\to\infty}\omega^2(H(j\omega)+H(-j\omega)^T)=\begin{bmatrix}4\varrho_1\xi\omega_r-2\varrho_2 & \omega_r^2\varrho_1+2\varrho_2\xi\omega_r-\varrho_3\\ \omega_r^2\varrho_1+2\varrho_2\xi\omega_r-\varrho_3 & 2\omega_r^2\varrho_2\end{bmatrix}. \tag{4.43}$$

Therefore, the condition $\lim_{\omega\to\infty}\omega^2(H(j\omega)+H(-j\omega)^T)>0$ is equivalent to

$$2\varrho_1\xi\omega_r>\varrho_2,\quad \varrho_2>0, \tag{4.44}$$

and

$$\begin{gathered}4(2\varrho_1\xi\omega_r-\varrho_2)(\omega_r^2\varrho_2)>(\omega_r^2\varrho_1+2\varrho_2\xi\omega_r-\varrho_3)^2\\ \Downarrow\\ \varrho_3^2-2\varrho_3(\omega_r^2\varrho_1+2\xi\omega_r\varrho_2)+(\omega_r^2\varrho_1-2\xi\omega_r\varrho_2)^2+4\omega_r^2\varrho_2^2<0\\ \Downarrow\\ \left(\varrho_3>(\omega_r^2\varrho_1+2\xi\omega_r\varrho_2)-2\omega_r\sqrt{2\xi\omega_r\varrho_1\varrho_2-\varrho_2^2}\right)\wedge\\ \left(\varrho_3<(\omega_r^2\varrho_1+2\xi\omega_r\varrho_2)+2\omega_r\sqrt{2\xi\omega_r\varrho_1\varrho_2-\varrho_2^2}\right).\end{gathered} \tag{4.45}$$

When $n-m=3$, condition (4.43) is re-written as

$$\begin{bmatrix}4\varrho_1\xi\omega_r-2\varrho_2 & \omega_r^2\varrho_1+2\varrho_2\xi\omega_r-\varrho_3-K_n\beta_1\\ \omega_r^2\varrho_1+2\varrho_2\xi\omega_r-\varrho_3-K_n\beta_1 & 2\omega_r^2\varrho_2-2K_n\beta_2\end{bmatrix}>0, \tag{4.46}$$

which is equivalent to

$$2\varrho_1\xi\omega_r>\varrho_2,\quad \omega_r^2\varrho_2>K_n\beta_2, \tag{4.47}$$

and

$$\begin{gathered}4(2\varrho_1\xi\omega_r-\varrho_2)(\omega_r^2\varrho_2-K_n\beta_2)>(\omega_r^2\varrho_1+2\varrho_2\xi\omega_r-\varrho_3-K_n\beta_1)^2\\ \Downarrow\\ \left(\varrho_3>(\omega_r^2\varrho_1-K_n\beta_1+2\xi\omega_r\varrho_2)-2\sqrt{2\xi\omega_r^3\varrho_1\varrho_2+K_n\varrho_2\beta_2-\omega_r^2\varrho_2^2}\right)\wedge\\ \left(\varrho_3<(\omega_r^2\varrho_1-K_n\beta_1+2\xi\omega_r\varrho_2)+2\sqrt{2\xi\omega_r^3\varrho_1\varrho_2+K_n\varrho_2\beta_2-\omega_r^2\varrho_2^2}\right)\wedge\\ \left(2\xi\omega_r^3\varrho_1\varrho_2+K_n\varrho_2\beta_2>\omega_r^2\varrho_2^2\right).\end{gathered} \tag{4.48}$$

Step 3: When $L(s)$ has at least one pole at the origin, by (4.42)

$$\lim_{\omega\to 0}H(j\omega)+H(-j\omega)^T=\begin{bmatrix}2K_{s_0}\beta_1 & K_{s_0}\beta_2+2K_{s_0}\beta_1\xi\omega_r-\varrho_1\\ K_{s_0}\beta_2+2K_{s_0}\beta_1\xi\omega_r-\varrho_1 & 4K_{s_0}\beta_2\xi\omega_r-2\varrho_2\end{bmatrix}>0, \tag{4.49}$$

which is equivalent to

$$K_{s_0}\beta_1>0,\quad 2K_{s_0}\beta_2\xi\omega_r>\varrho_2, \tag{4.50}$$

and

$$\begin{gathered}4(K_{s_0}\beta_1)(2K_{s_0}\beta_2\xi\omega_r-\varrho_2)>(K_{s_0}\beta_2+2K_{s_0}\beta_1\xi\omega_r-\varrho_1)^2\\ \Downarrow\\ \varrho_1^2-2\varrho_1(2K_{s_0}\beta_1\xi\omega_r+K_{s_0}\beta_2)+(2K_{s_0}\beta_1\xi\omega_r-K_{s_0}\beta_2)^2+4K_{s_0}\beta_1\varrho_2<0\\ \Downarrow\\ \left(\varrho_1>K_{s_0}(2\beta_1\xi\omega_r+\beta_2)-2\sqrt{2K_{s_0}^2\xi\omega_r\beta_1\beta_2-K_{s_0}\beta_1\varrho_2}\right)\wedge\\ \left(\varrho_1<K_{s_0}(2\beta_1\xi\omega_r+\beta_2)+2\sqrt{2K_{s_0}^2\xi\omega_r\beta_1\beta_2-K_{s_0}\beta_1\varrho_2}\right).\end{gathered} \tag{4.51}$$

Step 4: In the case in which $L(s)$ has poles at the origin, denote $Q_1 = \frac{\varrho_1}{\beta_1}$, $Q_2 = \frac{\varrho_2}{\beta_1}$, $Q_3 = \frac{\varrho_3}{\beta_2}$ and $Q_4 = \frac{\varrho_2}{\beta_2}$. Furthermore, since $K_{s_0}\beta_1$, $K_{s_0}\beta_2$, and $|\kappa(\omega)|^2$ are positive, condition (4.42) is equal to

$$\begin{bmatrix} 2K_{s_0} f_1(Q_1, Q_2, 1, \omega) & f_1(Q_2, \frac{Q_2 Q_3}{Q_4}, \frac{Q_2}{Q_4}, \omega) + f_2(Q_2, Q_1, 1, \omega) \\ f_1(Q_4, Q_3, 1, \omega) + f_2(Q_4, \frac{Q_1 Q_4}{Q_2}, \frac{Q_4}{Q_2}, \omega) & \frac{2}{K_{s_0}} f_2(Q_3, Q_4, 1, \omega) \end{bmatrix} > 0. \tag{4.52}$$

Therefore, for all $\omega \in (0, \infty)$, there exist Q_1, Q_2, Q_3, and Q_4 such that

$$K_{s_0} f_1(Q_1, Q_2, 1, \omega) > 0,\ K_{s_0} f_2(Q_3, Q_4, 1, \omega) > 0, \tag{4.53}$$

and since $f_1(Q_1, Q_2, 1, \omega) f_2(Q_3, Q_4, 1, \omega) > 0$,

$$\frac{(f_1(Q_2, \frac{Q_2 Q_3}{Q_4}, \frac{Q_2}{Q_4}, \omega) + f_2(Q_2, Q_1, 1, \omega))(f_1(Q_4, Q_3, 1, \omega) + f_2(Q_4, \frac{Q_1 Q_4}{Q_2}, \frac{Q_4}{Q_2}, \omega))}{f_1(Q_1, Q_2, 1, \omega) f_2(Q_3, Q_4, 1, \omega)} < 4. \tag{4.54}$$

Thus, since the condition (4.54) must hold for all $\omega \in (0, \infty)$, $\min_{Q_i} G_1(Q_1, Q_2, Q_3, Q_4) < 4$, with $i = 1, 2, 3, 4$. Moreover, re-writing equations (4.38), (4.40) (4.45), and (4.51) using the variables Q_1, Q_2, Q_3, and Q_4, the constraints $\mathcal{S}_3 - \mathcal{S}_7$ of Definition 14 are obtained.

When $L(s)$ does not have any pole at the origin, let $Q_1' = \frac{\beta_1}{\varrho_1}$, $Q_2' = \frac{\varrho_2}{\varrho_1}$, $Q_3' = \frac{\beta_2}{\varrho_3}$ and $Q_4' = \frac{\varrho_2}{\varrho_3}$. With this change of variables, since ϱ_3, ϱ_1 and $|\kappa(\omega)|^2$ are positive, condition (4.42) is equivalent to

$$\begin{bmatrix} 2 f_1(1, Q_2', Q_1', \omega) & f_1(Q_2', \frac{Q_2'}{Q_4'}, \frac{Q_2' Q_3'}{Q_4'}, \omega) + f_2(Q_2', 1, Q_1', \omega) \\ f_1(Q_4', 1, Q_3', \omega) + f_2(Q_4', \frac{Q_4'}{Q_2'}, \frac{Q_1' Q_4'}{Q_2'}, \omega) & 2 f_2(1, Q_4', Q_3', \omega) \end{bmatrix} > 0. \tag{4.55}$$

Therefore, for all $\omega \in [0, \infty)$,

$$f_1(1, Q_2', Q_1', \omega) > 0,\ f_2(1, Q_4', Q_3', \omega) > 0, \tag{4.56}$$

and since $f_1(1, Q_2', Q_1', \omega) f_2(1, Q_4', Q_3', \omega) > 0$,

$$\frac{(f_1(Q_2', \frac{Q_2'}{Q_4'}, \frac{Q_2' Q_3'}{Q_4'}, \omega) + f_2(Q_2', 1, Q_1', \omega))(f_1(Q_4', 1, Q_3', \omega) + f_2(Q_4', \frac{Q_4'}{Q_2'}, \frac{Q_1' Q_4'}{Q_2'}, \omega))}{f_1(1, Q_2', Q_1', \omega) f_2(1, Q_4', Q_3', \omega)} < 4. \tag{4.57}$$

Therefore, since condition (4.57) must hold for all $\omega \in [0, \infty)$, $\min_{Q_i'} G_2(Q_1', Q_2', Q_3', Q_4') < 4$, with $i = 1, 2, 3, 4$. Re-writing equations (4.40) and (4.45) with the variables Q_1', Q_2', Q_3', and

Q_4', the constraints $\mathcal{S}_3-\mathcal{S}_5$ of Definition 15 are achieved. Similarly, using these variables in equations (4.40) and (4.48), the constraints $\mathcal{S}_3-\mathcal{S}_6$ of Definition 16 are obtained.
By Steps 1-4, $A_\rho^T \varrho A_\rho - \varrho < 0$, $H(s)$ is SPR [27], $(\bar{A}, C_0)$ is observable and $(\bar{A}, B_0)$ is controllable, and the base linear system is stable. Thus, the H_β condition is satisfied for the reset control system (4.8) with GSORE (4.6). Hence, the zero equilibrium of the system is globally uniformly asymptotically stable when $w = 0$ and according to Lemma 5, it has the UBIBS property for any initial condition x_0 and any input w which is a Bohl function. □

Remark 9. The minimum value of the function $\Gamma(\gamma_1, \gamma_2)$ occurs when $\gamma_1 = \gamma_2$. In other words, if $\gamma_1 = \gamma_2 \Rightarrow \Gamma(\gamma_1, \gamma_2) = \min_{\gamma_1,\, \gamma_2} \Gamma(\gamma_1, \gamma_2) = 1$. Thus, if Theorem 5 holds for a pair of (γ_1, γ_2), it also holds for $A_\rho = \gamma I,\ -1 < \gamma < 1$.

4

Note that unlike linear controllers, the GSORE (4.5) with a different state-space realization yields different performance, and Theorem 5 can not be used for such realizations. For example, the GSORE (4.5) can also be realized in observable canonical form, that is with

$$A_r = \begin{bmatrix} 0 & -\omega_r^2 \\ 1 & -2\xi\omega_r \end{bmatrix},\ B_r = \begin{bmatrix} 1 \\ 0 \end{bmatrix},\ C_r = \begin{bmatrix} 0 & 1 \end{bmatrix},\ D_r = 0, \tag{4.58}$$

or it can be realized with two GFORE yielding the realization (provided $\xi \geq 1$)

$$A_r = \begin{bmatrix} -\omega_{r_1} & 0 \\ 1 & -\omega_{r_2} \end{bmatrix},\ B_r = \begin{bmatrix} 1 \\ 0 \end{bmatrix},\ C_r = \begin{bmatrix} 0 & 1 \end{bmatrix},\ D_r = 0,\ \omega_{r_1} + \omega_{r_2} = 2\xi\omega_r,\ \omega_{r_1}\omega_{r_2} = \omega_r^2, \tag{4.59}$$

which results in different closed-loop performance.

Corollary 10. *Suppose hypotheses of Theorem 5 hold for the reset control system (4.8) with the GSORE (4.5) in the controllable canonical form (4.6) for a pair (γ_1, γ_2). Then the reset control system (4.8) with GSORE (4.5) with realization (4.58) or (4.59) and $A_\rho = \gamma I,\ -1 < \gamma < 1$ has the following property. For each initial condition x_0 such that $x_0 = \begin{bmatrix} 0 & 0 & \zeta_0^T \end{bmatrix}^T$ and each bounded input w which is a Bohl function, there exists $\epsilon > 0$ such that $||x(t, x_0, w(t))|| < \epsilon$ for $t \geq 0$.*

Proof. See 4.D. □

4.4.2. RESET CONTROL SYSTEMS WITH SOSRE

In this section stability analysis for the reset control system (4.8) with the SOSRE [22] is presented. In [22] GSORE (4.6) with $A_\rho = \begin{bmatrix} \gamma & 0 \\ 0 & 1 \end{bmatrix}$, which is termed SOSRE, is used to improve the performance of the reset control system (4.8). In the case of SOSRE one state of GSORE is reset and the other state is utilized to reduce the high order harmonics of the reset element.

Corollary 11. *Consider the reset control system (4.8) with SOSRE. Define the NSV vector as*

$$\overrightarrow{\mathcal{N}}_{SOS}(\omega) = [\mathcal{N}_{SOS_\chi} \quad \mathcal{N}_{SOS_\Upsilon}]^T =$$

$$\left[\Re(L(j\omega)\kappa(j\omega)\mathcal{C}_s(j\omega)) \quad -\Im(\omega\kappa(j\omega)C_R(j\omega))\right]^T.$$

Suppose that the reset instants have the well-posedness property and $-1 < \gamma < 1$. *Then, with this definition of NSV the zero equilibrium of the reset control system (4.8) with SOSRE is globally uniformly asymptotically stable when* $w = 0$, *and the system has the UBIBS property for any input* w *which is a Bohl function if all of the following conditions are satisfied.*

- *The base linear system is stable and the open-loop transfer function does not have any pole-zero cancellation.*
- *The reset control system (4.8) is either of Type I and/or of Type II.*

Proof. Let $\beta' = -\beta$. The transfer function (4.10) with C_0 as in (4.15) can be rewritten as (see also Figure. 4.5, transfer function from r_1 to y_1 with $\varrho_2 = 0$)

$$H(s) = \frac{\beta' L(s)\mathcal{C}_s(s) + \varrho s C_R(s)}{1 + L(s)}. \tag{4.60}$$

Step 1 and Step 4 of the proof of Theorem 4 are repeated with small modifications. When the open-loop system has poles at the origin

$$\lim_{\omega \to 0} \Re(H(j\omega)) = K_{s_0}\beta' > 0. \tag{4.61}$$

In the case of SOSRE one has $n - m \geq 3$. Consequently,

$$\lim_{\omega \to \infty} \omega^2 \Re(H(j\omega)) = 2\varrho\xi\omega_r > 0, \tag{4.62}$$

and the proof is complete. □

Note that it is impossible to satisfy Assumption 3 for this configuration. Thus, the reset instants must have the well-posedness property.

4.5. ILLUSTRATIVE EXAMPLES

In this section two examples showing how the proposed methods can be used to study stability properties of reset control systems are presented. In particular, stability properties of a precision positioning system [17] (knows as a spider stage) controlled by a reset controller are considered. In this system (see Figure. 4.6), three actuators are angularly spaced to actuate three masses (labeled as B1, B2, and B3) which are constrained by parallel flexures and connected to the central mass D through leaf flexures. Only one of the actuators (A1) is considered and used for controlling the position of the mass B1 attached to the same actuator, which results in a SISO system. For using these stability methods the FRF measurement of the plant (Figure. 4.7) is needed. In [17] a non linear phase compensator, which is termed “Constant in gain Lead in phase" (CgLp) (for more detail see [15, 17, 43]), has been used to improve the performance of this precision positioning stage. CgLp compensators, consisting of a first/second order lead filter and a GFORE/GSORE, have been utilized along with a PID controller to enhance the precision of the system. In the following, stability properties of two CgLp+PID controllers, one of

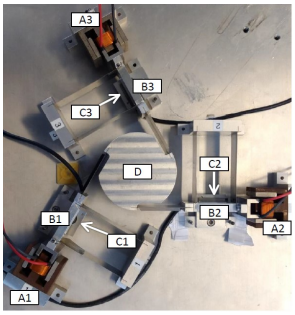

Figure 4.6: Spider stage

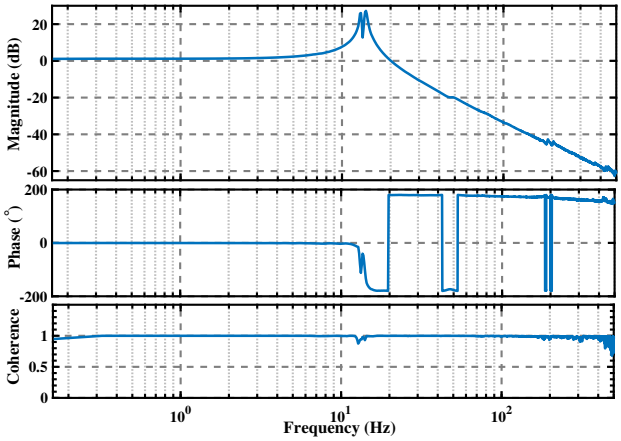

Figure 4.7: FRF measurement of Spyder stage

which has GSORE and the other has SOSRE, are assessed with the proposed methods. The general structure of the controller is

$$C(s) = K_p \overbrace{\underbrace{\left(\frac{1}{s^2+2\xi\omega_r s+\omega_r^2}\right)}_{\text{GSORE}}\underbrace{\left(\frac{s^2+2\xi_d\omega_d s+\omega_d^2}{s^2+20\omega_c+100\omega_c^2}\right)}_{\text{Lead}}}^{\text{CgLp}}\overbrace{\underbrace{\left(1+\frac{\omega_c}{10s}\right)}_{\text{PI}}\underbrace{\left(\frac{\frac{3s}{\omega_c}+1}{\frac{s}{3\omega_c}+1}\right)}_{\text{Lead}}}^{\text{PID}}, \tag{4.63}$$

in which ω_c is the cross-over frequency and K_p, γ, ω_d, ω_r, ξ, and ξ_d are tuning parameters. The PID part is tuned on the basis of [44, 45] and the CgLp part is tuned on the basis of [17, 22, 46], and K_p is set so that $\omega_c = 200\pi$, considering the Describing Function (DF) method [17]. In addition, no shaping filter is used for modifying the performance of the reset controller (i.e. $C_s(s) = 1$). Note that the tuning of the CgLp compensator is not within the scope of this paper, and we only discuss how to assess stability properties of reset control systems with these compensators.

Remark 10. Suppose that the H_β condition is/is not satisfied for the reset control system (4.8) with $\mathcal{C}_s(s)$, $C_{L_1}(s)$, $C_{L_2}(s)$, $C_R(s)$, $G(s)$, and A_ρ. Then the H_β condition is/is not satisfied for the reset control system (4.8) with $\mathcal{C}_s(s)$, $C'_{L_1}(s)$, $C'_{L_2}(s)$, $C_R(s)$, $G'(s)$, and A_ρ if $C'_{L_1}(s)C'_{L_2}(s)G'(s) = C_{L_1}(s)C_{L_2}(s)G(s)$ and $G'(s)$ is strictly proper. In other words, the "position" of the reset element does not change in the H_β condition. However, the "position" of the reset element has effects on the performance of the reset control systems [26] (see Appendix B). In the two following examples, the sequence of control filters is such that the tracking error is the input of the reset element and other linear parts following in series.

4.5.1. A RESET CONTROL SYSTEM WITH GSORE

In the case of GSORE, the control parameters are $\gamma_1 = \gamma_2 = 0.5$, $\omega_r = 800\pi$, $\omega_d = 720\pi$, $K_p = 8.5273e^7$, and $\xi = \xi_d = 1$. Since the controller has a pole at the origin, we use Definition 14 to assess stability properties of this reset control system. Using Proposition 1 yields $340 < \dfrac{Q_2}{Q_1} < 5057$ and $1132 < \dfrac{Q_3}{Q_4}$ for $\mathcal{S}_1$ and $\mathcal{S}_2$, respectively. Thus, we have to solve the optimization problem

$$
\begin{aligned}
M = \min_{Q_1,Q_2,Q_3,Q_4} \quad & G_1(Q_1,Q_2,Q_3,Q_4) \\
\mathcal{S}_1: \quad & \forall \omega \in (0,\infty): \ f_1(Q_1,Q_2,1,\omega) > 0 \\
\mathcal{S}_2: \quad & \forall \omega \in (0,\infty): \ f_2(Q_3,Q_4,1,\omega) > 0 \\
\mathcal{S}_3: \quad & \frac{1600\pi}{Q_1} + \frac{Q_2}{Q_1Q_4} + \frac{2}{Q_1}\sqrt{\frac{1600\pi Q_2}{Q_4} - Q_2} > 1 \\
\mathcal{S}_4: \quad & \frac{1600\pi}{Q_1} + \frac{Q_2}{Q_1Q_4} - \frac{2}{Q_1}\sqrt{\frac{1600\pi Q_2}{Q_4} - Q_2} < 1 \\
\mathcal{S}_5: \quad & \frac{640000\pi^2 Q_1}{Q_2} + 1600\pi\left(1 + 2\sqrt{\frac{1600\pi Q_1}{Q_2} - 1}\right) > \frac{Q_3}{Q_4} \\
\mathcal{S}_6: \quad & \frac{640000\pi^2 Q_1}{Q_2} + 1600\pi\left(1 - 2\sqrt{\frac{1600\pi Q_1}{Q_2} - 1}\right) < \frac{Q_3}{Q_4} \\
\mathcal{S}_7: \quad & Q_i > 0,\ 1600\pi > Q_4,\ 1600\pi < \frac{Q_2}{Q_1} < 5057,\ 1132 < \frac{Q_3}{Q_4},\ \frac{Q_1Q_3}{Q_2Q_4} > 1,
\end{aligned}
\tag{4.64}
$$

This optimization problem is solved using Genetic Algorithm and Proposition 1. The optimal solution is $Q_1 = 13172$, $Q_2 = 12001144$, $Q_3 = 8113151$, and $Q_4 = 1055$, yielding $M = 3.5$. Furthermore, $(\tilde{A}, C_0)$ is observable and $(\tilde{A}, B_0)$ is controllable. Hence, the reset control system is of Type III and using Theorem 5 this GSORE has the UBIBS property for $A_\rho = \gamma I$, $-1 < \gamma < 1$. Furthermore, since $\dfrac{Q_1Q_3}{Q_2Q_4} > \Gamma(-0.5, 0.5)$ and $\dfrac{Q_1Q_3}{Q_2Q_4} > \Gamma(0.5, -0.5)$, Theorem 5 holds for the considered closed-loop system with $A_\rho = \begin{bmatrix} 0.5 & 0 \\ 0 & -0.5 \end{bmatrix}$ or $A_\rho = \begin{bmatrix} -0.5 & 0 \\ 0 & 0.5 \end{bmatrix}$. In Figure. 4.8 the step responses of the closed-loop Spider stage (Figure. 4.6)

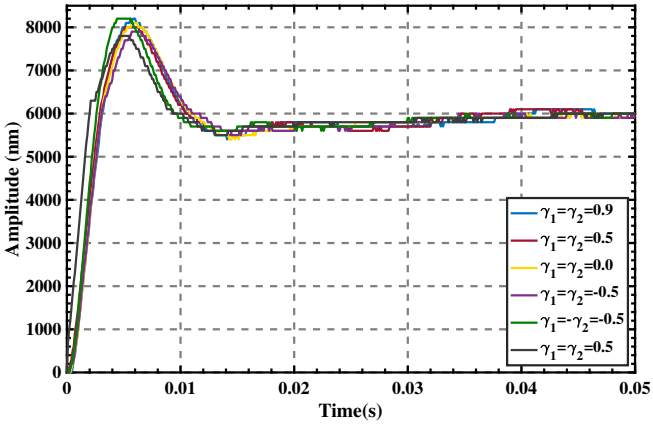

Figure 4.8: Step response of the closed-loop system with designed GSORE for different values of γ_i

with the designed controller for different values of γ_i are displayed. As it can be observed, the values of γ_i have effect on the performance of the system. In the sense of transient response, the reset controller with $\gamma_1 = \gamma_2 = 0.5$ has better performance among other configurations (for more detail see [17, 22]).

4.5.2. A RESET CONTROL SYSTEM WITH SOSRE

In the case in which the controller is a SOSRE the control parameters are $-1 < \gamma < 1$, $\omega_r = 150\pi$, $\omega_d = 96\pi$, $K_p = 1.135e^6$, and $\xi = \xi_d = 1$. Since the controller has a pole at the origin, we use Definition 12 with the NSV defined in Corollary 11 to assess stability properties. The phase of the NSV for this example is shown in Figure. 4.9. Since the phase of the NSV for this example is between $(-\frac{\pi}{2}, \pi)$ and the difference between its maximum and its minimum is less than π, by Remark 6 the reset control system is of Type I. Moreover, the time regularization technique (to prevent successive reset instants, i.e. if the reset happened at one sample time before, the system does not reset) is used to guarantee the well-posedness property. Consequently, by Corollary 11 the designed SOSRE yields a closed-loop system which has the UBIBS property. The step responses of the closed-loop Spider stage (Figure. 4.6) with the designed controller for different values of γ are shown in Figure. 4.10. In the sense of transient response, reset control system with $\gamma = 0.5$ has better performance among other controllers. For deeper insights on the performance of closed-loop reset control systems with SOSRE see [22, 46].

4.6. CONCLUSION

In this paper a novel frequency-domain approach based on the H_β condition for assessing stability properties of reset control systems has been proposed. This method can be used to determine stability properties of control systems with first and second order reset elements using FRF measurements of their base linear open-loop system. Consequently, the methods do not need an accurate parametric model of the system and the

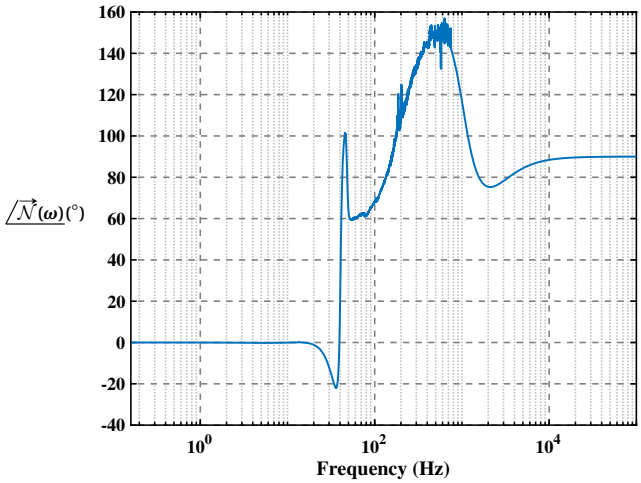

Figure 4.9: $\angle\vec{\mathcal{N}}(\omega)$ for the reset control systems with SOSORE

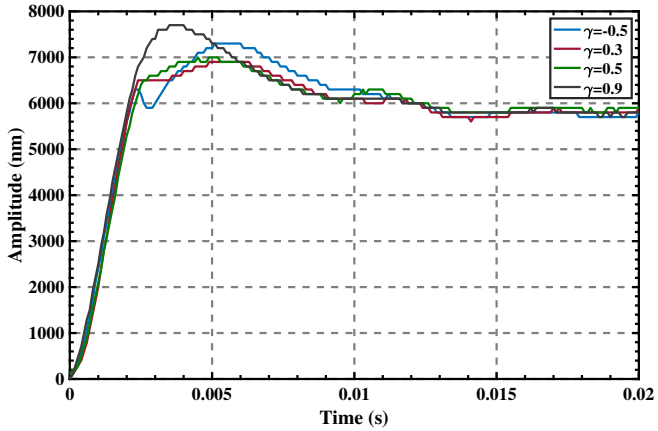

Figure 4.10: Step response of the closed-loop system with designed SOSRE for different values of γ

solution of LMIs. In addition, these methods are applicable to the case in which partial reset techniques are used. The effectiveness of the proposed methods have been illustrated with a practical example.

4.A. PROOF OF LEMMA 5

It has been shown in [2] that when $A_\rho = 0$, $\mathcal{C}_s(s) = 1$, Assumption 3 holds, and the H_β condition is satisfied, the reset control system has the UBIBS property. In what follows, we provide a slight modification of the proof in [2] to deal with the case $A_\rho \neq 0$. The base

linear dynamic of the reset control system is given by

$$\begin{cases} \dot{x}_l(t) = \bar{A}x_l(t) + \bar{B}w(t), \\ y_l(t) = \bar{C}x_l(t), \end{cases} \tag{4.65}$$

where $x_l(t) = [x_{r_l}(t)^T \ \zeta_l(t)^T]^T \in \mathbb{R}^{n_p+n_r}$. Denoting $z(t) : x(t) - x_l(t) = [z_p(t)^T \ \ z_r(t)^T]^T$, yields

$$\begin{cases} \dot{z}(t) = \bar{A}z(t), & e(t) \neq 0, \\ z(t^+) = \bar{A}_\rho z(t) + (\bar{A}_\rho - I)x_l(t), & e(t) = 0. \end{cases} \tag{4.66}$$

According to [2], it is sufficient to show that $z(t)$ is bounded. Since the H_β condition is satisfied, there exists a matrix $P = P^T > 0$ such that

$$P = \begin{bmatrix} P_1 & (\beta\bar{C}_e)^T \\ \beta\bar{C}_e & \varrho \end{bmatrix}, \ P_1 = P_1^T > 0. \tag{4.67}$$

Consider now the quadratic Lyapunov function $V(t) = z(t)^T P z(t)$. Using the same procedure as in [2] yields

$$V(t) \leq e^{-\epsilon(t-t_i)}V(t_i), \quad t \in (t_i, t_{i+1}], \ \epsilon > 0, \tag{4.68}$$

and

$$V(t_i^+) = V(t_i) + x_r^T(t_i)(A_\rho^T\varrho A_\rho - \varrho)x_r(t_i) + 2(A_\rho^T - I)x_r^T(t_i)\beta\bar{C}_e z_p(t_i) - 2x_r^T(t_i)A_\rho^T\varrho x_{r_l}(t_i), \tag{4.69}$$

in which t_i are the reset instants. Now, let the maximum eigenvalue of $A_\rho^T\varrho A_\rho - \varrho$ be $\lambda_{\max}$ and note that $\lambda_{\max} < 0$ since $A_\rho^T\varrho A_\rho - \varrho < 0$. As a result

$$\begin{gathered} V(t_i^+) \leq V(t_i) - |\lambda_{\max}|x_r^T(t_i)x_r(t_i) + 2(A_\rho^T - I)x_r^T(t_i)\beta\bar{C}_e z_p(t_i) - 2x_r^T(t_i)A_\rho^T\varrho x_{r_l}(t_i), \\ V(t_i^+) \leq V(t_i) + 2\|x_r(t_i)\|(\|A_\rho^T - I\|\left\|\beta\bar{C}_e z_p(t_i)\right\| + \|A_\rho\varrho x_{r_l}(t_i)\|). \end{gathered} \tag{4.70}$$

At the reset instants $|\bar{C}_e z_p(t_i)| \leq |D_e r(t_i)|$ which implies that $|\bar{C}_e z_p(t_i)|$ is bounded. Moreover, since the base linear system is stable, $x_{r_l}(t_i)$ is bounded. Assume now that $x_r(t_i)$ is unbounded. By (4.68) and (4.70), we conclude that $\lim_{i\to\infty} V(t_i) = 0$. This is a contradiction because $z(t) = 0 \Rightarrow x(t) = x_l(t)$ which implies that the system is a stable linear system with bounded state. Therefore, $x_r(t_i)$ is bounded. Now, we prove that $\dot{x}_r(t_i)$ is bounded. If reset happens when the input of the reset element is zero (i.e. $\mathcal{C}_s(s) = 1$) and Assumption 3 holds, then

$$\frac{dx_r(t)}{dt}\Big|_{t=t_i^-} = A_r\left(e^{A_r(t_i-t_{i-1})}x_r(t_{i-1}) + \int_{t_{i-1}}^{t_i} e^{A_r(t_i-\tau)}B_r e(\tau)d\tau\right) = A_r x_r(t_i) \Rightarrow \left|\dot{x}_r(t_i^-)\right| = |A_r x_r(t_i)|. \tag{4.71}$$

Thus, since $|x_r(t_i)|$ is bounded, $\left|\dot{x}_r(t_i^-)\right|$ is bounded. As a result, since $|x_r(t_{i-1}^+)| \leq |A_\rho||x_r(t_{i-1})|$, $|x_r(t_i)|$ and $\left|\dot{x}_r(t_i^-)\right|$ are bounded,

$$\exists \ K_1 > 0, \ \alpha > 0 \text{ such that } |x_r(t_i)| \leq K_1\left(1 - e^{\alpha(t_i-t_{i-1})}\right), \ \forall \ t_i. \tag{4.72}$$

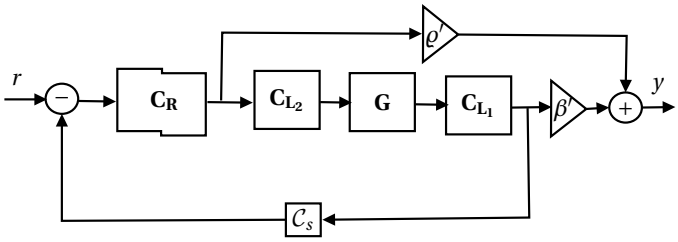

Figure 4.11: The block diagram of H_β condition for the modified architecture Figure. 4.4 with GFORE or PCI

Now assume that there exist t_i and t_{i-1} such that for any $\epsilon > 0$, $t_i - t_{i-1} < \epsilon$. Thus, by (4.72) and for sufficient small ϵ, $x_r(t_i) \to 0$. This is a contradiction because $(I - \bar{A}_\rho)x_r(t_i) \to 0$ which means that t_i is not a reset instant. Thus, there exists $\lambda > 0$ such that, for all $k \in \mathbb{N}$, $\lambda \leq t_{k+1} - t_k$. Therefore, the reset instants have the the well-posedness property (see Definition 10).
In the case in which $\mathcal{C}_s = 1$ or Assumption 3 does not hold, (4.71) can not be concluded. However, if the well-posedness property of the reset instants holds, then there exists $\lambda > 0$ such that, for all $k \in \mathbb{N}$, $\lambda \leq t_{k+1} - t_k$. In addition, since $|x_r(t_{i-1}^+)| \leq |A_\rho||x_r(t_{i-1})|$ and $|x_r(t_i)|$ are bounded, we conclude (4.72). Since the system has the well-posedness property, the reset control system (4.8) has an unique well-defined solution for any initial condition x_0 and any input w which is a Bohl function [39]. The rest of the proof is the same as the proof in [2].

4.B. PROOF OF COROLLARY 9

Let $\beta' = -\beta$ and $\varrho' = \dfrac{\varrho}{C_r}$. By the proof of the H_β condition in [2] the transfer function (4.10) for the configuration shown in Figure. 4.4) can be rewritten as (see also Figure. 4.11)

$$H(s) = \frac{\beta' \dfrac{L'(s)}{\mathcal{C}_s(s)} + \varrho' C_R(s)}{1 + L'(s)}. \tag{4.73}$$

Let $C_{L_1}(s)C_{L_2}(s)C_R(s)G(s) = \dfrac{k_m s^m + k_{m-1}s^{m-1} + \ldots + k_0}{s^n + k'_{n-1}s^{n-1} + \ldots + k'_0}$. Using the NSV defined in (4.35), one could repeat Steps 1 to 4 of the proof of Theorem 4. Note that $K_{s_0}\beta'$ in (4.20)-(4.24) and (4.28) has to be replaced by $\dfrac{\beta'}{K_{s_0}}$ and K_n has also to be replaced by k_n in (4.25).

4.C. PROOF OF PROPOSITION 1

Consider $Q_1\mathcal{F}_1(\omega) + Q_2\mathcal{F}_2(\omega)$ as the scalar product of the two vectors $\vec{\mathcal{F}}(\omega)$ and $\vec{\mathcal{Q}}$. Thus, for all $\omega \in \mathbb{R}^+$, the condition (4.33) can be re-written as

$$\sqrt{Q_1^2 + Q_2^2}\sqrt{\mathcal{F}_1^2(\omega) + \mathcal{F}_2^2(\omega)}\cos(\vartheta) > \mathcal{F}_3(\omega). \tag{4.74}$$

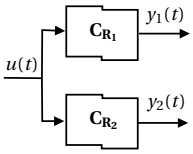

Figure 4.12: Two reset controllers C_{R_1} and C_{R_2} with different realization configurations

As a result, when $\mathcal{F}_3(\omega) \geq 0$, $\cos(\vartheta)$ must be positive and

$$\sqrt{Q_1^2+Q_2^2} > \max_{\omega\in\omega_p} \frac{\mathcal{F}_3(\omega)}{\cos(\vartheta)\sqrt{\mathcal{F}_1^2(\omega)+\mathcal{F}_2^2(\omega)}} = \eta_1(\frac{Q_2}{Q_1}). \tag{4.75}$$

Positivity of $\cos(\vartheta)$ implies $\dfrac{Q_2}{Q_1} \in g_p$. When $\mathcal{F}_3(\omega) < 0$, there are two solutions for condition (4.74). $\cos(\vartheta) \geq 0$ which requiers $\dfrac{Q_2}{Q_1} \in g_N$, or

$$\sqrt{Q_1^2+Q_2^2} < \min_{\omega\in\omega_N} \frac{\mathcal{F}_3(\omega)}{\cos(\vartheta)\sqrt{\mathcal{F}_1^2(\omega)+\mathcal{F}_2^2(\omega)}} = \eta_2(\frac{Q_2}{Q_1}). \tag{4.76}$$

Therefore, by (4.75) and (4.76) $\eta_2(\dfrac{Q_2}{Q_1}) > \eta_1(\dfrac{Q_2}{Q_1})$ and the proof is complete.

4.D. PROOF OF COROLLARY 10

First, a preliminary result is stated and proved.

Lemma 6. *Consider the reset controllers C_{R_1} and C_{R_2} shown in Figure. 4.12. Suppose C_{R_1} and C_{R_2} have the same base linear system, are strictly proper, and have different state-space realizations. Then if $A_\rho = \gamma I$ and their initial conditions are zero, $y_1(t) = y_2(t)$, for $t \geq 0$.*

Proof. Let A_{r_1}, B_{r_1}, and C_{r_1} be the state-space realization of $C_{R_1}(s)$ and A_{r_2}, B_{r_2}, and C_{r_2} be the state-space realization of $C_{R_2}(s)$. Since the base transfer function of $C_{R_1}(s)$ and $C_{R_2}(s)$ are the same,

$$C_{r_1}\int_{t_0}^{t} e^{A_{r_1}(t-\tau)}B_{r_1}u(\tau)d\tau = C_{r_2}\int_{t_0}^{t} e^{A_{r_2}(t-\tau)}B_{r_2}u(\tau)d\tau. \tag{4.77}$$

Let t_k, $k \in \mathbb{N}$, be the reset instants of C_{R_1} and C_{R_2}. Since the initial condition is zero,

$$y_1(t) = C_{r_1}\left(\int_{t_k}^{t} e^{A_{r_1}(t-\tau)}B_{r_1}u(\tau)d\tau + \gamma\int_{t_{k-1}}^{t_k} e^{A_{r_1}(t-\tau)}B_{r_1}u(\tau)d\tau + \cdots + \gamma^k\int_{t_0}^{t_1} e^{A_{r_1}(t-\tau)}B_{r_1}u(\tau)d\tau\right), \tag{4.78}$$

$$y_2(t) = C_{r_2}\left(\int_{t_k}^{t} e^{A_{r_2}(t-\tau)}B_{r_2}u(\tau)d\tau + \gamma\int_{t_{k-1}}^{t_k} e^{A_{r_2}(t-\tau)}B_{r_2}u(\tau)d\tau + \cdots + \gamma^k\int_{t_0}^{t_1} e^{A_{r_2}(t-\tau)}B_{r_2}u(\tau)d\tau\right). \tag{4.79}$$

As a result, $y_1(t) = y_2(t)$, for all $t \geq 0$ by (4.77). □

The corollary is now proved. Using Lemma 6, since the initial condition of the reset part are zero and $A_\rho = \gamma I$, the states $\zeta(t)$ are the same for different state-space realizations of $C_R(s)$ of the reset control system (4.8). Thus, since Theorem 5 holds for the reset control system (4.8) with GSORE (4.5) with the controllable realization (4.6), $\zeta(t)$, which contains $u_1(t)$ and $u_r(t)$, is also bounded in the reset control system (4.8) with GSORE (4.5) with realization configurations (4.58) and (4.59). Therefore, it is just needed to show that the reset state $x_r(t)$ is bounded. Consider the reset controller (4.1). Now assume that $x_r(t)$ is unbounded, since $u_1(t)$ is bounded and by state-space realization (4.58) and (4.59), $u_r(t)$ becomes unbounded which is a contradiction. Therefore, $x_r(t)$ must be bounded and the proof is complete.

REFERENCES

[1] J. C. Clegg, *A nonlinear integrator for servomechanisms,* Transactions of the American Institute of Electrical Engineers, Part II: Applications and Industry **77**, 41 (1958).

[2] O. Beker, C. Hollot, Y. Chait, and H. Han, *Fundamental properties of reset control systems,* Automatica **40**, 905 (2004).

[3] W. H. T. M. Aangenent, G. Witvoet, W. P. M. H. Heemels, M. J. G. van de Molengraft, and M. Steinbuch, *Performance analysis of reset control systems,* International Journal of Robust and Nonlinear Control **20**, 1213 (2010).

[4] F. Forni, D. Nešić, and L. Zaccarian, *Reset passivation of nonlinear controllers via a suitable time-regular reset map,* Automatica **47**, 2099 (2011).

[5] A. F. Villaverde, A. B. Blas, J. Carrasco, and A. B. Torrico, *Reset control for passive bilateral teleoperation,* IEEE Transactions on Industrial Electronics **58**, 3037 (2011).

[6] A. Baños and A. Barreiro, *Reset control systems* (Springer Science & Business Media, 2011).

[7] S. van Loon, K. Gruntjens, M. Heertjes, N. van de Wouw, and W. Heemels, *Frequency-domain tools for stability analysis of reset control systems,* Automatica **82**, 101 (2017).

[8] S. H. HosseinNia, I. Tejado, and B. M. Vinagre, *Fractional-order reset control: Application to a servomotor,* Mechatronics **23**, 781 (2013).

[9] Y. Guo, L. Xie, and Y. Wang, *Analysis and Design of Reset Control Systems* (Institution of Engineering and Technology, 2015).

[10] A. Bisoffi, R. Beerens, W. Heemels, H. Nijmeijer, N. van de Wouw, and L. Zaccarian, *To stick or to slip: A reset pid control perspective on positioning systems with friction,* Annual Reviews in Control **49**, 37 (2020).

[11] I. Horowitz and P. Rosenbaum, *Non-linear design for cost of feedback reduction in systems with large parameter uncertainty,* International Journal of Control **21**, 977 (1975).

[12] L. Hazeleger, M. Heertjes, and H. Nijmeijer, *Second-order reset elements for stage control design,* in *American Control Conference (ACC)* (2016) pp. 2643–2648.

[13] Y. Guo, Y. Wang, and L. Xie, *Frequency-domain properties of reset systems with application in hard-disk-drive systems,* IEEE Transactions on Control Systems Technology **17**, 1446 (2009).

[14] S. J. A. M. Van den Eijnden, Y. Knops, and M. F. Heertjes, *A hybrid integrator-gain based low-pass filter for nonlinear motion control,* in *IEEE Conference on Control Technology and Applications (CCTA)* (2018) pp. 1108–1113.

[15] L. Chen, N. Saikumar, and S. H. HosseinNia, *Development of robust fractional-order reset control,* IEEE Transactions on Control Systems Technology **28**, 1404 (2020).

[16] D. Valério, N. Saikumar, A. A. Dastjerdi, N. Karbasizadeh, and S. H. HosseinNia, *Reset control approximates complex order transfer functions,* Nonlinear Dynamics , 1 (2019).

[17] N. Saikumar, R. K. Sinha, and S. H. HosseinNia, *'Constant in gain Lead in phase' element-application in precision motion control,* IEEE/ASME Transactions on Mechatronics **24**, 1176 (2019).

[18] R. Beerens, A. Bisoffi, L. Zaccarian, W. Heemels, H. Nijmeijer, and N. van de Wouw, *Reset integral control for improved settling of pid-based motion systems with friction,* Automatica **107**, 483 (2019).

[19] R. Beerens, A. Bisoffi, L. Zaccarian, W. Heemels, H. Nijmeijer, and N. van de Wouw, *Reset integral control for improved settling of pid-based motion systems with friction,* Automatica **107**, 483 (2019).

[20] M. Heertjes, K. Gruntjens, S. van Loon, N. Kontaras, and W. Heemels, *Design of a variable gain integrator with reset,* in *American Control Conference (ACC), Chicago, USA* (2015) pp. 2155–2160.

[21] L. Zaccarian, D. Nesic, and A. R. Teel, *First order reset elements and the Clegg integrator revisited,* in *American Control Conference* (2005) pp. 563–568 vol. 1.

[22] N. Karbasizadeh, A. Ahmadi Dastjerdi, N. Saikumar, D. Valerio, and S. HosseinNia, *Benefiting from linear behaviour of a nonlinear reset-based element at certain frequencies,* in *Australian and New Zealand Control Conference (ANZCC)* (2020).

[23] A. Barreiro, A. Baños, S. Dormido, and J. A. González-Prieto, *Reset control systems with reset band: Well-posedness, limit cycles and stability analysis,* Systems & Control Letters **63**, 1 (2014).

[24] A. Baños and M. A. Davó, *Tuning of reset proportional integral compensators with a variable reset ratio and reset band,* IET Control Theory & Applications **8**, 1949 (2014).

[25] J. Zheng, Y. Guo, M. Fu, Y. Wang, and L. Xie, *Improved reset control design for a pzt positioning stage,* in *2007 IEEE International Conference on Control Applications* (IEEE, 2007) pp. 1272–1277.

[26] C. Cai, A. A. Dastjerdi, N. Saikumar, and S. HosseinNia, *The optimal sequence for reset controllers,* in 18^{th} *European Control Conference (ECC 2020)* (2020).

[27] H. K. Khalil and J. W. Grizzle, *Nonlinear systems*, Vol. 3 (Prentice hall Upper Saddle River, NJ, 2002).

[28] D. Nešić, L. Zaccarian, and A. R. Teel, *Stability properties of reset systems,* Automatica **44**, 2019 (2008).

[29] A. Baños, J. Carrasco, and A. Barreiro, *Reset times-dependent stability of reset control systems,* IEEE Transactions on Automatic Control **56**, 217 (2010).

[30] K. Rifai and J.-J. Slotine, *Compositional contraction analysis of resetting hybrid systems,* IEEE Transactions on Automatic Control **51**, 1536 (2006).

[31] S. Polenkova, J. W. Polderman, and R. Langerak, *Stability of reset systems,* in *Proceedings of the 20th International Symposium on Mathematical Theory of Networks and Systems* (2012) pp. 9–13.

[32] P. Vettori, J. W. Polderman, and R. Langerak, *A geometric approach to stability of linear reset systems,* Proceedings of the 21st Mathematical Theory of Networks and Systems (2014).

[33] A. Banos, J. Carrasco, and A. Barreiro, *Reset times-dependent stability of reset control with unstable base systems,* in *2007 IEEE International Symposium on Industrial Electronics* (IEEE, 2007) pp. 163–168.

[34] D. Paesa, J. Carrasco, O. Lucia, and C. Sagues, *On the design of reset systems with unstable base: A fixed reset-time approach,* in *IECON 2011-37th Annual Conference of the IEEE Industrial Electronics Society* (IEEE, 2011) pp. 646–651.

[35] W. M. Griggs, B. D. Anderson, A. Lanzon, and M. C. Rotkowitz, *A stability result for interconnections of nonlinear systems with "mixed" small gain and passivity properties,* in *2007 46th IEEE Conference on Decision and Control* (IEEE, 2007) pp. 4489–4494.

[36] J. Carrasco, A. Baños, and A. van der Schaft, *A passivity-based approach to reset control systems stability,* Systems & Control Letters **59**, 18 (2010).

[37] C. Hollot, Y. Zheng, and Y. Chait, *Stability analysis for control systems with reset integrators,* in *Proceedings of the 36th IEEE Conference on Decision and Control*, Vol. 2 (IEEE, 1997) pp. 1717–1719.

[38] O. Beker, C. Hollot, Q. Chen, and Y. Chait, *Stability of a reset control system under constant inputs,* in *Proceedings of the 1999 American Control Conference (Cat. No. 99CH36251)*, Vol. 5 (IEEE, 1999) pp. 3044–3045.

[39] A. Banos, J. I. Mulero, A. Barreiro, and M. A. Davo, *An impulsive dynamical systems framework for reset control systems,* International Journal of Control **89**, 1985 (2016).

[40] C. Hollot, O. Beker, Y. Chait, and Q. Chen, *On establishing classic performance measures for reset control systems,* in *Perspectives in robust control* (Springer, 2001) pp. 123–147.

[41] A. A. Dastjerdi, A. Astolfi, and S. H. HosseinNia, *A frequency-domain stability method for reset systems,* in *IEEE 59th Conference on Decision and Control* (2020).

[42] N. Karbasizadeh, A. A. Dastjerdi, N. Saikumar, and S. H. HosseinNia, *and-passing nonlinearity in reset elements,* arXiv preprint arXiv:2005.02887 (2020).

[43] A. Palanikumar, N. Saikumar, and S. H. HosseinNia, *No more differentiator in PID: Development of nonlinear lead for precision mechatronics,* in *European Control Conference (ECC)* (2018) pp. 991–996.

[44] R. M. Schmidt, G. Schitter, and A. Rankers, *The Design of High Performance Mechatronics High-Tech Functionality by Multidisciplinary System Integration* (IOS Press, 2014).

[45] A. A. Dastjerdi, N. Saikumar, and S. H. HosseinNia, *Tuning guidelines for fractional order PID controllers: Rules of thumb,* Mechatronics **56**, 26 (2018).

[46] N. Karbasizadeh, N. Saikumar, and S. H. Hoseinnia, *Fractional-order single state reset element,* Nonliner Dynamics (2021).

5

A FREQUENCY-DOMAIN TUNING METHOD FOR CGLP COMPENSATORS

Ali AHMADI DASTJERDI

In this chapter, the frequency-domain framework and the frequency-domain stability method, which are described in previous chapters, are utilized based on the loop-shaping approach to provide a reliable frequency-domain tuning method for CgLp compensators. Furthermore, different performance metrics of a CgLp compensator, which is tuned by the proposed method, are compared with those of a PID controller on a precision positioning stage. The results show that this method is effective, and the tuned CgLp can achieve more favourable dynamic performance than the PID controller for the precision motion stage. It is observed that the precision of the system is improved by 60% *without devastating the transient response of the system (throughput). In addition, by calculating the integral of the sensitivity numerically, it has been shown that the "water-bed" effect is broken using the CgLp compensator.*

This chapter has been published in IEEE-Access (2021 [1]).

5.1. INTRODUCTION

PROPORTIONAL Integral Derivative (PID) controllers have been used in the industry for several decades. However, since they suffer from fundamental limitations such as "water-bed" effect, satisfying the ever-increasing demands for high precision and accuracy operations calls for a better alternative [2–4]. Among non-linear controllers, it has been widely demonstrated that reset controllers have prospects to reduce the limitation of linear control systems [5–17].

The first reset element, which is Clegg Integrator (CI), was introduced by Clegg in 1958 [8]. CI is an integrator which resets its state to zero when its input crosses zero. Next, to have more design freedom and applicability, First Order Reset Element (FORE) [5, 18, 19] and Second Order Reset Element (SORE) have been proposed [12, 18]. Besides, to enhance the performance of reset control systems, several techniques such as reset band [20, 21], fixed reset instants [22], Partial Reset, and PI+CI approaches [23] have been studied.

Considering only the first harmonic of the steady-state output of reset elements (Describing Function (DF) analysis [24]) reveals that reset elements provide less lag phase in comparison with their base linear structures. Based on this phase advantage, several new phase compensators have been proposed [6, 18, 25–27]. One of these novel reset compensators is “Constant in gain Lead in phase" (CgLp) which has a constant gain with a phase lead considering DF [6, 18, 26]. As a consequence of replacing derivative part in PID by CgLp [18, 26], the open-loop of the system gets higher gains at low frequencies and lower gains at high frequencies which leads to enhance the closed-loop performance of the system.

There are few studies which investigate tuning of CgLp compensators [18, 26, 28, 29]. In those studies, CgLp is mainly tuned to achieve a specific amount of phase lead at the cross-over frequency considering the DF method. In addition, the High Order Sinusoidal Input Describing Function (HOSIDF) method is used in some of those studies to increase the accuracy of their approaches. However, these methods have several significant drawbacks which make them unreliable. First and foremost, the condition for the existence of the steady-state performance of the closed-loop, which is essential for relying on the closed-loop performance prediction, has not been checked. Second, the DF method, which is conventionally used for tuning, can not precisely predict the closed-loop performance even considering the open-loop high order harmonics of reset control systems [30–39]. Finally, stability could only be assessed after the tuning process. Hence, obtaining a reliable frequency-domain tuning method for CgLp compensators that handles these challenges is still an important open question.

Recently, the sufficient condition for the existence of the steady-state response of the closed-loop reset control systems has been given in Chapter 3. Also, in that work, pseudo-sensitivities for reset control systems are defined which combine high order harmonics to well predict the closed-loop steady-state performance of reset control systems. Furthermore, a frequency-domain method for assessing the stability of reset control systems has been proposed which allows for determining the stability during the tuning process (see Chapter 5).

The contributions of this paper to tune CgLp elements are:

- Based on the loop-shaping approach, we utilize the pseudo-sensitivities (see Chap-

ter 3) and the frequency-domain stability method (see Chapter 5) to provide a reliable frequency-domain tuning method for CgLp compensators.

- To show the effectiveness of the proposed tuning method, a CgLp compensator is tuned and implemented on a high-tech precision positioning stage. Furthermore, the paper delves deeper into the precision position stage performance metrics, like disturbance rejection, noise rejection, tracking performance, obtained using the CgLp compensator.
- Although it is not proven theoretically, we practically show that “water-bed" effect is beaten for this application.

In the remainder of this paper, an overview of CgLp compensators is presented in Section 5.2. In Section 5.3, the frequency-domain tuning procedure is elaborated. In Section 5.4, the tuned CgLp is applied to the precision positioning stage, and its performance is compared with a PID controller. Conclusions are provided in Section 5.5.

5.2. OVERVIEW OF CGLP COMPENSATORS

IN this section, frequency-domain descriptions of reset elements, CgLp compensators, the H_β condition, pseudo-sensitivities, and effects of the sequence of filters of reset control systems on the performance of systems are briefly recalled.

5.2.1. FREQUENCY-DOMAIN DESCRIPTIONS FOR RESET ELEMENTS

The state-space representation of reset elements is,

$$\begin{cases} \dot{x}_r(t) = A_r x_r(t) + B_r e(t), & e(t) \neq 0, \\ x_r(t^+) = A_\rho x(t), & e(t) = 0, \\ u_r(t) = C_r x(t) + D_r r(t), \end{cases} \tag{5.1}$$

where A_r, B_r, C_r, and D_r are the dynamic matrices of the base linear system of the reset element, $e(t)$ and $u_r(t)$ are the input and control input, respectively. States' values after reset action are determined by the resetting matrix A_ρ. In the case of Generalized First Order Reset Element (GFORE), $A_\rho = \gamma$ while in the case of Generalized Second Order Reset Element (GSORE), $A_\rho = \gamma I$, with $-1 < \gamma < 1$ [18]. Note that the transfer function $C_r(sI - A_r)^{-1}B_r + D_r$ is called the base linear transfer function of the reset element.

Similar to other non-linear controllers, the DF analysis is popularly used in literature to study frequency-domain behaviour of reset elements. To have a well-defined steady-state response for a sinusoidal reference input $r(t) = a_0 \sin(\omega t)$, it is assumed that A_r has all eigenvalues with a negative real part and A_ρ has all eigenvalues with a magnitude smaller than one [7]. The sinusoidal input DF of reset elements (5.1) is given in [7] as

$$\mathcal{N}_r(j\omega) = C_r \left(j\omega I - A_r\right)^{-1} B_r \left(I + j\Theta(\omega)\right) + D_r, \tag{5.2}$$

in which Θ is

$$\Theta(\omega) = \frac{-2\omega^2}{\pi}(I + e^{\frac{\pi A_r}{\omega}})\left((I + A_\rho e^{\frac{\pi A_r}{\omega}})^{-1} A_\rho (I + e^{\frac{\pi A_r}{\omega}}) - I\right)(\omega^2 I + A_r^2)^{-1}. \tag{5.3}$$

In [30], the DF method is extended to HOSIDF method in which a non-linear controller is considered as a virtual harmonic generator, and HOSIDF is defined as

$$H_n(j\omega) = \frac{a_n(\omega)e^{j\varphi_n(a_0,\omega)}}{a_0}, \tag{5.4}$$

where a_n and φ_n are the n^{th} component of the Fourier series expansion of the steady-state output of the controller for a sinusoidal input. HOSIDF of reset elements in the open-loop configuration is provided in [33] as

$$H_n(j\omega) = \begin{cases} C_r(j\omega I - A_r)^{-1}(I + j\Theta(\omega))B_r + D_r, & n = 1, \\ C_r(jn\omega I - A_r)^{-1} j\Theta(\omega)B_r, & n > 1 \text{ odd}, \\ 0, & n \text{ even}, \end{cases} \tag{5.5}$$

where n is the order of harmonics.

5.2.2. CGLP COMPENSATOR

A CgLp compensator (5.6) is constructed utilizing a GFORE or a GSORE with the series combination of a corresponding order of a lead filter. Considering the DF analysis, this compensator has a constant gain with a lead phase (Figure. 5.1) [6, 18, 40]. In this paper, without loss of generality, we consider the first order CgLp which is

$$C_{CgLp}(s) = \left(\frac{1}{\frac{s}{\omega_r\alpha} + 1}\right)^{A_\rho}\left(\frac{\frac{s}{\omega_r} + 1}{\frac{s}{\omega_t} + 1}\right), \tag{5.6}$$

where ω_r is the corner frequency of DF of the reset element, $A_\rho = \gamma$ is the reset matrix ($\overset{A_\rho}{(\nearrow)}$ denotes the controller resets with the reset matrix A_ρ), and ω_d and ω_t are the corner frequency of the lead filter. To provide a constant gain, $\omega_{r\alpha} = \omega_r/\alpha$, where α is a correction factor which is provided in Table 5.1, and $\omega_t \gg \omega_r$.

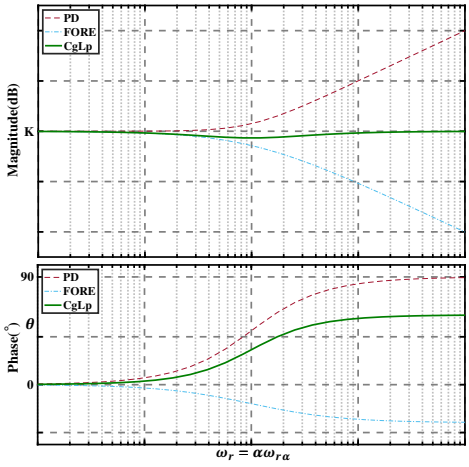

Figure 5.1: The DF of a CgLp compensator

Table 5.1: Correction factor α of first order CgLp [18]

γ	-0.9	-0.8	-0.7	-0.6	-0.5	-0.4	-0.3	-0.2	-0.1	0	0.1	0.2	0.3	0.4	0.5	0.6	0.7	0.8	0.9
α	16.71	8.19	5.26	3.85	3.01	2.47	2.09	1.81	1.60	1.44	1.32	1.23	1.16	1.11	1.07	1.04	1.02	1.01	1.0

5.2.3. H_β CONDITION

There exist several approaches to determine the stability of reset control systems [9, 23, 41–47]. Among these methods, the H_β condition method [23, 45] received a lot of attention due to its simplicity and its frequency-domain applicability. In Chapter 5, a method is proposed to test the H_β condition using the frequency response of the plant directly. Let $L(j\omega)$ and $C_R(j\omega)$ be the frequency response of the base linear system of the open-loop and of the reset element, respectively. Then, the Nyquist Stability Vector (NSV=$\overrightarrow{\mathcal{N}}(\omega) \in \mathbb{R}^2$), for all $\omega \in \mathbb{R}^+$, is $\overrightarrow{\mathcal{N}}(\omega) = [\mathcal{N}_\chi \quad \mathcal{N}_\Upsilon]^T$ in which

$$\mathcal{N}_\chi = \left| L(j\omega) + \frac{1}{2} \right|^2 - \frac{1}{4}, \; \mathcal{N}_\Upsilon = \Re(L(j\omega) \cdot C_R(j\omega)) + \Re(C_R(j\omega)).$$

Now, considering $\theta_1 = \min_{\omega \in \mathbb{R}^+} \angle\overrightarrow{\mathcal{N}}(\omega)$ and $\theta_2 = \max_{\omega \in \mathbb{R}^+} \angle\overrightarrow{\mathcal{N}}(\omega)$, the H_β condition can be examined by the following theorem, which is provided in Chapter 5.

Theorem 6. *Suppose $-1 < \gamma \leq 1$. Then, the H_β condition for a reset control system is satisfied and its response is uniformly bounded-input bounded-state (UBIBS) stable for any bounded input if*

$$\left(-\frac{\pi}{2} < \theta_1 < \pi\right) \wedge \left(-\frac{\pi}{2} < \theta_2 < \pi\right) \wedge (\theta_2 - \theta_1 < \pi). \tag{5.7}$$

5.2.4. PSEUDO-SENSITIVITIES FOR RESET CONTROL SYSTEMS

For Linear Time Invariant (LTI) systems, the tracking error and required control action are calculated by sensitivity transfer functions. Although reset control systems may be analyzed using the DF method in the closed-loop, this yields an approximation which is not precise due to the existence of high order harmonics. In order to analyze reset control systems more accurately, pseudo-sensitivity functions for a sinusoidal reference $r(t) = r_0 \sin(\omega t)$ are defined in Chapter 3 to combine all high order harmonics to a single function. To this end, the sufficient condition for the existence of the steady-state solution is asserted in Chapter 3.

Theorem 7. *A closed-loop reset control system has a well-defined steady-state solution for any Bohl function input if the H_β condition is satisfied and reset instants have the well-posedness property (see Chapter 3).*

Also, the tracking error and control input of a reset control system for $r(t) = \sin(\omega t)$ is a periodic function with the period of $2\pi/\omega$ if the H_β condition is satisfied. Therefore, from the precision viewpoint, the pseudo-sensitivity can be defined as the ratio of the maximum error of the reset control system with $r(t) = r_0 \sin(\omega t)$ to the amplitude of the reference at each frequency.

Definition 17. *Pseudo-sensitivity S_∞*

$$\forall \omega \in \mathbb{R}^+ : \; S_\infty(j\omega) = e_{\max}(\omega) e^{j\varphi_{max}},$$

where

$$e_{\max}(\omega) = \left(\frac{\max\limits_{t_{ss_0} \le t \le t_{ss_m}} (r(t) - y(t))}{r_0} \right) = \sin(\omega t_{\max}) - \frac{y(t_{\max})}{r_0},\ \varphi_{max} = \frac{\pi}{2} - \omega t_{max},$$

$y(t)$ is the steady-state response of the closed-loop reset control system, and t_{ss_0} and $t_{ss_m} = t_{ss_0} + 2\pi/\omega$ are the steady-state reset instants of the closed-loop reset control system ($e(t_{ss_0}) = e(t_{ss_m}) = 0$). Similarly, pseudo-control sensitivity $CS_\infty(j\omega)$ (transfer function from reference to control input), pseudo-complementary sensitivity $T_\infty(j\omega)$ (transfer function from reference to output of the system), and pseudo-process sensitivity $PS_\infty(j\omega)$ (transfer function from disturbance to error of the system) are defined in Chapter 3.

5.2.5. SEQUENCE OF RESET ELEMENTS

Unlike linear controllers, the sequence of filters of reset control systems affects the performance of reset control systems, which is investigated in Appendix B. It is revealed that if the sequence of the control parts is lead elements of the linear controller, reset element, and lag elements of the linear controller, then, the system has a better tracking performance in some frequencies than other sequences. Also, using this sequence, the reset control system has an over-damp step response, and its rise time is increased (also seen in [48]). However, the performance of the system is drastically hampered in this sequence if the signal to noise ratio is low. To solve this issue, a shaping filter $\mathfrak{C}_s$ is used to roll-off the noise from the reset instants of the reset control system as shown in Figure. 5.2.

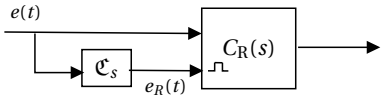

Figure 5.2: Structure of the shaping filter

The transfer function of the shaping filter is described in Appendix B as

$$\mathfrak{C}_s = \left(\frac{1}{1 + \frac{s}{2\omega_c}} \right) \left(\frac{1 + \frac{1.62s}{\omega_c}}{1 + \frac{s}{1.62\omega_c}} \right), \tag{5.8}$$

in which ω_c is the cross-over frequency of the open-loop considering the DF method. In this research, we use the traditional configuration, in which the tracking error is the input of the reset element. Also, we will analyze the performance of different sequences of filters of a reset control systems experimentally.

5.3. TUNING PROCEDURE

IN this section, the pseudo-sensitivities and the frequency-domain stability method are utilized based on the loop-shaping approach [49–57] to provide an appropriate

frequency-domain tuning method for CgLp compensators. The structure of the controller C_R is CgLp.PID as

$$C_R = K_p \overbrace{\underbrace{\left(\frac{1}{\frac{\alpha s}{\omega_r}+1}\right)}^{\text{FORE}} \overbrace{\left(\frac{\frac{s}{\omega_r}+1}{\frac{s}{\omega_t}+1}\right)^{\gamma}}^{\text{Lead}_1}}^{\text{CgLp}} \overbrace{\left(1+\frac{\omega_i}{s}\right)}^{\text{PI}} \overbrace{\left(\frac{\frac{s}{\omega_d}+1}{\frac{s}{\omega_f}+1}\right)}^{\text{Lead}_2}}^{\text{PID}}, \tag{5.9}$$

in which set $(K_p, \omega_r, \gamma, \omega_d, \omega_t, \omega_f, \omega_i)$ is the tuning parameter set, and α is provided in Table 5.1. Following the loop-shaping method described in [49], to have an acceptable rise time, control effort level, tracking performance, and disturbance and noise rejection capabilities, four frequency-domain inequality constraints (Figure. 5.3)

$$|T_\infty(j\omega)| \leq |T_u(\omega)|, \tag{5.10}$$
$$|S_\infty(j\omega)| \leq |S_u(\omega)|, \tag{5.11}$$
$$|CS_\infty(j\omega)| \leq |CS_u(\omega)|, \tag{5.12}$$
$$|PS_\infty(j\omega)| \leq |PS_u(\omega)|, \tag{5.13}$$

have to be fulfilled, for all $\omega \in \mathbb{R}^+$.

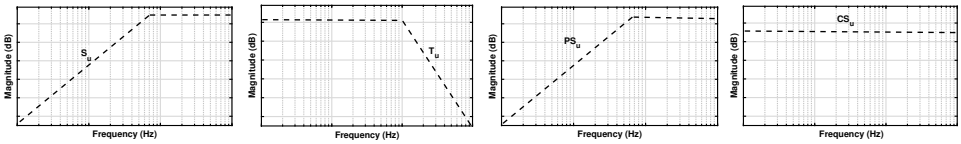

(a) $S_u(j\omega)$ (b) $T_u(j\omega)$ (c) $PS_u(j\omega)$ (d) $CS_u(j\omega)$

Figure 5.3: Loop-shaping constraints

As shown in Figure. 5.3a, $S_u(j\omega)$ restrains the lowest value of the cross-over frequency, limits the magnitude of the peak of sensitivity, and guarantees an acceptable tracking performance. $T_u(j\omega)$ (Figure. 5.3b) limits the effect of noise on the performance of the system. Moreover, $PS_u(j\omega)$ (Figure. 5.3c) places a limit on the effects of the disturbance on the system performance, and $CS_u(j\omega)$ (Figure. 5.3d) confines the control effort level. Besides, to assure stability and be allowed to use pseudo-sensitivities, the tuning parameter set has to satisfy the conditions of Theorem 6. Furthermore, to make the controller robust against gain variations (iso-damping), the tuning parameter set is selected such that

$$\frac{d(\angle \mathcal{N}_{CgLp}(j\omega)\text{PID}(j\omega)G(j\omega))}{d\omega}\Big|_{\omega=\omega_c} = 0, \tag{5.14}$$

in which

$$\mathcal{N}_{CgLp}(j\omega) = \mathcal{N}_r(j\omega)\left(\frac{\frac{j\omega}{\omega_r}+1}{\frac{j\omega}{\omega_t}+1}\right), \tag{5.15}$$

and ω_c is obtained by

$$|\mathcal{N}_{CgLp}(j\omega_c)\text{PID}(j\omega_c)G(j\omega_c)| = 1. \tag{5.16}$$

All in all, the considered constraints for tuning the control structure (5.9) are summarized as:

(I) The H_β condition: Equation (5.7) and $-1 < \gamma \leq 1$

(II) Iso-damping Behaviour: Equation (5.14)

(III) Loop-shaping constraints: Equations (5.10)-(5.13)

Now, it is needed to define a suitable cost function to accomplish the tuning procedure of the control structure (5.9). According to [49], to have a more favourable tracking performance in the interested region of frequencies, the following cost function is obtained.

$$J = \max_{\omega \leq \omega_l} \left| \frac{S_\infty(j\omega)}{\omega} \right|_{\text{dB}}, \tag{5.17}$$

where $\omega_l \leq \omega_c$ determines the interested region of frequencies over which the reset control system is expected to track references and reject disturbances.

5

5.3.1. SOLVING THE OPTIMIZATION PROBLEM

For simplicity, the control structure (5.9) is re-written as

$$C_{\text{R}}(s) = K_p \overbrace{\underbrace{\left(\frac{1}{\frac{\alpha\chi_1 s}{\omega_c}+1}\right)^{\gamma}}_{\text{FORE}} \underbrace{\left(\frac{\frac{\chi_1 s}{\omega_c}+1}{\frac{s}{\chi_2\omega_c}+1}\right)}_{\text{Lead}_1}}^{\text{CgLp}} \overbrace{\underbrace{\left(1+\frac{\omega_c}{\chi_3 s}\right)}_{\text{PI}} \underbrace{\left(\frac{\frac{\chi_4 s}{\omega_c}+1}{\frac{s}{\chi_5\omega_c}+1}\right)}_{\text{Lead}_2}}^{\text{PID}}, \tag{5.18}$$

in which $\chi_i > 0$ and $-1 < \gamma \leq 1$. In addition, limits for ω_c is found based on $S_u(j\omega)$ and $T_u(j\omega)$. Here, we use Genetic Algorithm (GA) method for solving this optimization problem. To speed up the process, we propose the following procedure:

- For each potential solution $(\omega_c, \gamma, \chi_1, \chi_2, \chi_3, \chi_4, \chi_5)$ produced by GA, α and K_p are obtained by γ (Table 5.1) and (5.16), respectively.
- Check constraint (I), (II), and (III) in tandem to reduce computational efforts.
- If all constraints are satisfied, calculate J (5.18).
- Continue until the stop criterion of GA method are satisfied.

PROVIDE AN APPROPRIATE INITIAL GUESS

Here, we provide a method to obtain an appropriate initial guess for the GA method. To this end, we suggest using a grid search method to explore an appropriate feasible solution. First, provide a wide range for χ_i considering $S_u(j\omega)$, $T_u(j\omega)$, $PS_u(j\omega)$, and stability of the base linear of the system. Suppose we obtain vectors l_B and u_B which set the lower

and higher limits for the tuning parameter set (i.e. $l_B < [\omega_c \ \gamma \ \chi_1 \ \chi_2 \ \chi_3 \ \chi_4 \ \chi_5]^T < u_B$). Then, with a small resolution, we grid the parameters and provide a parameter space. Now, we check constraints (I)-(III) in tandem for every point in this space, and eliminate the points which do not satisfy the constraints. Finally, suppose there are N parameter sets which satisfy the aforementioned constraints, then the parameter set with the minimum J value is selected as the initial guess for the optimization problem proposed in Section 5.3.1. Since the performance of the controller is not so sensitive to a small change of the tuning set parameter, it is highly possible that this initial guess does not have far distance from the final solution of the GA method.

5.4. APPLICATION TO A PRECISION MOTION STAGE

To show the effectiveness of the proposed tuning method, a precision positioning stage (Figure. 5.4), which is termed "Spider", is considered as a benchmark. In this system, three actuators are angularly spaced to actuate three masses (labelled by B1, B2, and B3) which are constrained by parallel flexures and connected to the central mass D through leaf flexures. Only one of the actuators (A1) is considered and used for controlling the position of mass B1 attached to the same actuator which results in a SISO system. A linear power amplifier is utilized to drive the Lorentz actuator, and Mercury M2000 linear encoder is used to obtain position feedback with the resolution of 0.1 µm.

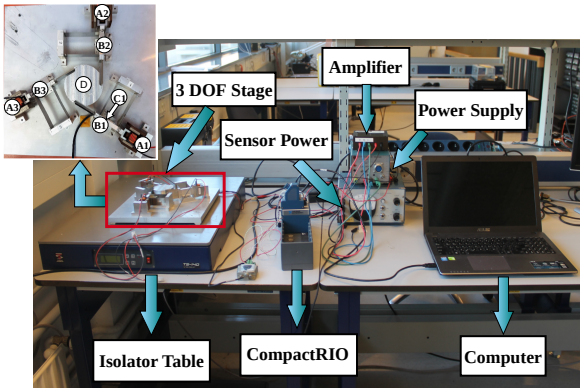

Figure 5.4: The whole setup including computer, CompactRio, power supply, sensor power, amplifier, isolator, sensor and, stage

The identified frequency response data of the system is shown in Figure. 5.5.

As illustrated in Figure. 5.5, although the plant is a collocated double mass-spring system, the identified frequency response data is well approximated by a mass-spring-damper system via the transfer function

$$G(s) \approx \frac{Ke^{-\tau s}}{\frac{s^2}{\omega_r^2} + \frac{2\zeta s}{\omega_r} + 1} = \frac{1.14e^{-0.00014s}}{\frac{s^2}{7627} + \frac{0.05s}{87.3} + 1}. \tag{5.19}$$

Note that to use relations provided in Chapter 3, the time delay ($e^{-0.00014s}$) is approximated by the first order Pade method [58] as $(-s+14400)/(s+14400)$. To provide an

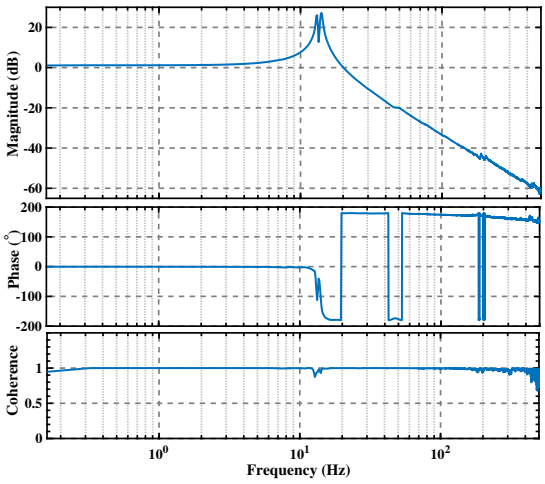

Figure 5.5: Identification of the stage

acceptable closed-loop performance for the positioning stage, without loss of generality, we consider similar constraints as in [49]:

$$T_u(\omega) = \begin{cases} 5\text{ dB}, & \omega \le 200\pi, \\ \left(\dfrac{850}{\omega}\right)^2, & \omega > 200\pi, \end{cases} \quad S_u(\omega) = \begin{cases} \dfrac{\omega}{300}, & \omega \le 160\pi, \\ 4.5\text{ dB}, & \omega > 160\pi, \end{cases}$$

$$PS_u(\omega) = \begin{cases} \dfrac{\omega}{600}, & \omega \le 30\pi, \\ -15\text{ dB}, & \omega > 30\pi, \end{cases} \text{ and } CS_u(\omega) = 60\text{ dB}.$$ Figure 5.6 shows the frequency behaviour of T_u, S_u, PS_u, and CS_u. Since the cut-off frequency of T_u and S_u are 150 Hz and 50 Hz, respectively, ω_c is limited to 50 Hz $< \omega_c <$ 150 Hz. Moreover, we take $\omega_l = 20\pi$ as the maximum limit of the interest frequency region for tracking. Now, the control structure (5.9) is tuned based on the described method in Section 5.3. To simplify constraint (II), according to phase plot of the stage (Figure. 5.5) and the variation range of ω_c (50 Hz,150 Hz), we can approximate $\left.\dfrac{d(\angle G(j\omega))}{d\omega}\right|_{\omega=\omega_c} \approx -\tau$. Therefore, constraint (II) can be re-written as

$$\left.\frac{d(\angle \mathcal{N}_{CgLp}(j\omega) + \angle \text{PID}(j\omega))}{d\omega}\right|_{\omega=\omega_c} \approx \tau = 0.00014. \tag{5.20}$$

To this end, as described in Subsection 5.3.1, we consider a wide parameter range for tuning parameters as $[100\pi\ -1\ 1\ 2\ 2\ 2\ 2]^T < [\omega_c\ \gamma\ \chi_1\ \chi_2\ \chi_3\ \chi_4\ \chi_5]^T < [300\pi\ 1\ 20\ 20\ 20\ 10\ 20]^T$ to find an appropriate initial guess for the GA method. The initial guess is obtained as $[190\pi\ 0.5\ 2\ 10.8\ 7.5\ 3.4\ 1.7]^T$. Then, the control structure (5.9) is tuned by the method presented in Subsection 5.3.1. The tuned CgLp.PID controller is:

$$C_R(s) = 17.05\left(\frac{1}{\dfrac{s}{86\pi}+1}\right)^{0.3}\left(\frac{\dfrac{s}{100\pi}+1}{\dfrac{s}{1440\pi}+1}\right)\left(1+\frac{20\pi}{s}\right)\left(\frac{\dfrac{s}{66\pi}+1}{\dfrac{s}{300\pi}+1}\right). \tag{5.21}$$

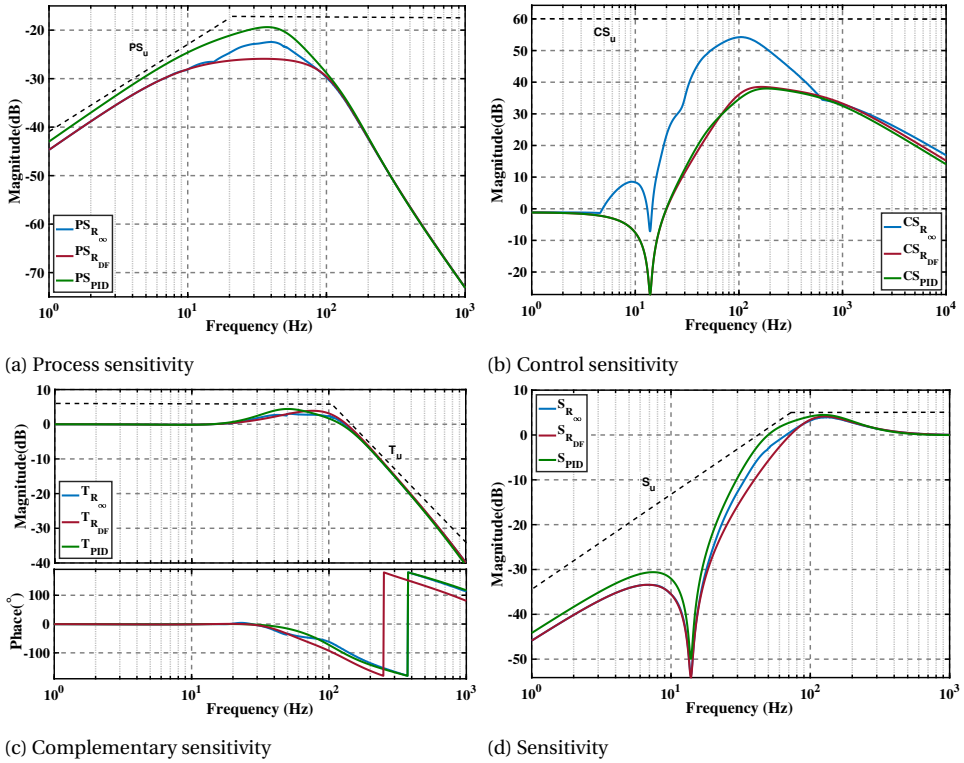

(a) Process sensitivity

(b) Control sensitivity

(c) Complementary sensitivity

(d) Sensitivity

Figure 5.6: The DFs (._ DF) and pseudo-sensitivities (._ ∞) of the closed-loop of the system with the controllers C_{R}, and the closed-loop sensitivities of the system with the controller C_{PID}

As predicted before, the optimum point is not so far from the initial guess. This happens because the closed-loop performance is not so sensitive to a small change of the tuning set parameter which implies that a grid search with a small resolution also can converge to the optimum point.

In order to compare the performance of the tuned controller with a linear controller, a PID structure is also tuned with the same method explained in Section 5.3. To have a fair comparison, the structure of the PID controller is similar to the control structure (5.9) in which FORE is replaced with a low-pass filter. Finally, the C_{PID} is tuned as:

$$C_{\mathrm{PID}} = 7.28\left(\frac{1}{\frac{s}{1480\pi}+1}\right)\left(\frac{\frac{s}{105\pi}+1}{\frac{s}{360\pi}+1}\right)\left(1+\frac{46.5\pi}{s}\right)\left(\frac{\frac{s}{90\pi}+1}{\frac{s}{300\pi}+1}\right). \tag{5.22}$$

Figure 5.7 presents the open-loop frequency response of the system with controllers C_{PID} and the DF of the open-loop of the system with the controller C_{R}. As it is observed, the system with the controller C_{R} has a higher cross-over frequency in comparison with the one with the controller C_{PID}. Moreover, the system with these controllers must indicate iso-damping behaviour as a result of the flatness region around the cross-over frequency.

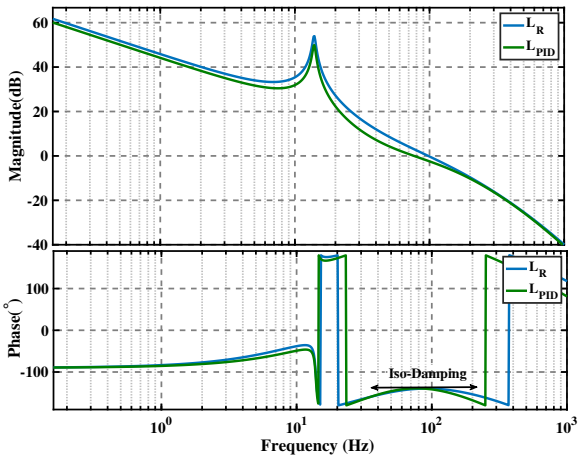

Figure 5.7: Open-loop frequency responses of the system with controllers C_{PID} and C_{R}

The closed-loop frequency responses of the systems with the controller C_{R} including the pseudo-sensitivities and the DF methods, and the closed-loop sensitivities of the system with the controller C_{PID} are also shown in Figure. 5.6. These frequency responses are obtained utilizing the toolbox in [59]. As illustrated in Figure. 5.6a, the disturbance rejection capability of the system with the controller C_{R} is better than that of with the controller C_{PID}. Besides, the control input of the system with the controller C_{R} is more than the one with the controller C_{PID}. This is explained by the fact that reset elements produce jumps in their output signal and differentiation of jumps produces a large control input. Moreover, there are discrepancies between the results obtained by the DF method and pseudo-sensitivities at certain frequency ranges which are due to the existence of high order harmonics. This implies that using pseudo-sensitivities for tuning CgLp compensators is more reliable than using the DF method, particularly for precision motion applications.
As shown in Figure. 5.6c, the noise rejection capabilities of the system with these two controllers are the same (the same roll-off at high frequencies). Furthermore, as shown in Figure. 5.6d, the system with the controller C_{R} has a better tracking performance than that of with the controller C_{PID} at frequencies less than 100Hz while the peak value of the sensitivity of the system with the controller C_{R} is less than that of with the controller C_{PID}.

5.4.1. BREAKING WATER-BED EFFECT

To recall, according to linear control theory,

$$\int_0^\infty \text{Ln}(|S(j\omega)|)d\omega = 0, \tag{5.23}$$

for every stable linear control systems without RHP poles and zeros which has at least two more poles than zeros. Thus, if the sensitivity amplitude is reduced by some control

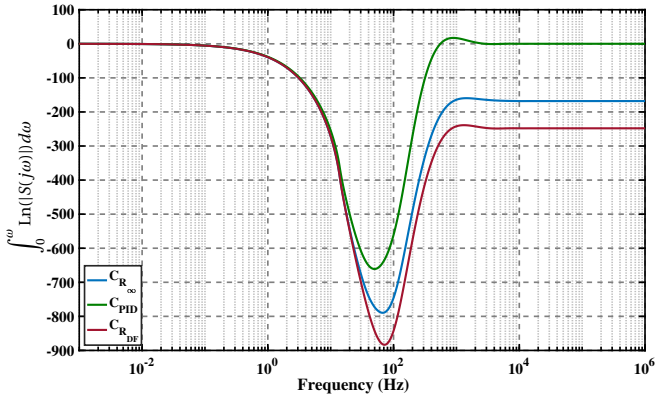

Figure 5.8: The magnitude of the integral of the sensitivity versus frequency

actions in a certain frequency range, then the sensitivity will increase in other frequency ranges. We calculate this integral numerically for the system with both controllers C_R and C_{PID} (Figure. 5.8). For the case of C_R, this integral is calculated using the DF method and pseudo-sensitivity. As observed in Figure. 5.8, the integral (5.23) for the system with the controller C_{PID} converges to zero as expected by linear control theory. Note that, for linear systems with RHP poles and zeros, the water-bed effect situation is even worse because integral (5.23) converges to a positive value [60]. In our system, although time delay can be modelled as a zero-pole transfer function with RHP zero, this integral approximately converges to zero since the time-delay is very small for our system (i.e. 140 μs). Whereas, the integral (5.23) for the system with the controller C_R converges to -160 and -250 using the pseudo-sensitivity and the DF method, respectively. This implies that the sensitivity is decreased in a certain frequency range without increasing in other frequency ranges. Note that calculating relation (5.23) using the DF method is the ideal performance which can be obtained using CgLp compensators. However, using pseudo-sensitivity for calculating this integral for the controller C_R consider all high order harmonics. Although high order harmonics leads to deviation from the ideal case, CgLp compensator is still better than the PID controller and breaks the water-bed effect.

5.4.2. TIME-DOMAIN RESULTS

In this part, the time domain results of the system with these two designed controllers are compared with each other. To implement these designed controllers (Figure. 5.9), each controller is discretized with the sample time $T_s = 100$ µs using the Tustin method [49, 61]. Furthermore, to provide the well-posedness property (see [23, 45]), we prevent consecutive reset instants.

In Figure. 5.10, the step responses (step of 20 µm) of the system with these controllers are shown. The step responses have almost the same rise and settling time while the overshoot of the system with the controller C_R is less than that of with the controller C_{PID} as the peak of the sensitivity of the system with the controller C_R is less than the one with the controller C_{PID}. To examine the iso-damping behaviour of the system, the

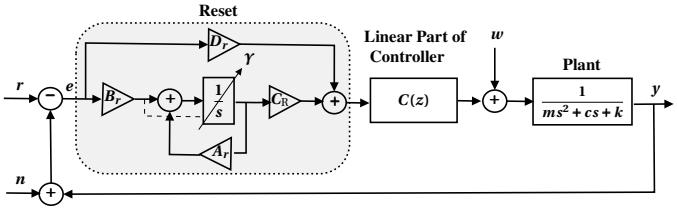

Figure 5.9: The block diagram of the whole system for implementing the designed controllers (reset matrices are discretized)

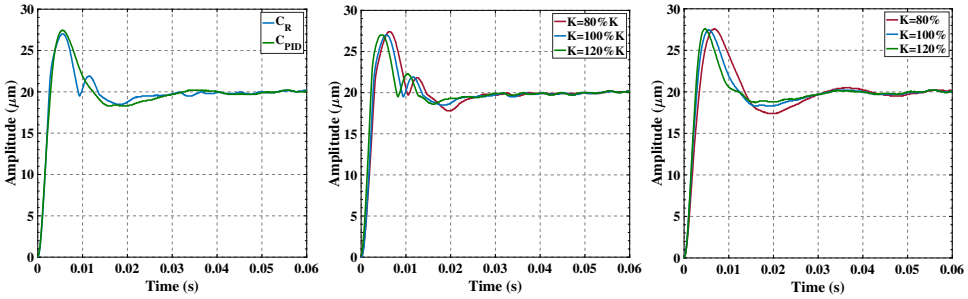

(a) Step responses of controllers (b) Iso-damping behaviour of C_{R} (c) Iso-damping behaviour of C_{PID}

Figure 5.10: The step responses of controllers with gain variation between 80% to 120% of their nominal values

K_p values of the controllers are changed between 80% to 120% of their nominal values. As it is observed, step responses of these perturbed systems show the same overshoot.

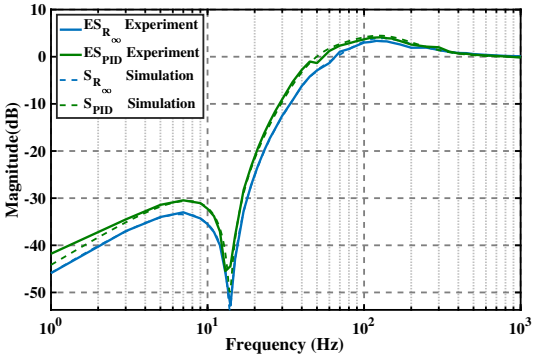

Figure 5.11: The pseudo-sensitivity and sensitivity of the system with the CgLp and PID controllers which are deduced experimentally, ES_{R_∞} and ES_{PID} are practical sensitivity of the system with the controller C_{R} and C_{PID}, respectively

In order to compare the tracking performances of the systems with both controllers, we draw the sensitivity responses practically (Figure. 5.11). In other words, Figure. 5.11

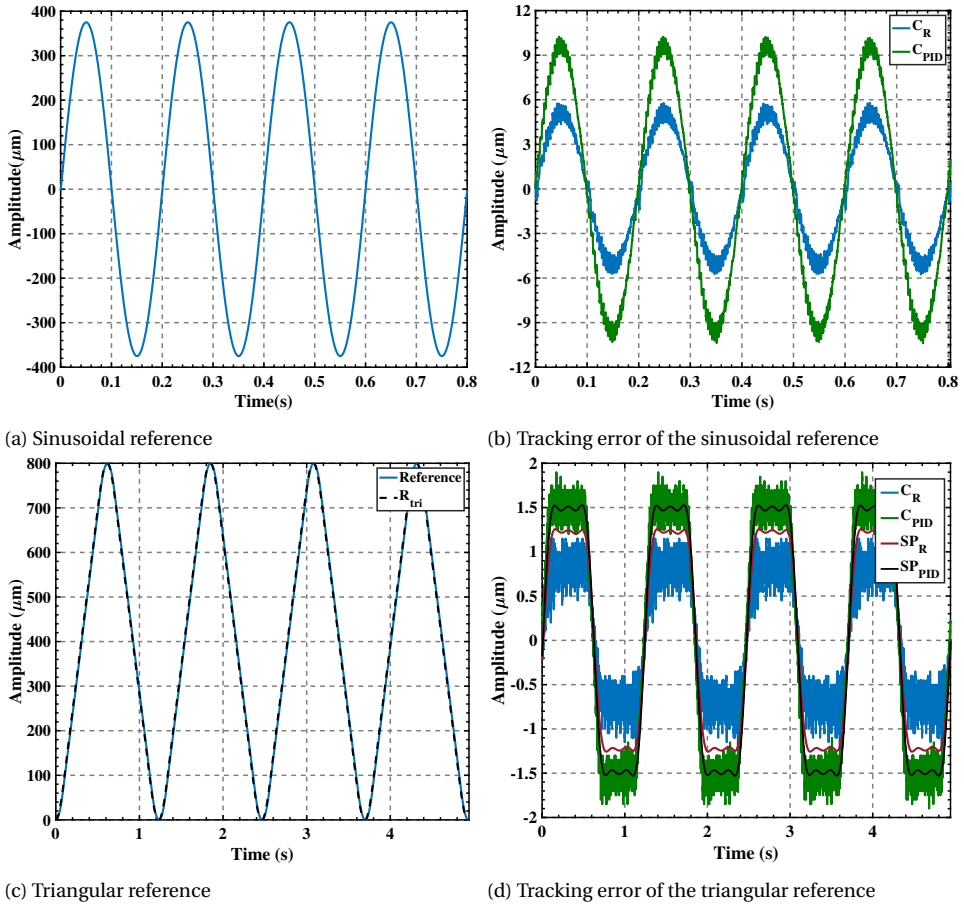

(a) Sinusoidal reference

(b) Tracking error of the sinusoidal reference

(c) Triangular reference

(d) Tracking error of the triangular reference

Figure 5.12: Tracking performance of the system with the designed controllers for a triangular and a sinusoidal references. SP_{R} and SP_{PID} are obtained using super-position law and sensitivity responses for three harmonics of R_{tri} which resembles the triangular reference, respectively.

shows $(\max e(t))/r_0$ for the sinusoidal reference in several frequencies. As shown in Figure. 5.11, S_∞ precisely predicts the maximum error of the system with the controller C_{R} for the sinusoidal references. Besides, it shows that the tracking performance of the system with the controller C_{R} is better than the one with the controller C_{PID} for the sinusoidal reference for all frequencies less than $100Hz$. In order to have a closer look, we show the time response of the system with these controllers for a sinusoidal reference (Figure. 5.12a) at 5 Hz in Figure. 5.12b. Moreover, a triangular trajectory with the amplitude of 800 μm (Figure. 5.12c) is applied to the system. As shown in Figure. 5.12d, the system with the controller C_{R} also has a better tracking performance than that of with the controller C_{PID} for the triangular reference, which consists of several frequencies. For this trajectory and sinusoidal references, the tracking performance of the system is improved by 60% using the controller C_{R}. As was seen in Figure. 5.13, there is a small de-

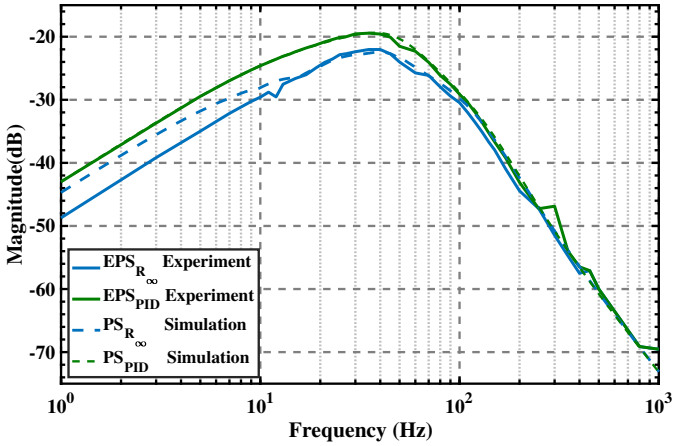

Figure 5.13: The process pseudo-sensitivity and process sensitivity of the system with the CgLp and PID controllers which are deduced experimentally, EPS_{R_∞} and EPS_{PID} are practical process sensitivity of the system with the controller C_R and C_{PID}, respectively

5

viation between pseudo-process sensitivity and the practical results at low frequencies. This deviation is because of quantisztion and sensor noise of the precision stage, which fortunately reduce effects of disturbances at low frequencies in this case.

To have a closer look, we show time response of the system with these controllers for a sinusoidal disturbance (Figure. 5.14a) at 15 Hz in Figure. 5.14b. Moreover, a step disturbance is applied to the system and the amplitude of the error is shown in Figure. 5.14c. It can be said that the disturbance rejection capability of the system is enhanced by 70% using the controller C_R for sinusoidal disturbances. As it is shown, the system with the controller C_R attenuates the step disturbance better than that of with the controller C_{PID}. To study the noise rejection capabilities of the system with these controllers, a white noise with a maximum amplitude of 5 µm is applied to the system (Figure. 5.14d). The Power Spectrum Density (PSD) of the output of the system with these controllers are shown in Figure 5.15. Although it was predicted by Figure. 5.6c that the system with these controllers have the same noise rejection capability, the noise rejection capability of the system with the controller C_R is slightly better than the one with the controller C_{PID} (Figure. 5.10b).

To sum up, the system with the tuned CgLp compensator has a smaller overshoot, the same rise time, better tracking performance and disturbance rejection capability for frequencies less than 100 Hz, a smaller peak of the sensitivity, and a better noise rejection capability than those of the system with the controller PID.

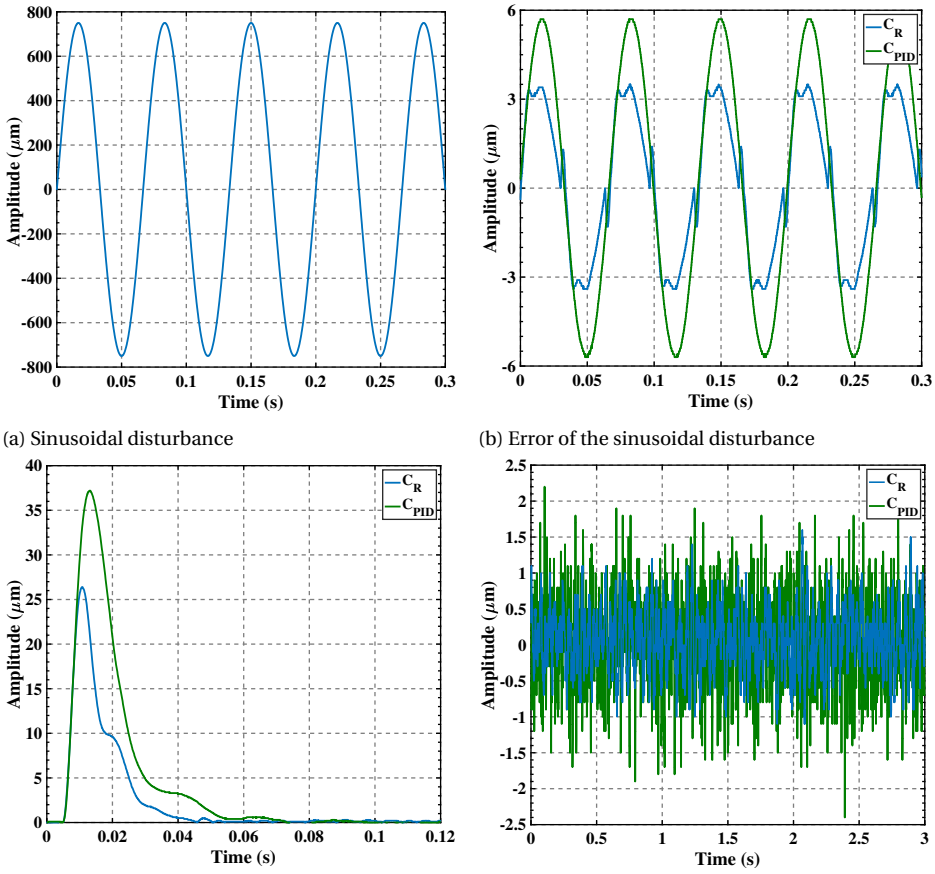

(a) Sinusoidal disturbance

(b) Error of the sinusoidal disturbance

(c) Error of the step disturbance

(d) Noise rejection

Figure 5.14: Disturbance rejection capability of the system for a step and a sinusoidal disturbance, and noise rejection capability of the system

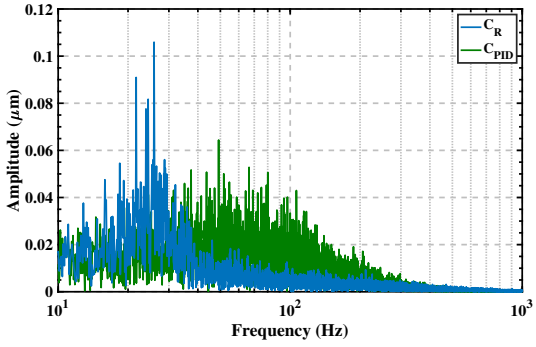

Figure 5.15: PSD of the output of the system with controllers C_R and C_{PID} for a white noise

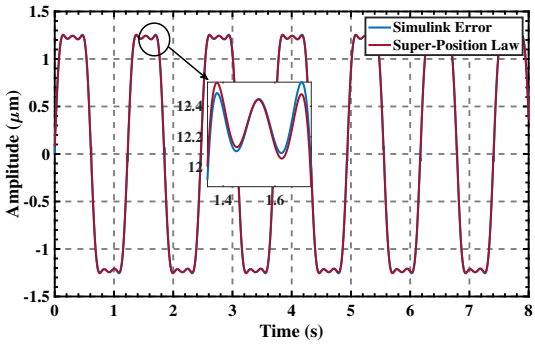

Figure 5.16: Comparison between the predicted error by super-position law and simulated error without quantization and noise for system with C_R

5.4.3. INVESTIGATION OF SUPER-POSITION LAW

In this section, we evaluate that how much the output of the system with the controller C_R follows the super-position law. To this end, we consider the triangular trajectory (Figure. 5.12c), which is the combination of several harmonics. As it is shown in Figure. 5.12c, the reference is accurately approximated with

$$R_{\text{tri}}(t)=363.7\sin(5.1t-1.54)+31.27\sin(15.3t-1.5)+6\sin(25.5t-1.45)+400. \quad (5.24)$$

Since the H_β condition is satisfied and controller C_R has a PI, the steady-state error of tracking is independent of the constant value [9]. In Figure. 5.12d, the predicted errors, which are obtained using super-position law and sensitivity responses for these three harmonics, for both controllers C_R (SP_R) and C_{PID} (SP_{PID}) are drawn. As it is observed, there are differences (16% maximum relative error) between predicted errors by super-position law and practical errors for both controllers C_R and C_{PID}. These differences are mainly due to quantization and noise of sensor (for more details about effects of noise and quantization on the performance of reset control systems, see [62]). Fortunately, in this application, noise and quantization positively affect the performance and reduce the tracking error. In Figure. 5.16, we compare the simulation error, in which we do not consider the noise and quantization, and the predicted error obtained by super-position law for controller C_R. As it is seen, when noise and quantization do not exist, the total error almost follows the super-position law for this trajectory. The identification of the closed-loop system with the controller C_R is demonstrated in Figure. 5.17. The coherence plot is an indicator of existed noise and non-linearity in the output of the closed-loop system in the presence of the input signal $r(t)$. Since the coherence is almost one at low and high frequencies ($f<40$ and $f>120$), the relation between $r(t)$ and $y(t)$ can be well approximated as a linear system in this range of frequency. This can be justified by the fact that in the frequency range ($40<f<120$) the high order harmonics amplitudes of the complementary-sensitivity are maximum near the cross-over frequencies, and they are filtered out outside of this frequency range (Figure. 5.18). In this figure,

$$\left\| \sum_{n=3}^{\infty} T_n(j\omega) \right\|_\infty : \sup_{t_{ss_0}\le t\le t_{ss_m}} \sum_{n=3}^{\infty} |T_n(j\omega)|\sin(n\omega t+\angle T_n(j\omega)),$$

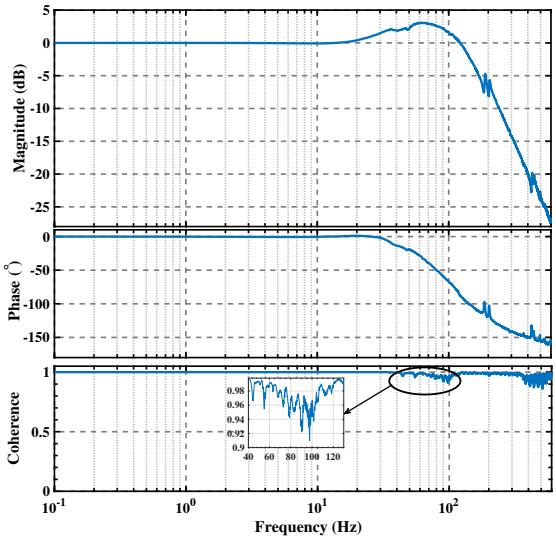

Figure 5.17: Identification of the closed-loop of the system with controller C_R

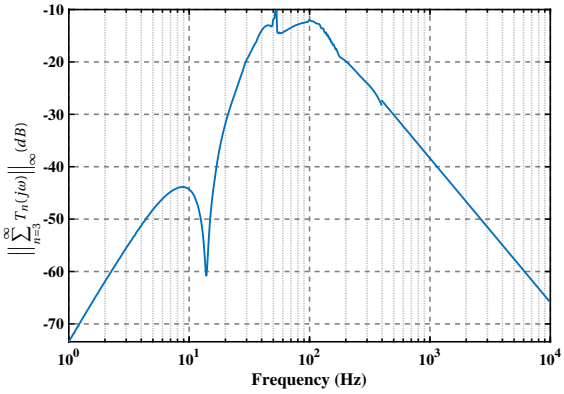

Figure 5.18: The infinity norm of summation of high order harmonics of the complementary-sensitivity of system with the controller C_R

for all $\omega \in \mathbb{R}^+$, which is an appropriate indicator of effects of high order harmonics on the output of the systems (for more details about $T_n(j\omega)$, see Chapter 3). Indeed, there is a relation between the amplitudes of high order harmonics of the complementary-sensitivity and the coherence of identification which should be investigated in future studies.

5.4.4. CHANGING SEQUENCE OF RESET ELEMENT

In this subsection, we investigate the effects of changing the sequence of control filters C_R on the performance of the precision positioning stage. The controller C_R has

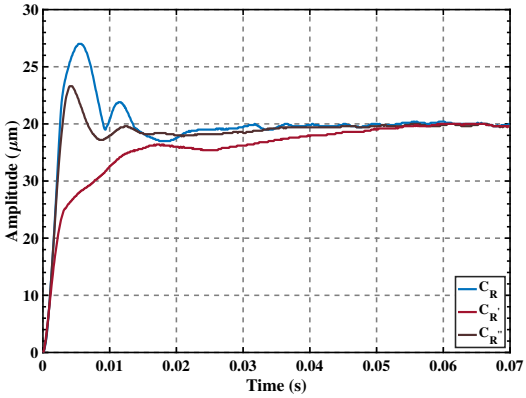

Figure 5.19: Step responses of the system with CgLp compensators

the traditional sequence which is FORE-Lead-PI (for the sake of simplicity, Lead means $\text{Lead}_1.\text{Lead}_2$ in (5.18)). Let's assume C_{R}, $C_{\text{R}'}$, and $C_{\text{R}''}$ have the same base linear system. The sequence of filters in controllers $C_{\text{R}'}$ and $C_{\text{R}''}$ is Lead-FORE-PI. In addition, $C_{\text{R}''}$ has a shaping filter in the reset-instants line as explained in Subsection 5.2.5. Note that since changing the sequence does not alter the H_β condition (see Remark 10 in Chapter 4), the H_β condition is also satisfied for the system with the controller $C_{\text{R}'}$, and the stability of the system with the controller $C_{\text{R}''}$ is assured with the method described in Chapter 4.

In Figure. 5.19, the step responses (step of 20 μm) of the system with these CgLp controllers are shown. As it is shown, the system with the controller $C_{\text{R}''}$ has less over-shoot than that of with the controller C_{R}. Furthermore, the system with the controller $C_{\text{R}'}$ has an over-damp response with the highest rise and settling time. It can be said that this configuration is similar to a reset system which resets when the differentiation of the tracking error is zero ($\dot{e}(t) = 0$). Consequently, the reset control system resets sooner than the case in which the resetting law is $e(t) = 0$. This can be reason the over-damp response with high settling time. It is noteworthy to recall that the open-loop DFs of the system with controllers C_{R} and $C_{\text{R}'}$ are exactly the same. However, the step response specifications, including rise time and over-shoot, are totally different due to different amplitudes of high order harmonics. Thus, the effect of the structure of reset elements on the accuracy of the DF method can be considered as an interesting topic for future study. The disturbance rejection capabilities of the system with these CgLp controllers for the step disturbance and the sinusoidal disturbance at 15 Hz are shown in Figure. 5.20a and Figure. 5.20b, respectively. Besides, a white noise with a maximum amplitude of 5 μm is applied to examine the noise rejection capabilities of the system with these CgLp controllers (Figure. 5.20c). The system with controller C_{R} has the best disturbance and noise rejection capabilities among these CgLp controllers. Similarly, using the shaping filter significantly improves the disturbance and noise rejection capabilities of the system with controller $C_{\text{R}'}$. To see effects of the changing sequence on the tracking performance, the triangular reference and the sinusoidal reference at 5 Hz are applied to the system (Figure. 5.21). As shown in Figure. 5.21a and Figure. 5.21b, the system with the controller

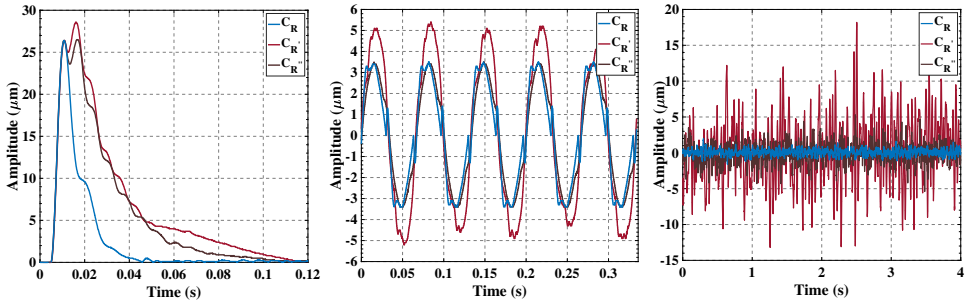

(a) Error of the step diturbance (b) Sinusoidal disturbance error (c) Noise rejection capability

Figure 5.20: Disturbance and noise rejection capability of the system with CgLp controllers

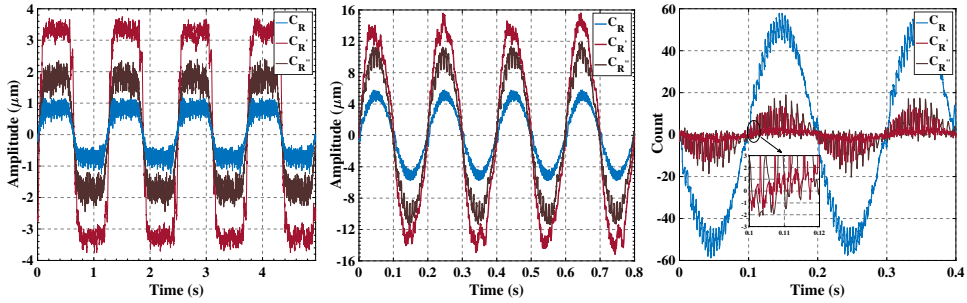

(a) Error of the triangular reference (b) Error of the sinusoidal reference (c) The input of the reset instant line

Figure 5.21: Tracking performance of the system with CgLp controllers and the input of the reset instant line of the reset element of CgLp controllers

C_{R} has the best tracking performance for the triangular and the sinusoidal references. As discussed in Appendix B, for low frequency references, when the lead element of the controller comes first, the existing noise and quantization error are amplified and dominate the tracking error. Consequently, the reset instants are changed considerably by amplified noise which deteriorates the tracking performance of the system. In this case, as suggested in Appendix B, using the shaping filter ($C_{\mathrm{R}''}$) solves the problem to some extent. To show this, in Figure. 5.21c, we draw the signal that enters to the reset line of the reset element for these CgLp controllers as a result of the sinusoidal input at 5 Hz in the presence of noise. For a deeper insight, in Table 5.2, the Signal to Noise Ratio (SNR) of these there signals are provided. In this paper, SNR is calculated using

$$SNR = \frac{P_{signal}}{P_{noise}}, \tag{5.25}$$

where P_{signal} and P_{noise} are power of signal (considering till the fifth harmonic) and noise, respectively. As it can be seen from Table 5.2, the SNR value in the case of C_{R} is significantly higher than the case of $C_{\mathrm{R}'}$. Although using the shaping filter ($C_{\mathrm{R}''}$) leads to reducing the effect of the noise, it is still far from the case of C_{R} in which the reference frequency dominates the reset instants line.

Table 5.2: SNR of the entered signal to the reset line of the reset element for these CgLp controllers

Signal	C_{R}	$C_{\mathrm{R}'}$	$C_{\mathrm{R}''}$
SNR (dB)	20.26	0.10	1.14

It can be concluded that C_{R} has the best steady-state performance, $C_{\mathrm{R}'}$ has the best transient response, and $C_{\mathrm{R}''}$ can be considered as a trade-off between C_{R} and $C_{\mathrm{R}'}$. This trade-off can be set by tuning the cut-off frequency of the shaping filter. Increasing the cut-off frequency brings $C_{\mathrm{R}''}$ near to $C_{\mathrm{R}'}$ which means improving the transient response. While reducing the cut-off frequency brings $C_{\mathrm{R}''}$ near to C_{R} which results in improving the steady-state response.

5.5. CONCLUSION

THIS paper has proposed a frequency-domain tuning method for CgLp compensators based on the defined pseudo-sensitivities for reset control systems. In this method, a PID.CgLp structure was considered, and its parameters were tuned such that the pseudo-sensitivity was minimized under several loop-shaping and stability constraints. To show the effectiveness of the proposed approach, the performance of this tuned CgLp was compared with a linear PID. The results showed that the proposed method achieved more favourable dynamic performance than the PID controller for the precision motion stage. The tracking performance, the disturbance rejection capability, and the noise rejection capability of the system were improved using the CgLp compensator. In addition, it was practically shown that the water-bed effect was broken for this application. Also, without considering quantization and noise, the super-position law almost held for the specified reference. Finally, among different sequences, it was demonstrated that the traditional sequence of reset control systems has the best steady-state performance while putting lead filters first has an over-damped response. For future study, effects of noise and quantization error on the super-position law and tuning and configuration of the shaping filter should be deeply investigated.

REFERENCES

[1] A. A. Dastjerdi and S. H. HosseinNia, *A frequency-domain tuning method for a class of reset control systems,* IEEE-Access (2021).

[2] A. A. Dastjerdi, B. M. Vinagre, Y. Chen, and S. H. HosseinNia, *Linear fractional order controllers; a survey in the frequency domain,* Annual Reviews in Control (2019).

[3] R. Middleton, *Trade-offs in linear control system design,* Automatica **27**, 281 (1991).

[4] R. M. Schmidt, G. Schitter, and A. Rankers, *The Design of High Performance Mechatronics High-Tech Functionality by Multidisciplinary System Integration* (IOS Press, 2014).

[5] I. Horowitz and P. Rosenbaum, *Non-linear design for cost of feedback reduction in systems with large parameter uncertainty,* International Journal of Control **21**, 977 (1975).

[6] L. Chen, N. Saikumar, and S. H. HosseinNia, *Development of robust fractional-order reset control,* IEEE Transactions on Control Systems Technology **28**, 1404 (2020).

[7] Y. Guo, Y. Wang, and L. Xie, *Frequency-domain properties of reset systems with application in hard-disk-drive systems,* IEEE Transactions on Control Systems Technology **17**, 1446 (2009).

[8] J. C. Clegg, *A nonlinear integrator for servomechanisms,* Transactions of the American Institute of Electrical Engineers, Part II: Applications and Industry **77**, 41 (1958).

[9] O. Beker, C. Hollot, Y. Chait, and H. Han, *Fundamental properties of reset control systems,* Automatica **40**, 905 (2004).

[10] D. Wu, G. Guo, and Y. Wang, *Reset integral-derivative control for HDD servo systems,* IEEE Transactions on Control Systems Technology **15**, 161 (2007).

[11] A. Pavlov, B. Hunnekens, N. Wouw, and H. Nijmeijer, *Steady-state performance optimization for nonlinear control systems of Lure type,* Automatica **49**, 2087 (2013).

[12] L. Hazeleger, M. Heertjes, and H. Nijmeijer, *Second-order reset elements for stage control design,* in *American Control Conference (ACC)* (2016) pp. 2643–2648.

[13] R. Beerens, A. Bisoffi, L. Zaccarian, W. Heemels, H. Nijmeijer, and N. van de Wouw, *Reset integral control for improved settling of PID-based motion systems with friction,* Automatica **107**, 483 (2019).

[14] U. Raveendran Nair, R. Costa-Castello, and A. Banos, *Reset control for DC-DC converters: An experimental application,* IEEE Access **7**, 128487 (2019).

[15] J. Bernat, J. Kołota, and D.Cieślak, *Reset strategy for output feedback multiple models MRAC applied to DEAP,* IEEE Access **8**, 120905 (2020).

[16] Z. Gao, Y. Liu, and Z. Wang, *On stabilization of linear switched singular systems via PD state feedback,* IEEE Access **8**, 97007 (2020).

[17] Y. Liu, C. Dong, W. Zhang, and Z.-J. Zhou, *Performance-guaranteed switching adaptive control for nonlinear systems with multiple unknown control directions,* IEEE Access **8**, 35905 (2020).

[18] N. Saikumar, R. K. Sinha, and S. H. HosseinNia, *'Constant in gain Lead in phase' element-application in precision motion control,* IEEE/ASME Transactions on Mechatronics **24**, 1176 (2019).

[19] L. Zaccarian, D. Nesic, and A. R. Teel, *First order reset elements and the Clegg integrator revisited,* in *American Control Conference* (2005) pp. 563–568 vol. 1.

[20] A. Barreiro, A. Baños, S. Dormido, and J. A. González-Prieto, *Reset control systems with reset band: Well-posedness, limit cycles and stability analysis,* Systems & Control Letters **63**, 1 (2014).

[21] A. Baños and M. A. Davó, *Tuning of reset proportional integral compensators with a variable reset ratio and reset band,* IET Control Theory & Applications **8**, 1949 (2014).

[22] J. Zheng, Y. Guo, M. Fu, Y. Wang, and L. Xie, *Improved reset control design for a pzt positioning stage,* in *2007 IEEE International Conference on Control Applications* (IEEE, 2007) pp. 1272–1277.

[23] A. Baños and A. Barreiro, *Reset control systems* (Springer Science & Business Media, 2011).

[24] P. Nuij, M. Steinbuch, and O. Bosgra, *Experimental characterization of the stick/sliding transition in a precision mechanical system using the third order sinusoidal input describing function,* Mechatronics **18**, 100 (2008).

[25] S. J. A. M. Van den Eijnden, Y. Knops, and M. F. Heertjes, *A hybrid integrator-gain based low-pass filter for nonlinear motion control,* in *IEEE Conference on Control Technology and Applications (CCTA)* (2018) pp. 1108–1113.

[26] A. Palanikumar, N. Saikumar, and S. H. HosseinNia, *No more differentiator in PID: Development of nonlinear lead for precision mechatronics,* in *European Control Conference (ECC)* (2018) pp. 991–996.

[27] D. Valério, N. Saikumar, A. A. Dastjerdi, N. Karbasizadeh, and S. H. HosseinNia, *Reset control approximates complex order transfer functions,* Nonlinear Dynamics , 1 (2019).

[28] H. Xiaojun, A. Ahmadi Dastjerdi, N. Saikumar, and S. HosseinNia, *Tuning of 'Constant in gain Lead in phase (CgLp)' reset controller using Higher-Order Sinusoidal Input Describing Function (HOSIDF),* in *Australian and New Zealand Control Conference (ANZCC)* (2020).

[29] M. Shirdast Bahnamiri, N. Karbasizadeh, A. Ahmadi Dastjerdi, N. Saikumar, and S. HosseinNia, *Tuning of CgLp based reset controllers: Application in precision positioning systems,* in *Australian and New Zealand Control Conference (ANZCC)* (2020).

[30] P. Nuij, O. Bosgra, and M. Steinbuch, *Higher-order sinusoidal input describing functions for the analysis of non-linear systems with harmonic responses,* Mechanical Systems and Signal Processing **20**, 1883 (2006).

[31] S. Engelberg, *Limitations of the describing function for limit cycle prediction,* IEEE Transactions on Automatic Control **47**, 1887 (2002).

[32] M. Haeringer, M. Merk, and W. Polifke, *Inclusion of higher harmonics in the flame describing function for predicting limit cycles of self-excited combustion instabilities,* Proceedings of the Combustion Institute **37**, 5255 (2019).

[33] K. Heinen, *Frequency analysis of reset systems containing a Clegg integrator*, Master's thesis, Delft University of Technology (2018).

[34] A. Ahmadi Dastjerdi, N. Saikumar, D. Valerio, and S. Hassan HosseinNia, *Closed-loop frequency analyses of reset systems,* arXiv e-prints , arXiv:2001.10487 (2020), arXiv:2001.10487 [eess.SY] .

[35] P. Nataraj and J. Barve, *Reliable and accurate algorithm to compute the limit cycle locus for uncertain nonlinear systems,* IEE Proceedings-Control Theory and Applications **150**, 457 (2003).

[36] B. Armstrong-Helouvry and B. Amin, *Pid control in the presence of static friction: exact and describing function analysis,* in *Proceedings of 1994 American Control Conference - ACC '94*, Vol. 1 (1994) pp. 597–601 vol.1.

[37] P. Subramanian, V. Gupta, B. Tulsyan, and R. Sujith, *Can describing function technique predict bifurcations in thermoacoustic systems?* in *16th AIAA/CEAS Aeroacoustics Conference* (2010) p. 3860.

[38] C. Cai, A. A. Dastjerdi, N. Saikumar, and S. HosseinNia, *The optimal sequence for reset controllers,* in 18^{th} *European Control Conference (ECC 2020)* (2020).

[39] N. Karbasizadeh, A. Ahmadi Dastjerdi, N. Saikumar, D. Valerio, and S. HosseinNia, *Benefiting from linear behaviour of a nonlinear reset-based element at certain frequencies,* in *Australian and New Zealand Control Conference (ANZCC)* (2020).

[40] N. Saikumar, D. Valerio, and S. H. HosseinNia, *Complex order control for improved loop-shaping in precision positioning,* in *IEEE 58th Conference on Decision and Control* (2019) pp. 7956–7962.

[41] S. Polenkova, J. W. Polderman, and R. Langerak, *Stability of reset systems,* in *Proceedings of the 20th International Symposium on Mathematical Theory of Networks and Systems* (2012) pp. 9–13.

[42] P. Vettori, J. W. Polderman, and R. Langerak, *A geometric approach to stability of linear reset systems,* Proceedings of the 21st Mathematical Theory of Networks and Systems (2014).

[43] H. K. Khalil and J. W. Grizzle, *Nonlinear systems*, Vol. 3 (Prentice hall Upper Saddle River, NJ, 2002).

[44] S. van Loon, K. Gruntjens, M. Heertjes, N. van de Wouw, and W. Heemels, *Frequency-domain tools for stability analysis of reset control systems,* Automatica **82**, 101 (2017).

[45] Y. Guo, L. Xie, and Y. Wang, *Analysis and Design of Reset Control Systems* (Institution of Engineering and Technology, 2015).

[46] D. Nešić, L. Zaccarian, and A. R. Teel, *Stability properties of reset systems,* Automatica **44**, 2019 (2008).

[47] K. Rifai and J.-J. Slotine, *Compositional contraction analysis of resetting hybrid systems,* IEEE Transactions on Automatic Control **51**, 1536 (2006).

[48] S. J. A. M. van den Eijnden, M. F. Heertjes, W. P. M. H. Heemels, and H. Nijmeijer, *Hybrid integrator-gain systems: A remedy for overshoot limitations in linear control?* IEEE Control Systems Letters **4**, 1042 (2020).

[49] J. Sabatier, P. Lanusse, P. Melchior, and A. Oustaloup, *Fractional order differentiation and robust control design*, Vol. 77 (Springer, 2015).

[50] E. Grassi and K. Tsakalis, *Pid controller tuning by frequency loop-shaping: application to diffusion furnace temperature control,* IEEE Transactions on Control Systems Technology **8**, 842 (2000).

[51] R. Nagamune, *Closed-loop shaping based on nevanlinna-pick interpolation with a degree bound,* IEEE Transactions on Automatic Control **49**, 300 (2004).

[52] X. Chen, T. Jiang, and M. Tomizuka, *Pseudo Youla–Kucera parameterization with control of the waterbed effect for local loop shaping,* Automatica **62**, 177 (2015).

[53] T. Jiang, H. Xiao, J. Tang, L. Sun, and X. Chen, *Local loop shaping for rejecting band-limited disturbances in nonminimum-phase systems with application to laser beam steering for additive manufacturing,* IEEE Transactions on Control Systems Technology **28**, 2249 (2020).

[54] J. M. Díaz, R. Costa-Castelló, R. Muñoz, and S. Dormido, *An interactive and comprehensive software tool to promote active learning in the loop shaping control system design,* IEEE access **5**, 10533 (2017).

[55] B. Mohandes, I. Boiko, and Y. Abdel-Magid, *Control system loop-shaping as a mathematical optimization problem: An ensemble of models,* IEEE Access **8**, 137185 (2020).

[56] B. Mohandes, I. Boiko, and Y. Abdel-Magid, *Control system loop-shaping as a mathematical optimization problem: An ensemble of models,* IEEE Access **8**, 137185 (2020).

[57] W. Guan, W. Cao, J. Sun, and Z. Su, *Steering controller design for smart autonomous surface vessel based on csf L_2 gain robust strategy,* IEEE Access **7**, 109982 (2019).

[58] S. Al-Amer and F. Al-Sunni, *Approximation of time-delay systems,* in *Proceedings of the 2000 American Control Conference. ACC (IEEE Cat. No. 00CH36334)*, Vol. 4 (IEEE, 2000) pp. 2491–2495.

[59] A. A. Dastjerdi, *Toolbox for frequency analysis of reset control systems,* .

[60] A. Emami-Naeini and D. de Roover, *Bode's sensitivity integral constraints: The waterbed effect revisited,* arXiv preprint arXiv:1902.11302 (2019).

[61] A. A. Dastjerdi, N. Saikumar, and S. H. HosseinNia, *Tuning guidelines for fractional order PID controllers: Rules of thumb,* Mechatronics **56**, 26 (2018).

[62] B. Kieft, *Proposed solutions for quantization induced performance deterioration in reset controllers,* Ph.D. thesis, Delft University of Technology (2020).

6

CONCLUSIONS AND RECOMMENDATIONS

This thesis has proposed a non-linear loop-shaping framework to allow frequency-domain analyzing of CgLp reset compensators. This final chapter draws the main relevant conclusions of this study presented in the preceding chapters. In addition, the limitations of this research approach are discussed, and recommendations for solving those in future studies are provided.

6.1. CONCLUSIONS

THIS research contributed to solving a significant challenge which is providing a method to enhance the precision of the steady-state performance without devastating the transient response (throughput) of motion systems. The main aim of this thesis was to develop a non-linear loop-shaping framework to enable analyzing CgLp compensators in the frequency-domain. For this purpose, three major questions, which are how to study steady-state performance, assess the stability, and tune parameters of CgLp compensators in the frequency-domain, have been answered through Chapter 3 to Chapter 5.

As was explained in Chapter 1, this performance limitation is irrespective of how optimally linear controllers are tuned and comes from the inherent linearity of these controllers. As a result, linear controllers are not suited to increase precision and speed simultaneously. In order to show that even using advanced FO calculus in linear controllers can not impressively solve this problem, a comprehensive literature study on linear FO controllers in the frequency-domain was carried out in Chapter 2. In that chapter, the structures and tuning methods of four well-known types of FO controllers were discussed. These controllers need approximation methods for realization which leads to high order transfer functions that make the implementation of FO controllers more difficult than IO ones. In fact, it can be anticipated that IO-PID controllers are replaced with FO ones in the near future if a direct method for implementation of FO controllers will be found. Finally, it was concluded that even ignoring the implementation problem, although FO-PID controllers are offering more design freedom compared to classical PID controllers and improve the performance of motion systems (see our work in [1]), they are a type of linear controller and their performance are confined. Thus, to further increase in precision performance without reducing the speed of the system, non-linear controllers like CgLp compensators had to be considered.

In Chapter 3, an analytical approach was proposed to accurately obtain closed-loop frequency responses of reset control systems, including high order harmonics. Unlike linear controllers, proving stability by itself does not guarantee the existence of the steady-state solution for non-linear control systems. Without proving the existence of the steady-state solution, it is not even allowed to utilize the DF method for predicting the closed-loop performance of non-linear control systems. First, this crucial problem was solved asserting that satisfying the H_β condition [2, 3] is sufficient for the existence of the steady-state solution of the closed-loop reset control systems driven by periodic inputs. In addition, it was proved that if the H_β condition is satisfied, the response of reset control systems for a sinusoidal reference $r(t) = r_0 \sin(\omega t)$ only contains the odd harmonics $((2n-1)\omega,\ n \in \mathbb{N})$, and the system does not produce any subharmonics. In addition, satisfying the H_β condition assured that the response of the reset control system for a periodic input $w_P(t) = w_P(t + T_P)$ is periodic with the same period time T_P. This property is important because looking at a time frame of steady-state response with duration T_P gives all essential information about the performance of the reset control system for that periodic input.

After that, the steady-state solution was obtained for a sinusoidal reference, and the closed-loop frequency responses including high order harmonics were formalized using HOSIDF technique [4]. Besides, to study reset control systems more efficiently, all har-

monics were combined to define pseudo-sensitivities, which serve as a graphical tool for performance analysis of reset control systems. The defined frequency responses and pseudo-sensitivities are independent of the input amplitude. Therefore, considering $\tilde{x}_r$ as the steady-state solution of a reset control system for reference r implies that $k\tilde{x}_r$, with $k \in \mathbb{R}$, is the solution of the systems for the reference kr.

After comparing results of pseudo-sensitivity results with results obtained by the DF method in several practical examples, it was demonstrated that pseudo-sensitivities can predict the closed-loop performance of reset control systems more accurately that the DF method (in some examples up to 60%) due to consideration of high order harmonics. Actually, that pseudo-sensitivities revealed important features of reset control systems which could not be exposed by the DF method. One of these features is effects of filter sequence of reset control systems on their performance. Although different sequences of filters result in the same DF, their high order harmonics are different which results in different closed-loop performances. Moreover, another feature was that the actual implementation of reset elements has significant effects on the performance of the system which cannot be understood by the DF method. Pseudo-sensitivities revealed that a CI should be used in the parallel architecture, yielding a system with better precision (up to 25% in one example) and lower control input (up to 80% in one example) once compared to the system with the CI in the series architecture.

As it was explained in Chapter 3, satisfaction of the H_β condition not only guarantees the stability of reset control systems, but also it is the sufficient condition for the existence of the steady-state solution. Thus, in Chapter 4, a novel frequency-domain method for assessing the stability of reset control systems was proposed based on the H_β condition. Note that since the method was developed based on the H_β condition, it is able to assure the existence of the steady-state solution of reset control systems. The method is applicable for all reset elements with the first and second order base linear transfer functions which are introduced in this thesis. Apart from the applicability of this method in the case of partial reset technique (resetting to non-zero values), another advantage of this method in comparison with the conventional H_β condition is that in the case of resetting one state, it provides a graphical tool for determining stability of reset control systems. Similar to the Nyquist plot in the linear control systems, this approach simplifies the stability analysis of reset control systems in the frequency-domain.

Another important result of Chapter 4 was that satisfying the H_β condition results in the well-posedness property of reset instants (according to the definition provided in [5]) for CI, PCI, GFORE, and GSORE. In addition, it was obtained that if the H_β condition is/is not satisfied for a reset control system, the H_β condition is/is not satisfied for other reset control systems with the same base linear and reset matrix but with the different sequence of their filters. In the case of the reset element with the second order base linear transfer function, if the H_β condition is/is not satisfied for a reset control system with a specified state-space realization (e.g. controllable or observable) of the reset element, it does not imply that the H_β condition is/is not satisfied for other reset control systems with the same base linear and reset matrix but with the different state-space realization of the reset element. In short, since the proposed method can directly verify the stability of reset control systems using frequency responses of their base linear open-loop transfer functions, it does not need an accurate parametric model of the system and solving

LMI equations. The developed theories in Chapter 3 and Chapter 4 were embedded in a user-friendly toolbox, which is presented in the appendix C.

In Chapter 5, pseudo-sensitivities and the frequency-domain stability method, which were described in the preceding chapters, were utilized to form a non-linear loop-shaping approach for tuning CgLp compensators. To show the effectiveness of non-linear loop-shaping, different performance metrics of a tuned CgLp were compared with a linear PID, which was also tuned optimally using the same constraints. The results showed that the tuned CgLp achieved more favourable dynamic performance than the PID controller for a precision motion stage. The tracking performance and the disturbance rejection capability of the system were improved by 60% using the CgLp compensator.

In addition, it was practically shown that the “water-bed" effect was broken in this application. To show this, the integral of the pseudo-sensitivity of the system with the CgLp compensator was calculated numerically. Using the CgLp compensator, the integral of the pseudo-sensitivities converged to a negative value which means that the sensitivity was decreased in a certain frequency range without increasing in other frequency ranges. Therefore, the steady-state precision was increased while the transient response was not changed.

Furthermore, it was demonstrated that without considering quantization and noise errors, super-position almost holds (with the maximum relative error 2%) for a specified reference in this practical example. The closed-loop identification of the system with the CgLp compensator was performed which showed that the coherence was around 1 in a wide range of frequencies. This implied that super-position law approximately holds at that wide range of frequencies. It can be said that setting the corner frequency of a GFORE near the cross-over frequency of the system and considering a positive value for the reset matrix, reduce effects of the non-linearity on the output of the GFORE. This was also demonstrated by the identification of a GFORE in [6]. Looking at the coherence function provided in [6], it was understood that GFORE compensator can be well approximated by a linear element at a wide range of frequencies.

In this thesis, effects of changing the filter sequence on the closed-loop performance of reset control systems were studied. It was demonstrated that putting the lead elements of controllers first and then the reset element and other linear parts following in series has an over-damped transient response. However, since noise and quantization errors are amplified before entering the reset element which leads to a drastic change of reset instants in this structure, the steady-state performance of this sequence is not favourable. Although this problem was solved to some extent using the proposed shaping filter [7], the traditional sequence, in which the tracking error is the input of the reset element and other linear parts following in series, has shown a better steady-state performance. It can be said that using the proposed shaping filter provided a trade-off between these two sequences.

All in all, based on several experiments, it can be concluded that using a CgLp compensator, which is tuned based on this non-linear loop-shaping approach, is able to improve the precision of linear motion systems while it does not change the transient response. In particular, as shown in several practical examples, properly replacing part of D action of PID with a CgLp compensator can provide the same rise time, the same overshoot, the same settling time, a better tracking performance (up to 60% in precision

motion applications), a better disturbance rejection capability, and a better noise rejection capability than those of the system with the PID controller. In addition, based on the closed-loop identification, it can be concluded that non-linearity of CgLp compensators at low frequencies is small enough such that systems with these novel compensators can be considered as a linear system at that range of frequencies. Based on our observations, the noise and quantization errors enhance the precision performance of CgLp compensators instead of reducing it in several cases. It is noteworthy to recall that all of these mentioned advantages are obtainable if the CgLp compensator is tuned appropriately according to guidelines provided in this thesis. Otherwise, it may provide a performance worse than linear controllers. Finally, the developed non-linear loop-shaping method in this thesis makes the CgLp compensator an advanced industry-compatible controller such that:

- It improves the precision and speed of motion systems simultaneously.
- Similar to linear controllers, their performance and stability can be analyzed in the frequency-domain.
- Similar to linear controllers, it almost follows super-position law in a wide range of frequencies.

Hence, it is anticipated that D-action part of linear controllers will be substituted with this type of reset compensators in the precision motion systems.

6.2. RECOMMENDATIONS

This research has proposed a non-linear loop-shaping approach for frequency-domain analysis of CgLp compensators. However, during this research, several new aspects have been identified which where excluded form this thesis. Here, most of those important aspects which might be tackled in future are mentioned.

- Predicting coherence of the closed-loop system upon open-loop HOSIDF is an outstanding topic which helps engineers to design CgLp compensators such that they follow the super-position law that is important in industrial applications.
- Although the deviation between the DF method and pseudo-sensitivities can be related to HOSIDF, the relation should be mathematically formalized to enable tuning CgLp compensators on the basis of the open-loop HOSIDF.
- Finding a method for assessing the H_β condition using the open-loop HOSIDF is a future step toward tuning CgLp compensators in the open-loop configuration.
- The H_β condition is a conservative method to analyze stability and existence of the steady-state solution. Based on our observations, when the base linear of the system was stable and the maximum absolute eigenvalues of the reset matrix was less than one, the reset control system was stable, and it had a steady-state solution. It is an extraordinary achievement to prove this hypothesis mathematically.

- An optimization solution was provided for assessing the stability of reset control systems with GSORE, which is computationally expensive. Finding a simple method for solving that optimization problem leads to wider the applicability of the proposed method.

- It is believed in literature that when the open-loop filters out high-order harmonics, the DF approximation is reliable. However, in this work, it has been demonstrated that while DFs of several cases are the same, their performances are completely different. For example, different sequences of filters of reset control systems and parallel or series placement of reset elements have different performances while their DFs are the same. These initial results open a path for further study of effects of the structure of non-linear elements on the accuracy of the DF method.

- In some applications, it has been practically demonstrated that the “water-bed" effect was overcome using CgLp compensators. However, it is not a general result and needs to be proved mathematically that using CgLp compensators will overcome this limitation for motion systems.

- The focus of this thesis was mostly on the performance of CgLp compensators designed by GFORE. However, the performance of different types of CgLp compensators, which have been introduced based on modified GFORE, GSORE, FOSRE, and SOSRE in our group, has not been studied. Thus, it is needed to carry out a comprehensive comparison between the performance of different types of CgLp compensators.

- Based on our observations in several practical examples, the noise and quantization effects reduced the tracking error of the system. One study can be performed to see under which conditions noise and quantization have advantages for reset control systems.

REFERENCES

[1] A. A. Dastjerdi, N. Saikumar, and S. H. HosseinNia, *Tuning guidelines for fractional order PID controllers: Rules of thumb,* Mechatronics **56**, 26 (2018).

[2] O. Beker, C. Hollot, Y. Chait, and H. Han, *Fundamental properties of reset control systems,* Automatica **40**, 905 (2004).

[3] A. Baños and A. Barreiro, *Reset control systems* (Springer Science & Business Media, 2011).

[4] P. Nuij, O. Bosgra, and M. Steinbuch, *Higher-order sinusoidal input describing functions for the analysis of non-linear systems with harmonic responses,* Mechanical Systems and Signal Processing **20**, 1883 (2006).

[5] A. Banos, J. I. Mulero, A. Barreiro, and M. A. Davo, *An impulsive dynamical systems framework for reset control systems,* International Journal of Control **89**, 1985 (2016).

[6] N. Saikumar, R. K. Sinha, and S. H. HosseinNia, *'Constant in gain Lead in phase' element-application in precision motion control,* IEEE/ASME Transactions on Mechatronics **24**, 1176 (2019).

[7] C. Cai, *The Optimal Sequence for Reset Controllers*, Master's thesis, Delft University of Technology (2019).

ACKNOWLEDGEMENTS

Although this thesis might introduce me as the author, supports of many people are behind of this thesis which must be appreciated by me. First and foremost, I would like to thank my supervisor Dr. S.H. HosseinNia for his commitment to build my characteristic as a researcher. When I started my PhD, I was far from the filed of mechatronic, but he dedicated remarkably so much time to train me that I could write this thesis. He was incredibly tolerant and supportive. During my scientific journey, I was faced with some significant obstacles which I passed by his inspiration. We had a lot of challenging and scientific discussion meetings from which I enjoyed so much. He not only taught me mechatronic lessons, but also he enlightened me how to live appropriately. I do not want to exaggerate, but I could not complete my PhD without his encouragement, guidance, and involvements. I want to express my sincere gratitude to my promoter Prof. Just Herder. He always gave me supportive feedbacks and comments. He tried to keep me in line with my PhD and carefully has tracked my improvement during these four years.

Besides my supervisors, I would particularly thank Prof. Alessandro Astolfi who helped me a lot during my stay in Imperial College of London. He had unbelievable contributions toward completing the first and second chapter of this thesis. He was very patient and precise. I learned from him how to write and discuss precisely. He believes that control is a kind of mathematical major, and people have to prove their hypothesis very rigorously and unquestionably. Another important thing that I learned from him is that I have to be patient and perform my jobs perfectly. I was lucky that I had the opportunity to collaborate with him who is one of the most reputed scientists in the field of control. I would thank Dr. HosseinNia, Prof. Just Herder, Erasmus Institute, and Imperial College of London for providing this great opportunity for me.

I had an awesome work environment to collaborate with my best colleagues. I would like to thank my colleagues Dr. Niranjan Saikumar, Nima Karbasizadeh, Dr. Durate Valerio, Dr. Andres Hunt, and Wan Hasbullah for their significant effects on my research. I notably want to thank Jo Spronck who taught me a lot of practical aspects of mechatronics. I did not feel passing time when I was talking with him. For all memorable time that we had together, I would thank my roommates Davood, Thijs, Freek, Jelle, Reinier, Ad, Joep, Jelle Snieder, Werner, Qi Wang, and Alden. I would like to thank our department assistants, Corine, Birgit, Marli, Mariane, and Lisette for providing a comfortable work environment for me. For sharing enjoyable time during my PhD, I express my gratitude to my dear Iranian friends at 3ME, Saleh, Ali Sarafraz, Ali Amoozandeh, Mostafa, and Soroush. My favourite activities during my leisure time are exploring Europe, sitting with my friends, going to the gym, and playing football. For all of these moments, I would like to thank Javad, Hadi, Elahe, Amir, Amir Hossein, Alireza, Ali Latifi, Ali Vahidi, Babak, Masood, Iman, Mohammad, Ehsan, Mahyar, Sina, Hamed, and Mehdi.

I owe my deepest gratitude to my parents, my brother Amir, and my sister Fateme for all they have done for me during my life. Particularly, I am forever grateful for my wife

Azar who was very patient during my PhD. During last years, Azar has supported me a lot and trained my lovely son Amir Abbas who makes our life very beautiful. I would also thank Azar's family who tolerates the separation from their daughter. I would also thank Prof. Movahedi and Prof. Akbari who were my supervisors at Sharif University and encouraged me during my PhD. I am grateful to TU Delft for hosting me nicely and provided the needed resources for accomplishing my research. Finally, I owe a very important debt to Iranian people who financially supported me during my study.

Ali Ahmadi Dastjerdi
Delft, May, 2021

A

A FREQUENCY-DOMAIN STABILITY METHOD FOR RESET SYSTEMS

Ali AHMADI DASTJERDI

In this appendix, an intuitive frequency-domain approach is proposed for assessing stability of reset control systems with reset elements with the first order base linear transfer function, which is the primary results of Chapter 4. Furthermore, the effectiveness of the proposed approach is demonstrated through a practical example.

This appendix has been presented in in Conference on Decision and Control (CDC 2020) [1].

A

A.1. INTRODUCTION

TECHNOLOGY developments in cutting edge industries have control requirements that cannot be fulfilled by linear controllers. To overcome this problem, linear controllers should be substituted with non-linear ones, for example reset controllers. These controllers have attracted significant attention due to their simple structure [2–10]. The advantages of reset controllers have been utilized to enhance the performance of several mechatronic systems (see, e.g. [11–17]). In 1958, the first reset element was introduced by Clegg [2]. The Clegg Integrator (CI) is an integrator which resets its state to zero when its input signal crosses zero. Extensions of the CI, which provide additional design freedom and flexibility, include First Order Reset Elements (FORE) [11, 18], Generalized First Order Reset Element (GFORE) [17], Second Order Reset Elements (SORE) [12], and Generalized Second Order Reset Element (GSORE) [17]. Several reset techniques, such as those based on reset bands [19, 20], fixed reset instants, partial reset (resetting to a non-zero value or resetting a selection of the controller states) [21], and the PI+CI approach [21] have also been studied to improve the performances of these controllers.

Stability is one of the most important requirements of every control system, and reset control systems are no exception [3, 7, 8, 10, 22–25]. Several researchers have analyzed the stability of reset controllers using quadratic Lyapunov functions [7, 10, 26, 27], reset instants dependant methods [24, 28, 29], passivity, small gain, and IQC approaches [22, 30–32]. However, most of these approaches are complex, need parametric models of the system, require solving LMI's, and are only applicable to specific types of plants. As a result, these methods do not interface well with the current control design in industry which favours the use of frequency-domain methods. Several researchers have proposed frequency-domain approaches for assessing stability of reset controllers [3, 8, 33]. In [33], an approach for determining stability of a FORE in closed-loop with a mass-spring damper system has been proposed. The result in [8] is applicable to reset control systems under the specific condition $e(t)u(t) < \frac{u^2}{\varepsilon}$, $\varepsilon > 0$, in which $e(t)$ and $u(t)$ are the input and the output of the reset controller, respectively. This method is not usable in the case of partial reset techniques.

The H_β condition has gained significant attention among existing approaches for assessing stability of reset systems [3, 10, 24]. When the base linear system of the reset controller is a first order transfer function, it provides sufficient frequency-domain conditions for uniform bounded-input bounded-state (UBIBS) stability. However, assessing the H_β condition in the frequency-domain is complex, especially for high dimensional plants. Moreover, it cannot be used to assess UBIBS stability of reset control systems in the case of partial reset techniques. As a result, obtaining a general easy-to-use frequency-domain method for assessing stability of reset control systems is an important open problem.

In this chapter, based on the H_β condition, a novel frequency-domain method for reset controllers with first order base linear system is proposed. This can assess UBIBS stability of reset control systems in the frequency-domain. In this method, stability is determined on the basis of the frequency response of the base linear open-loop transfer function, and the H_β condition does not have to be explicitly tested. Besides, this method is applicable to partial reset techniques.

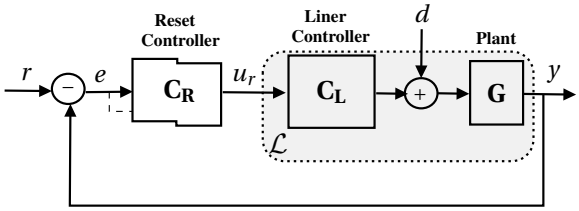

Figure A.1: The closed-loop architecture of a reset controller

The remainder of this chapter is organized as follows. In Section A.2 the problem is formulated. In Section A.3 the frequency-domain approach for determining stability of reset control systems is presented. In Section A.4 the effectiveness of this approach is demonstrated via a practical example. Finally, some remarks and suggestions for future studies are presented in Section A.5.

A.2. PROBLEM FORMULATION

In this section the well-known reset structures GFORE and Proportional Clegg Integrator (PCI) are recalled. Then, the problem under investigation is posed. The focus of this chapter is on the single-input-single-output (SISO) control architecture illustrated in Figure. A.1. The closed-loop system consists of a linear plant with transfer function $G(s)$, a linear controller with transfer function $C_L(s)$, and a reset controller with base linear transfer function $C_R(s)$. The state-space representation of the first order reset controller is

$$\begin{cases} \dot{x}_r(t) = A_r x_r(t) + B_r e(t), & e(t) \neq 0, \\ x_r(t^+) = \gamma x(t), & e(t) = 0, \\ u_r(t) = C_r x(t) + D_r e(t), \end{cases} \tag{A.1}$$

in which $x_r(t) \in \mathbb{R}$ is the reset state, A_r, B_r, and C_r are the dynamic matrices of the reset controller, $-1 < \gamma < 1$ determines the value of the reset state after the reset action, $r(t) \in \mathbb{R}$ is the reference signal, $y(t) \in \mathbb{R}$ is the output of the plant, and $e(t) = r(t) - y(t)$ is the tracking error. The focus of this chapter is on GFORE and PCI, which have been mostly used in practice. In the case of GFORE one has

$$C_R(s) = \frac{1}{\frac{s}{\omega_r} + 1}, \tag{A.2}$$

whereas for PCI one has

$$C_R(s) = 1 + \frac{\omega_r}{s}. \tag{A.3}$$

Thus, for GFORE, $A_r = -C_r = -\omega_r$ (ω_r is the so-called corner frequency), $D_r = 0$ and $B_r = 1$, whereas for the PCI, $A_r = 0$, $C_r = \omega_r$ and $B_r = D_r = 1$.
Let now $\mathcal{L}(s) = C_L(s)G(s)$ and assume that $G(s)$ is strictly proper. Let the state-space realization of $\mathcal{L}(s)$ be

$$\begin{cases} \dot{\zeta}(t) = A\zeta(t) + Bu_r(t) + B_d d(t), \\ y(t) = C\zeta(t), \end{cases} \tag{A.4}$$

where $\zeta(t) \in \mathbb{R}^{n_p}$ describes the state of the plant and of the linear controller (n_p is the number of states of the whole linear part), A, B, and C are the dynamic matrices, and $d(t) \in \mathbb{R}$ is an external disturbance. The closed-loop state-space representation of the overall system can, therefore, be written as

$$\begin{cases} \dot{x}(t) = \bar{A}x(t) + \bar{B}r(t) + \bar{B}_d d(t), & e(t) \neq 0, \\ x(t^+) = \bar{A}_\rho x(t), & e(t) = 0, \\ y(t) = \bar{C}x(t), \end{cases} \tag{A.5}$$

where $x(t) = [x_r(t)^T \quad \zeta(t)^T]^T \in \mathbb{R}^{n_p+1}$, and $\bar{A} = \begin{bmatrix} A_r & -B_r C \\ BC_r & A - BD_r C \end{bmatrix}$, $\bar{B} = \begin{bmatrix} 1 \\ D_r B \end{bmatrix}$, $\bar{B}_d = \begin{bmatrix} 0 \\ B_d \end{bmatrix}$, $\bar{A}_\rho = \begin{bmatrix} \gamma & 0 \\ 0 & I_{n_p \times n_p} \end{bmatrix}$, and $\bar{C} = \begin{bmatrix} 0 & C \end{bmatrix}$. The main goal of this chapter is to provide frequency-domain sufficient conditions to assess UBIBS stability of the reset control system (A.5) with the control structure depicted in Figure. A.1.

A.3. FREQUENCY-DOMAIN STABILITY ANALYSIS

IN this section the main results, which are based on the so-called H_β-condition [3, 7, 10], are presented. Let

$$C_0 = [\rho \quad \beta C], \quad B_0 = \begin{bmatrix} 1 \\ 0_{n_p \times 1} \end{bmatrix}, \quad \rho > 0, \quad \beta \in \mathbb{R}. \tag{A.6}$$

The H_β condition, in the case of the PCI and of the GFORE, states that the reset control system (A.5) with $-1 \leq \gamma \leq 1$, and $r = d = 0$ is quadratically stable if and only if there exist $\rho > 0$ and β such that the transfer function

$$H(s) = C_0(sI - \bar{A})^{-1}B_0 \tag{A.7}$$

is Strictly Positive Real (SPR). This condition requires finding the parameters ρ and β, which may be very difficult when the system has a high order transfer function. In the following, a method to determine stability without finding ρ and β is proposed.

To this end, define the Nyquist Stability Vector (NSV=$\vec{\mathcal{N}}(\omega) \in \mathbb{R}^2$) in a plane with axis $\chi - \Upsilon$ (see Figure. A.2) as follows.

Definition 18. *The Nyquist Stability Vector is, for all $\omega \in \mathbb{R}^+$, the vector*

$$\vec{\mathcal{N}}(\omega) = [\mathcal{N}_\chi \quad \mathcal{N}_\Upsilon]^T = \left[\left| L(j\omega) + \tfrac{1}{2} \right|^2 - \tfrac{1}{4} \quad \Re(L(j\omega) \cdot C_R(j\omega)) + \Re(C_R(j\omega)) \right]^T,$$

$L(s) = \mathcal{L}(s)C_R(s)$.

Let, for simplicity and without loss of generality, $\angle\vec{\mathcal{N}}(\omega) = \theta_{\mathcal{N}} \in [-\frac{\pi}{2}, \frac{3\pi}{2})$, and define the open sets

$$\mathcal{I}_1 = \left\{ \omega \in \mathbb{R}^+ \mid 0 < \angle\vec{\mathcal{N}}(\omega) < \frac{\pi}{2} \right\}, \mathcal{I}_2 = \left\{ \omega \in \mathbb{R}^+ \mid \frac{\pi}{2} < \angle\vec{\mathcal{N}}(\omega) < \pi \right\},$$

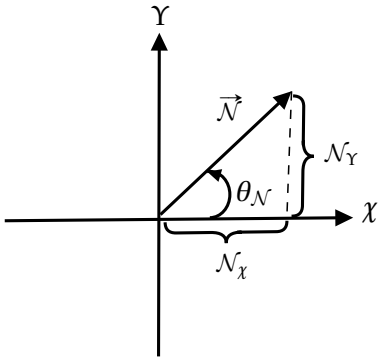

Figure A.2: Representation of the NSV in the $\chi - \Upsilon$ plane

$$\mathcal{I}_3 = \left\{\omega \in \mathbb{R}^+ | \ \pi < \angle\vec{\mathcal{N}}(\omega) < \frac{3\pi}{2}\right\}, \ \mathcal{I}_4 = \left\{\omega \in \mathbb{R}^+ | \ -\frac{\pi}{2} < \angle\vec{\mathcal{N}}(\omega) < 0\right\}.$$

Define now the H_β circle in the complex plane with centre $(-\frac{1}{2}, 0)$ and radius $\frac{1}{2}$ (see Figure. A.3). Then, the following statements hold.

- For all ω such that $L(j\omega)$ is outside the H_β circle $\mathcal{N}_\chi > 0$.
- For all ω such that $L(j\omega)$ is on the H_β circle $\mathcal{N}_\chi = 0$.
- For all ω such that $L(j\omega)$ is inside the H_β circle $\mathcal{N}_\chi < 0$.

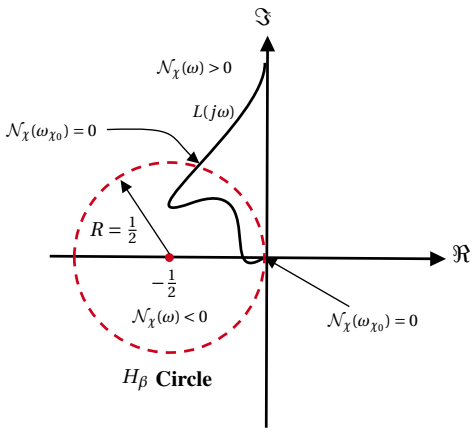

Figure A.3: H_β circle in the Nyquist diagram

On the basis of the definition of the NSV, systems of Type I and of Type II, which are used to assess the stability of the reset control systems, are defined.

Definition 19. *The reset control system (A.5) is of Type I if the following conditions hold.*

(1) For all $\omega \in \mathcal{M} = \{\omega \in \mathbb{R}^+ \mid \mathcal{N}_\chi(\omega) = 0\}$ *one has* $\mathcal{N}_\Upsilon(\omega) > 0$.

(2) For all $\omega \in \mathcal{Q} = \{\omega \in \mathbb{R}^+ \mid \mathcal{N}_\Upsilon(\omega) = 0\}$ *one has* $\mathcal{N}_\chi(\omega) > 0$.

(3) At least one of the following statements is true:

(a) $\forall\, \omega \in \mathbb{R}^+ : \mathcal{N}_\Upsilon(\omega) \geq 0$.

(b) $\forall\, \omega \in \mathbb{R}^+ : \mathcal{N}_\chi(\omega) \geq 0$.

(c) Let $\delta_1 = \max_{\omega \in \mathcal{I}_4} \left| \frac{\mathcal{N}_\Upsilon(\omega)}{\mathcal{N}_\chi(\omega)} \right|$ *and* $\Psi_1 = \min_{\omega \in \mathcal{I}_2} \left| \frac{\mathcal{N}_\Upsilon(\omega)}{\mathcal{N}_\chi(\omega)} \right|$. *Then* $\delta_1 < \Psi_1$ *and* $\mathcal{I}_3 = \varnothing$.

Remark 11. Let

$$\theta_1 = \min_{\omega \in \mathbb{R}^+} \angle \vec{\mathcal{N}}(\omega) = \angle \vec{\mathcal{N}}_1 \text{ and } \theta_2 = \max_{\omega \in \mathbb{R}^+} \angle \vec{\mathcal{N}}(\omega) = \angle \vec{\mathcal{N}}_2, \tag{A.8}$$

where $\vec{\mathcal{N}}_1$ and $\vec{\mathcal{N}}_2$ are implicitly defined by equation (A.8). Then, the conditions identifying Type I systems are equivalent to the condition

$$\left(-\frac{\pi}{2} < \theta_1 < \pi\right) \wedge \left(-\frac{\pi}{2} < \theta_2 < \pi\right) \wedge (\theta_2 - \theta_1 < \pi). \tag{A.9}$$

Definition 20. *The reset control system (A.5) is of Type II if the following conditions hold:*

(1) $\mathcal{L}(s)$ *does not have any pole at origin.*

(2) For all $\omega \in \mathcal{M}$ *one has* $\mathcal{N}_\Upsilon(\omega) > 0$.

(3) For all $\omega \in \mathcal{Q}$ *one has* $\mathcal{N}_\chi(\omega) < 0$

(4) At least, one of the following statements is true:

(a) $\forall\, \omega \in \mathbb{R}^+ : \mathcal{N}_\Upsilon(\omega) \geq 0$.

(b) $\forall\, \omega \in \mathbb{R}^+ : \mathcal{N}_\chi(\omega) \leq .0$

(c) Let $\delta_2 = \max_{\omega \in \mathcal{I}_3} \left| \frac{\mathcal{N}_\Upsilon(\omega)}{\mathcal{N}_\chi(\omega)} \right|$ *and* $\Psi_2 = \min_{\omega \in \mathcal{I}_1} \left| \frac{\mathcal{N}_\Upsilon(\omega)}{\mathcal{N}_\chi(\omega)} \right|$. *Then,* $\delta_2 < \Psi_2$ *and* $\mathcal{I}_4 = \varnothing$.

Remark 12. The conditions identifying the Type II systems are equivalent to the following conditions.

(1) $\mathcal{L}(s)$ does not have any pole at origin.

(2)

$$\left(0 < \theta_1 < \frac{3\pi}{2}\right) \wedge \left(0 < \theta_2 < \frac{3\pi}{2}\right) \wedge (\theta_2 - \theta_1 < \pi). \tag{A.10}$$

On the basis of the above definitions the main result of this chapter, which is a frequency-domain tool for determining stability of reset control systems, is presented.

Theorem 8. *The reset control system (A.5) with GFORE or PCI is UBIBS stable if all the following conditions are satisfied.*

- *The base linear system is stable and the open-loop transfer function does not have any pole-zero cancellation.*
- *The reset control system (A.5) is either of Type I and/or of Type II.*

Proof. Theorem 8 is proved in several steps.

- Step 1: It is shown that, by Hypothesis (II) of Theorem 8, it is possible to find β and $\rho > 0$ such that $\Re(H(j\omega)) > 0,\ \forall\ \omega \in \mathbb{R}^+$.
- Step 2: For systems with poles at origin, it is shown that $\lim_{\omega \to 0} \Re(H(j\omega)) > 0$.
- Step 3: It is shown that either $\lim_{s \to \infty} H(s) > 0$ or $\lim_{\omega \to \infty} \omega^2 \Re(H(j\omega)) > 0$.
- Step 4: It is shown that (A, C_0) and (A, B_0) are observable and controllable, respectively. Thus, $H(s)$ is SPR and the H_β condition is satisfied, and reset control system (A.5) with GFORE or PCI is UBIBS stable.

Step 1: The transfer function (A.7) can be rewritten as

$$H(s) = \frac{y}{r} = \frac{\beta L(s) + \rho' C_R(s)}{1 + L(s)}, \text{ (see also Figure. A.4).} \tag{A.11}$$

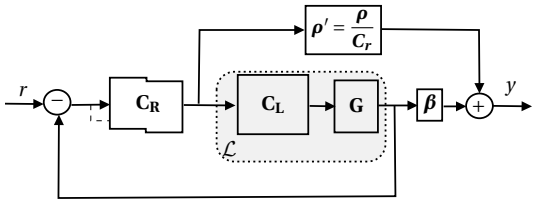

Figure A.4: The block diagram representative of $H(s)$

Let $L(j\omega) = a + bj$ and $C_R(j\omega) = a_R + b_R j$. Then,

$$\Re(H(j\omega)) = \frac{\beta\left((a+\frac{1}{2})^2 + b^2 - \frac{1}{4}\right) + \rho'(a_R a + b_r b + a_R)}{(a+1)^2 + b^2}. \tag{A.12}$$

Define now the vector $\vec{\xi} \in \mathbb{R}^2$ as $\vec{\xi} = [\beta \quad \rho]^T$ in the $\chi - \Upsilon$ plane. Using Definition 18, equation (A.12) can be re-written as

$$\Re(H(j\omega)) = \frac{\vec{\xi} \cdot \vec{\mathcal{N}}}{(a+1)^2 + b^2}. \tag{A.13}$$

Then, the H_β condition reduces to

$$\forall \omega \in \mathbb{R}^+ : \Re(H(j\omega)) > 0 \iff \vec{\xi} \cdot \vec{\mathcal{N}} > 0 \iff -\frac{\pi}{2} < \angle(\vec{\xi}, \vec{\mathcal{N}}) < \frac{\pi}{2} \ \wedge\ \left|\vec{\mathcal{N}}\right| \neq 0 \ \wedge\ \left|\vec{\xi}\right| \neq 0. \tag{A.14}$$

By (A.8), $\forall \omega \in \mathbb{R}^+$, $\overrightarrow{\mathcal{N}}(\omega)$ is placed between the vectors $\overrightarrow{\mathcal{N}_1}$ and $\overrightarrow{\mathcal{N}_2}$ illustrated in Figure. A.5. In other words,

$$\forall\, \omega \in \mathbb{R}^+ : \theta_1 \leq \angle\overrightarrow{\mathcal{N}}(\omega) \leq \theta_2. \tag{A.15}$$

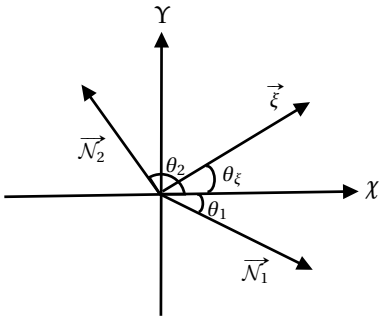

Figure A.5: Representation of $\vec{\mathcal{N}}(\omega)$ and $\vec{\xi}$ in the $\chi - \Upsilon$ plane

If $\beta > 0$, since $0 < \angle\overrightarrow{\xi} = \theta_\xi < \frac{\pi}{2}$, then $\theta_1 \in (-\frac{\pi}{2}, \pi)$ and $\theta_2 \in (-\frac{\pi}{2}, \pi)$. This implies the conditions (1) and (2) in Definition 19 and $\mathcal{I}_3 = \varnothing$. If $\beta \leq 0$, then $\theta_1 \in (0, \frac{3\pi}{2})$ and $\theta_2 \in (0, \frac{3\pi}{2})$, which implies the conditions (1) and (2) in Definition 20 hold and $\mathcal{I}_4 = \varnothing$. If $\theta_1 \in [0, \frac{\pi}{2}]$ and $\theta_2 \in [0, \frac{\pi}{2}]$, then

$$\Re(H(j\omega)) > 0 \iff \begin{cases} \theta_\xi \in (0, \frac{\pi}{2}) \iff \beta > 0, \\ \theta_\xi \in [\frac{\pi}{2}, \frac{\pi}{2} + \theta_1) \Rightarrow \beta \leq 0 \ \wedge\ \theta_1 > 0. \end{cases} \tag{A.16}$$

If $\theta_1 \in [0, \frac{\pi}{2}]$ and $\theta_2 \in [\frac{\pi}{2}, \pi]$, then

$$\Re(H(j\omega)) > 0 \iff \begin{cases} \theta_\xi \in (\theta_2 - \frac{\pi}{2}, \frac{\pi}{2}) \Rightarrow \beta > 0 \wedge\ \theta_2 < \pi, \\ \theta_\xi \in [\frac{\pi}{2}, \frac{\pi}{2} + \theta_1) \Rightarrow \beta \leq 0 \ \wedge\ \theta_1 > 0. \end{cases} \tag{A.17}$$

If $\theta_1 \in [\frac{\pi}{2}, \pi]$ and $\theta_2 \in [\frac{\pi}{2}, \pi]$, then

$$\Re(H(j\omega)) > 0 \iff \begin{cases} \theta_\xi \in (\theta_2 - \frac{\pi}{2}, \frac{\pi}{2}) \Rightarrow \beta > 0 \wedge\ \theta_2 < \pi, \\ \theta_\xi \in [\frac{\pi}{2}, \pi) \iff \beta \leq 0. \end{cases} \tag{A.18}$$

If $\theta_1 \in [\frac{\pi}{2}, \frac{3\pi}{2})$ and $\theta_2 \in [\pi, \frac{3\pi}{2})$, then

$$\Re(H(j\omega)) > 0 \iff \theta_\xi \in (\theta_2 - \frac{\pi}{2}, \pi) \Rightarrow \beta < 0. \tag{A.19}$$

If $\theta_1 \in (0, \frac{\pi}{2}]$ and $\theta_2 \in [\pi, \frac{3\pi}{2})$, then $\Re(H(j\omega)) > 0$ if and only if

$$\left(\theta_\xi \in (\theta_2 - \frac{\pi}{2}, \theta_1 + \frac{\pi}{2}) \wedge \theta_2 - \theta_1 < \pi\right) \Rightarrow \beta < 0. \tag{A.20}$$

As a result.

$$\theta_2 - \theta_1 < \pi \iff \delta_2 < \psi_2. \tag{A.21}$$

Hence, by (A.16)-(A.21), Condition (3) of Definition 20 and Condition (2) of Remark 12 are obtained. If $\theta_1 \in (-\frac{\pi}{2}, 0]$ and $\theta_2 \in (-\frac{\pi}{2}, \frac{\pi}{2}]$, then

$$\Re(H(j\omega)) > 0 \iff \theta_\xi \in (0, \theta_1 + \frac{\pi}{2}) \Rightarrow \beta > 0. \tag{A.22}$$

If $\theta_1 \in (-\frac{\pi}{2}, 0]$ and $\theta_2 \in [\frac{\pi}{2}, \pi)$, then $\Re(H(j\omega)) > 0$ if and only if

$$\left(\theta_\xi \in (\theta_2 - \frac{\pi}{2}, \theta_1 + \frac{\pi}{2}) \wedge \theta_2 - \theta_1 < \pi\right) \Rightarrow \beta > 0, \tag{A.23}$$

hence

$$\theta_2 - \theta_1 < \pi \iff \delta_1 < \psi_1. \tag{A.24}$$

Therefore, by (A.16)-(A.18) and (A.22)-(A.24), Condition (3) of Definition 19 and Remark 11 are obtained.

Step 2: Let $L(s) = \dfrac{L'(s)}{s^n}$, with $n \geq 1$, $L'(0) \neq 0$. Equation (A.12) yields

$$\lim_{\omega \to 0} \Re(H(j\omega)) = \lim_{|L| \to \infty} \frac{\beta |L|^2 + \rho' \left(|L||C_R(0)| \cos(\angle \overrightarrow{C_R(0), L(0)}) + \Re(C_R(0)) \right)}{|L|^2}. \tag{A.25}$$

For GFORE, equation (A.25) becomes

$$\lim_{\omega \to 0} \Re(H(j\omega)) = \beta + \rho' \lim_{|L| \to \infty} \frac{\cos(\angle \overrightarrow{C_R(0), L(0)})}{|L|} + \frac{1}{|L|^2} = \beta > 0, \tag{A.26}$$

whereas in the case of PCI with $n = 1$ (A.25) becomes

$$\lim_{\omega \to 0} \Re(H(j\omega)) = \beta + \rho' \lim_{\omega \to 0} \left(\frac{|C_R|}{|L|} + \frac{1}{|L|^2} \right) = \beta + \frac{\rho' \omega_r}{|\mathcal{L}(0)|} \tag{A.27}$$

which, setting $\overrightarrow{\mathcal{N}'} = [1 \quad \frac{\rho' \omega_r}{|\mathcal{L}(0)|}]^T$, yields

$$\lim_{\omega \to 0} \Re(H(j\omega)) = \overrightarrow{\xi} \cdot \overrightarrow{\mathcal{N}'}. \tag{A.28}$$

In addition,

$$\angle \overrightarrow{\mathcal{N}'} = \lim_{\omega \to 0} \angle \overrightarrow{\mathcal{N}} \xrightarrow{(A.15)} \theta_1 \leq \angle \overrightarrow{\mathcal{N}'} \leq \theta_2. \tag{A.29}$$

As a result, by Step 1, $\lim_{\omega\to 0}\Re(H(j\omega)) = \vec{\xi}\cdot\overrightarrow{\mathcal{N}'} > 0$. For PCI with $n>1$

$$\lim_{\omega\to 0}\Re(H(j\omega)) = \beta + \rho'\lim_{\omega\to 0}\frac{\omega^n\cos(\angle(\overrightarrow{C_R(0)},\overrightarrow{L(0)}))}{\omega} = \beta > 0. \tag{A.30}$$

It is therefore concluded that for systems with poles at the origin (i.e. $\mathcal{L}(s) = \frac{\mathcal{L}'(s)}{s^n}$, $n\geq 1$, $\mathcal{L}'(0)\neq 0$), $\beta>0$. If $\mathcal{L}(s)$ does not have any pole at origin, β can be either positive or negative. As a result, by Step 1 and Step 2, if Hypothesis (II) holds

$$\exists\,(\beta\in\mathbb{R},\ \rho'>0)\mid\forall\,\omega\in\mathbb{R}^+:\ \Re(H(j\omega))>0, \tag{A.31}$$

and also, the claims in Remark 11 and Remark 12 are true.

Step 3: Since $\mathcal{L}(s)$ is strictly proper, it is possible to consider $\lim_{\omega\to\infty}|L| = \frac{|a_\infty + jb_\infty|}{|\omega|^n}$, $n\geq 2$. For GFORE, $|C_R|\approx\frac{\omega_r}{|\omega|}$ and $a_R\approx\frac{\omega_r^2}{\omega^2}$ for ω sufficiently large, hence, for $n=2$ and setting $\overrightarrow{\mathcal{N}''} = [a_\infty \quad \omega_r^2]^T$, yields

$$\lim_{\omega\to\infty}\omega^2\Re(H(j\omega)) = (\beta a_\infty + \rho'\omega_r^2) = \vec{\xi}\cdot\overrightarrow{\mathcal{N}''}. \tag{A.32}$$

In addition

$$\angle\overrightarrow{\mathcal{N}''} = \lim_{\omega\to\infty}\angle\overrightarrow{\mathcal{N}} \overset{(A.15)}{\Longrightarrow} \theta_1\leq\angle\overrightarrow{\mathcal{N}''}\leq\theta_2. \tag{A.33}$$

Thus, by Step 1, $\lim_{\omega\to\infty}\omega^2\Re(H(j\omega)) = \vec{\xi}\cdot\overrightarrow{\mathcal{N}''} > 0$. For GFORE with $n>2$, $\lim_{\omega\to\infty}\omega^2\Re(H(j\omega)) = \rho'\omega_r^2 > 0$. For PCI, $\lim_{s\to\infty}H(s) = \rho > 0$. Hence, by Hypothesis (II), $\lim_{s\to\infty}H(s) > 0$ or $\lim_{\omega\to\infty}\omega^2\Re(H(j\omega)) > 0$.

Step 4: In order to show that the pairs (A, C_0) and (A, B_0) are observable and controllable, respectively, it is sufficient to show that the denominator and the numerator of $H(s)$ do not have any common root. Let $a_0 + jb_0$ be a root of the denominator. Then

$$1 + R_L(a_0,b_0) + jI_L(a_0,b_0) = 0 \Rightarrow \begin{cases} R_L(a_0,b_0) = -1, \\ I_L(a_0,b_0) = 0 \Rightarrow b_0 = \mathcal{P}(a_0). \end{cases} \tag{A.34}$$

If the numerator does not have a root at $a_0 + jb_0$, then

$$\begin{aligned} &\beta\left(1 + R_L(a_0,b_0) + jI_L(a_0,b_0)\right) + \rho'\left(R_{C_R}(a_0,b_0) + I_{C_R}(a_0,b_0)\right)\neq 0 \\ &\overset{(A.34)}{\Longrightarrow} \beta\neq\rho' R_{C_R}(a_0,b_0)\ \vee\ I_{C_R}(a_0,b_0)\neq 0. \end{aligned} \tag{A.35}$$

For GFORE, by (A.35), this yields

$$\beta\neq\frac{\rho'\omega_r}{a_0+\omega_r}\ \vee\ b_0\neq 0, \tag{A.36}$$

and for PCI

$$\beta\neq\frac{\rho'(a_0+\omega_r)}{a_0}\ \vee\ b_0\neq 0. \tag{A.37}$$

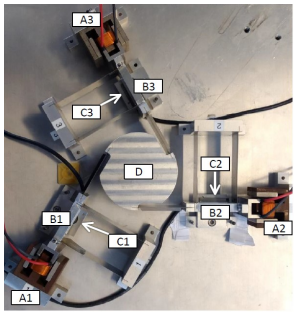

Figure A.6: Spider stage

Therefore, by Step 1, (A.36) and (A.37), it is possible to find a pair (β, ρ') such that $H(s)$ does not have any pole-zero cancellation.
Step 5: By Steps 1-4 and Hypothesis (I), we concluded that $H(s)$ is SPR, and (A, C_0) and (A, B_0) are observable and controllable, respectively. Hence, according to the H_β condition [3, 7, 10], the system is quadratically stable. To complete the proof we have to show that the system is UBIBS stable. In [3], it has been shown that, for GFORE and PCI , when $\gamma = 0$ and the H_β condition is satisfied, the system is UBIBS. If $-1 < \gamma < 1$, that proof is true and the system is UBIBS. □

Remark 13. Since this frequency-domain theorem is based on the H_β condition, if one of the conditions (I) and (II) is not satisfied, then the system is not quadratically stable.

A.4. ILLUSTRATIVE EXAMPLE

IN this section an example is used to show how Theorem 8 can be used to study stability of reset control systems. For this purpose, the stability of a precision positioning system [17] controlled by a reset controller is considered. In this system (Figure. A.6), three actuators are angularly spaced to actuate 3 masses (indicated by B1, B2, and B3) which are constrained by parallel flexures and connected to the central mass D through leaf flexures. Only one of the actuators (A1) is considered and used for controlling the position of mass B1 attached to the same actuator which results in a SISO system. This positioning stage with its amplifier is well modelled by the second order mass-spring-damper system [17] as following.

$$G(s) = \frac{1.429 \times 10^8}{175.9s^2 + 7738s + 1.361 \times 10^6} \tag{A.38}$$

In [17], a non-linear phase compensator, which is termed Constant in gain Lead in phase (CgLp) (for more details see [15, 17, 34]), has been used to improve the performance of the precision positioning stage. CgLp compensators, consisting of a lead filter and a

A

Table A.1: Tuning parameters of controller (A.39) [17]

Tuning Parameters	C_1	C_2	C_3	C_4	C_5
K_p	0.070	0.163	0.201	0.197	0.183
γ	0	0.2	0.4	0.6	0.8
d	1.44	1.23	1.11	1.04	1.01
g	1.98	2.12	2.27	2.43	2.63

GFORE, have been utilized along with a PID controller to give the overall controller

$$C(s)=K_p\overbrace{\overbrace{\left(\frac{1}{\frac{ds}{\omega_c}+1}\right)^{\gamma}}^{\text{GFORE}}\overbrace{\left(\frac{\frac{s}{\omega_c}+1}{\frac{s}{10\omega_c}+1}\right)}^{\text{Lead}}}^{\text{Reset Compensator}}\overbrace{\overbrace{\left(1+\frac{\omega_c}{10s}\right)}^{\text{PI}}\overbrace{\left(\frac{\frac{gs}{\omega_c}+1}{\frac{s}{g\omega_c}+1}\right)}^{\text{Lead}}\overbrace{\left(\frac{1}{\frac{s}{10\omega_c}+1}\right)}^{\text{Low-Pass}}}^{\text{PID}}. \tag{A.39}$$

in which ω_c is the cross-over frequency and K_p, γ, d, and g are tuning parameters. In [17], five controllers with different values of K_p, γ, d, and g (see Table A.1) have been designed to provide 45° phase margin at $\omega_c = 200\pi$(rad/s). This results in

$$\mathcal{L}_i(s)=\left(\frac{K_p(\frac{s}{200\pi}+1)(10s+200\pi)(\frac{gs}{200\pi}+1)1.429\times10^8}{s(\frac{s}{200\pi}+1)(\frac{s}{200\pi g}+1)(\frac{s}{2000\pi}+1)(175.9s^2+7738s+1.361\times10^6)}\right), \tag{A.40}$$

$$C_{R_i}(s)=\left(\frac{1}{\frac{ds}{200\pi}+1}\right), \tag{A.41}$$

$$L_i(s)=C_R\mathcal{L}. \tag{A.42}$$

As the reset element used in these controllers is a GFORE and $\mathcal{L}_i$ have a pole at the origin, we use Definition 19 to assess stability. The properties of $\mathcal{N}_\chi(\omega)$ and $\mathcal{N}_\Upsilon(\omega)$ for these controllers are listed in Table A.2. On the basis of this table all of these reset control systems are of Type I. To provide a better insight, the angels $\angle\overrightarrow{\mathcal{N}(\omega)}$ for these reset systems are plotted in Figure. A.7. As demonstrated by the figure, for all of these systems $\theta_1 \in (-\frac{\pi}{2},\pi)$, $\theta_2 \in (-\frac{\pi}{2},\pi)$ and $\theta_2-\theta_1<\pi$, therefore, the condition in Remark 11 holds. Furthermore, the base linear systems of these controllers are stable and do not have any pole-zero cancellation in the open-loop transfer functions. Hence, by Theorem 8, all of these controllers give UBIBS stable reset control systems.

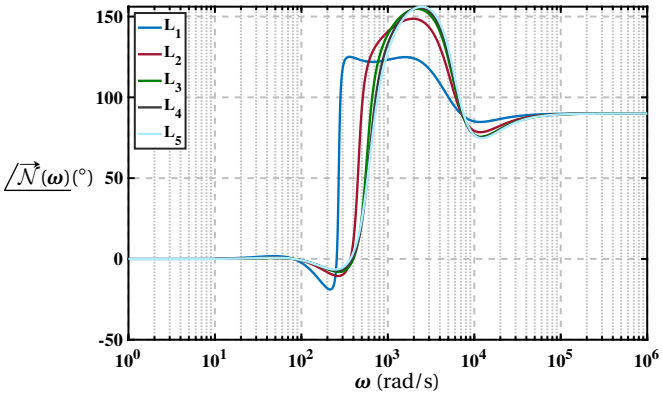

Figure A.7: $\angle\vec{\mathcal{N}}(\omega)$ for the five considered reset control systems

Table A.2: Properties of $\vec{\mathcal{N}}(\omega)$ for the five considered reset control systems

Systems	L_1	L_2	L_3	L_4	L_5
$\mathcal{L}$ has a pole at origin	Yes	Yes	Yes	Yes	Yes
$\mathcal{M}$	279.2-6945.0	495.7-7090.7	630.0-7225.6	686.8-7354.4	718.3-7488.7
$\mathcal{Q}$	80.9-256.3	80.7-370.2	81.2-398.9	81.8-388.1	82.6-368.0
Sign($\mathcal{N}_Y(\omega \in \mathcal{M})$)	+	+	+	+	+
Sign($\mathcal{N}_\chi(\omega \in \mathcal{Q})$)	+	+	+	+	+
$\mathcal{I}_3$	$\varnothing$	$\varnothing$	$\varnothing$	$\varnothing$	$\varnothing$
$\delta_1 < \psi_1$	$0.11 < 0.44$	$0.12 < 0.45$	$0.14 < 0.47$	$0.18 < 0.61$	$0.34 < 1.42$
Type	(I)	(I)	(I)	(I)	(I)

In order to verify the results, the H_β parameters for each reset system are listed in Table A.3. As demonstrated by the table, the H_β condition is satisfied which is consistent with our conclusion. The step responses of the reset control systems are plotted in Figure. A.8 which demonstrates the performances of these controllers. In summary, as shown by Table A.2 and Figure. A.7, the proposed results allow us determining stability of these reset control systems without computing values for the pair (ρ, β).

Table A.3: Pairs (ρ', β) for the five considered reset control systems

Systems	L_1	L_2	L_3	L_4	L_5
Equivalent H_β ($\beta > 0$)	$2.24 < \frac{\rho'}{\beta} < 8.77$	$2.19 < \frac{\rho'}{\beta} < 8.7.94$	$2.12 < \frac{\rho'}{\beta} < 6.85$	$1.63 < \frac{\rho'}{\beta} < 5.36$	$0.7 < \frac{\rho'}{\beta} < 2.91$

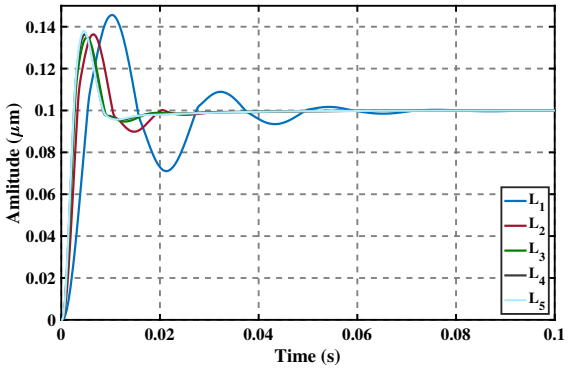

Figure A.8: Step responses of the five considered reset control systems

A.5. CONCLUSION

IN this chapter a novel frequency-domain method for determining stability properties of reset control systems has been proposed. This method is based on the H_β condition and it can assess stability of reset control systems using the frequency response of their base linear open-loop transfer function. Consequently, this method does not need an accurate parametric model of the system and solving LMIs. The effectiveness of the proposed method has been illustrated by one practical example. This method may increase usage of reset controllers in high-precision industry to improve performances of control systems.

REFERENCES

[1] A. A. Dastjerdi, A. Astolfi, and S. H. HosseinNia, *A frequency-domain stability method for reset systems,* in *IEEE 59th Conference on Decision and Control* (2020).

[2] J. Clegg, *A nonlinear integrator for servomechanisms,* Transactions of the American Institute of Electrical Engineers, Part II: Applications and Industry **77**, 41 (1958).

[3] O. Beker, C. Hollot, Y. Chait, and H. Han, *Fundamental properties of reset control systems,* Automatica **40**, 905 (2004).

[4] W. Aangenent, G. Witvoet, W. Heemels, M. Van De Molengraft, and M. Steinbuch, *Performance analysis of reset control systems,* International Journal of Robust and Nonlinear Control **20**, 1213 (2010).

[5] F. Forni, D. Nešić, and L. Zaccarian, *Reset passivation of nonlinear controllers via a suitable time-regular reset map,* Automatica **47**, 2099 (2011).

[6] A. F. Villaverde, A. B. Blas, J. Carrasco, and A. B. Torrico, *Reset control for passive bilateral teleoperation,* IEEE Transactions on Industrial Electronics **58**, 3037 (2011).

[7] A. Baños and A. Barreiro, *Reset control systems* (Springer Science & Business Media, 2011).

[8] S. Van Loon, K. Gruntjens, M. F. Heertjes, N. van de Wouw, and W. Heemels, *Frequency-domain tools for stability analysis of reset control systems,* Automatica **82**, 101 (2017).

[9] S. H. HosseinNia, I. Tejado, and B. M. Vinagre, *Fractional-order reset control: Application to a servomotor,* Mechatronics **23**, 781 (2013).

[10] Y. Guo, L. Xie, and Y. Wang, *Analysis and design of reset control systems* (Institution of Engineering and Technology, 2015).

[11] I. Horowitz and P. Rosenbaum, *Non-linear design for cost of feedback reduction in systems with large parameter uncertainty,* International Journal of Control **21**, 977 (1975).

[12] L. Hazeleger, M. Heertjes, and H. Nijmeijer, *Second-order reset elements for stage control design,* in *American Control Conference (ACC)* (IEEE, 2016) pp. 2643–2648.

[13] Y. Guo, Y. Wang, and L. Xie, *Frequency-domain properties of reset systems with application in hard-disk-drive systems,* IEEE Transactions on Control Systems Technology **17**, 1446 (2009).

[14] S. Van den Eijnden, Y. Knops, and M. F. Heertjes, *A hybrid integrator-gain based low-pass filter for nonlinear motion control,* in *IEEE Conference on Control Technology and Applications (CCTA)* (IEEE, 2018) pp. 1108–1113.

[15] L. Chen, N. Saikumar, and S. H. HosseinNia, *Development of robust fractional-order reset control,* IEEE Transactions on Control Systems Technology , 1 (2019).

[16] D. Valério, N. Saikumar, A. A. Dastjerdi, N. Karbasizadeh, and S. H. HosseinNia, *Reset control approximates complex order transfer functions,* Nonlinear Dynamics , 1 (2019).

[17] N. Saikumar, R. K. Sinha, and S. H. HosseinNia, *"Constant in Gain Lead in Phase" Element-Application in Precision Motion Control,* IEEE/ASME Transactions on Mechatronics **24**, 1176 (2019).

[18] L. Zaccarian, D. Nesic, and A. R. Teel, *First order reset elements and the clegg integrator revisited,* in *Proceedings of the 2005, American Control Conference* (2005) pp. 563–568 vol. 1.

[19] A. Barreiro, A. Baños, S. Dormido, and J. A. González-Prieto, *Reset control systems with reset band: Well-posedness, limit cycles and stability analysis,* Systems & Control Letters **63**, 1 (2014).

[20] A. Baños and M. A. Davó, *Tuning of reset proportional integral compensators with a variable reset ratio and reset band,* IET Control Theory & Applications **8**, 1949 (2014).

[21] J. Zheng, Y. Guo, M. Fu, Y. Wang, and L. Xie, *Improved reset control design for a PZT positioning stage,* in *IEEE International Conference on Control Applications* (2007) pp. 1272–1277.

A

[22] H. K. Khalil and J. W. Grizzle, *Nonlinear systems*, Vol. 3 (Prentice hall Upper Saddle River, NJ, 2002).

[23] D. Nešić, L. Zaccarian, and A. R. Teel, *Stability properties of reset systems,* Automatica **44**, 2019 (2008).

[24] A. Baños, J. Carrasco, and A. Barreiro, *Reset times-dependent stability of reset control systems,* IEEE Transactions on Automatic Control **56**, 217 (2010).

[25] K. Rifai and J.-J. Slotine, *Compositional contraction analysis of resetting hybrid systems,* IEEE Transactions on Automatic Control **51**, 1536 (2006).

[26] S. Polenkova, J. W. Polderman, and R. Langerak, *Stability of reset systems,* in *Proceedings of the 20th International Symposium on Mathematical Theory of Networks and Systems* (2012) pp. 9–13.

[27] P. Vettori, J. W. Polderman, and R. Langerak, *A geometric approach to stability of linear reset systems,* Proceedings of the 21st Mathematical Theory of Networks and Systems (2014).

[28] A. Banos, J. Carrasco, and A. Barreiro, *Reset times-dependent stability of reset control with unstable base systems,* in *IEEE International Symposium on Industrial Electronics* (2007) pp. 163–168.

[29] D. Paesa, J. Carrasco, O. Lucia, and C. Sagues, *On the design of reset systems with unstable base: A fixed reset-time approach,* in *Annual Conference of the IEEE Industrial Electronics Society* (2011) pp. 646–651.

[30] W. M. Griggs, B. D. Anderson, A. Lanzon, and M. C. Rotkowitz, *A stability result for interconnections of nonlinear systems with "mixed" small gain and passivity properties,* in *46th IEEE Conference on Decision and Control* (2007) pp. 4489–4494.

[31] J. Carrasco, A. Baños, and A. van der Schaft, *A passivity-based approach to reset control systems stability,* Systems & Control Letters **59**, 18 (2010).

[32] C. Hollot, Y. Zheng, and Y. Chait, *Stability analysis for control systems with reset integrators,* in *Proceedings of the 36th IEEE Conference on Decision and Control*, Vol. 2 (1997) pp. 1717–1719.

[33] O. Beker, C. Hollot, Q. Chen, and Y. Chait, *Stability of a reset control system under constant inputs,* in *Proceedings of the American Control Conference (Cat. No. 99CH36251)*, Vol. 5 (1999) pp. 3044–3045.

[34] A. Palanikumar, N. Saikumar, and S. H. HosseinNia, *No more differentiator in PID: Development of nonlinear lead for precision mechatronics,* in *European Control Conference (ECC)* (2018) pp. 991–996.

B

THE OPTIMAL SEQUENCE FOR RESET CONTROLLERS

Ali AHMADI DASTJERDI

Unlike linear controllers, the performance of reset control systems vary depending on the relative sequence of their filers. In this appendix, the effects of sequence of filters on the performance of reset control systems are investigated utilizing High Order Sinusoidal Input Describing Function (HOSIDF) method. Note that, since these results were obtained before completing Chapter 3 and 4, the H_β constraint was not considered for tuning reset control systems in this appendix.

This appendix has been presented in European Control Conference (ECC 2020) [1].

B.1. INTRODUCTION

PRECISION positioning is an important topic in the high-tech industry with applications such as photolithography machines and atomic force microscopes. In these applications, nano-precision controllers with high bandwidth and stability are required to ensure high production quality and speeds. PID controllers, which are one of the most used controllers in the industry owing to their simplicity and ease of tuning, cannot fulfil these control requirements due to their linear nature. This is explained by the water-bed effect which confines the performance of linear controllers so that it is impossible to achieve high bandwidth, stability and precision simultaneously [2–5]. Reset controllers are a popular nonlinear alternative and have attracted a lot of attention from academia and industry due to their simple structure [6–13].

Reset control is a nonlinear control strategy which was introduced in 1958. A traditional reset element resets its state/s to zero when the input signal crosses zero. Clegg introduced the first reset controller by applying reset strategy on a linear integrator [6]. In [14] and [15], reset controllers have been extended to First Order Reset Element (FORE) and Second Order Reset Element (SORE) respectively, enabling greater tune-ability and hence applicability in complex systems. Also, several additional strategies have been developed to tune the degree of non-linearity of reset elements such as partial reset and PI+CI [16–19]. Reset control has been used to introduce new compensators such as CgLp, CLOC, etc. [11, 20–23].

One of the frequency domain tools for the study of nonlinear controllers is Describing Function (DF), in which the nonlinear controller output is approximated with the first harmonic of Fourier series expansion. Although DF is widely used to analyze and tune reset controllers as well, neglecting of the high order harmonics can be seen in the deviation between expected and measured performance [21, 23]. To investigate the influence of high order harmonics in general nonlinear systems, the concept of high order sinusoidal input describing functions (HOSIDF) was proposed in [24], which was applied for reset controllers in [25].

The HOSIDF tool shows that the plant, as well as the linear parts of the controller, influence the high order harmonics. Further, although traditionally the nonlinear reset element is placed to receive error signal as its input, changing the sequence of linear parts and nonlinear reset elements results in different high order harmonic shapes which should result in different resetting laws and closed-loop performance. However, the effects of this sequence on the performance of reset systems have not been investigated so far. In this paper, the effects of different sequences of controller parts on the performance of reset systems are studied using the HOSIDF tool. The best sequence is selected from HOSIDF theory to achieve the highest precision while also ensuring the lowest magnitude control input. This sequence is then tested for closed-loop performance in simulation and on a high precision positioning setup.

In section B.2, relevant preliminaries of reset control and frequency domain tools are presented. Theoretical investigation of different sequences of controller parts is presented in section B.3. In section B.4, the simulation results from closed-loop for the different sequences are analysed. The experimental results and conclusion are described in sections B.5 and B.6, separately.

B.2. PRELIMINARIES

B.2.1. RESET CONTROL

A general SISO reset element is defined by the following state-space equations according to [10] as

$$\begin{cases} \dot{x}_r(t) = A_r x_r(t) + B_r u_r(t), & u_r(t) \neq 0, \\ x_r(t^+) = A_\rho x_r(t), & u_r(t) = 0, \\ y_r(t) = C_r x_r(t) + D_r u_r(t), \end{cases} \tag{B.1}$$

where A_r, B_r, C_r and D_r are state-space matrices of the corresponding base linear system, A_ρ is the reset matrix determining the states' value ($x_r(t^+)$) after reset action, $u_r(t)$ is the input and is traditionally the error signal $e(t)$ and $y_r(t)$ is the output. To simplify the design of the reset element, reset matrix A_ρ is often defined as a diagonal matrix as

$$A_\rho = \gamma I_{n_r \times n_r}, \quad \gamma \in [-1, 1], \tag{B.2}$$

where n_r is the order of the reset controller. Although several reset laws exist in literature, we utilize the zero input crossing, i.e., $u_r(t) = 0$ as the reset law in this paper. To avoid Zeno behaviour, two consecutive reset instants are prevented.
DF of the defined reset element for a sinusoidal input is obtained in [26] as

$$\mathcal{N}_{DF} = C_r^T (j\omega I - A_r)^{-1} (I + j\Theta_\rho(\omega)) B_r + D_r, \tag{B.3}$$

where

$$\Theta_\rho = \frac{2\left(I + e^{\frac{\pi A_r}{\omega}}\right)(I - A_\rho)}{\pi\left(I + A_\rho e^{\frac{\pi A_r}{\omega}}\right)\left((\frac{A_r}{\omega})^2 + I\right)}. \tag{B.4}$$

In addition, HOSIDF for general reset elements are obtained in [25] as

$$H_n(j\omega) = \begin{cases} C_r (j\omega I - A_r)^{-1} (I + j\Theta_\rho(\omega)) B_r + D_r, & n = 1, \\ C_r (j\omega n I - A_r)^{-1} j\Theta_\rho(\omega) B_r, & \text{odd } n \geq 2, \\ 0, & \text{even } n \geq 2, \end{cases} \tag{B.5}$$

where n is the order of the harmonic.

The linear part of the controller which receives the error input is defined as C_{L_1} and the linear part following the reset element is defined as C_{L_2}. This is as shown in Figure. B.1. If the input of reset element is error ($C_{L_1} = 1$), then it results in the zero error crossing as introduced by Clegg. If the plant is defined as G, then the DF and HOSIDF of the open-loop L is obtained as

$$L_n(j\omega) = C_{L_1}(j\omega) H_n(j\omega) C_{L_2}(nj\omega) G(nj\omega). \tag{B.6}$$

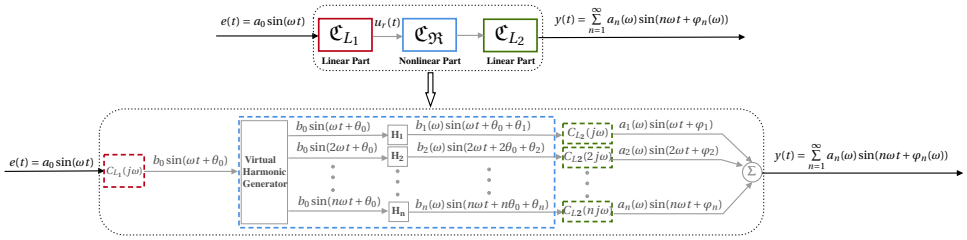

Figure B.1: HOSIDF Representation

B.2.2. PSEUDO SENSITIVITY FUNCTIONS

In linear systems, tracking error is obtained through sensitivity function which is defined as:

$$\frac{e}{r} = S(j\omega) = \frac{1}{1 + L(j\omega)} \tag{B.7}$$

where $L(j\omega)$ is the open loop frequency response of the linear system. In order to get sensitivity function of nonlinear systems, DF can be used to get $L_1(j\omega)$. However, DF only considers the first harmonic. To take into account the influence of high order harmonics, from a precision perspective, a pseudo-sensitivity function is defined for nonlinear systems as the ratio of the maximum tracking error of the system to the magnitude of the reference at each frequency. In other words,

$$\forall \omega \in \mathbb{R}^+ : \; S_\partial(\omega) = \frac{\max(|e(t)|)}{|r|}, \qquad \text{for } t \geq t_{ss}, \tag{B.8}$$

where t_{ss} is the time when system reaches steady state and r is the amplitude of sinusoidal reference input. Since $\max(|e(t)|)$ is the summation error of all the harmonics, this pseudo sensitivity function is more reliable than (B.7) for nonlinear controllers and will be used for closed-loop performance analyses.

B.3. METHODOLOGY

IN linear controllers, the sequence of the different linear filters does not affect the performance since they result in the same transfer function. However, when reset elements are used, the performance of the system can vary depending on the relative sequence of controller parts because the magnitude of high order harmonics depends on the chosen sequence and this in-turn influences the closed-loop performance. As shown in (B.6), while the DF (when $n = 1$) is not affected by the sequence, the magnitude of high order harmonics of the whole controller are influenced by $\mathfrak{C}_{L_1}$, $\mathfrak{C}_{L_2}$ and even the plant G. Therefore, HOSIDF tool is used to investigate and compare the magnitude of high order harmonics of different sequences.

In general, linear controllers can be divided into lead $\mathfrak{C}_{lead}$ and lag $\mathfrak{C}_{lag}$ filters. With the inclusion of the reset element, resulting in three controller parts, there are six different sequences possible. However, if linear lead and lag elements are interchanged, no difference will be seen in performance. Hence the number of sequences for investigation reduces to four and these are listed in TABLE B.1.

Table B.1: Different sequences of general case

No.	Sequence	nth order harmonic
1	**Lead-Reset-Lag**	$\mathfrak{C}_{lead}(j\omega)H_n(j\omega)\mathfrak{C}_{lag}(nj\omega)G(nj\omega)$
2	Lag-Reset-Lead	$\mathfrak{C}_{lag}(j\omega)H_n(j\omega)\mathfrak{C}_{lead}(nj\omega)G(nj\omega)$
3	Reset-Lead-Lag	$H_n(j\omega)\mathfrak{C}_{lead}(nj\omega)\mathfrak{C}_{lag}(nj\omega)G(nj\omega)$
4	Lead-Lag-Reset	$\mathfrak{C}_{lead}(j\omega)\mathfrak{C}_{lag}(j\omega) \times H_n(j\omega)G(nj\omega)$

Based on the equations in TABLE B.1, the first harmonic ($n = 1$) or DF for all 4 sequences are the same. However, for high order harmonics, since lead filters are ascending functions in magnitude while lag filters are descending functions with respect to the frequency, it is obvious that the first (No.1) and second (No.2) sequence has the smallest and largest magnitude of high order harmonics, respectively.

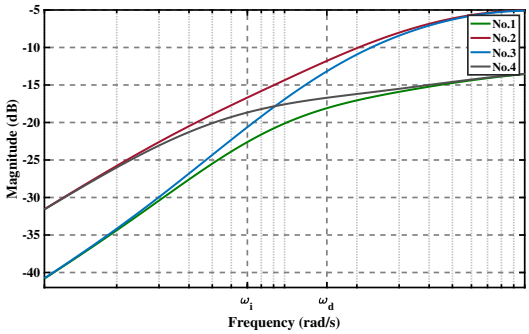

Figure B.2: The magnitude of the third order harmonic for different sequences of FORE

For a simple example, let us combine a FORE with a first-order lead filter $(1+\frac{s}{\omega_d})$ and a first-order lag filter: $(1+\frac{\omega_i}{s})$, with the magnitude of the third order harmonic for the four different sequences visualized in Figure. B.2. It is clear that before ω_i, the lag filter plays a role so that *No.*1 and *No.*3 have a smaller magnitude of high order harmonics. After ω_i, the lag filter effect has been terminated and the lead filter comes into play, therefore, *No.*1 and *No.*4 become smaller. In all range of frequencies, *No.*1 always has the smallest magnitude while *No.*2 has the largest magnitude of high order harmonics. The other two sequences are a trade-off between the extremes. Since the high order harmonics deteriorate the closed-loop performance, the optimal sequence is hypothesized to be the one with the lowest magnitude of high order harmonics. Based on HOSIDF theory, we can say that the optimal sequence for reset systems results in all linear lead elements preceding and all linear lag elements following the reset element i.e., *No.*1.

B.4. CLOSED-LOOP PERFORMANCE

To validate our hypothesis and investigate the closed-loop performances of different sequences, a Lorentz-actuated precision positioning stage is used as a benchmark.

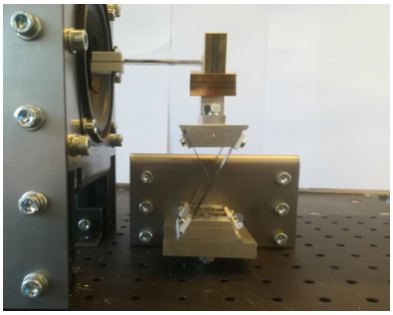

Figure B.3: Precision positioning stage actuated by a loud speaker

B.4.1. SYSTEM OVERVIEW

The system shown in Figure. B.3 consists of a mass guided using flexure cross hinge and actuated by a Visaton FR10-4 loudspeaker. With a Mercury 2000 reflective linear encoder, the horizontal position of the stage is measured with a resolution of 100nm. The controllers are implemented using FPGA module via compact RIO real-time hardware. Figure. B.4 shows the frequency response of the system.

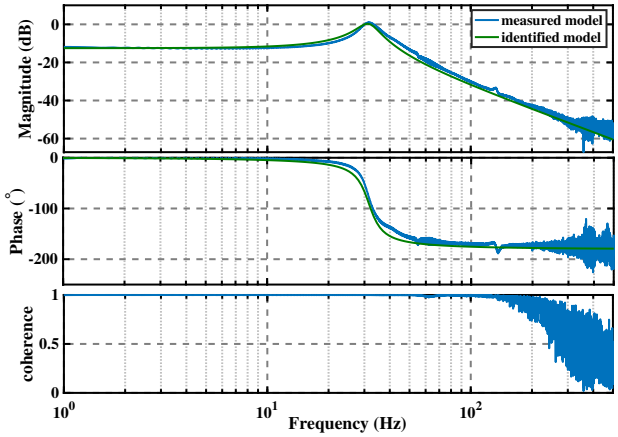

Figure B.4: Frequency response of the system identification

This system is identified as a second order mass-spring-damper system with the transfer function

$$P(s) = \frac{1}{1.077 \times 10^{-4} s^2 + 0.0049 s + 4.2218}. \tag{B.9}$$

B.4.2. CONTROLLER DESIGN

For controlling this system, a Proportional Integration (PI) with a Constant in gain Lead in phase (CgLp) compensator used. CgLp element is made up of a reset lag filter and a corresponding linear lead filter as proposed in [21]. Consider a FORE and a linear lead

part D as given below:

$$\text{FORE}(s) = \frac{1}{\cancel{s/\omega_r + 1}^{\gamma}}, \tag{B.10}$$

and

$$D(s) = \frac{s/\omega_d + 1}{s/\omega_t + 1}, \tag{B.11}$$

where ω_r is the corner frequency of reset element, γ determines the reset value (as defined in (B.2)), ω_d and ω_t are starting and taming frequencies of linear lead filter. By tuning $\omega_r = \omega_d/\alpha$, where α is a correction factor chosen according to [21], broadband phase lead can be achieved in the range of $[\omega_d, \omega_t]$ with constant gain (based on DF) as shown in Figure. B.5.

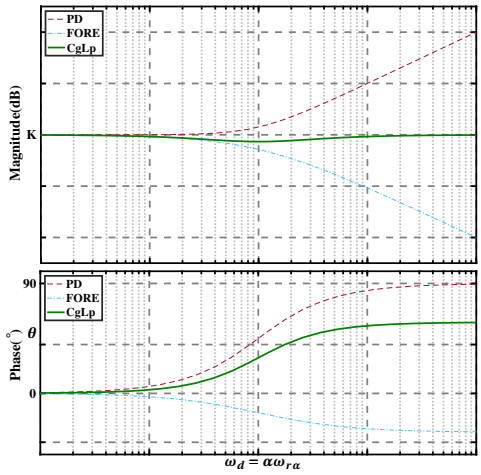

Figure B.5: The DF of a CgLp compensator

By replacing the D part of a traditional PID controller with a CgLp element, PI+CgLp controller is defined as

$$\Sigma_{RC} = \underbrace{K_p\left(1 + \frac{\omega_i}{s}\right)}_{PI} \underbrace{\left(\frac{1 + \frac{s}{\omega_d}}{1 + \frac{s}{\omega_t}}\right)\left(\frac{1}{\cancel{\frac{s}{\omega_r} + 1}^{\gamma}}\right)}_{CgLp}, \tag{B.12}$$

where ω_i is the corner frequency of the integrator element, and K_p is the proportional gain.

Based on the DF, controllers are designed to have the cross-over frequency ω_c = 100Hz with 30° phase margin. γ is selected as zero (classical reset), and according to [21, 27], ω_d is chosen to be $\omega_c/4$, ω_i=$\omega_c/10$ and ω_t=6ω_c, and correction factor α is taken as 1.62 ($\omega_r = \omega_d/1.62$). Also, K_p is tuned to get the required cross-over frequency. The

Table B.2: Tuning parameters of PI+CgLp controller

symbol	parameter	Value
ω_c	bandwidth	100 Hz
ω_d	corner frequency of lead filter	25Hz
ω_t	taming frequency of lead filter	600 Hz
ω_r	corner frequency of reset lag filter	15.43 Hz
ω_i	corner frequency of integrator	10 Hz
K_p	proportional gain of the controller	3980

parameters of the controller are listed in TABLE B.2. A PI+CgLp consists of a lag element (PI), a lead element (D) and a reset element (FORE). As TABLE B.1, four relative sequences are to be considered.

B.4.3. CLOSED-LOOP PERFORMANCE ANALYSIS IN SIMULATION

The defined pseudo-sensitivity function of (B.8) is used to compare the closed-loop tracking performance in simulation. Disturbance and white noise are added to mimic a more realistic situation as shown in Figure. B.6. Control elements are discretized for a sampling frequency of 20 KHz. A disturbance signal between $0.5Hz$ and $30Hz$ which can cause 10% positioning deviation is applied for all sequences to mimic floor vibration. White noise with the magnitude of $(1\% - 3\%)$ of the reference is considered to imitate the noise present in the real setup. However, to consider the effect of noise on overall performance, different levels of noise are used during simulation for analysis.

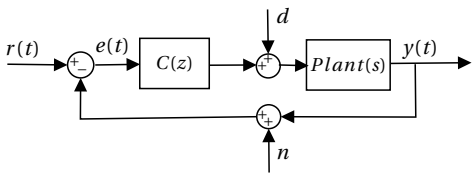

Figure B.6: Block diagram of closed-loop performance analyses

Sinusoidal signal is given as input at different frequencies and the maximum steady-state value of $|e(t)|$ was recorded and used to plot $S_\partial(\omega)$ with different levels of noise as shown in Figure. B.7. Also, the DF sensitivity is plotted using DF of reset element and linear sensitivity relation of (B.7). The first thing that should be noted is that the DF based sensitivity is not appropriate at estimating closed-loop performance of any of the sequences. Next, concerning the different sequences, as shown in Figure. B.7a, the sequence Lead-Reset-Lag ($No.1$) has the smallest $S_\partial(\omega)$ at all frequencies when the magnitude of noise signal is 0.1% of reference. When the magnitude of noise increases to more than 1%, the performances of sequence $No.1$ and $No.4$ deteriorate at low frequencies while the sequences $No.2$ and $No.3$ do not change a lot. This deterioration in performance with the increase in noise amplitude can be explained by the fact that both $No.1$ and $No.4$ have a lead filter before the reset element which amplifies noise which is present at high frequencies. This amplified noise influences the zero crossing

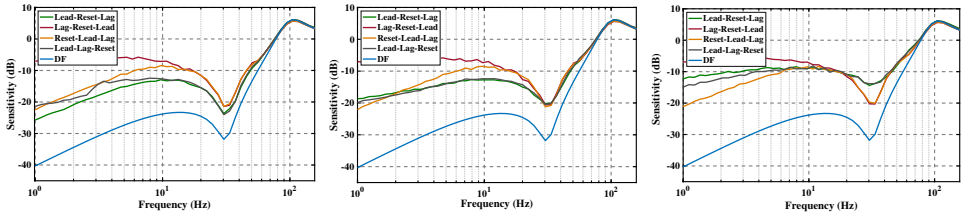

(a) Sensitivity with 0.1% noise (b) Sensitivity with 1% noise (c) Sensitivity with 3% noise

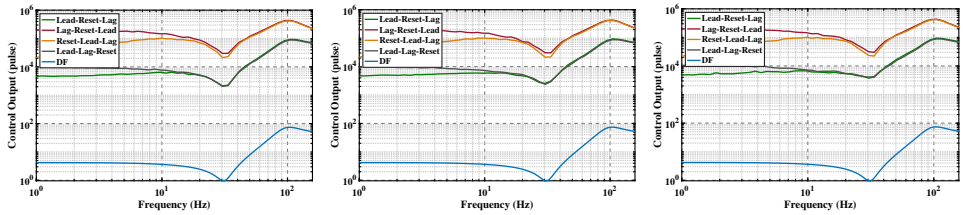

(d) Control output with 0.1% noise (e) Control output with 1% noise (f) Control output with 3% noise

Figure B.7: Pseudo-sensitivity functions and maximum control inputs with different level of noise

instants. This is especially true at low frequencies of the reference where the error signal in the absence of noise and disturbances would be quite low. In the presence of amplified noise, noise starts dominating the combined error signal. As a result, the zero crossings are dominantly determined by noise resulting in the performance deterioration seen. At higher frequencies especially above ω_d (25Hz), the error due to reference is also amplified by the lead filter hence cancelling out the detrimental influence of noise.

In terms of the control input, since the maximum amplitude is important for avoiding saturation, the maximum control input values at each frequency are compared for all sequences. As shown in Figure. B.7e, Figure. B.7d, and Figure. B.7f, sequences *No*.2 and *No*.3 always have much larger control input compared with others. This is because these two structures have a lead filter after the reset element. In these sequences, the resetting action which results in the output of the reset element jumping is fed to the lead filter whose amplification of jump leads to large control input to the system. Since low control input is preferred, the optimal sequence from a precision perspective is also the optimal sequence from the control input viewpoint.

B.4.4. SHAPING FILTER

To attenuate the influence of noise, in sequence *No*.1 and *No*.4, a shaping filter $\mathfrak{C}_s$ is proposed whose output is used to determine the reset instants as shown in Figure. B.8.

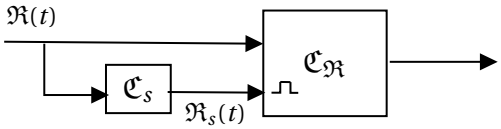

Figure B.8: Structure of shaping filter

This shaping filter consists of a low pass filter (LPF) and a tamed lead filter. It is represented as

$$\mathfrak{C}_s = \underbrace{\left(\frac{1}{1+\frac{s}{\omega_f}}\right)}_{LPF}\underbrace{\left(\frac{1+\frac{s}{\omega_c/a}}{1+\frac{s}{\omega_c a}}\right)}_{Lead}, \tag{B.13}$$

where ω_f is the corner frequency of the LPF,ω_c is the bandwidth and a is a tuning knob. The LPF plays the role of decreasing the magnitude of noise. However, the LPF also introduces phase lag into the signal used for resetting, which changes the reset instants and hence deteriorates performance. To compensate for this, a tamed lead filter is used. The phase of LPF at bandwidth can be calculated by

$$\phi_c = -\tan^{-1}\left(\frac{\omega_c}{\omega_f}\right). \tag{B.14}$$

To compensate for this phase change, the constant a is tuned such that

$$\tan^{-1}(a) - \tan^{-1}\left(\frac{1}{a}\right) = -\phi_c. \tag{B.15}$$

A smaller ω_f results in greater noise attenuation, but a corresponding large value for a, creating a magnitude peak due to the lead filter. As a trade-off, the corner frequency of LPF is set as $\omega_f = 2\omega_c$, with the corresponding $a = 1.62$.

Considering the phase of this shaping filter as $\phi(\omega)$, the HOSIDOFs of the reset element with shaping filter are re-established using a similar process in [26] and [25] as

$$H_n(j\omega) = \begin{cases} C_r(j\omega I - A_r)^{-1}(I + e^{j\phi} j\Theta_s(\omega))B_r + D_r, & n = 1, \\ C_r(j\omega n I - A_r)^{-1} e^{j\phi} j\Theta_s(\omega) B_r, & \text{for odd } n \geq 2, \\ 0, & \text{for even } n \geq 2, \end{cases} \tag{B.16}$$

where

$$\Theta_s = \Theta_\rho\left(\frac{-A_r \sin\phi + \omega\cos\phi I}{\omega}\right).$$

The first and third order DF of the traditional FORE and the FORE with shaping filter are shown in Figure. B.9. It can be seen that the shaping filter does not change the DF significantly, but the magnitude of the third order harmonic is reduced after ω_f.

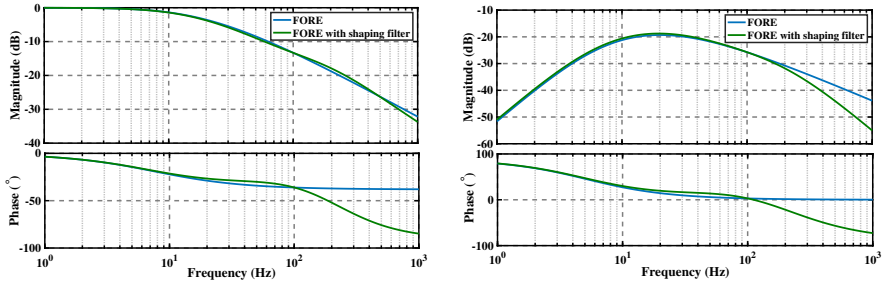

(a) The first order DFs

(b) The third order DFs

Figure B.9: The first and third order DFs of FORE and FORE with shaping filter

The pseudo sensitivity $S_\partial(\omega)$ is obtained with the use of shaping filter for sequences *No.*1 and *No.*4 and is shown in Figure. B.10 with 3% noise added. This shaping filter drastically reduces the effect of noise and improves tracking performance. Although the performance deteriorates slightly around the bandwidth, this will not affect the tracking performance of trajectory signals in reality, where high-frequency components are often pre-filtered out [28]. Simulation performance for noise levels larger than 3% showed poor performance for the chosen shaping filter and hence are not shown. For larger levels of noise, shaping filter with smaller ω_f needs to be used. However, the 3% noise level is already quite large for several precision positioning applications and hence this technique can be successfully used in practice.

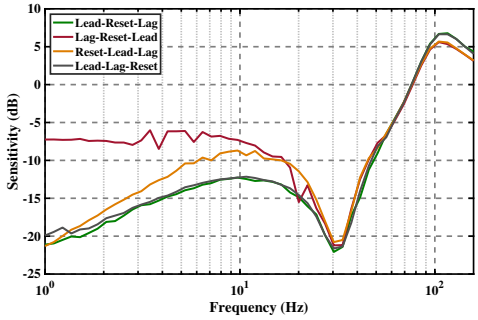

Figure B.10: Sensitivity function with 3% noise when shaping filter is applied on sequence 1 and 4

In summary, the sequence *No.*1 has the optimal sequence for tracking performance for noise signal up-to 1% amplitude compared to the reference. For larger noise levels, a shaping filter can be used to attenuate effects of noise in the performance. Furthermore, the sequence *No.*1 has the minimum control input among all possible sequences.

B.4.5. STEP RESPONSE

The step responses of different sequences are compared in Figure. B.11. It can be seen that steady state error is seen when integrator (lag filter) is in front of the reset element (the system is not asymptotically stable). Also, overshoot occurs when differentiator (lead) is located after the reset element. Although putting the lead filter after the reset element has less rise time than putting it before the reset element, both sequences have the same settling time. From the time domain perspective, Lead-Reset-Lag (sequence *No.*1) is still the optimal sequence.

B.5. EXPERIMENTAL VALIDATION

To validate the simulation results, a series of experiments are conducted for all the four sequences without any shaping filters. The maximum error values along with the maximum control input values are obtained for five different frequencies of reference input. Further, to avoid problems due to control input saturation, different amplitudes are chosen for the sinusoidal reference signals at different frequencies as given in TABLE B.3. The amplitude of the noise in the system is found to be (100nm) for the exper-

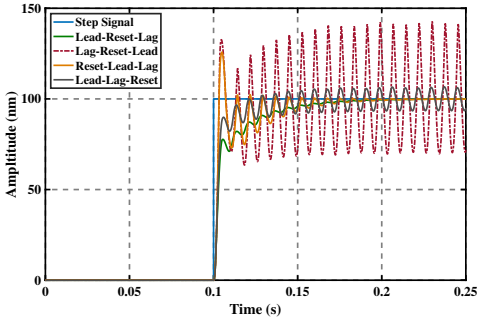

Figure B.11: Step responses of different sequences

iments. The maximum steady-state error signal ($\max(|e(t)|)$) and maximum steady-state digital control input are recorded in TABLE B.4 and TABLE B.5 respectively.

Table B.3: Magnitude of sinusoidal reference and the level of noise

Reference signal		level of noise
Frequency(Hz)	Magnitude ($0.1\mu m$)	Percentage
1	100	1%
5	120	0.83%
10	120	0.83%
15	150	0.67%
20	200	0.5%

Table B.4: Maximum steady-state error of four different sequences

Reference	$\max(\|e(t)\|)$ ($0.1\mu m$)			
(Hz)	No.1	No.2	No.3	No.4
1	15	73	14	15
5	37	78	56	40
10	42	73	67	48
15	54	84	86	54
20	55	97	86	55

The results in the tables validate the theory and simulation results as sequence $No.1$ provides the lowest error at almost all tested frequencies except at 1Hz, where $No.3$ has a lower error. This is consistent with the simulation results since the noise level being 1% of reference amplitude at this frequency results in performance deterioration. In addition, at $15Hz$ and $20Hz$ which are both more than ω_i, the effect of the integrator is vanished ($\frac{\omega_i}{s}|_{\omega>\omega_i} \approx 0$). Consequently, the sequences $No.1$ and $No.4$ have the same performance.

To check the effect of noise at low frequencies and the effect of shaping filter in over-

Table B.5: Maximum steady-state control input of four different sequences

Reference	Digital control input (count)			
(Hz)	No.1	No.2	No.3	No.4
1	486	26173	3103	1222
5	884	26806	12785	1513
10	941	24476	16972	1306
15	1364	25718	19539	1473
20	1677	27541	22038	1471

coming this problem, a different set of experiments is conducted at 1Hz with 3% noise. Since sequence *No*.2 is the worst sequence in terms of both tracking performance and control input as seen in Tables. B.4 and B.5, this sequence is not tested for and only the performance of the other three sequences are compared in TABLE B.6. Without the shaping filter, the performance of *No*.1 and *No*.4 significantly deteriorates, while the performance of *No*.3 does not change a lot with an increase in noise levels. When the shaping filter is applied, the performances of *No*.1 and *No*.4 are improved significantly which means that the effect of noise is effectively suppressed. The efficacy of the shaping filter is hence verified in practice.

Table B.6: Influence of shaping filter on maximum steady-state error

Configuration	level of noise	$\max(\|e(t)\|)$ $(0.1\mu m)$		
		No.1	No.3	No.4
without shaping filter	1%	15	14	15
without shaping filter	3%	49	20	32
with shaping filter	3%	19	19	21

B.6. CONCLUSION

THIS paper has proposed an optimized strategy for the sequence of controller parts when a reset element is used. Firstly, the frequency responses of the different sequences were investigated by considering high order harmonics using HOSIDF theory. The optimal sequence is hypothesized to be the one in which the magnitude of high order harmonics is minimum. Next, the closed-loop performances of a high-tech positioning stage with PI+CgLp controller were analyzed in both simulation and experiment for different sequences of controller parts. The results illustrate that when the magnitude of noise within the system is smaller than 1% of the reference signal, it is safe to say that the suggested sequence has the best performance. Otherwise, the performance of the suggested sequence will deteriorate at low frequencies. In this case, a shaping filter is proposed to deal with the problem. It is revealed that this shaping filter attenuates the influence of noise successfully and allows the suggested sequence to provide the best tracking performance with up to 3% noise. In addition, the suggested sequence also has the smallest control input, which provides greater flexibility for actuator choice/design.

These results can facilitate the use of reset controllers in a broad range of applica-

tions in high-tech industry. Application of this approach for other kinds of nonlinear controllers for improved performances is a promising topic for investigation in the future.

B

REFERENCES

[1] C. Cai, A. A. Dastjerdi, N. Saikumar, and S. HosseinNia, *The optimal sequence for reset controllers,* in 18^{th} *European Control Conference (ECC 2020)* (2020).

[2] R. H. Middleton, *Trade-offs in linear control system design,* Automatica **27**, 281 (1991).

[3] S. Skogestad and I. Postlethwaite, *Multivariable feedback control: analysis and design*, Vol. 2 (Wiley New York, 2007).

[4] R. M. Schmidt, G. Schitter, and A. Rankers, *The Design of High Performance Mechatronics-: High-Tech Functionality by Multidisciplinary System Integration* (IOS Press, 2014).

[5] A. A. Dastjerdi, B. M. Vinagre, Y. Chen, and S. H. HosseinNia, *Linear fractional order controllers; a survey in the frequency domain,* Annual Reviews in Control (2019).

[6] J. Clegg, *A nonlinear integrator for servomechanisms,* Transactions of the American Institute of Electrical Engineers, Part II: Applications and Industry **77**, 41 (1958).

[7] L. Chen, N. Saikumar, S. Baldi, and S. H. HosseinNia, *Beyond the waterbed effect: Development of fractional order crone control with non-linear reset,* in *2018 Annual American Control Conference (ACC)* (IEEE, 2018) pp. 545–552.

[8] S. H. HosseinNia, I. Tejado, and B. M. Vinagre, *Basic properties and stability of fractional-order reset control systems,* in *2013 European Control Conference (ECC)* (IEEE, 2013) pp. 1687–1692.

[9] L. Marinangeli, F. Alijani, and S. H. HosseinNia, *Fractional-order positive position feedback compensator for active vibration control of a smart composite plate,* Journal of Sound and Vibration **412**, 1 (2018).

[10] A. Baños and A. Barreiro, *Reset control systems* (Springer Science & amp; Business Media, 2011).

[11] D. Valério, N. Saikumar, A. A. Dastjerdi, N. Karbasizadeh, and S. H. HosseinNia, *Reset control approximates complex order transfer functions,* Nonlinear Dynamics , 1 (2019).

[12] G. Zhao, D. Nešić, Y. Tan, and C. Hua, *Overcoming overshoot performance limitations of linear systems with reset control,* Automatica **101**, 27 (2019).

[13] G. Zhao and J. Wang, *On l2 gain performance improvement of linear systems with lyapunov-based reset control,* Nonlinear Analysis: Hybrid Systems **21**, 105 (2016).

[14] I. Horowitz and P. Rosenbaum, *Non-linear design for cost of feedback reduction in systems with large parameter uncertainty,* International Journal of Control **21**, 977 (1975).

[15] L. Hazeleger, M. Heertjes, and H. Nijmeijer, *Second-order reset elements for stage control design,* in *2016 American Control Conference (ACC)* (IEEE, 2016) pp. 2643–2648.

[16] J. Zheng, Y. Guo, M. Fu, Y. Wang, and L. Xie, *Development of an extended reset controller and its experimental demonstration,* IET Control Theory & Applications **2**, 866 (2008).

[17] A. Baños and A. Vidal, *Definition and tuning of a pi+ ci reset controller,* in *2007 European Control Conference (ECC)* (IEEE, 2007) pp. 4792–4798.

[18] A. Barreiro, A. Baños, S. Dormido, and J. A. González-Prieto, *Reset control systems with reset band: Well-posedness, limit cycles and stability analysis,* Systems & Control Letters **63**, 1 (2014).

[19] J. Zheng, Y. Guo, M. Fu, Y. Wang, and L. Xie, *Improved reset control design for a pzt positioning stage,* in *2007 IEEE International Conference on Control Applications* (IEEE, 2007) pp. 1272–1277.

[20] A. Palanikumar, N. Saikumar, and S. H. HosseinNia, *No more differentiator in PID: Development of nonlinear lead for precision mechatronics,* in *2018 European Control Conference (ECC)* (IEEE, 2018) pp. 991–996.

[21] N. Saikumar, R. Sinha, and S. H. Hoseinnia, *'constant in gain lead in phase' element-application in precision motion control,* IEEE/ASME Transactions on Mechatronics (2019).

[22] N. Saikumar, R. K. Sinha, and S. H. HosseinNia, *Resetting disturbance observers with application in compensation of bounded nonlinearities like hysteresis in piezo-actuators,* Control Engineering Practice **82**, 36 (2019).

[23] N. Saikumar, D. Valério, and S. H. HosseinNia, *Complex order control for improved loop-shaping in precision positioning,* arXiv preprint arXiv:1907.09249 (2019).

[24] P. Nuij, O. Bosgra, and M. Steinbuch, *Higher-order sinusoidal input describing functions for the analysis of non-linear systems with harmonic responses,* Mechanical Systems and Signal Processing **20**, 1883 (2006).

[25] K. Heinen, *Frequency analysis of reset systems containing a clegg integrator: An introduction to higher order sinusoidal input describing functions,* (2018).

[26] Y. Guo, Y. Wang, and L. Xie, *Frequency-domain properties of reset systems with application in hard-disk-drive systems,* IEEE Transactions on Control Systems Technology **17**, 1446 (2009).

[27] X. Hou, *Tuning of the "Constant in gain Lead in phase" Element for Mass-like Systems*, Master's thesis, Delft University of Technology (2019).

[28] P. Lambrechts, M. Boerlage, and M. Steinbuch, *Trajectory planning and feedforward design for electromechanical motion systems,* Control Engineering Practice **13**, 145 (2005).

C

TOOLBOX

In order to facilitate using the developed non-linear loop-shaping, most of the complicated relations of this thesis are embedded in a user-friendly toolbox which is produced by Matlab. In this Appendix, a manual is provided to help how to use in this toolbox.

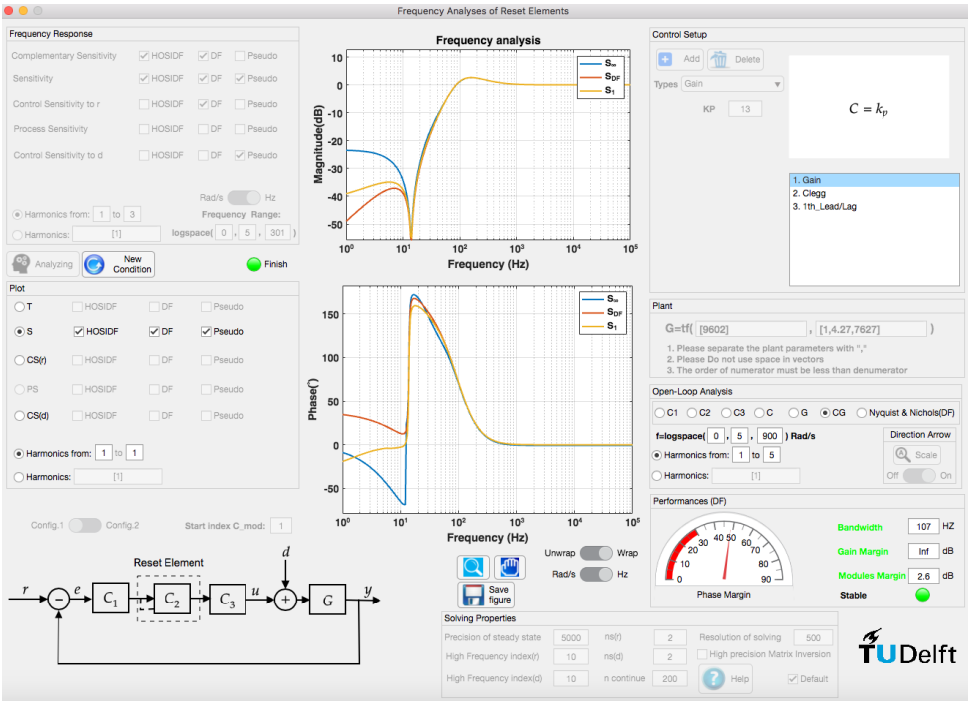

Figure C.1: Developed toolbox based on the proposed theory

This toolbox, which is available through the PME's website of Delft University of Technology[1], can be run in Matlab software (version 2018 or above). As it is shown in Fig. C.1, it consists of seven panels which are elaborated in following.

- **"Plant" panel**: In this part, the transfer function of the plant is specified.
- **"Control Setup" panel**: In this panel, filters of both linear and non-linear parts of the controller are tuned. Almost linear filters and reset elments consist of both zero and non-zero reset values of FORE, SORE, and Clegg are available in this panel. Note that the sequence of filters is the same as you entered in this part.
- **"Open-Loop Analysis" panel**: In this panel, it is possible to analyze the open-loop of the reset control system in the frequency-domain considering high order harmonics. It has to be noted that the Nyquist and Nichols plots in this panel are depicted using the Df method.
- **"Performances (DF)" panel**: In this part, the open-loop margins of the system can be observed in this panel. Note, all open-loop margins in this panel are calculated using the DF method. Although these margins are not accurate, they give an insight to the performance of the system.

[1] There is also a movie in the website which elaborates how to use the toolbox through one example

- **“Frequency Response" panel**: After tuning the controller and analyzing it in the open-loop, the frequency responses which have to be calculated are selected in this panel. Also, the number of closed-loop HOSIDF and the frequency range of the responses are set in this panel. Note, "DF" options in this panel approximate the closed-loop frequency responses through the DF method.
- **“Solving Properties" panel**: In this panel, solving properties for calculating frequency responses are set (for more details, read the help of toolbox).
- **“Plot" panel**: frequency responses which are selected in “Frequency Response" panel and obtained by the proposed method can be depicted in this panel.

CURRICULUM VITÆ

Ali AHMADI DASTJERDI

05-04-1991 Born in Tehran, Iran.

EDUCATION

2009–2013 Undergraduate in Mechanical Engineering
Amirkabir University of Technology, Tehran, Iran
Thesis: Optimizing of Distance Between Gas Pressure Stations
Supervisors: Prof. dr. N. Montazerin

2013–2015 Postgraduate in Solid Mechanics
Sharif University of Technology, Tehran, Iran
Thesis: Optimization of Warpage of Polymer Parts Produced by Selected Laser Sintering
Supervisors: Prof. dr. M. R. Movahedi, Prof. dr. J. Akbari

2017-2021 PhD. in Dept. Precision and Microsystems Engineering
Delft University of Technology, Delft, The Netherlands
Thesis: Frequency-Domain Analyzing of "Constant in gain Lead in phase (CgLp)" Reset Compensators
Supervisors: Prof. dr. J. Herder, Dr. S.H. HosseinNia

AWARDS

2020 Erasmus+fund

2020 IEEE CSS Student Travel Support Program of CDC

List of Publications

Journal Publications

7. **A. A. Dastjerdi**, A. Astolfi, N. Saikumar, N. Karbasizadeh, D. Valerio, S.H. HosseinNia, *Closed-loop Frequency Analyses of Reset Systems*, Submitted to IEEE Transaction on Automatic Control.

6. **A. A. Dastjerdi**, A. Astolfi, S.H. HosseinNia, *Frequency-Domain Stability Methods for Reset Systems*, Submitted to Automatica.

5. **A. A. Dastjerdi**, S.H. HosseinNia, *A Frequency-Domain Tuning Method For a Class of Reset Control Systems*, IEEE-Access (2021).

4. N. Karbasizadeh, **A. A. Dastjerdi**, N. Saikumar, S.H. HosseinNia, *A Frequency-Domain Tuning Method For a Class of Reset Control Systems*, Submitted to IEEE Transaction on System Control Technology.

3. **A. A. Dastjerdi**, B. M. Vinagre, Y. Q. Chen, S.H. HosseinNia, *Linear Fractional Order Controllers; A Survey in the Frequency Domain*, Annual Reviews in Control **47**, 51 (2019).

2. D. Valerio, N. Saikumar, **A. A. Dastjerdi**, N. Karbasizadeh, S.H. HosseinNia, *Reset Control Approximates Complex Order Transfer Functions*, Nonlinear Dynamics **97**, 2323 (2019).

1. **A. A. Dastjerdi**, B. M. Vinagre, Y. Q. Chen, S.H. HosseinNia, *Tuning Guidelines for Fractional Order PID Controllers: Rules of Thumb*, Mechatronics **56**, 26 (2018).

Conference Publications

6. **A. A. Dastjerdi**, N. Saikumar, S.H. HosseinNia, *Tuning of a Class of Reset Elements Using Pseudo-Sensitivities*, European Control Conference (ECC), Rotterdam, The Netherlands, 2021.

5. **A. A. Dastjerdi**, A. Astolfi, S.H. HosseinNia, *A Frequency-Domain Stability Methods for Reset Systems*, IEEE Conference on Decision and Control (CDC), Jeju Island, South Korea, 2020.

4. C. Cai, **A. A. Dastjerdi**, N. Saikumar, S.H. HosseinNia, *The Optimal Sequence for Reset Controllers*, European Control Conference (ECC), Saint Petersburg, Russia, 2020.

3. M.Shirdast, N. Karbasizadeh, **A. A. Dastjerdi**, N. Saikumar, S.H. HosseinNia, *Tuning of CgLp Based Reset Controllers: Application in Precision Positioning Systems.* IFAC World Congress, Berlin, Germany, 2020.

2. X. Hou, **A. A. Dastjerdi**, N. Saikumar, S.H. HosseinNia, *Tuning of "Constant in gain Lead in phase (CgLp)" Reset Controller using higher-order sinusoidal input describing function (HOSIDF)*, Australian and New Zealand Control Conference (ANZCC), Gold Coast, Australian, 2020.

1. N. Karbasizadeh, **A. A. Dastjerdi**, N. Saikumar, D. Valerio, S.H. HosseinNia, *Benefiting from Linear Behaviour of a Nonlinear Reset-based Element at Certain Frequencies*, Australian and New Zealand Control Conference (ANZCC), Gold Coast, Australian, 2020.